Thesis submitted for the Degree of

Doctor of Philosophy

in the

University of Oxford



RADIOGENIC ISOTOPE STUDIES OF CRUST-FORMING PROCESSES IN THE LOFOTEN-VESTERÅLEN PROVINCE OF NORTH NORWAY

(Volume Two: Plates, Tables and Figures)

by

Stephen James Rochfort Wade

Linacre College

and

Department of Earth Sciences

University of Oxford

1985



CONTENTS OF VOLUME TWO

	Page
CHAPTER ONE	
Figures	1
CHAPTER TWO	
Figures	2
Tables	6
CHAPTER THREE	
Plates	13
Tables	17
Figures	21
CHAPTER FOUR	
Plates	41
Tables	57
Figures	62
CHAPTER FIVE	
Plates	77
Tables	91
Figures	98
CHAPTER SIX	
Plates	125
Tables	151
Figures	170
CHAPTER SEVEN	
Plates	246
Tables	258
Figures	264
CHAPTER EIGHT	
Plates	276
Tables	284
Figures	288
CHAPTER NINE	
Figures	296

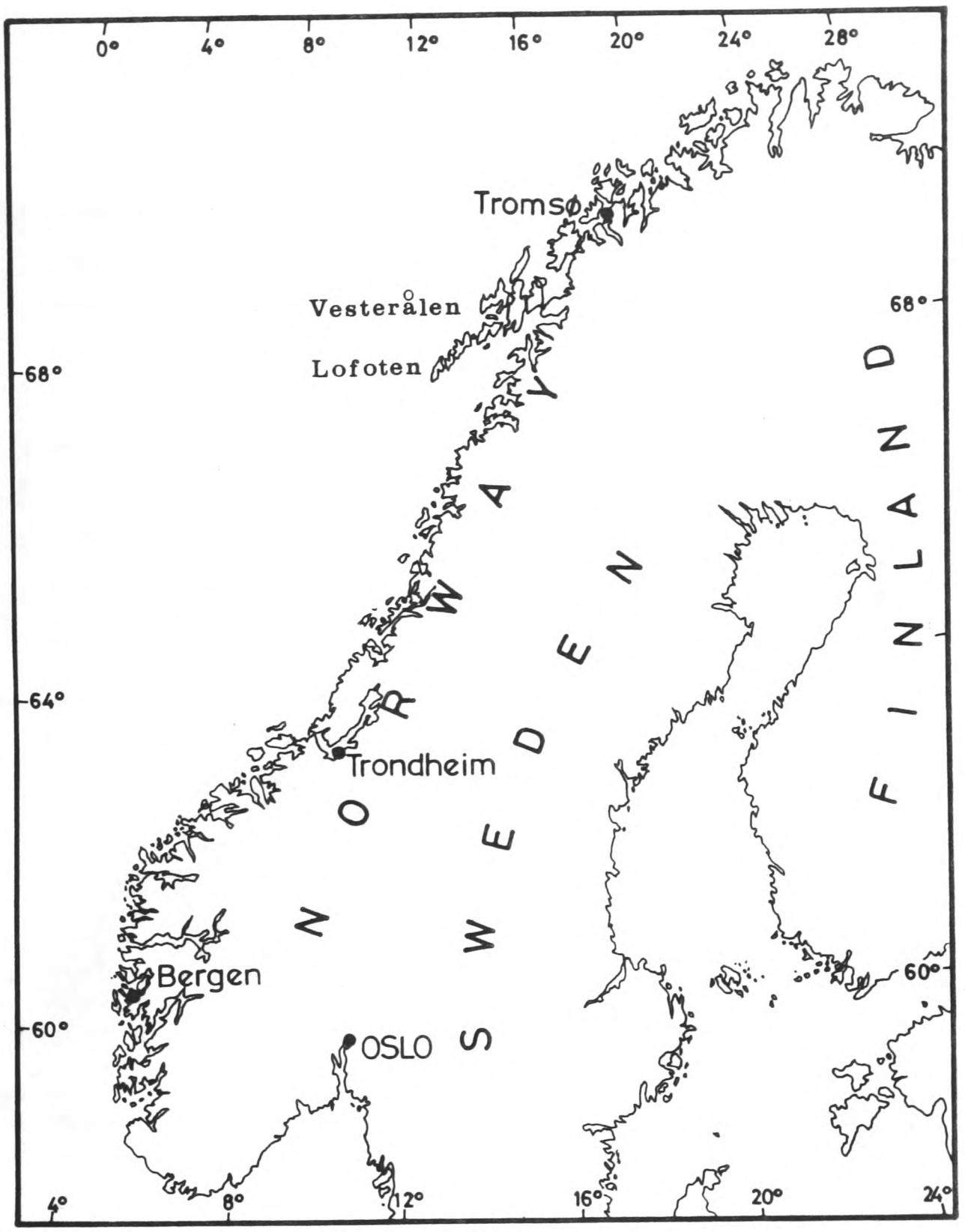


Fig. 1.1 The Location of the Lofoten-Vesterålen province, North Norway

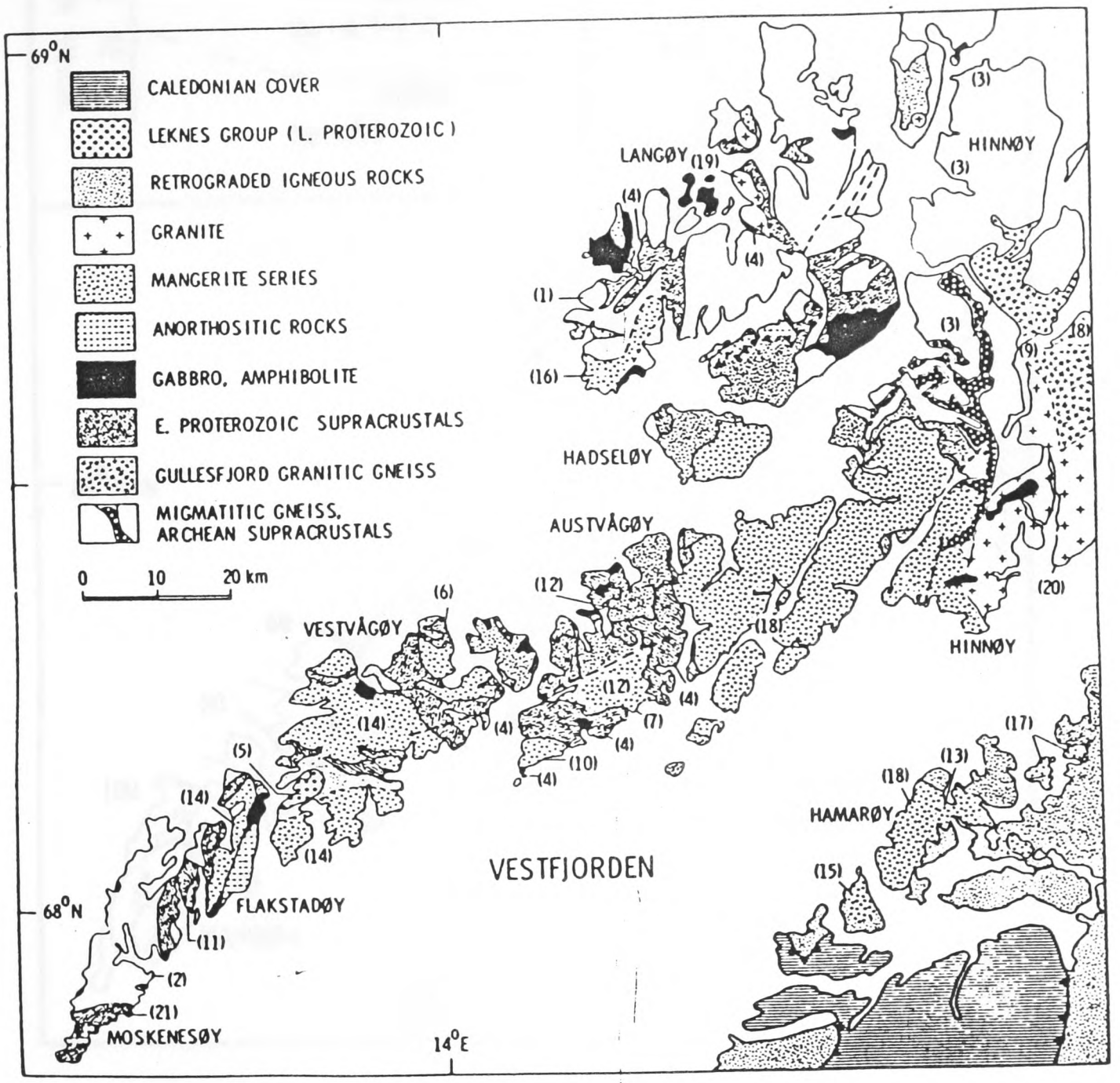


Fig. 2.1: Simplified geological map of Lofoten-Vesterålen. Numbers in parentheses refer to localities mentioned in Tables 2.3 and 2.6. (After Griffin et al., 1978)

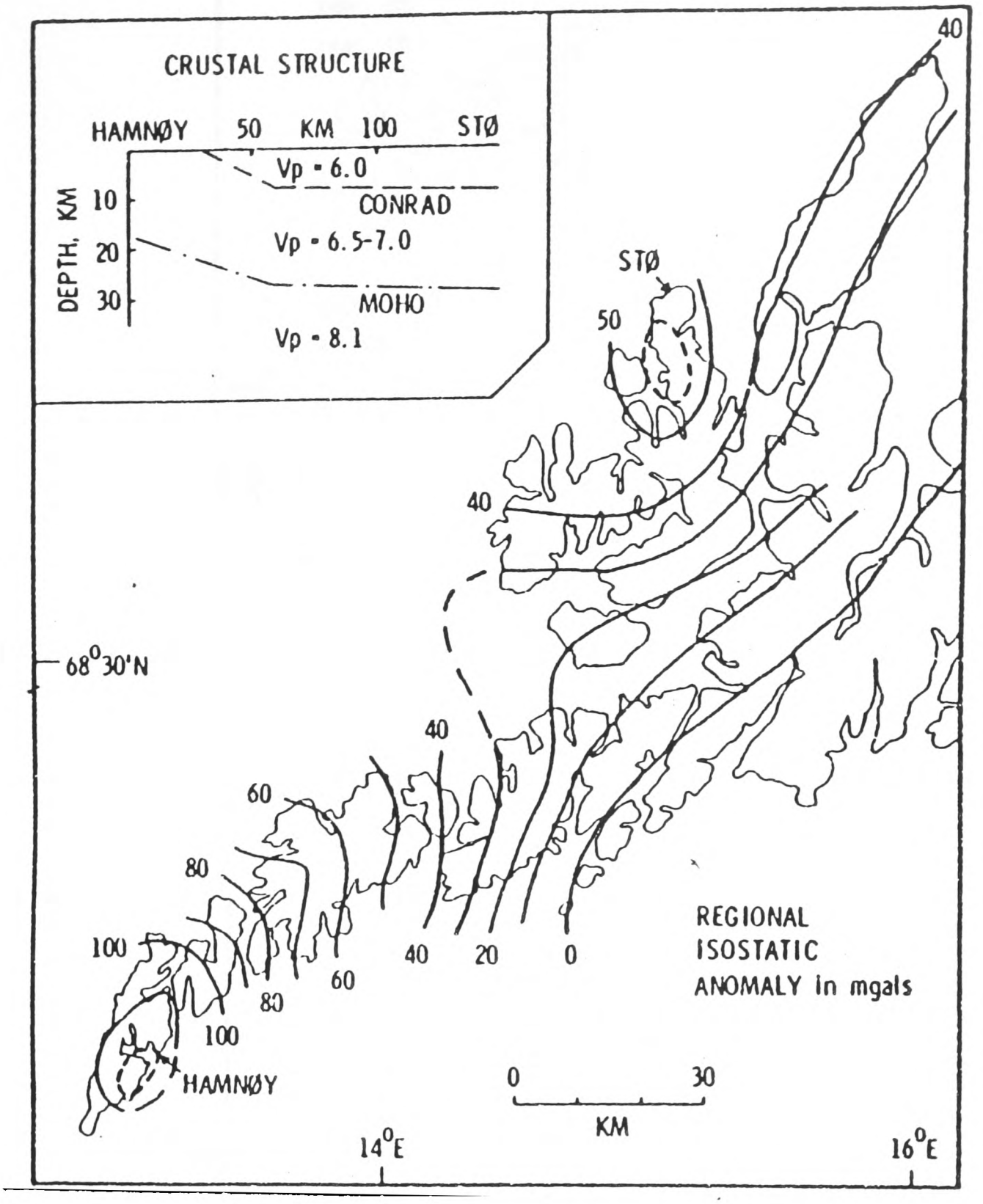


Fig. 2.2: Regional isostaticanomalies and summary of crustal structure, after Svela (1971) and Griffin et al. (1978).

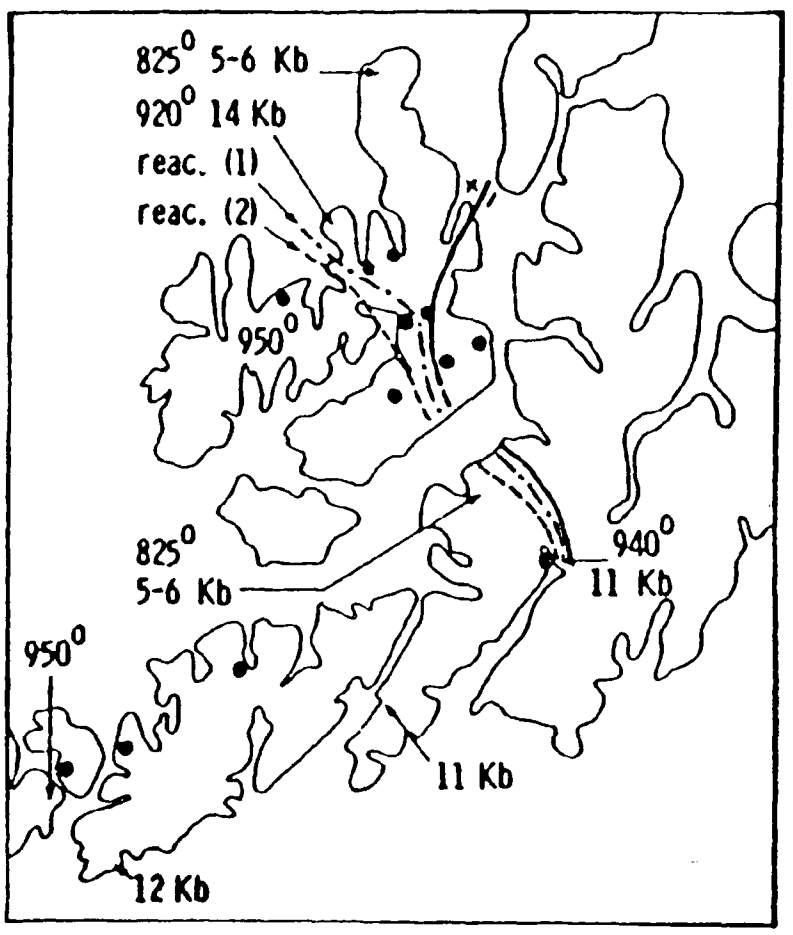


Fig. 2.3: Isograds and estimated maximum conditions during the c.1830Ma regional metamorphism. Solid line orthopyroxene isograd,(+) on upgrade side. Other isograds based oncarbonate reactions discussed in text (after Griffin et al., 1978).

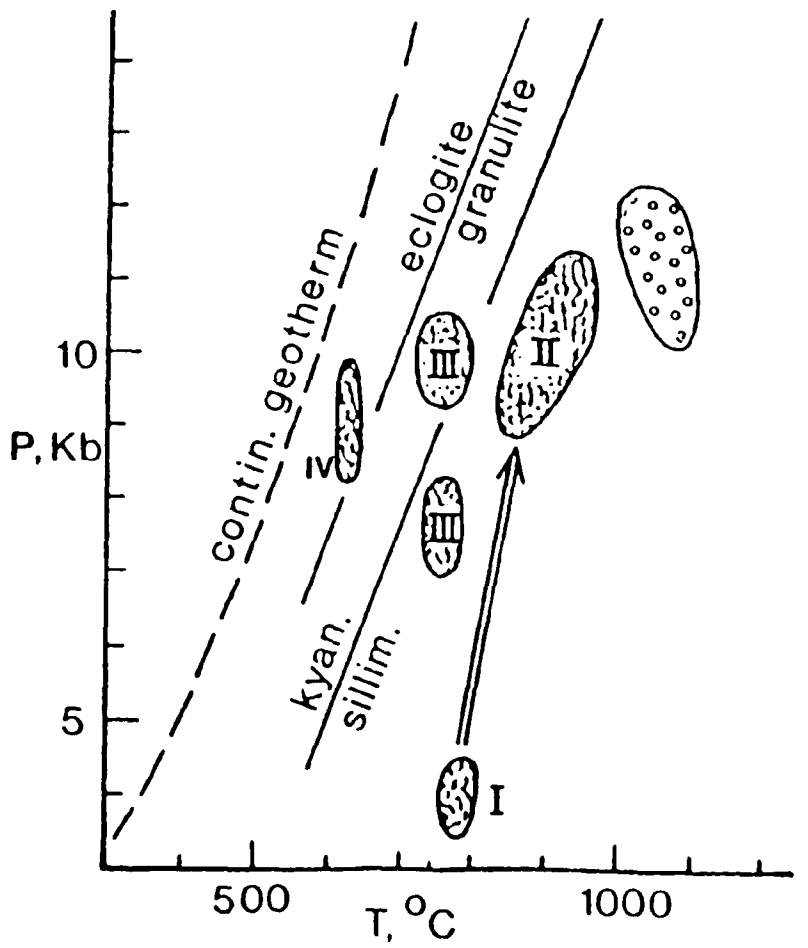


Fig. 2.4: Interpretation of P-T estimates based on mineral assemblages. Stippled field, crystallization of mangerites; hachured fields; metamorphic conditions. See also Table 2.4. After Griffin et al., (1978).

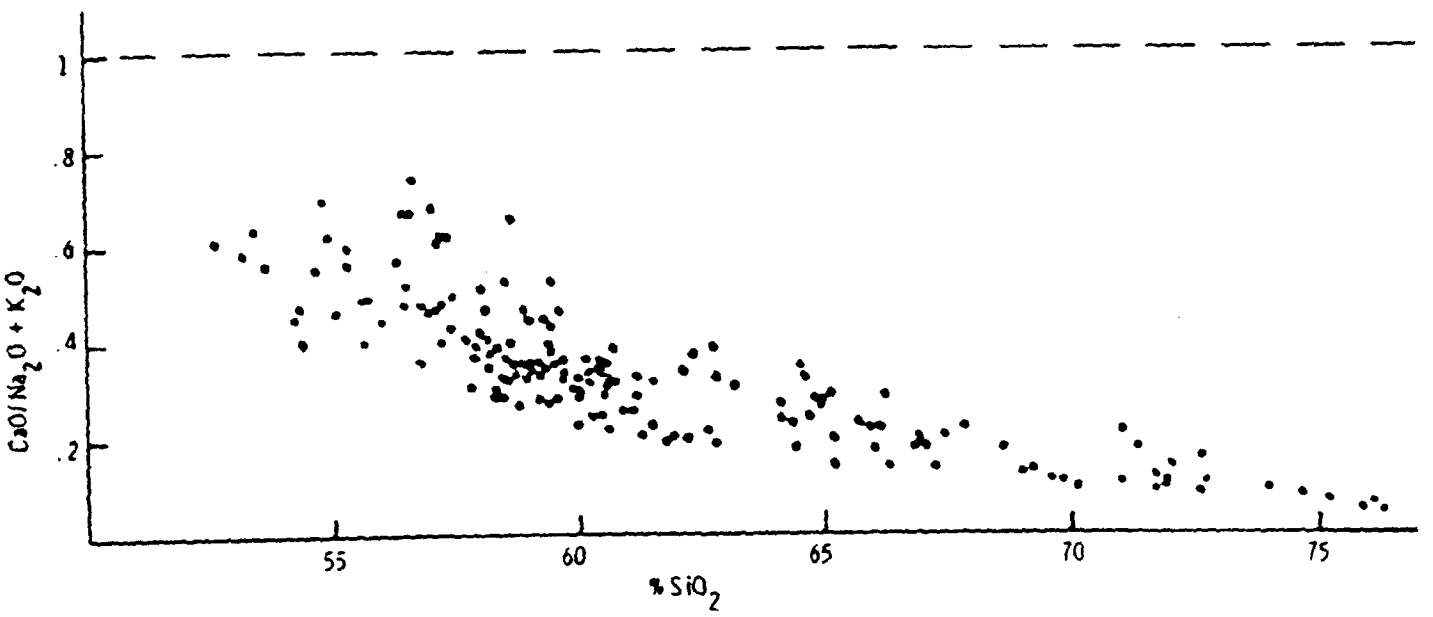


Fig. 2.6: Alkali-lime variation in the mangerite series (after Griffin et al., 1978)

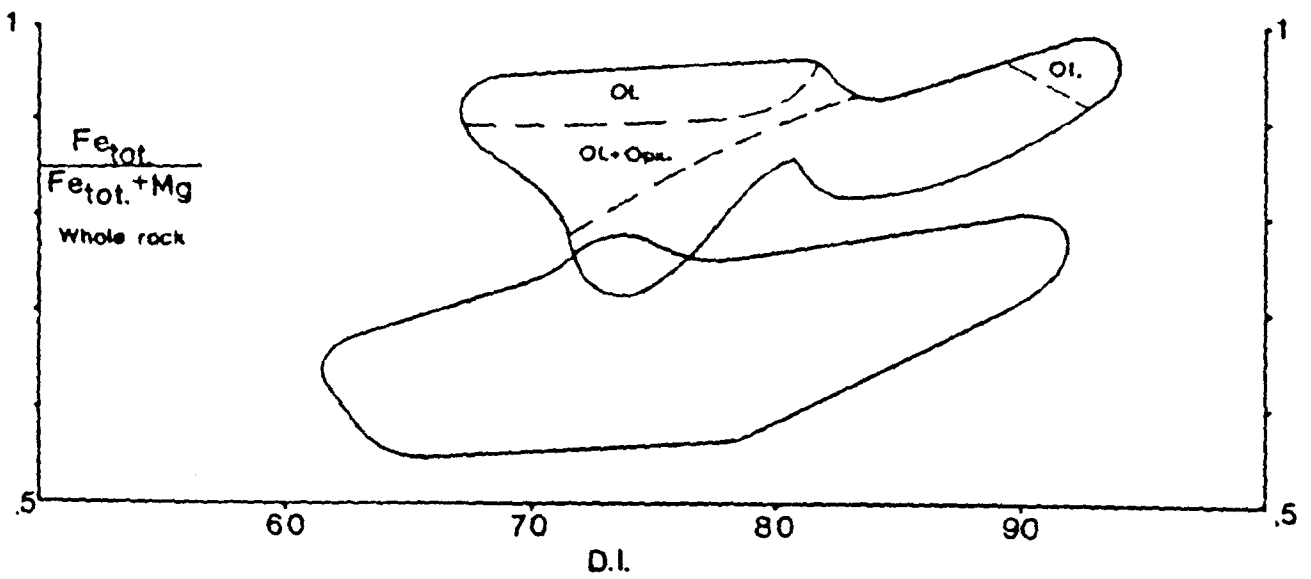


Fig. 2.5: Variation of Fe/Mg in mangerites with differentiation index (norm Ab + Q + Or), showing the occurrence of two series and the distribution of ol + cpx and ol + opx + cpx assemblages. Unlabelled fields enclose opx + cpx assemblages (after Ormaasen, 1976; Griffin et al., 1978).

Table 2.1: Compositions of Late Archaean Migmatitic Gneisses

(after Griffin et al., 1978)

	Langøy			Hinnøy			Moskenesøy			All migmatites			
	$\bar{x}$	σ	n	$\bar{x}$	σ	n	$\bar{x}$	σ	n	$\bar{x}$	σ	Range	n
SiO_2	66.1	6.3	56	61.7	6.4	40	54.8	5.6	22	62.6	7.4	48-77	116
TiO_2	0.5	0.2	"	0.7	0.3	"	1.0	0.4	"	0.6	0.4	0.03-1.9	"
Al_2O_3	15.8	1.8	"	16.2	1.7	"	18.2	1.5	"	16.4	1.9	12.0-21.9	"
$Fe_2O_3{}^t$	4.5	2.5	"	6.4	2.6	"	8.8	2.5	"	5.9	3.0	0.3-15.1	"
MnO	0.06	0.04	"	0.08	0.06	19	0.13	0.03	"	0.08	0.05	0.01-0.21	93
MgO	2.0	1.4	"	2.6	1.5	40	3.5	1.6	"	2.5	1.6	0.2-7.7	116
CaO	3.2	1.8	"	3.3	1.7	"	6.0	1.8	"	3.7	2.0	0.8-10.0	"
Na_2O	4.0	0.7	"	4.2	0.8	"	4.5	0.6	"	3.9	1.1	2.6-6.2	"
K_2O	3.3	1.8	"	3.2	1.4	"	2.7	0.9	"	3.2	1.6	0.4-8.2	"
P_2O_5	0.14	0.12	"	0.25	0.24	27	0.5	0.2	21	0.2	0.2	0-1.0	102
Rb	71	40	54	157	61	24	50	23	22	93	71	5-427	100
Sr	411	176	"	334	95	"	921	235	"	500	284	75-1340	"
U	1.0	1.7	37	0.7	0.4	"				0.9	1.3	0-9.7	65
Th	8.3	10.2	"	12.2	8.3	"				9.4	9.6	0-49.6	"
$\overline{K/Rb}$	537	321	54	216	91	"	541	333	"	464	318	115-1767	97
$\overline{Rb/Sr}$	0.24	0.23	"	0.58	0.60	"	0.08	0.11	"	0.29	0.38-	0.01-3.26	"

Table 2.2: Compositions of Early Proterozoic Supracrustal Gneisses
(after Griffin et al., 1978)

	Langøy			Austvågøy			Moskenesøy			All samples			
	$\bar{x}$	σ	n	$\bar{x}$	σ	n	$\bar{x}$	σ	n	$\bar{x}$	σ	Range	n
SiO_2	58.7	6.8	29	63.4	9.9	29	50.7	4.6	13	58.2	9.0	45-76	81
TiO_2	0.9	0.5	"	0.9	0.7	"	0.8	0.2	"	0.9	0.5	0.2-2.7	"
Al_2O_3	16.3	1.3	"	14.2	1.7	"	18.5	1.0	"	15.8	2.1	11.7-20.0	"
$Fe_2O_3^t$	7.8	3.4	"	6.9	4.8	"	10.2	2.1	"	8.4	4.1	1.0-18.8	"
MnO	0.10	0.06	22	0.09	0.08	26	0.15	0.03	"	0.10	0.06	0.02-0.27	89
MgO	3.2	1.7	29	1.9	2.1	29	5.2	1.7	"	3.4	2.4	0.2-8.6	81
CaO	4.6	2.4	"	3.0	2.5	"	8.1	1.6	"	5.1	3.3	0.6-15.9	"
Na_2O	4.5	0.9	"	4.4	1.3	"	4.1	0.6	"	4.3	1.0	1.9-6.5	"
K_2O	3.1	1.5	"	3.9	1.9	"	1.4	0.9	"	3.6	2.0	0.1-6.7	"
P_2O_5	0.4	0.4	28	0.4	0.3	15	0.4	0.4	"	0.4	0.3	0-1.9	63
Rb	76	75	16	75	43	19	19	30	"	60	58	2-236	48
Sr	441	279	"	265	197	"	928	110	"	503	342	44-1116	"
U	0.6	0.6	9							0.5	0.5	0-1.9	15
Th	5.5	5.9	"							5.1	6.0	0-16.4	"
$\overline{K/Rb}$	565	546	16	759	582	"	2086	2426	"	1059	1457	88-8837	48
$\overline{Rb/Sr}$	0.38	0.56	"	0.69	0.8	"	0.02	0.03	"	0.40	0.64	0.002-2.76	"

Table 2.3: Age Data on Metmorphic Rocks (after Griffin et al., 1978)

Locality	Method	Date (Ma)	Other Data	Interpretation
1. Vikan, Langøy	Pb/Pb w.r.	2685,1760	μ = 7.85	Transposed paleoisochron; protolith formation and granulite-facies metam.
3. N.W. Hinnøy	"	2685±65	μ = 7.85	Formation of migmatite protoliths
1. Vikan	Rb-Sr w.r.	2245±150	I.R.=0.7126±11	Disturb. of Rb-Sr systems during Proterozoic metam.
3. N.W. Hinnøy	"	2360±185	I.R.=0.7080±29	Proterozoic metam.
4. Langøy and Austvågøy	"	1830±35	I.R.=0.7037±5	High-grade metam.
5. Leknes, Vestvågøy	"	1140±135	I.R.=0.7052±21	Amph.-facies metam.
- Langøy	Rb-Sr bio/w.r.	930,1175	-	Retrograde metam.
6. Kvalnes, Vestvågøy	$^{40}Ar/^{39}Ar$(bio), K-Ar (bio)	1140,1144,1165	-	- " -
7. Svolvær, Austvågøy	Rb-Sr w.r. (1 sample)	1065	I.R.=0.710 (assumed)	- " -
5. Leknes	$^{40}Ar/^{39}Ar$,hbl.	460,615	-	Caledonian overprint
	- " - ,bio.	349±6,364±6	-	Caledonian resetting, uplift, cooling
8. N.W. Hinnøy	K-Ar, bio.	390±6		- " -

$^{40}Ar/^{39}Ar$ and K-Ar data by J. Sutter (Tull 1978)

TABLE 2.4: P-T Estimates for Lofoten-Vesterålen Rocks (after Griffin et al., 1978)

	Loc.	T°C	P, Kb	Method	Comments
			Magmatic crystallization		
	Raftsund, Hinnøy	1050	11 + 1	mgt/ilm oliv + opx	Krogh (1977). T estim. better than Griffin et al. (1975), P therefore higher.
	Hopen, Austvågøy	1000±25	12 + 1	mgt/ilm oliv + opx	Ormaasen (1976)
	Hamarøy	900-1075		Fe-rich subcalcic cpx	Malm (1976)
			Metamorphic conditions		
I	Langøy, Hinnøy	750-850	3-4	cord/gnt/bio	Olsen (1978)
II	S. Hinnøy	940	11±1	mgt/ilm	Krogh (1977). P=Raftsund mang.
	Langøy, Vestvågøy	950	-	mgt/ilm	Krogh (1975)
	Langøy, W. Hinnøy	850-900	8.5-10	gnt/opx, CO_2 incl.	Olsen (1978)
III	S. Hinnøy	770	9.5	cpx/opx/gnt	Krogh (1977)
	Austvågøy	750±50	10±1	cpx/opx	Ormaasen (1977). Min. conditions for fay + qtz ⟶ fs.
	Moskenesøy	770	-	cpx/opx	Ormaasen (1976)
	Langøy, W. Hinnøy	750-800	6.5-8	cpx/opx/gnt, CO_2 incl.	Olsen (1978)
IV	S. Hinnøy	630	8.5	phengite, alm/spin+qtz	Krogh (1977)
	Langøy, S. Hinnøy	625-675	9-11	gnt/bio, gnt/plag, CO_2 incl.	Olsen (1978)
V	Langøy, W. Hinnøy	550-600	5-6	gnt/pheng. gnt/bio H_2O and CO_2 incl.	Olsen (1978). 1100 m.y. event
VI	- " -	ca. 300	1-3	CO_2, H_2O incl.	Olsen (1978). Caledonian event?

Table 2.5

Average Major Element Chemistry of the Mangeritic Rocks (after Ormaasen, 1976)

	1	2	3	4	5	6	7	8	9	10
SiO_2	63.9	59.6	59.2	58.1	57.6	58.1	60.5	64.9	69.7	72.0
TiO_2	1.2	1.2	1.0	1.1	0.8	0.8	0.8	0.5	0.5	0.4
Al_2O_3	14.3	17.5	17.9	16.7	18.4	19.2	19.1	16.8	13.8	12.6
Fe_2O_3	6.6	5.9	6.0	9.3	6.8	5.4	3.8	4.5	4.7	4.3
MnO	0.1	0.1	0.1	0.2	0.1	0.1	0.1	0.1	0.1	0.1
MgO	1.6	1.4	1.7	0.7	2.4	1.5	0.8	0.37	0.25	0.09
CaO	2.9	3.6	3.9	3.4	5.2	4.6	3.5	2.0	1.2	0.9
Na_2O	3.8	5.0	4.9	4.8	5.2	5.2	5.7	5.0	4.3	4.0
K_2O	5.2	5.1	4.9	5.3	3.0	4.1	5.2	5.3	5.0	5.2
P_2O_5	0.5	0.5	0.4	0.2	0.3	0.3	0.4	0.1	0.1	0.1
Total	100.2	99.9	100.0	99.8	99.8	99.3	99.9	99.6	99.7	99.7

1. Southern Austvågøy Grey Mangerite
2. Vestvågøy Mangerite
3. Flakstadøy Mangerite
4. Raftsund Mangerite
5. Søberg Mangerite
6. Steine Mangerite
7. Northern Hovden Mangerite
8. Hopen acidic mangerite)
9. Hopen charnockite Type I) Ormaasen (1976,1977)
10. Hopen charnockite Type II)

Table 2.6: Rb-Sr whole-rock ages of intrusive rocks (after Griffin et al., 1978)

Loc.No.	Locality + Rock Type	Date (Ma)	$(^{87}Sr/^{86}Sr)_o$	Comments
9	Gullesfjord granodiorite	2715±120	0.6952±56	If I.R.=0.700, age lies near 2590 Ma
11	Sund-Ølkona mangerite	1800± 50	0.70333±58	7 points
12	Austvågøy grey mangerite	1805± 20	0.70318±32	9 points
10	Hopen mang.+charnockite	1790± 50	0.70456±72	9 points
13	Hamarøy basic mangerite	1770± 70	0.70463±78	5 points
14	SW Lofoten mangerite	1735± 25	0.70411±16	14 points
15	Lundøy mang.+orthogn.	1735± 30	0.70498±26	7 points
16	Steine mangerite, Langøy	1730± 40	0.70304±18	5 points
18	Raftsund mang., Hamarøy	1710± 60	0.70462±48	8 points
18	- " - , main body	1705± 30	0.70514±34	12 points
17	Hamarøy acid mangerite + charnockite	1695± 15	0.7034±28	10 points
19	Torset granite, Langøy	1665± 80	0.7057±36	Brueckner (1971)
20	Lødingen granite, Nes	1380± 80	0.7118±15	Anatexis?
21	Moskenesøy pegmatite	418±2 (bio) 317±3 (musc.)		K-Ar, R.M. McIntyre (unpubl.)

Rb-Sr ages based on ^{87}Rb $\lambda = 1.42 \times 10^{-11}/yr.$

Table 2.7: Sequence of Events (after Griffin et al., 1978)

1)	Form. of migmatite protoliths, metamorphism, anatexis, intrusion of Gullesfjord granitic gneiss	2700-2600 Ma
2)	Uplift and erosion	
3)	Deposition of supracrustal rocks	2100-1830 Ma
4)	High-grade metamorphism	ca. 1830 Ma
5)	Intrusion of gabbros, anorthosites, mangerites & charnockites	1800-1700 Ma
6)	Intrusion of dolerite dike swarm	
7)	Crustal anatexis at depth, intrusion of Lødingen Granite	ca. 1400 Ma
8)	Uplift and erosion	
9)	Emplacement and metamorphism of Leknes Group schists; retrograde metam. of granulite-facies rocks	ca. 1150-900 Ma
10)	Uplift and erosion	
11)	Minor Caledonian heating, intr. of pegmatites, thrust faulting	600-400 Ma
12)	Mesozoic and Tertiary uplift and erosion	

Plate 3.1. Late Archaean migmatitic gneisses, Festvåg, South-West Austvågøy; 50m west of WL549-WL562 isochron suite. Rounded palaeosome blocks up to 2 x 1.5m. Neosome volume is much smaller than palaeosome volume. The neosome may represent veins from the Hopen Mangerite/Charnockite.

Plate 3.2. Late Archaean migmatitic gneisses, Festvåg, South-West Austvågøy. More melano- and leucocratic gneisses sampled for the isochron suite, WL549-WL562.





Plate 3.3. 200m east of the road-cut from which the isochron suite, WL549-WL562, was collected and 100m south of the border between the Festvåg migmatites and the gabbroic margin to the Hopen Mangerite/Charnockite. Here, the migmatites consist of rounded, leucocratic blocks up to 0.4m across with melanocratic rims and surrounded by a leucocratic neosome. The latter intruded the palaeosome and extracted low-melting phases from the margins of the palaeosome blocks.

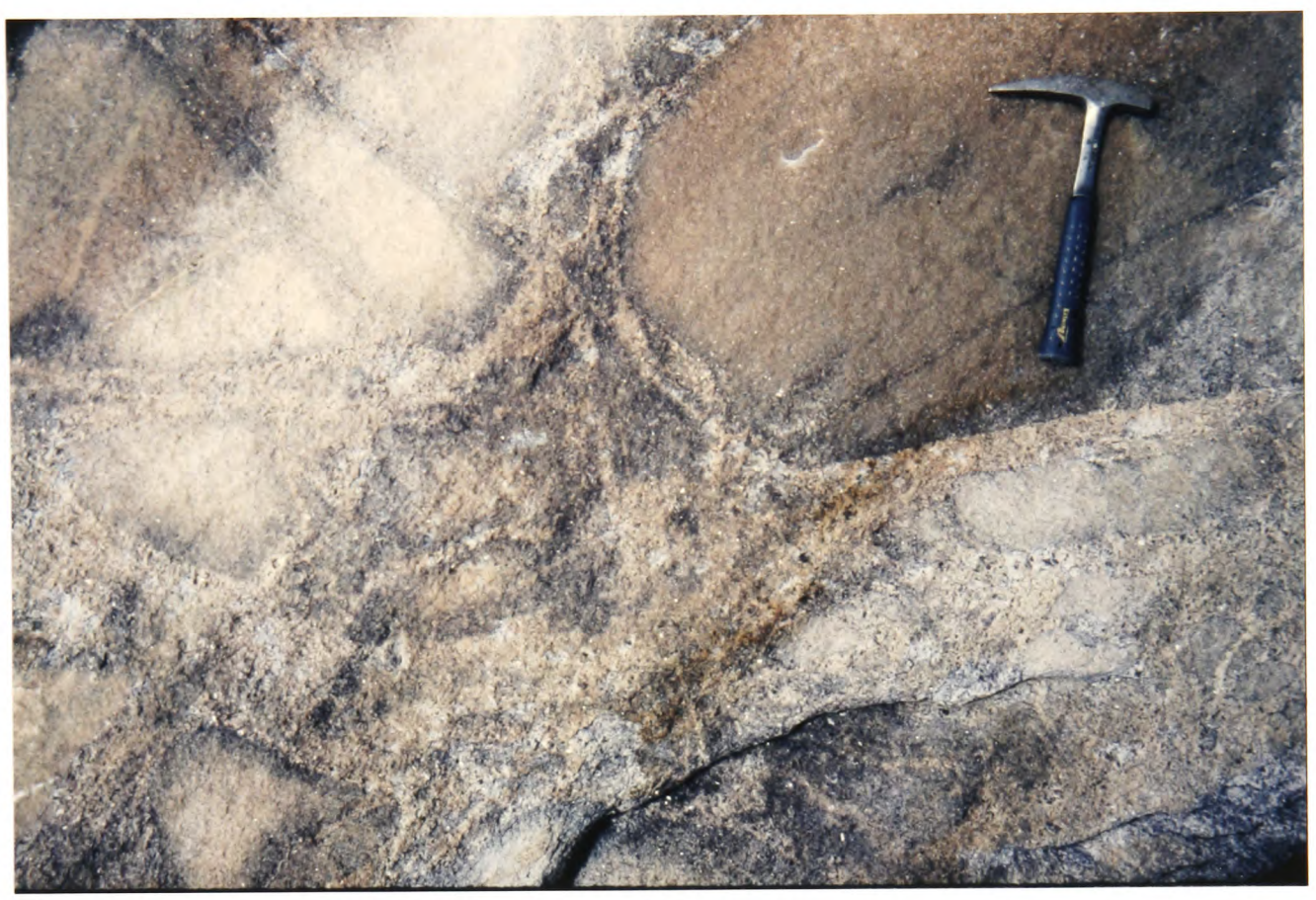


Table 3.1

Major Element Compositions and CIPW Norms of the Late Archaean Migmatites

	Moskenesøy	Austvågøy		Langøy		Hinnøy	
Sample	WL237	WL549	WL560	WL725	WL728	WL661	WL662
SiO_2	55.24	74.95	48.03	65.63	68.03	66.84	69.51
Al_2O_3	18.93	13.75	16.90	15.49	15.77	14.69	14.51
TiO_2	0.97	0.17	0.81	0.67	0.39	0.42	0.38
Fe_2O_3	7.62	1.17	10.73	4.27	3.40	5.76	3.97
MgO	2.68	0.21	7.58	1.60	1.28	2.44	2.05
CaO	5.13	0.87	9.82	2.61	2.38	2.29	2.63
Na_2O	4.94	3.78	3.66	4.34	4.33	4.27	3.89
K_2O	3.73	5.17	1.16	3.40	2.89	2.32	2.12
MnO	0.12	0.02	0.11	0.04	0.04	0.10	0.04
P_2O_5	0.43	0.02	0.13	0.16	0.08	0.13	0.10
LOI	0.22	0.30	0.43	1.57	0.67	0.71	0.59
Total	100.01	100.38	99.37	99.78	100.26	99.97	99.80
Norms calculated with $Fe^{3+}/Fe^{3+} + Fe^{2+} = 0.2$							
Q	-	31.40	-	21.98	21.79	25.09	30.71
Or	22.04	30.55	6.86	20.09	22.99	13.71	12.53
Ab	41.80	31.99	30.97	36.73	36.64	36.13	32.92
An	18.46	3.03	26.26	5.84	8.70	7.77	10.12
C	-	0.83	-	2.53	1.25	2.31	2.11
Cc	0.39	0.53	0.76	2.79	1.19	1.26	1.05
Di	2.70	-	15.85	-	-	-	-
Hy	1.29	0.86	7.30	5.04	4.27	8.35	6.49
Ol	5.58	-	16.24	-	-	-	-
Mt	1.14	0.35	3.18	1.26	1.01	1.74	1.18
Il	1.84	0.30	1.54	0.27	0.74	0.80	0.72
Ap	0.94	0.04	0.28	0.35	0.17	0.28	0.22
Plag(An_x)	45	15	62	23	31	29	37
Mg/Mg+Fe*	0.79	0.67	0.86	0.83	0.79	0.78	0.83

*for ferromagnesian minerals

Table 3.2

Sm-Nd Data for the Late Archaean Migmatites

Sample	Sm(ppm)	Nd(ppm)	$^{147}Sm/^{144}Nd$	$^{143}Nd/^{144}Nd$	T_{CHUR}(Ga)	T_{DM}(Ga)
WL237	6.900	39.130	0.1718	0.511507	1.90	2.17
WL548	3.231	20.585	0.09540	0.510653	2.94	3.06
WL560	2.305	12.874	0.10881	0.511701	1.60	1.92
WL725	2.083	13.032	0.09714	0.510933*	2.57	2.74
WL728	1.657	17.164	0.09407	0.510934	2.50	2.66
Errors (2σ)	±0.02%	±0.02%	0.10%	±0.000025	±0.04	±0.04
unless asterisked (*) and stated below						
WL725				±0.000031		

Table 3.3

Modelling of Sr Data for Sandset Gneisses, Central Langøy

Model: protoliths of the migmatites formed at 2.7Ga (from Nd data) with $(^{87}Sr/^{86}Sr)_o = 0.7013^*$. Sr isotope evolution was disturbed during the regional 1.8Ga granulite-facies metamorphism. From the measured values of $^{87}Sr/^{86}Sr$ and $^{87}Rb/^{86}Sr$, the value of $^{87}Sr/^{86}Sr$ can be calculated at 1.8Ga and subsequently $^{87}Rb/^{86}Sr$ can be calculated for the period 2.7 - 1.8 Ga. The change in $^{87}Rb/^{86}Sr$ affected by the metamorphism can be calculated.

Sample	Present Concentrations and Ratios				$\left(^{87}Rb/^{86}Sr\right)_{2.7-1.8}$	$\frac{(^{87}Rb/^{86}Sr)_{1.8-0}}{(^{87}Rb/^{86}Sr)_{2.7-1.8}}$ †
	Rb(ppm)	Sr(ppm)	$^{87}Rb/^{86}Sr$	$^{87}Sr/^{86}Sr$		
WL723	17	371	0.128	0.71089	0.48	0.27
WL724	47	369	0.369	0.72604	1.15	0.32
WL725	38	317	0.341	0.73574	1.94	0.18
WL726	12	349	0.087	0.70494	0.11	0.82
WL727	109	220	1.47	0.76619	2.04	0.72
WL728	112	290	1.14	0.75840	2.08	0.55

* assuming $^{87}Sr/^{86}Sr = 0.6990$ at 4.57Ga, and 0.7045 at present day (De Paolo and Wasserburg 1976)

† referred to as "depletion factor" in text since values <1 imply Rb-depletion

Table 3.4

Modelling of Sr Data for Festvåg Migmatites, South-West Austvågøy

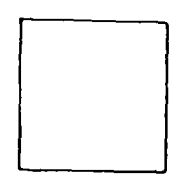
Model: as for Sandset data in Table 3.3

	Present Concentrations and Ratios					
	Rb(ppm)	Sr(ppm)	$^{87}Rb/^{86}Sr$	$^{87}Sr/^{86}Sr$	$\left(^{87}Rb/^{86}Sr\right)_{2.7-1.8}$	$\frac{(^{87}Rb/^{86}Sr)_{1.8-0}}{(^{87}Rb/^{86}Sr)_{2.7-1.8}}$
WL549	188	121	4.62	0.85912	2.89	1.60
WL550	183	184	2.96	0.82763	3.76	0.79
WL551	194	211	2.75	0.82292	3.83	0.72
WL552	179	173	3.09	0.82659	3.44	0.90
WL553	105	279	1.11	0.74691	1.28	0.86
WL554	77	606	0.369	0.72240	0.88	0.42
WL555	27	464	0.162	0.70910	0.27	0.59
WL556	60	251	0.691	0.72411	0.37	1.86
WL558	33	328	0.283	0.71059	0.15	1.87
WL559	36	359	0.283	0.71088	0.17	1.70
WL560	49	494	0.283	0.71161	0.23	1.25
WL561	100	1062	0.275	0.71288	0.34	0.81
WL562	67	245	0.807	0.76441	2.44	0.33

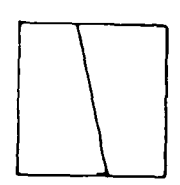
WL549-WL554 are acid; WL555-WL560 are basic; WL561-WL562 are intermediate.

A Nd model age (T_{DM} = 1.9Ga) for one of the basic samples (WL560) suggests that these samples are younger than 2.7Ga and hence the model is not applicable to them. All the remaining samples except WL549 show Rb-depletion at 1.8Ga.

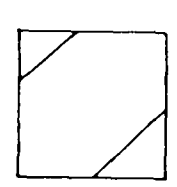
Fig. 3.1. Sample Locality Map for Moskenesøy: Late Archaean Migmatites, Ølkona Mangerite and Gabbro



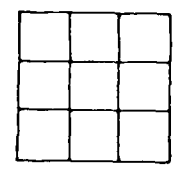
Late Archaean Migmatites



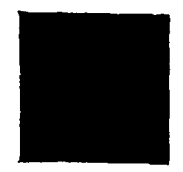
Retrograded Zone



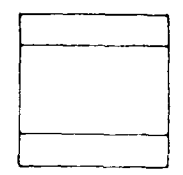
Early Proterozoic Supracrustal Gneisses



Anorthosite



Gabbro



Ølkona Mangerite

Mid-Proterozoic

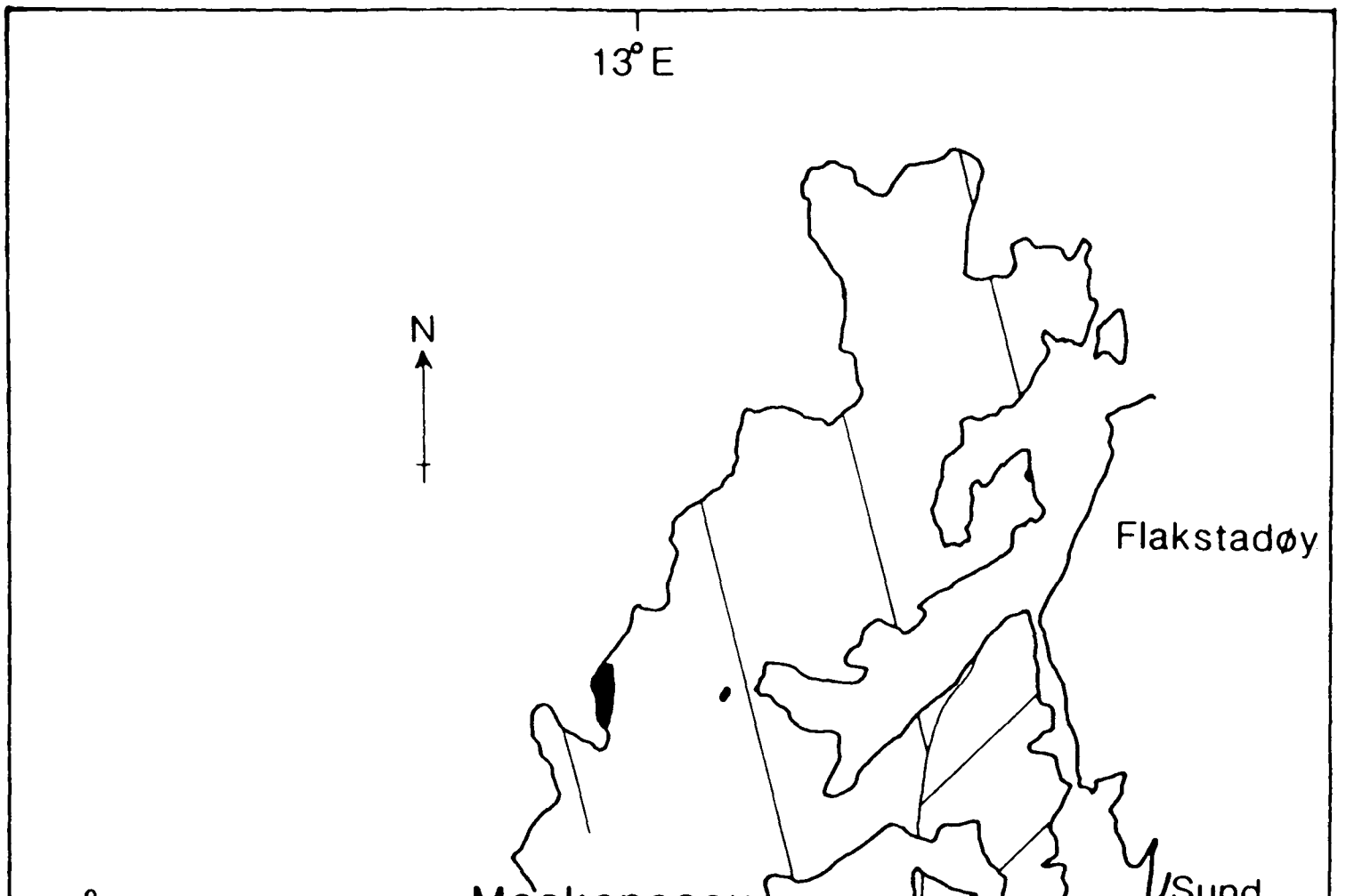
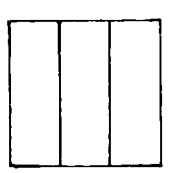
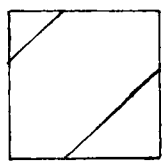

13° E
N
68° N
Flakstadøy
Moskenesoy
Sund
WL204
WL202 WL211
Ølkona WL210
WL224
Hamnøy
Reine
Djupfjord
WL237
Moskenes
Sørvågen
Å
Ånstad
Helle
0 km 5

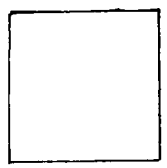
Fig. 3.2. Sample Locality Map for South-West Austvågøy: Late Archaean Migmatites



Late Archaean Migmatites



Early Proterozoic Supracrustal Gneisses



Mid-Proterozoic Mangerites

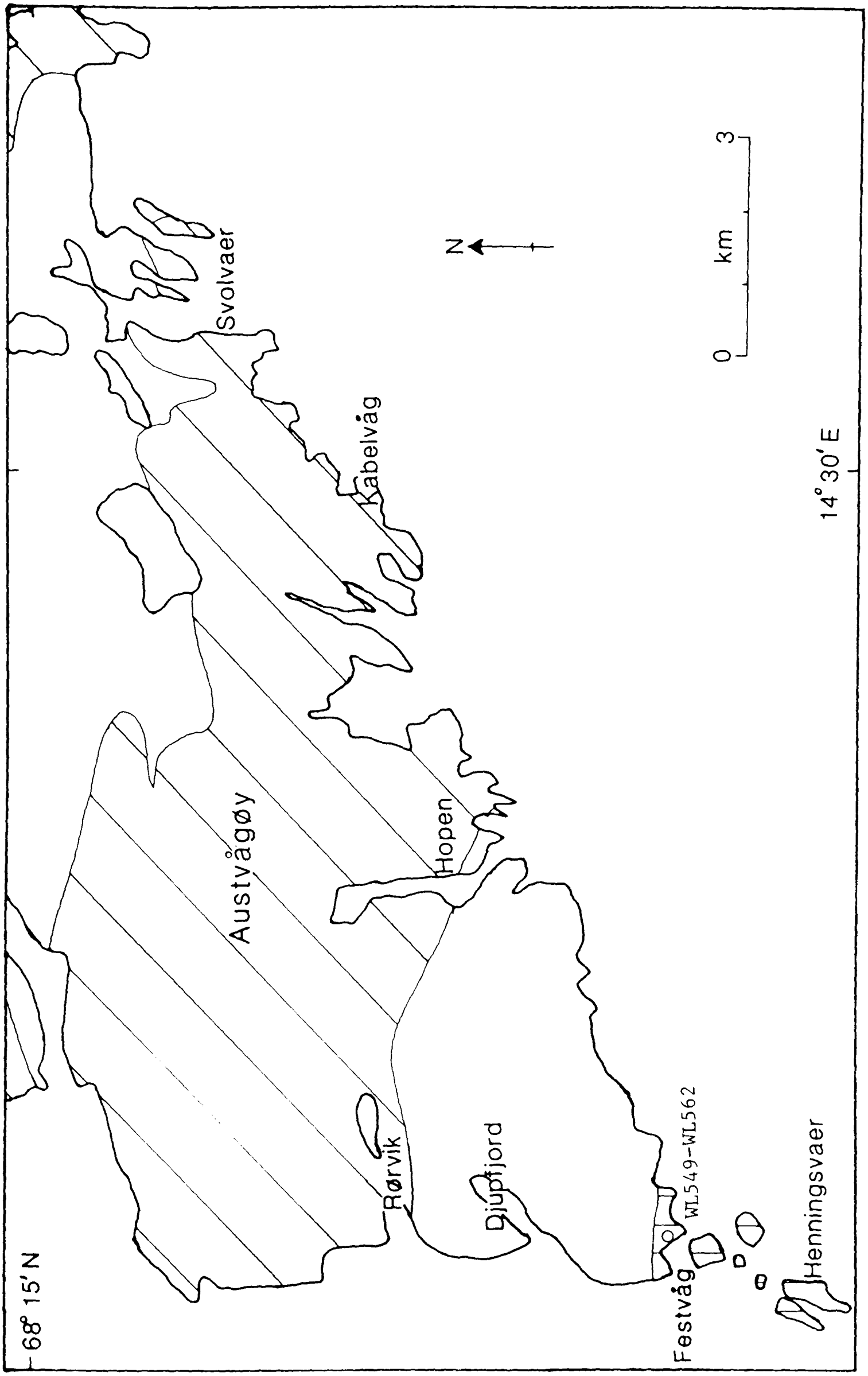
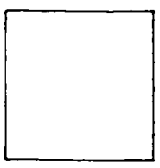
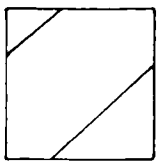

Svolvaer
Kabelvåg
Austvågøy
Hopen
Rørvik
Djupfjord
Festvåg
WL549-WL562
Henningsvaer
68° 15' N
14° 30' E
N
0
km
3

Fig. 3.3 Sample Locality Map for Langøy and North-West Hinnøy:

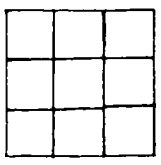
Late Archaean Migmatites



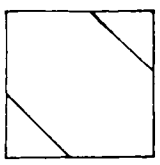
Late Archaean Migmatites



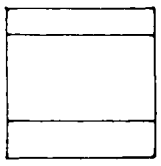
Early Proterozoic Supracrustal Gneisses



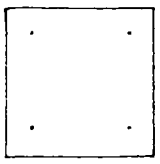
Anorthosite



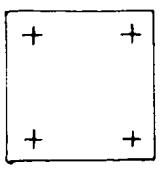
Gabbro



Mangerite



Retrograded Mangerite



Torset Granite

} Mid-Proterozoic

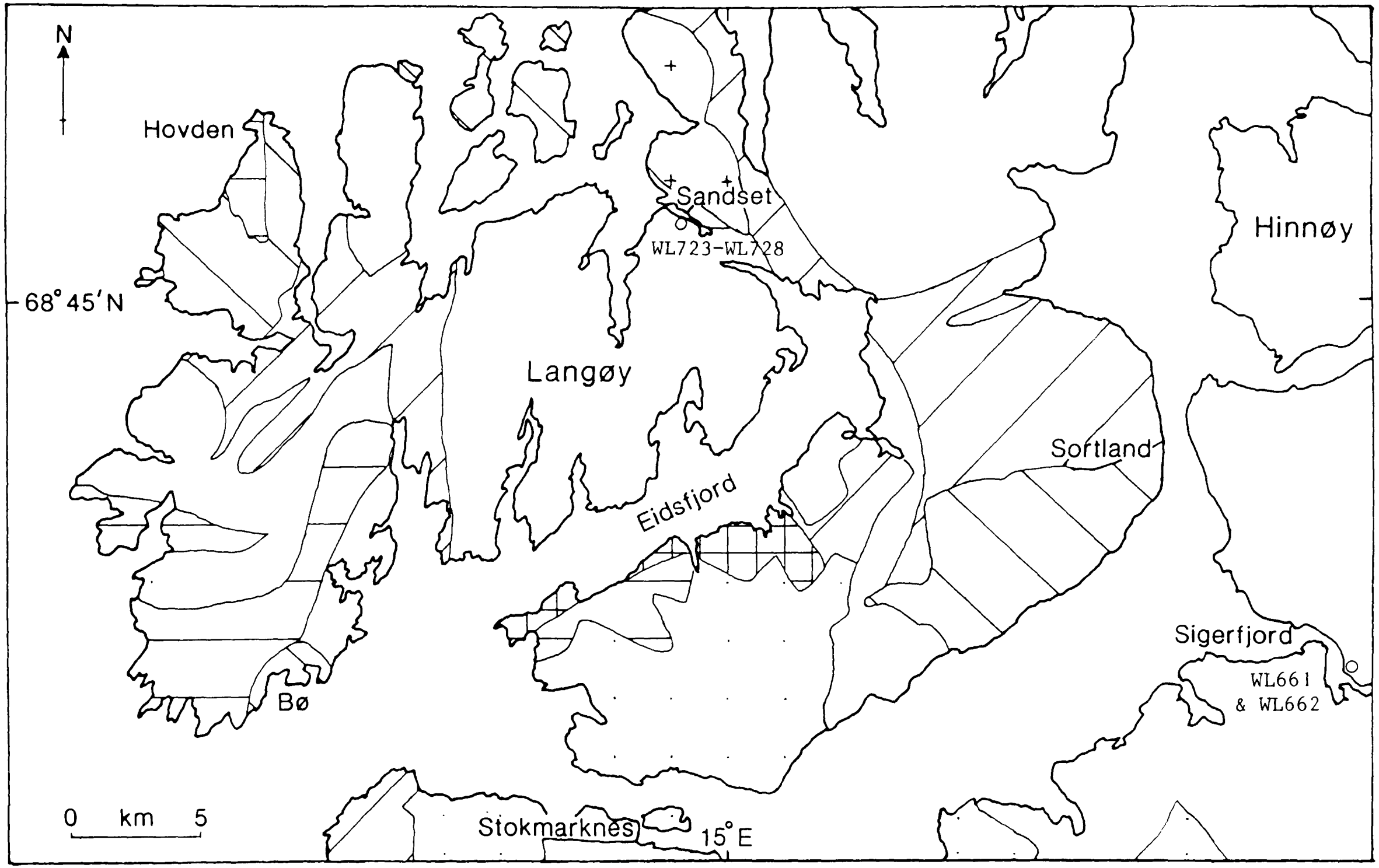

N
Hovden
Sandset
WL723-WL728
Hinnøy
68°45'N
Langøy
Sortland
Eidsfjord
Sigerfjord
WL661
& WL662
Bø
0 km 5
Stokmarknes
15°E

Fig. 3.4.

Sm-Nd evolution diagram for the Sandset Gneisses, Langøy. The two samples, WL725 and WL728, are petrographically the most different of the six samples collected from this locality (Fig. 3.3), but they have similar chemical compositions (Table 2.1) and their Sm-Nd isotopic compositions are very similar (Table 3.2). The T_{DM} model ages of both of the samples are within error of 2.7Ga, the age of formation of the protoliths of the migmatites according to Griffin et al. (1978), hence this figure confirms that the protoliths of the migmatitic gneisses of central Langøy were extracted from the depleted mantle in the late Archaean. The vertical lines define the age range 2.6 - 2.7 Ga.

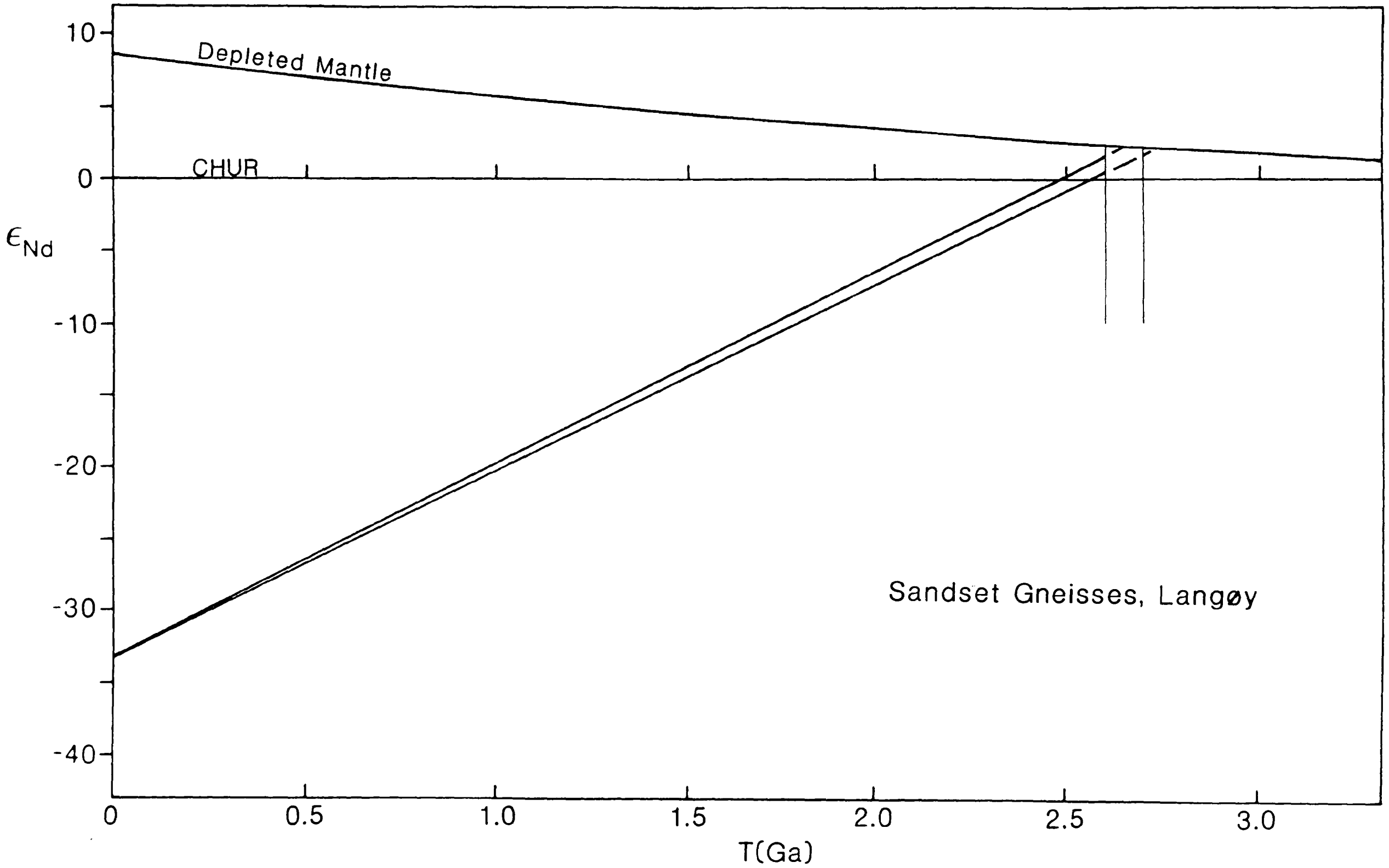

10
0
-10
-20
-30
-40
ϵ_{Nd}
Depleted Mantle
CHUR
Sandset Gneisses, Langøy
0
0.5
1.0
1.5
2.0
2.5
3.0
T(Ga)

Fig. 3.5.

Sm-Nd evolution diagram for the Festvåg Migmatites, South-West Austvågøy. At this locality (Fig. 3.2) the migmatites consist of acid and mafic components (Plate 3.2). The two samples shown in this figure reflect this bimodal chemistry (Table 4.1). The granitic sample, WL549, has a T_{DM} model age of 3.1Ga, whereas the gabbroic sample has a T_{DM} of 1.9Ga. The former confirms that a component of the migmatites on Austvågøy was extracted from the mantle in the late Archaean. The latter suggests an association of the basic components of the migmatites with the 1.8 - 1.7Ga intrusive activity. However none of the mangeritic or basic rocks analysed for this study (Chapters 5 and 6) have give- depleted mantle model ages as young as 1.9Ga. The sample could be associated with the post-mangeritic dolerite dykes, but no Nd studies have been conducted on these rocks. The vertical lines define the age range 2.6 - 2.7Ga.

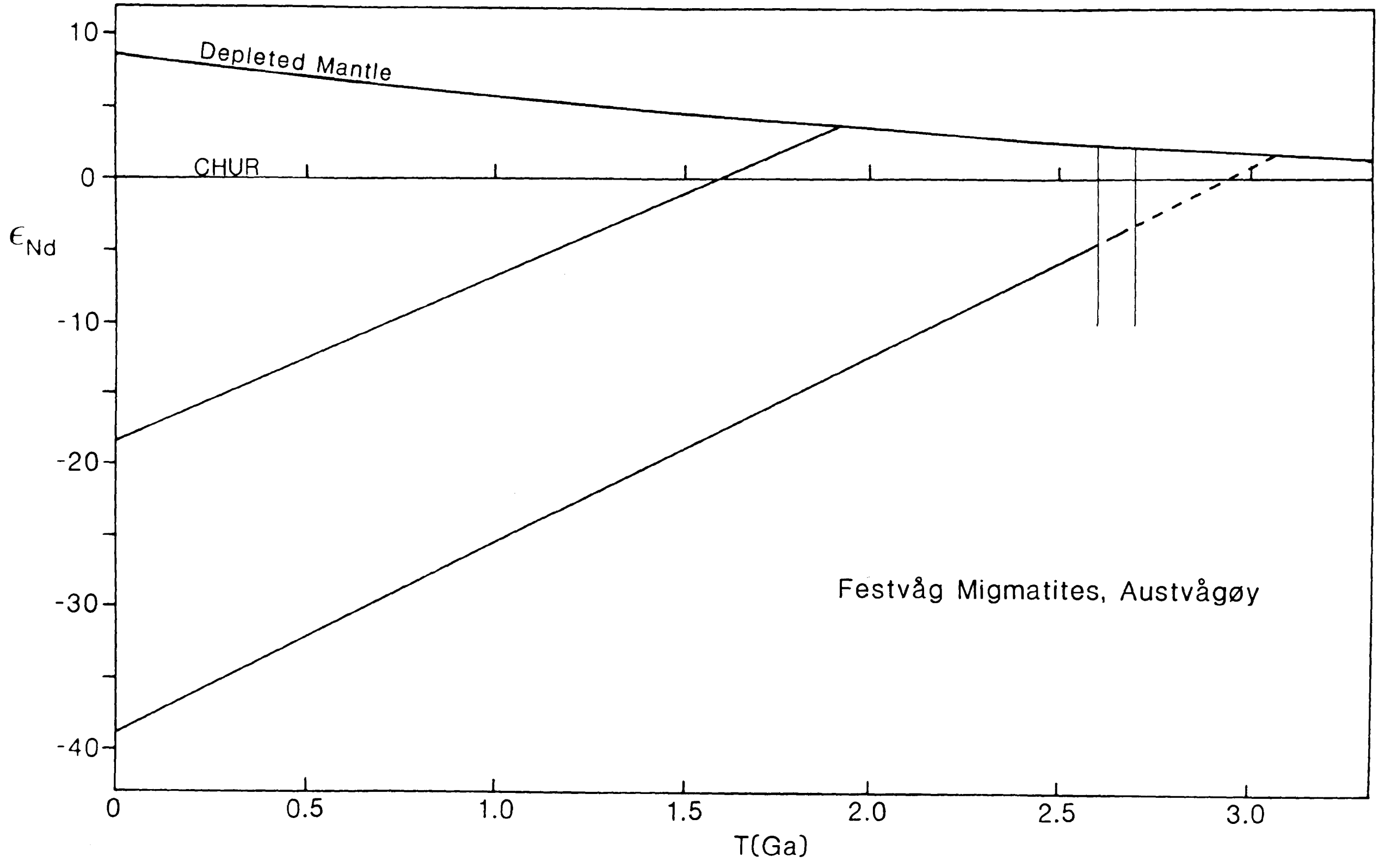

10
0
-10
-20
-30
-40
ϵ_{Nd}
Depleted Mantle
CHUR
Festvåg Migmatites, Austvågøy
0
0.5
1.0
1.5
2.0
2.5
3.0
T(Ga)

Fig. 3.6.

Sm-Nd evolution diagram for a gneiss sample, WL237, from the Moskenes Pegmatite Quarry, Moskenesøy (Fig. 3.1). It has a T_{DM} model age of 2.2Ga. Jacobsen and Wasserburg (1978) analysed a migmatite sample from Reine, Moskenesøy which also gave a significantly younger model age (T_{CHUR} = 2.0Ga) than the migmatites from Langøy and Hinnøy (T_{CHUR} = 2.6-2.7Ga). They concluded that the protoliths of the Moskenesøy migmatites are distinctly younger and not related to the Langøy and Hinnøy migmatites. This figure supports their conclusion. The vertical lines define the age range 2.6 - 2.7Ga.

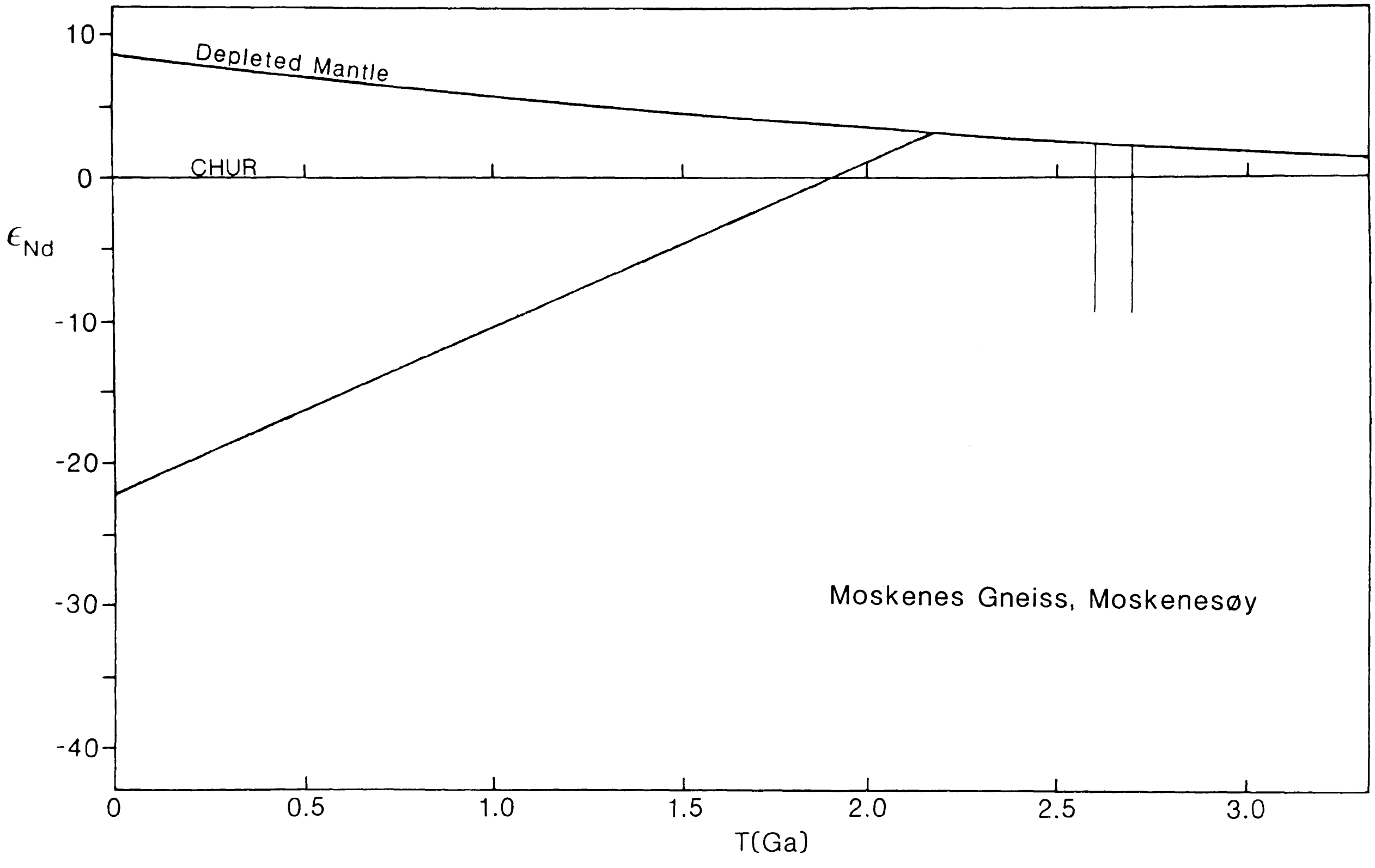

10
0
-10
-20
-30
-40
ϵ_{Nd}
Depleted Mantle
CHUR
Moskenes Gneiss, Moskenesøy
0
0.5
1.0
1.5
2.0
2.5
3.0
T(Ga)

Fig. 3.7.

Rb-Sr isochron diagram for the Sandset Gneisses, Langøy. A 2.7Ga reference isochron with initial $^{87}Sr/^{86}Sr$ of 0.7013 (assuming $^{87}Sr/^{86}Sr$ = 0.6990 at 4.57 Ga, and 0.7045 at present day (DePaolo and Wasserburg, 1976)) is shown in relation to the Rb-Sr whole-rock isotopic data for the six Sandset migmatite samples (Table 3.3). All of the data-points lie above and to the left of the 2.7Ga isochron. This distribution is best explained by Rbldepletion during the granulite-facies metamorphism at about 1.8Ga.

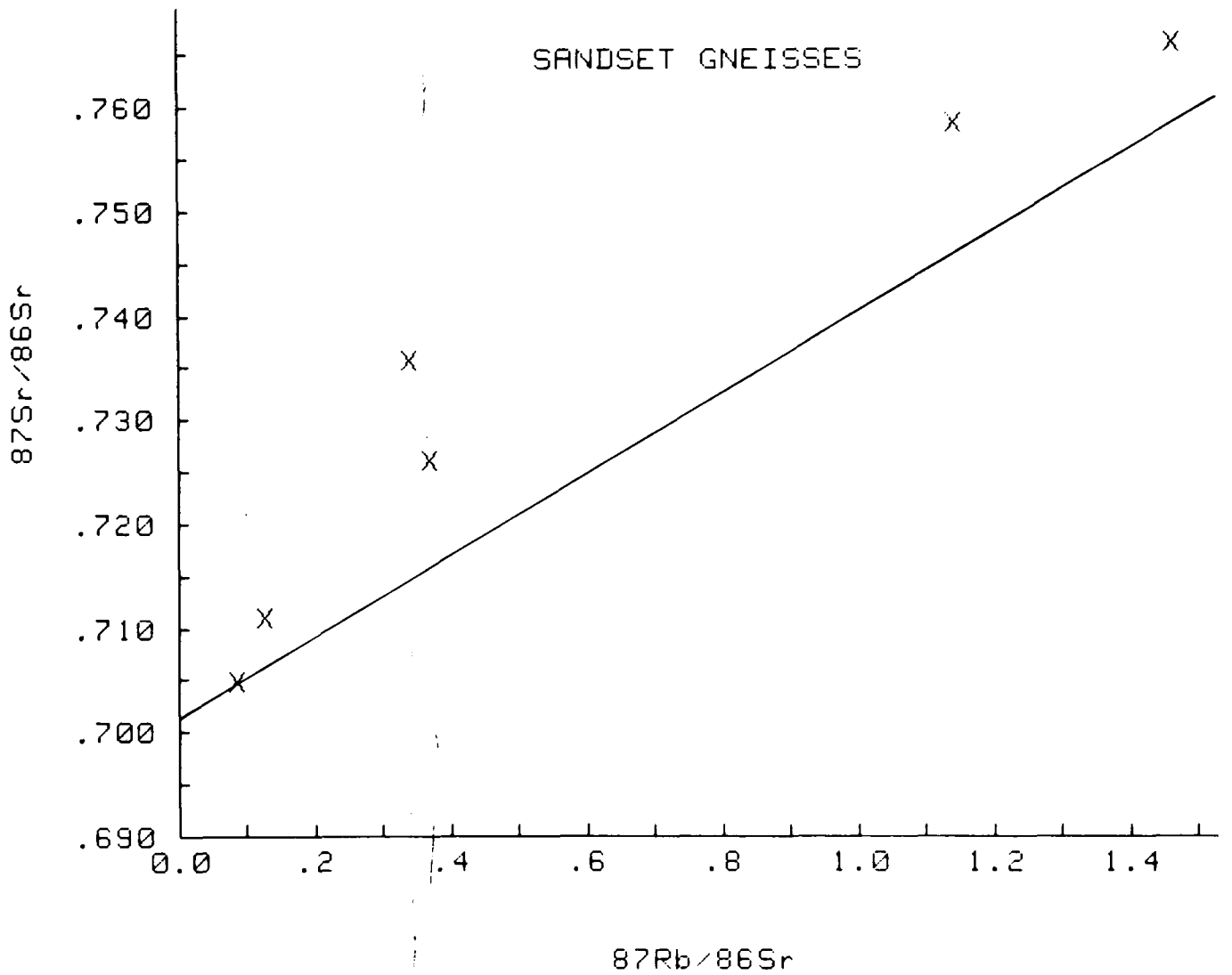

SANDSET GNEISSES
.760
.750
.740
.730
.720
.710
.700
.690
87Sr/86Sr
0.0
.2
.4
.6
.8
1.0
1.2
1.4
87Rb/86Sr

Fig. 3.8.

Rb-Sr isochron diagram for the Festvåg Migmatites, Austvågøy. A 2.7Ga reference isochron with initial $^{87}Sr/^{86}Sr$ of 0.7013 (as for Fig. 3.7) is shown in relation to the Rb-Sr whole-rock isotopic data for the thirteen Festvåg samples (Table 3.4). Most of the samples have suffered Rb-depletion at 1.8Ga. Those with apparent enrichment in radiogenic Sr are of gabbroic composition (except WL549). One of the gabbroic samples has a T_{DM} model age of 1.9Ga. A 1.8Ga reference isochron with initial $^{87}Sr/^{86}Sr$ of 0.7020 is shown compared to the gabbroic samples.

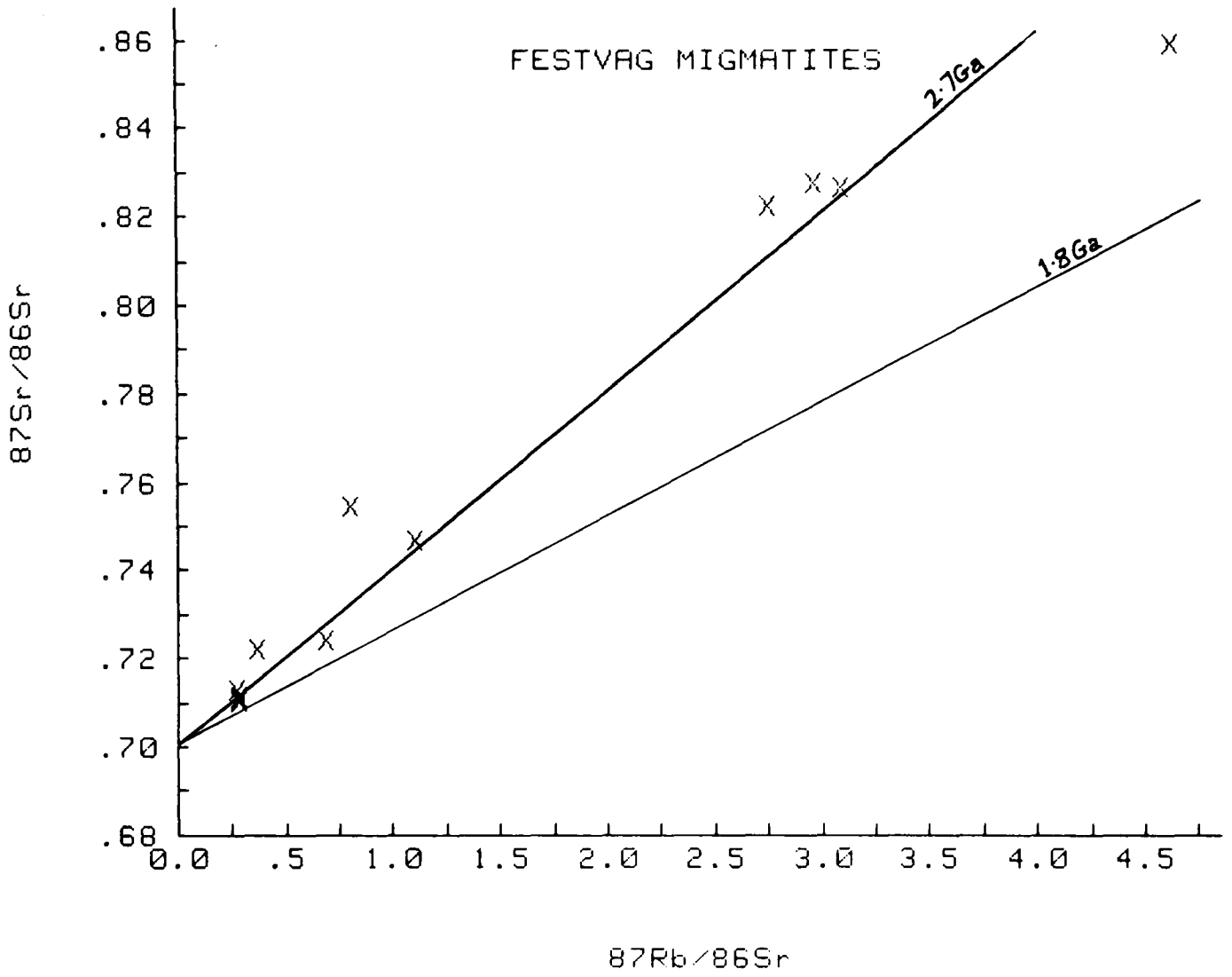

FESTVAG MIGMATITES
2·7Ga
1·8Ga
87Sr/86Sr
.86
.84
.82
.80
.78
.76
.74
.72
.70
.68
0.0
.5
1.0
1.5
2.0
2.5
3.0
3.5
4.0
4.5
87Rb/86Sr

Fig. 3.9.

Rb-Sr evolution diagram for the Sandset Gneisses, Langøy, showing how the present-day scatter of data-points on the Rb-Sr isochron diagram (Fig. 3.7) can be modelled as due to Rb depletion in the granulite-facies metamorphism at 1.8Ga. "Depletion factors" are listed in Table 3.3.

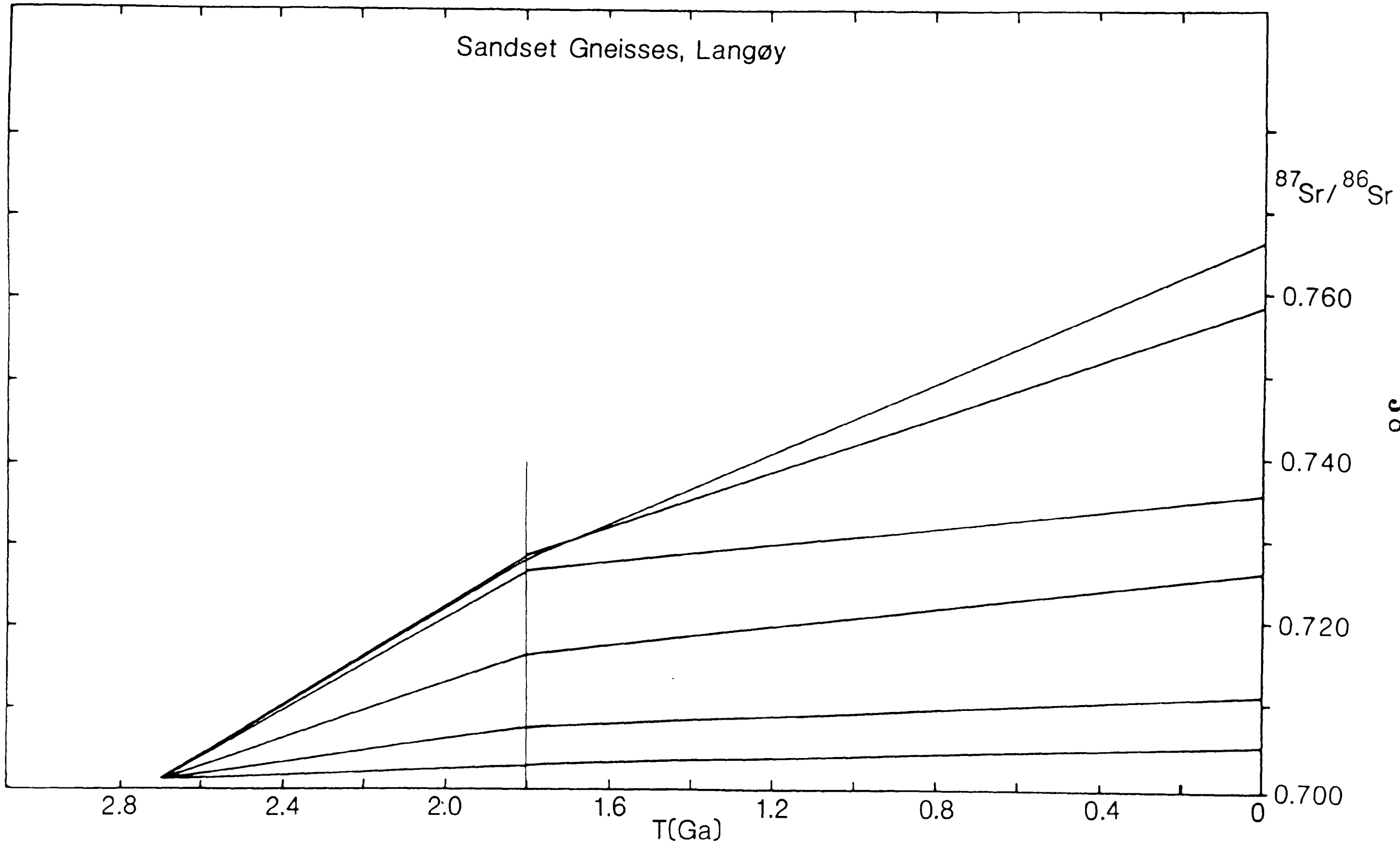

Sandset Gneisses, Langøy
$^{87}Sr/^{86}Sr$
0.760
0.740
0.720
0.700
2.8
2.4
2.0
1.6
1.2
0.8
0.4
0
T(Ga)

Fig. 3.10.

Rb-Sr evolution diagram for the Festvåg Migmatites, Austvågøy, showing how the present-day scatter of data-points on the Rb-Sr isochron diagram (Fig. 3.8) can be modelled as due to Rb-depletion in the granulite-facies metamorphism at 1.8Ga. The dashed lines are for the more basic samples from the Festvåg Migmatites for which there is evidence of formation at about 1.8Ga. Depletion factors are listed in Table 3.4.

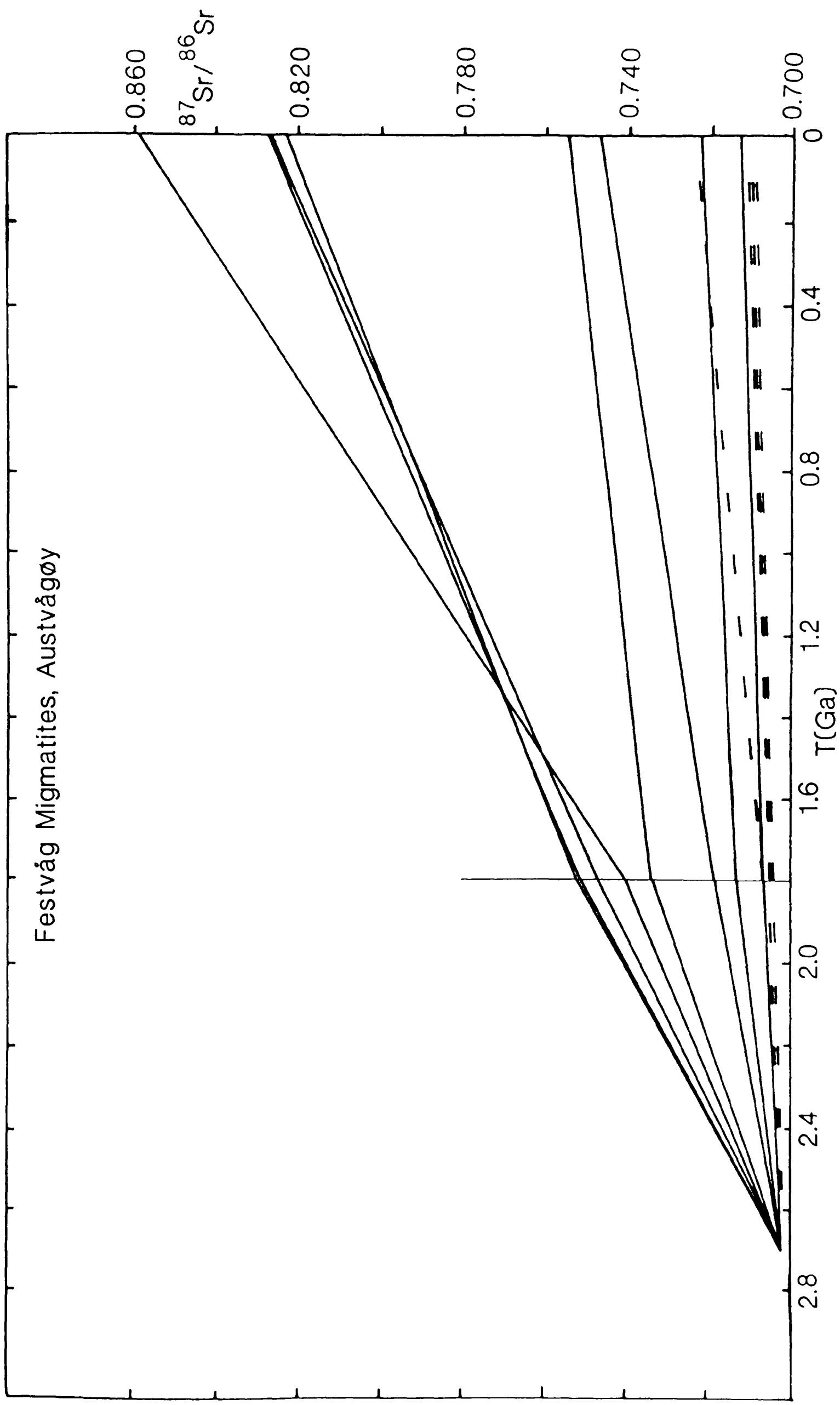

Festvåg Migmatites, Austvågøy
$^{87}Sr/^{86}Sr$
0.860
0.820
0.780
0.740
0.700
0
0.4
0.8
1.2
1.6
2.0
2.4
2.8
T(Ga)

Plate 4.1. Marble band (right) in early Proterozoic supracrustal gneisses at Ølkona. Phlogopite-rich bands at the margin of the 4m wide marble layer. Pyroxenite mantle (left) to the marble. The marble is zoned due to variations in P_{CO_2}. Mantle includes spinel-rich bands.

Plate 4.2. Diopside-rich layers in the core of the Ølkona Marble in the early Proterozoic supracrustal gneisses, broken up due to the competency contrast between the layers dominated by carbonate- and by silicate phases. Blocks of impure marble up to 25 x 12cm, with reaction rims against the less competent, more pure marble.





Plate 4.3. Boudins of competent pyroxene-rich layers in quartzo-feldspathic early Proterozoic supracrustal gneisses within 2m of the margin of the marble band at Ølkona.

Plate 4.4. Intensely defomed and broken-up early Proterozoic supracrustal gneisses at Ølkona, Moskenesøy. Melt development has occurred at this locality, represented today by leucocratic material between disrupted gneiss blocks.





Plates 4.5, and 4.6

14mm wide vein cutting quartzo-feldspathic gneisses of the early Proterozoic supracrustal sequence, and the pyroxenite mantle to the marble layer, but it is not observed cutting the marble layer itself. The vein contains rounded gneiss fragments, similar to the host gneisses. The match between opposite sides of the vein suggests that it was formed by dilatational opening. It is probably associated with the de-carbonation reactions observed in the Ølkona Marble (Table 4.1, Reaction 4.2).

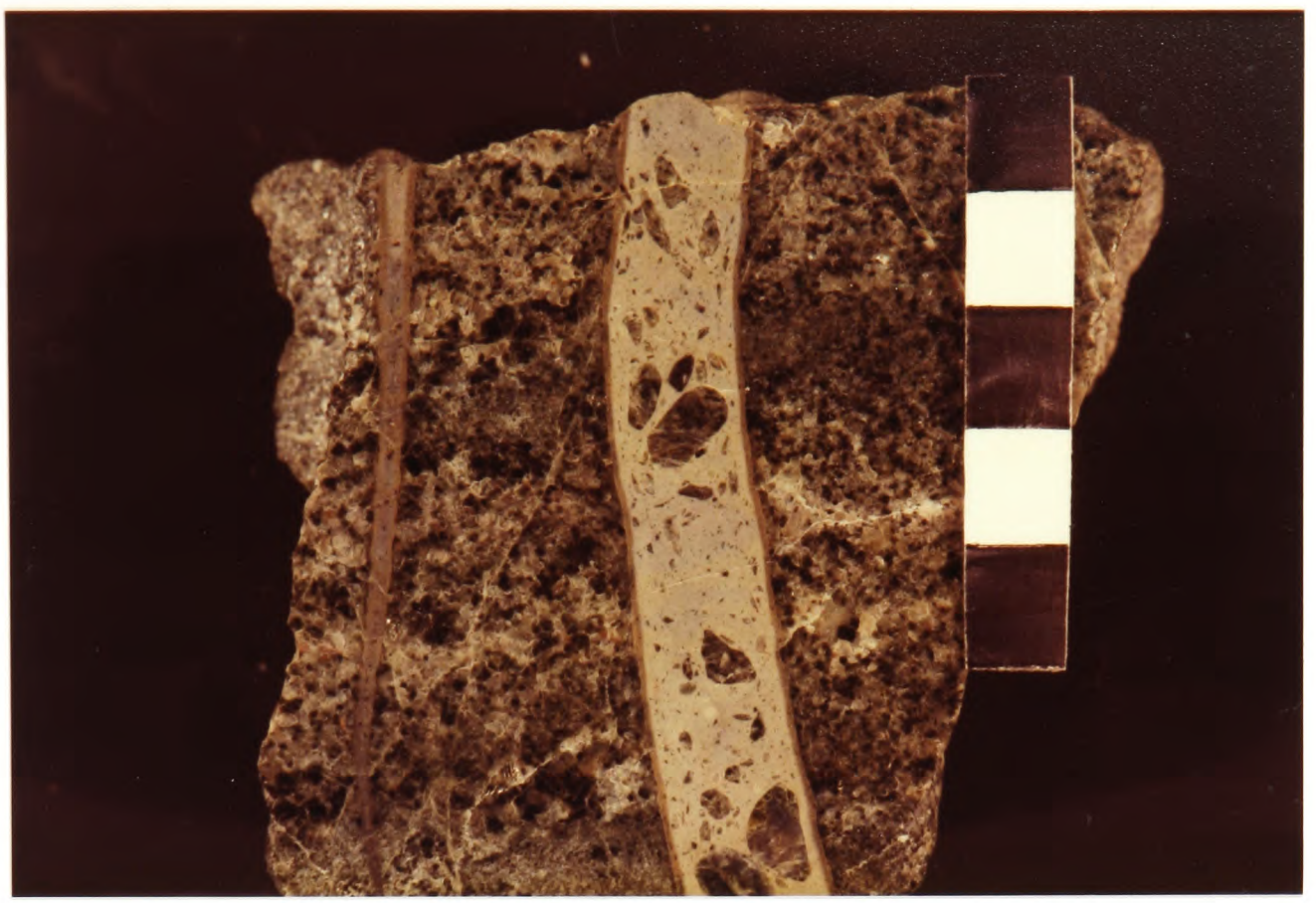




Plate 4.7. Early Proterozoic supracrustal gneisses, 1km south-west of the Ølkona Marble locality. Dark green rounded blocks of clinopyroxenite, orange-weathering monzonitic rock and white-weathering norite. The norite may be a restite after extraction of the monzonite rock as a partial melt.

Plate 4.8. Early Proterozoic supracrustal gneisses on the peninsula at the northern (Hamnøy) end of the Reine-Hamnøy bridge Moskenesøy. Coarse, granular stringers concordant to the gneiss foliation represent partial melts. The gneisses of Moskenesøy are the most basic in Lofoten-Vesterålen, probably due to the extraction of substantial volumes of partial melts.



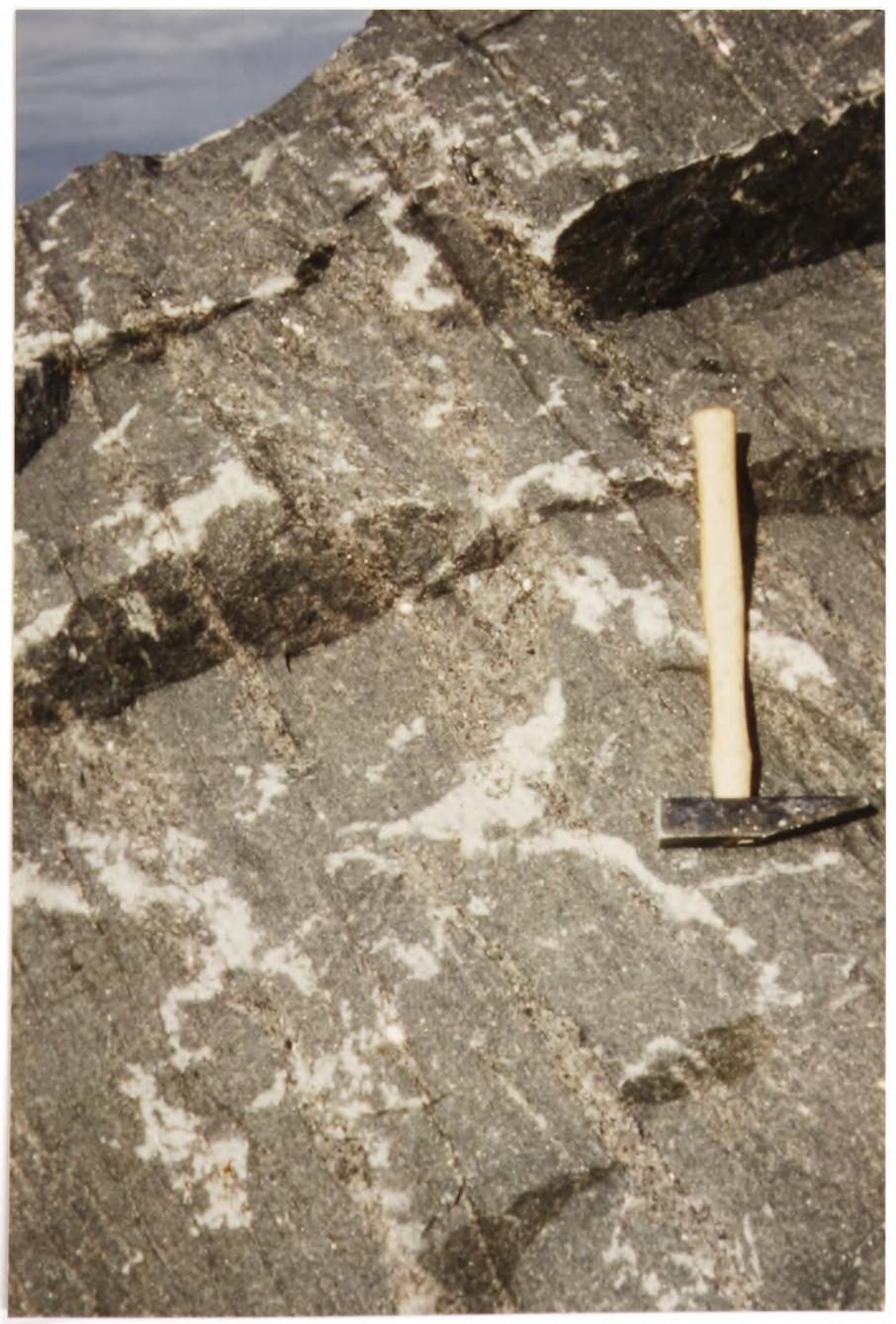


Plate 4.9. Early Proterozoic supracrustal gneisses at Hammøy, Moskenesøy, intruded by an anastomosing network of gabbroic veins. Thin veins of pinkish-grey melt are developed in the supracrustal gneisses around the gabbroic veins.

Plate 4.10. Early Proterozoic supracrustal gneisses at Hamnøy, Mosekensøy. Thin mafic veins are broken up by the development of leucocratic pinkish-grey, granular melts. This locality (illustrated in Plates 4.8 - 4.10) contains some of the best examples of in-situ anatexis in the Lofoten-Vesterålen province.



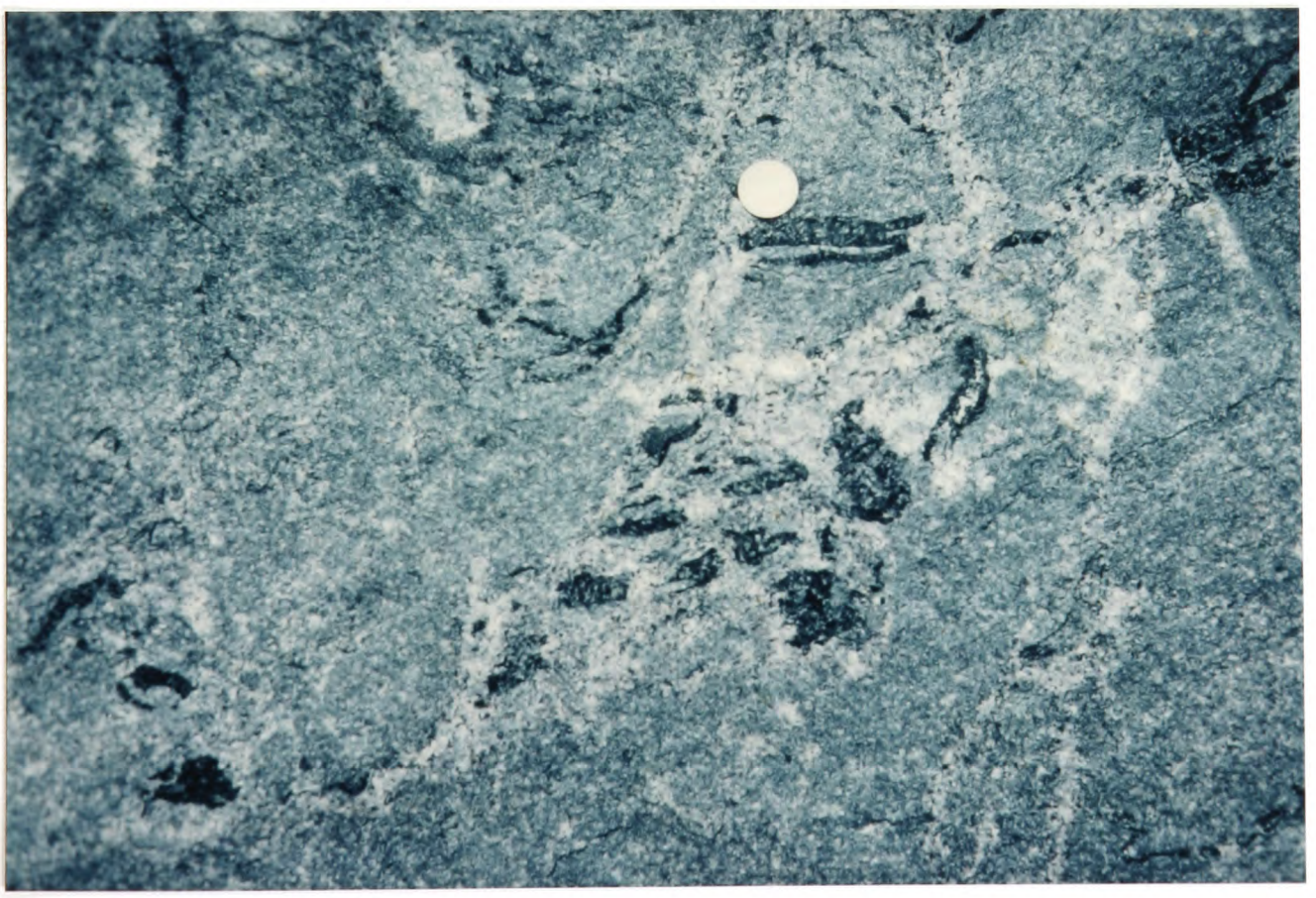


Plate 4.11. Early Proterozoic supracrustal gneisses at Vik, Vestvågøy. The isochron suite, WL427 to WL435, was collected from this locality. The gneisses are quartzo-feldspathic with a strong foliation defined by biotite and rare amphibolite layers. All the isochron samples contain epidote crystals with yellow-brown cores of allanite.

Plate 4.12. Augen gneiss from the early Proterozoic supracrustal gneisses 200m south of Ramberg Quarry, Vestvågøy. Alkali feldspar augen, up to 4cm across, have perthitic texture and contain inclusions of biotite, hornblende, opaques and quartz. Hornblende- and biotite-rich bands define the foliation and wrap around the augen.





Plate 4.13. Banded iron formation from the early Proterozoic supracrustal gneisses, Smorten, Vestvågøy. Magnetite, pyrite and bornite also occur at Smorten. These deposits have been mined for iron.

Plate 4.14. Quartzo-feldspathic gneiss from the early Proterozoic supracrustal gneisses, 6km north of Helle on the west side of Austnesfjord, Austvågøy. Plagioclase, microcline and quartz-rich layers alternate with biotite and epidote-rich layers. Sphene, pyrite, opaques, muscovite, apatite and calcite are accessory phases in this sample, WL537.



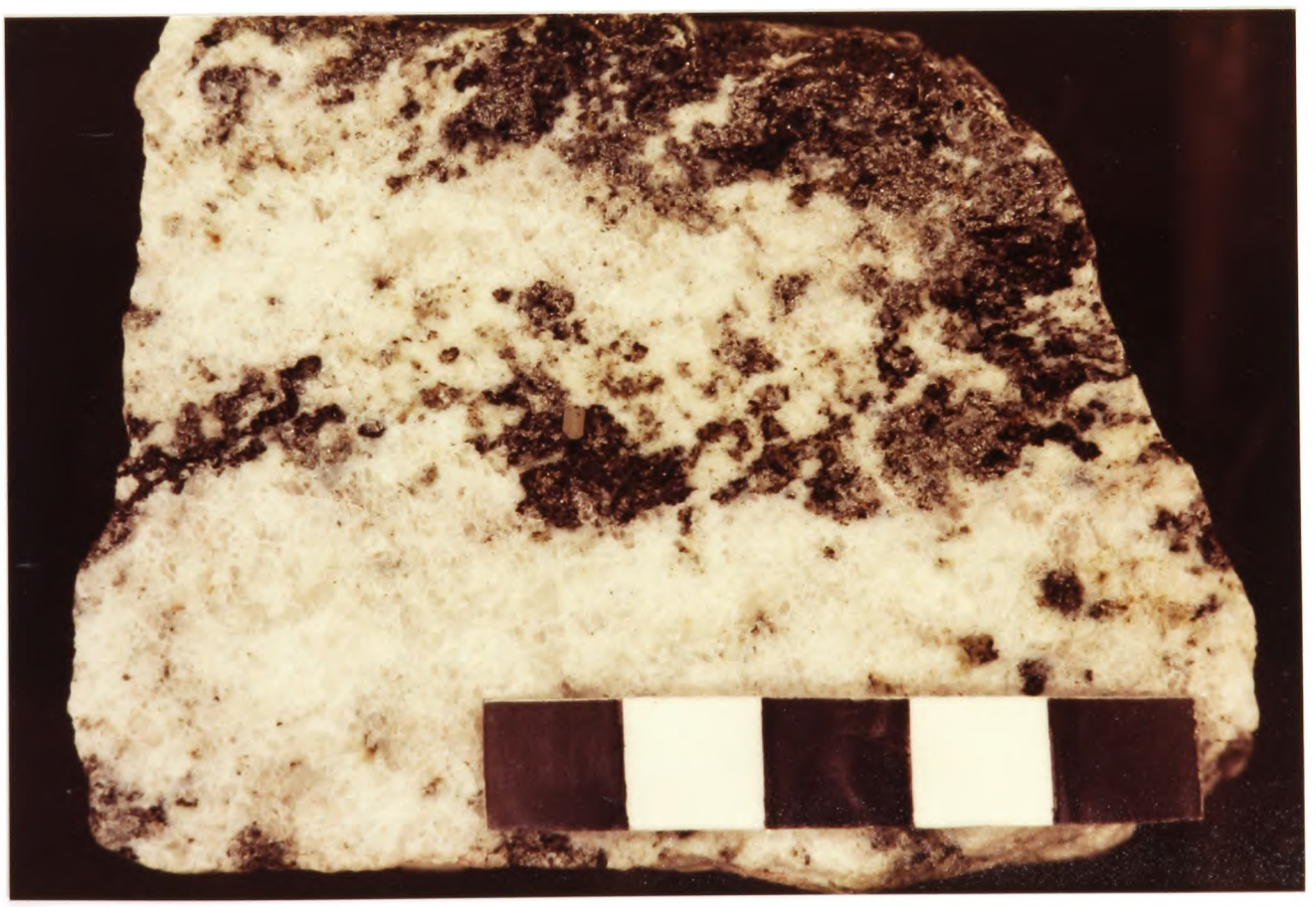
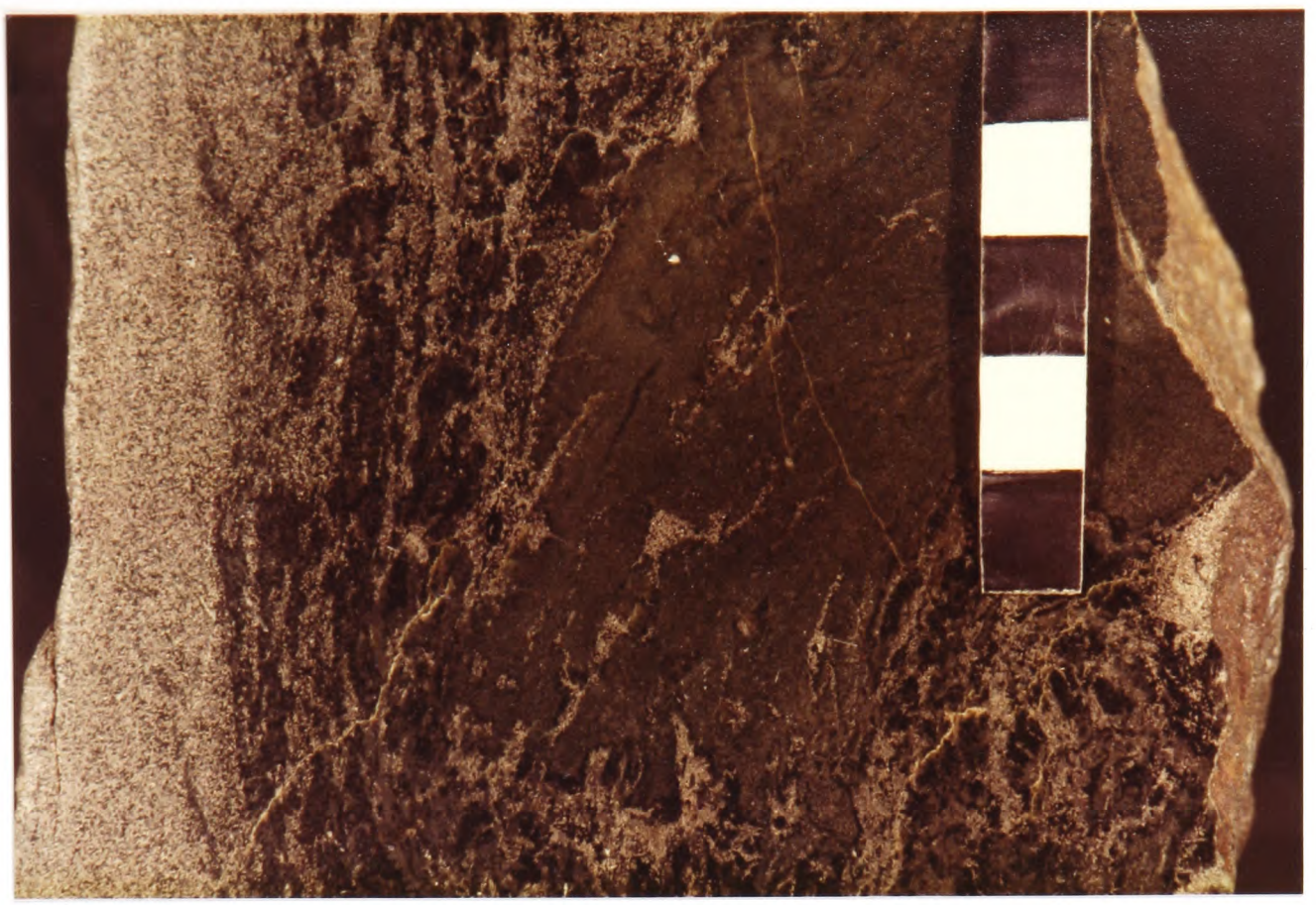


Plate 4.15. Sulphide-rich pyroxenite from an enclave of early Proterozoic supracrustal gneisses, greater than 100m long, in the Lødingen Granite, near Erikstad.

Plate 4.16. Banded iron formation from the early Proterozoic supracrustal gneisses, about 100m from the sulphide-bearing pyroxenite illustrated in Plate 4.15, within the same enclave in the Lødingen Granite, near Erikstad. It consists of hedenbergite- and grunerite-rich layers.



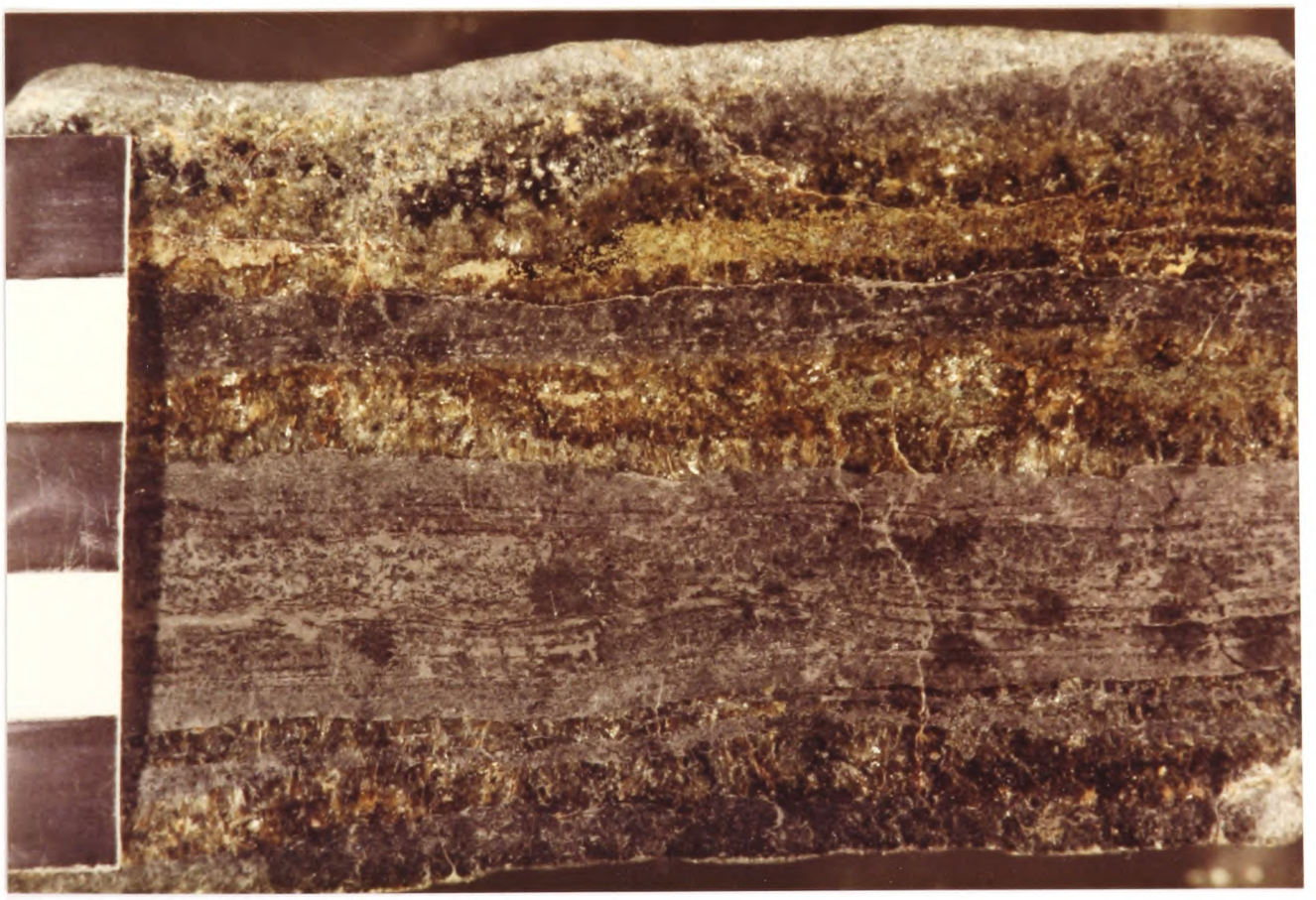


Table 4.1

Parageneses of the Ølkona Marble Samples

WL215:	cc - di - ch p phl	Margin
WL223:	cc - fo - phl	Margin
WL240:	cc - fo - di - do - ch - phl	Core
WL241:	cc - fo - do - phl - di - ch - ore	Core

cc = calcite; do = dolomite; fo = forsterite; di = diopside; phl = phlogopite; ch = chondrodite; ore = opaque. (Calcite - dolomite determined by staining (Dickson, 1965)).

The occurrence of diopside-dolomite as a mineral pair in the core of the mantle but not in the margin is similar to the marbles in Glassley's (1975) eastern province, but they also contained pargasitic hornblende; at Ølkona, chondrodite is present in the core of the carbonate (and in one of the marginal samples). Diopside overgrows forsterite in WL240.

$$CaMgSi_2O_6 + 3CaMg(CO_3)_2 \rightarrow 2Mg_2SiO_4 + 4CaCO_3 + 2CO_2$$

diopside dolomite forsterite calcite

Reaction 4.1

The presence of diopside-dolomite in the core of the marble demonstrates that the vapour phase had a higher partial pressure of CO_2 in the core of the marble than at its margins, as for some of the marbles analysed by Glassley (1975).

The formation of diopside around forsterite in which chondrodite is also formed, is a hydration reaction:

$$CaCO_3 + 6Mg_2SiO_4 + 2H_2O \rightarrow 2Mg_5(SiO_4)_2\,(OH_2) + CaMgSi_2O_6 + CO_2$$

calcite forsterite chondrodite diopside

Reaction 4.2

This takes place with decreasing T and/or P_{CO_2}. Internal buffering by CO_2 across the zoned carbonate from the core to the margin is likely to have controlled the reaction, i.e. P_{CO_2} decreased across the width of the marble, probably with accompanying increase in P_{H_2O}. In WL215, at the margin of the marble, the reaction has gone to completion: forsterite is absent. Rice (1980) has shown that the stability field of clinohumite (or chondrodite) increases with increasing mole fraction of fluorine in the clinohumite (Fig. 4.4). This diagram also shows that tremolite is present at $T < 600^{o}C$ for a wide range of X_{CO_2}, so the Ølkona Marble crystallized at $T > 600^{o}C$. Reaction 4.2 is also shown in this diagram, occurring at low X_{CO_2} and at $T > 650^{o}C$. This figure is for the $CaO-MgO-SiO_2-CO_2-H_2O$-HF system at 2kb. In Lofoten-Vesterålen, pressures reached 9-12kb at which pressures the temperatures of the above reactions would be rather higher.

Table 4.2

Major Element Compositions and CIPW Norms of Early Proterozoic Supracrustal Rocks

	Flakstadøy	Vestvågøy	
	WL339	WL428	WL432
SiO_2	52.90	74.76	75.52
Al_2O_3	19.35	13.60	13.17
TiO_2	0.62	0.13	0.12
Fe_2O_3	8.69	1.06	0.95
MgO	4.38	0.15	0.06
CaO	6.85	0.78	0.75
Na_2O	4.93	3.92	3.51
K_2O	0.81	5.22	5.46
MnO	0.14	0.04	0.03
P_2O_5	0.26	0.01	0.00
LOI	0.08	0.29	0.26
Total	99.00	99.96	99.83
Norms calculated with $Fe^{3+}/Fe^{3+} + Fe^{2+} = 0.2$			
Q	0.01	30.43	32.80
Or	4.79	30.85	32.27
Ab	41.72	33.17	29.70
An	28.28	2.69	2.72
C	-	0.52	0.49
Cc	0.14	0.52	0.46
Di	2.96	-	-
Hy	12.93	0.73	0.46
Ol	-	-	-
Mt	2.61	0.33	0.30
Il	1.18	0.25	0.23
Ap	0.57	0.02	-
Plag(An_x)	56	13	15
Mg/Mg+Fe*	0.81	0.58	0.39

*for ferromangesian minerals

Table 4.3

Sm-Nd Data for the Early Proterozoic Supracrustal Rocks

Sample	Sm(ppm)	Nd(ppm)	$^{147}Sm/^{144}Nd$	$^{143}Nd/^{144}Nd$	T_{CHUR}(Ga)	T_{DM}(Ga)
WL339	3.386	17.351	0.11861	0.511566	2.06	2.34
WL428	3.113	29.480	0.06419	0.510979	1.89	2.08
WL432	2.117	17.966	0.07160	0.511051	1.91	2.11
Errors (2σ)	±0.02%	±0.02%	±0.10%	±0.000025	±0.04	±0.04

Table 4.4

Modelling of Sr Data for Vik Gneisses, West Vestvågøy

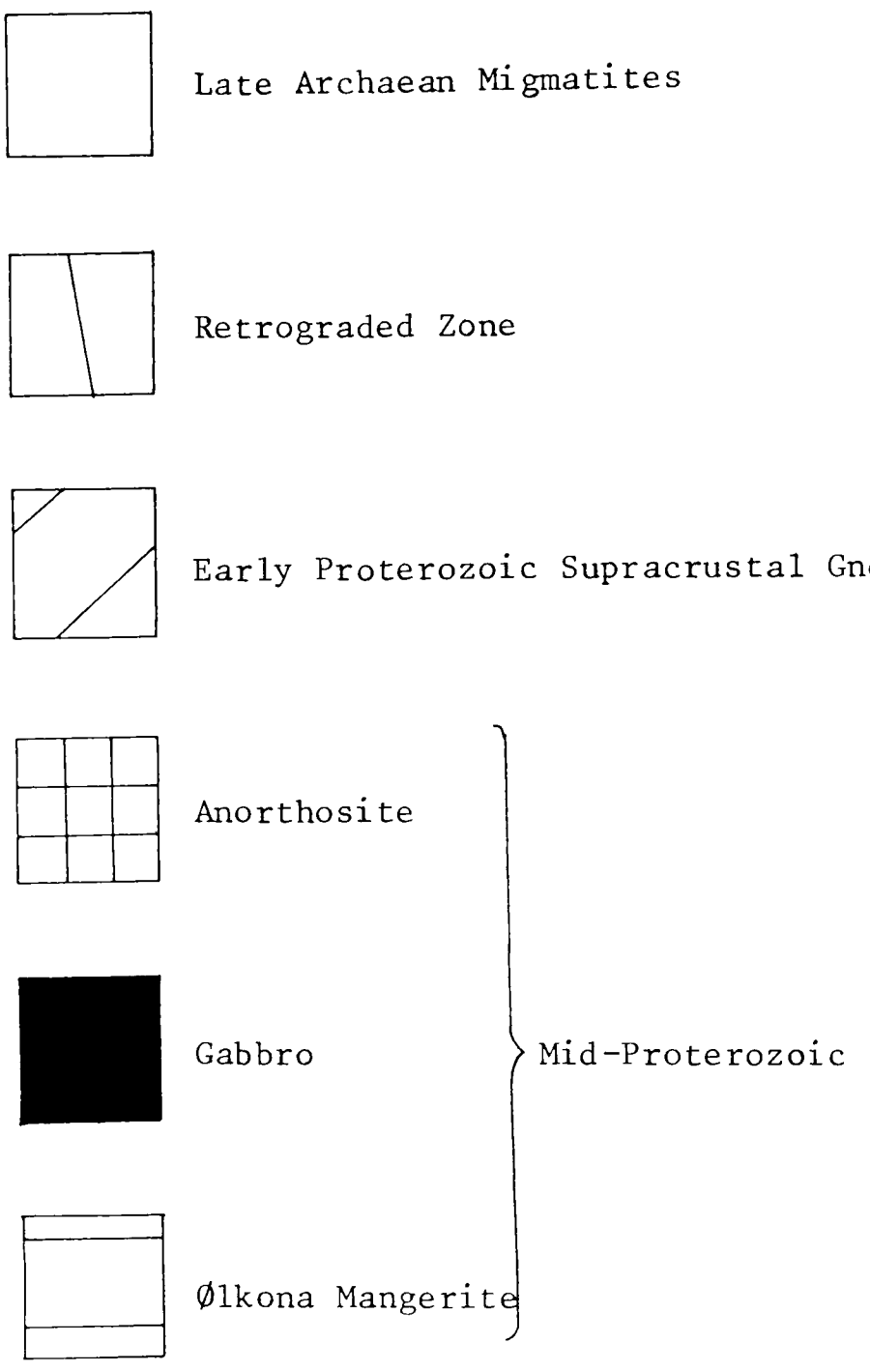
Model: supracrustal rocks formed at 2.1 Ga (from Nd data) with $(^{87}Sr/^{86}Sr)_o = 0.7020^*$. Sr isotope evolution was disturbed during the 1.1 Ga retrograde metamorphism. From the measured values of $^{87}Sr/^{86}Sr$ and $^{87}Rb/^{86}Sr$, the value of $^{87}Sr/^{86}Sr$ can be calculated at 1.1 Ga and subsequently $^{87}Rb/^{86}Sr$ can be calculated for the period 2.1 - 1.1 Ga. The change in $^{87}Rb/^{86}Sr$ effected by the metamorphism can be calculated.

Sample	Present Concentrations and Ratios				$\left(^{87}Rb/^{86}Sr\right)_{2.1-1.1}$	$\frac{(^{87}Rb/^{86}Sr)^{1.1-0}}{(^{87}Rb/^{86}Sr)_{2.1-1.1}}$ †
	Rb(ppm)	Sr(ppm)	$^{87}Rb/^{86}Sr$	$^{87}Sr/^{86}Sr$		
WL427	122	169	2.14	0.75782	1.54	1.39
WL428	135	160	2.49	0.77052	2.03	1.22
WL429	125	203	1.81	0.74630	1.10	1.65
WL430	135	178	2.24	0.75809	1.44	1.55
WL431	143	194	2.17	0.75234	1.12	1.93
WL432	129	181	2.10	0.75438	1.33	1.58
WL433	132	156	2.50	0.77137	2.08	1.21
WL434	116	212	1.62	0.74575	1.26	1.28
WL435	81	397	0.60	0.71879	0.52	1.15

*assuming $^{87}Sr/^{86}Sr = 0.6990$ at 4.57 Ga, and 0.7045 at present day (DePaolo and Wasserburg 1976).

† referred to as "enrichment factor" in text since values >1 imply Rb-enrichment.

Fig. 4.1 Sample Locality Map for Moskenesøy: Early Proterozoic Supracrustal Gneisses



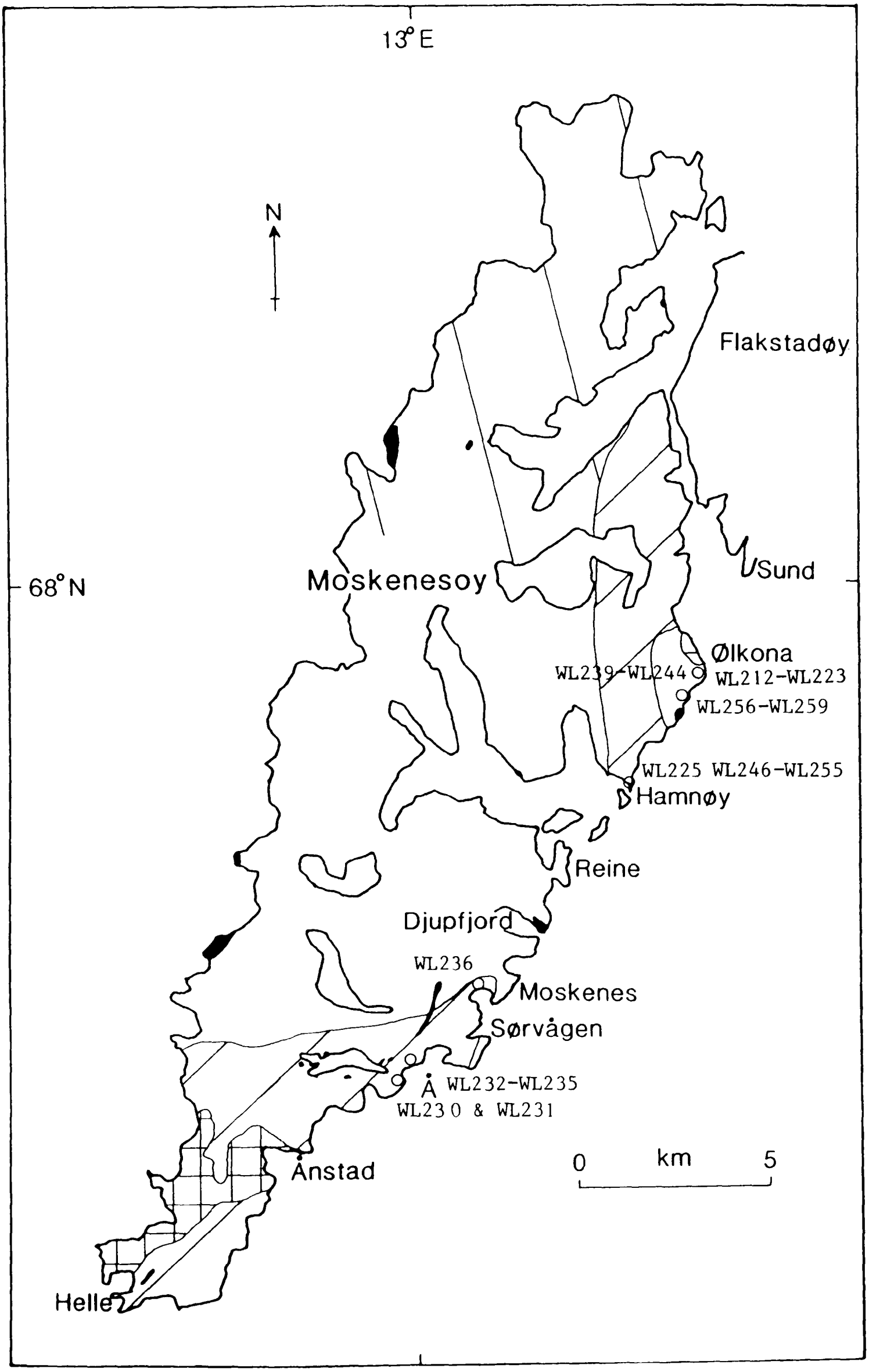
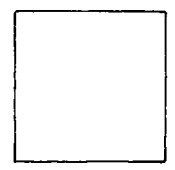
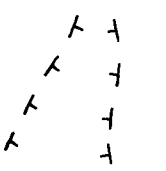

13°E
N
Flakstadøy
68°N
Moskenesoy
Sund
Ølkona
WL239-WL244
WL212-WL223
WL256-WL259
WL225 WL246-WL255
Hamnøy
Reine
Djupfjord
WL236
Moskenes
Sørvågen
Å WL232-WL235
WL230 & WL231
Ånstad
0 km 5
Helle

Fig. 4.2. Sample Locality Map for Flakstadøy and Vestvagøy: Early Proterozoic Supracrustal Gneisses



Late Archaean Migmatites

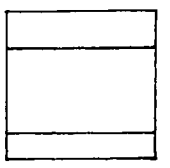


Mangerites

Early Proterozoic Supracrustal Gneisses

Retrograded Mangerites

Mid-Proterozoic Basic Intrusions



Leknes Metasediments

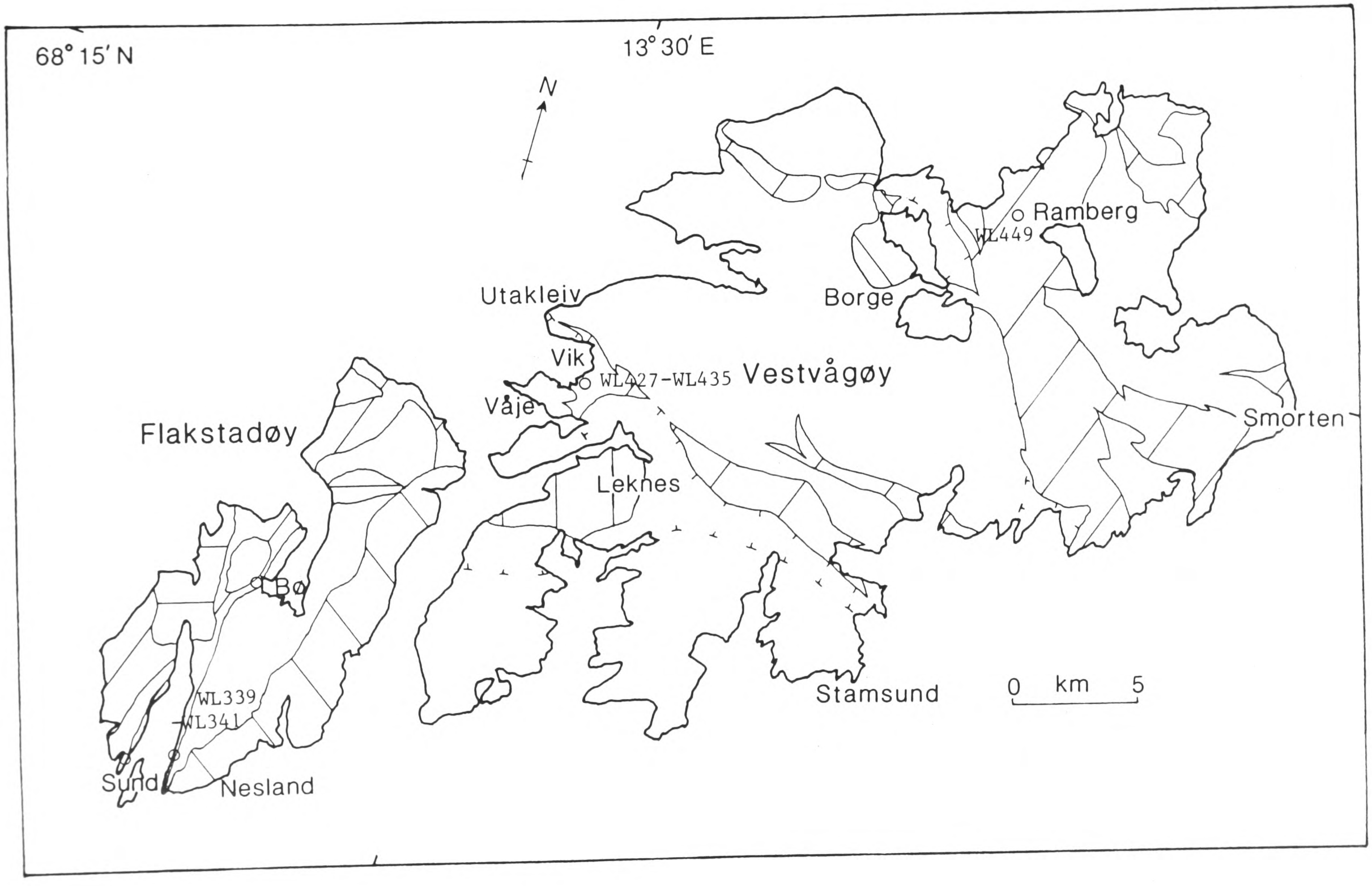
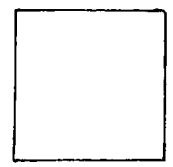
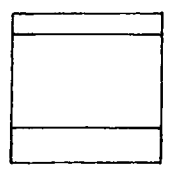

68° 15' N
13° 30' E
N
Ramberg
WL449
Utakleiv
Borge
Vik
WL427-WL435
Vestvågøy
Våje
Flakstadøy
Smorten
Leknes
Bø
WL339
WL341
Sund
Nesland
Stamsund
0 km 5

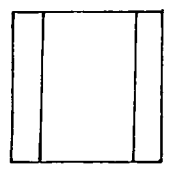
Fig. 4.3. Sample Locality Map for South-West Austvågøy: Early Proterozoic Supracrustal Gneisses



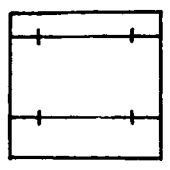
Early Proterozoic Supracrustal Gneisses



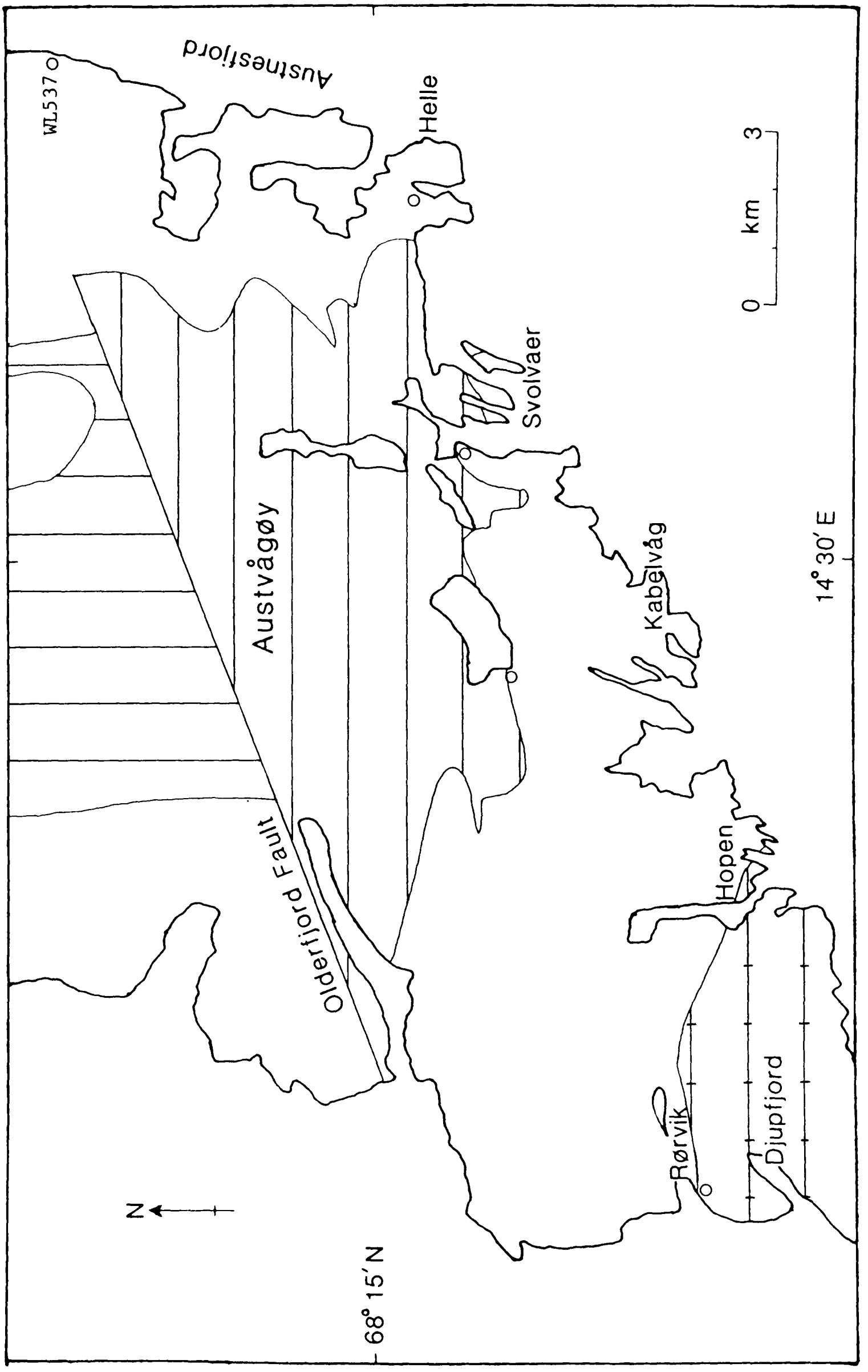
Austvågøy Grey Mangerite (Southern)



Austvågøy Grey Mangerite (Northern)



Hopen Mangerite


WL537
Austnesfjord
Helle
Svolvaer
Kabelvåg
Austvågøy
Hopen
Olderfjord Fault
Rørvik
Djupfjord
0 km 3
14° 30′ E
68° 15′ N
N

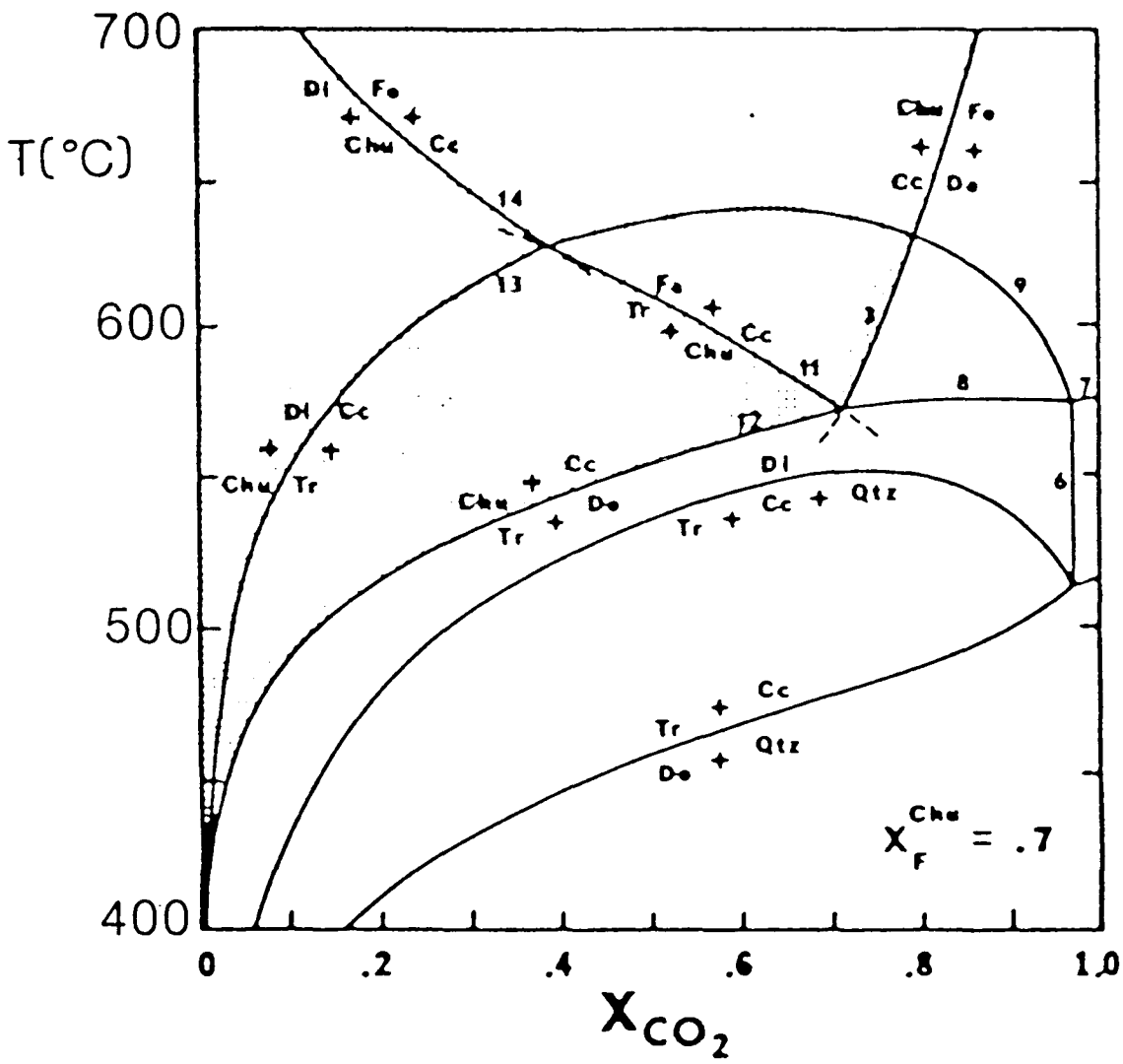


Fig. 4.4. Isobaric (2kb) temperature-fluid composition diagram for equilibria in the system CaO-MgO-SiO_2-CO_2-H_2O-HF. This diagram corresponds to a mole fraction of fluorine of 0.7 in clinohumite (Chu) and Tremolite (Tr).

The formation of trondite (humite group mineral) in the Ølkona Marble corresponds to the reaction Fo + Cc → Di + Chu (top left of diagram) (Table 4.1). The stability field of clinohumite (or chondrite) increases with increasing mole fraction of fluorine in the clinohumite. (After Rice, 1980).

Fig. 4.5.

Sm-Nd evolution diagram for the Vik Gneisses, Western Vestvågøy. At this locality (Fig. 4.2), the supracrustal gneisses are quartzo-feldspathic, and rhyolitic in composition (Table 4.2). The two samples shown in this figure, WL428 and WL432, both have T_{DM} model ages within error of 2.1Ga, the age of formation of the first supracrustal gneisses according to Griffin et al. (1978). The vertical lines define the age range 1.8 - 2.1Ga.

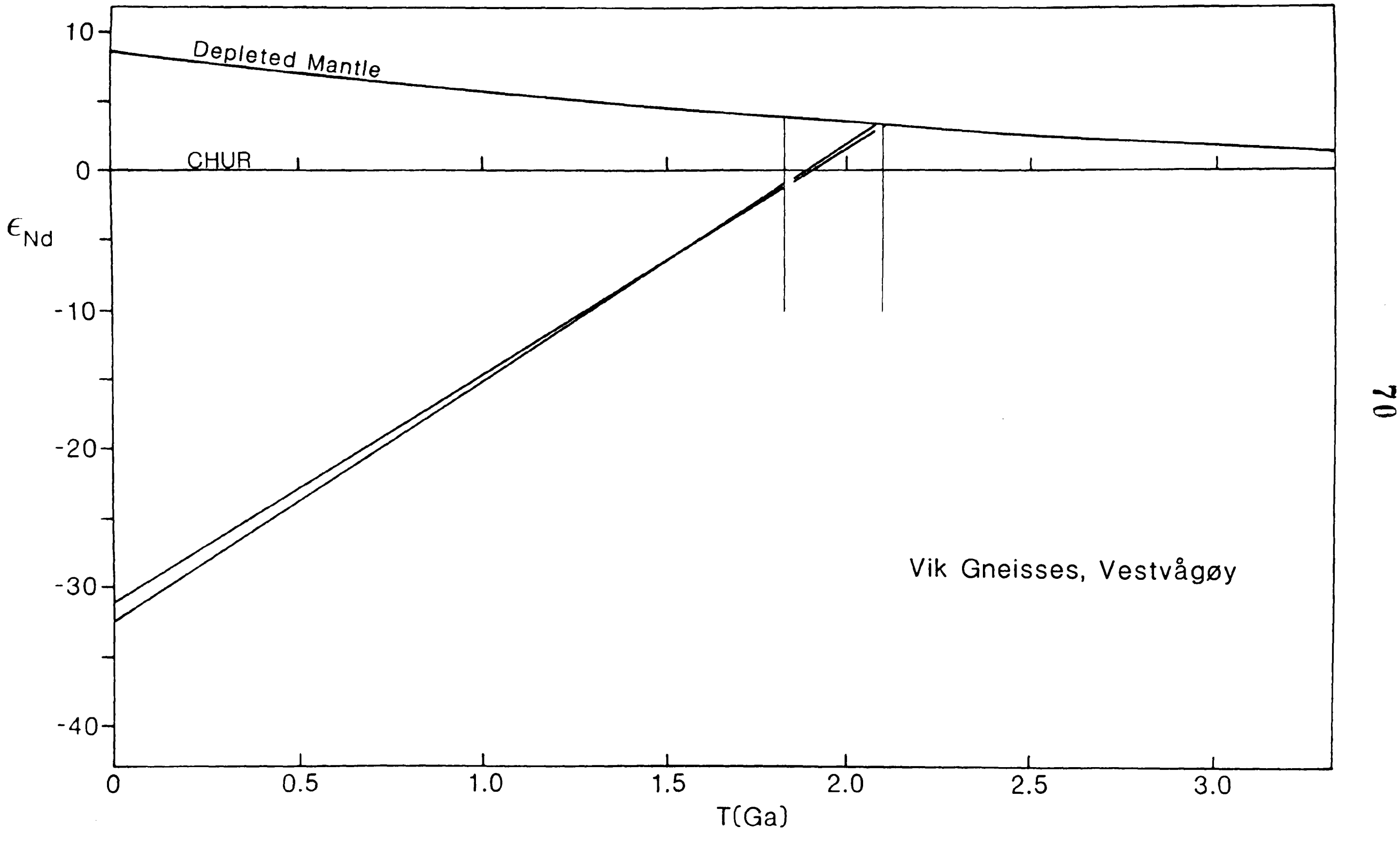

10
0
-10
-20
-30
-40
ϵ_{Nd}
Depleted Mantle
CHUR
Vik Gneisses, Vestvågøy
0
0.5
1.0
1.5
2.0
2.5
3.0
T(Ga)

Fig. 4.6.

Sm-Nd evolution diagram for a supracrustal gneiss sample, WL339, from north-west of Nesland, Flakstadøy (Fig. 4.2). It has a T_{DM} model age of 2.3Ga, which suggests that a component of the Nd may have been derived from an older crustal source, i.e. by contamination from the late Archaean migmatites at depth.

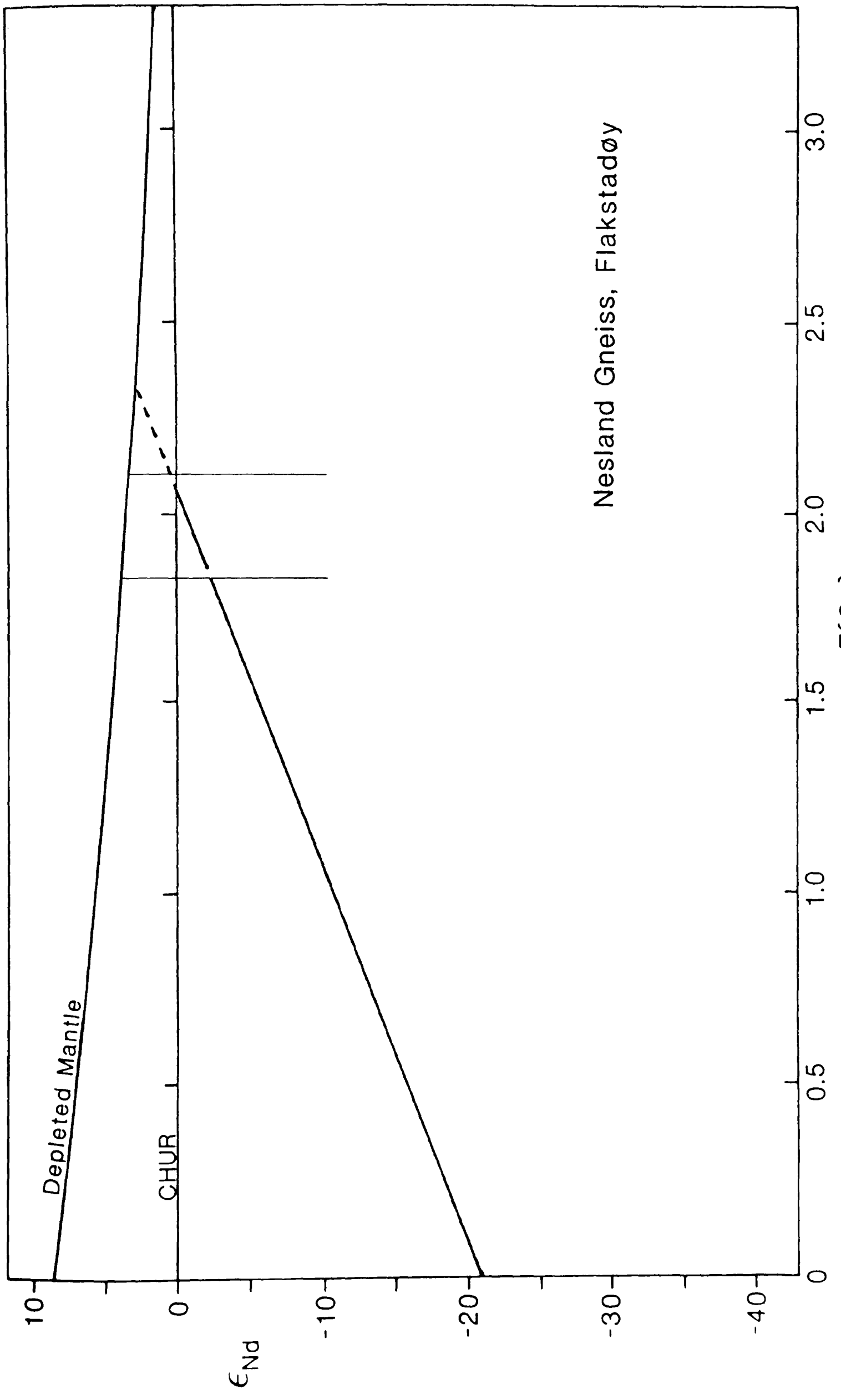

Nesland Gneiss, Flakstadøy
Depleted Mantle
CHUR
ϵ_{Nd}
10
0
-10
-20
-30
-40
0
0.5
1.0
1.5
2.0
2.5
3.0
T(Ga)

Fig. 4.7.

Rb-Sr isochron diagram for the Vik Gneisses, Vestvågøy. A 2.1Ga reference isochron with initial $^{87}Sr/^{86}Sr$ of 0.7020 (assuming $^{87}Sr/^{86}Sr$ 0 0.6990 at 4.57Ga, and 0.7045 at present day (DePaolo and Wasserburg, 1976)) is shown in relation to the Rb-Sr whole-rock isotopic data for the nine Vik gneiss samples (Table 4.4). All of the data-points lie below and to the right of 2.1Ga isochron. This distribution is best explained by Rb-enrichment during the retrograde metamorphism at about 1.1Ga.

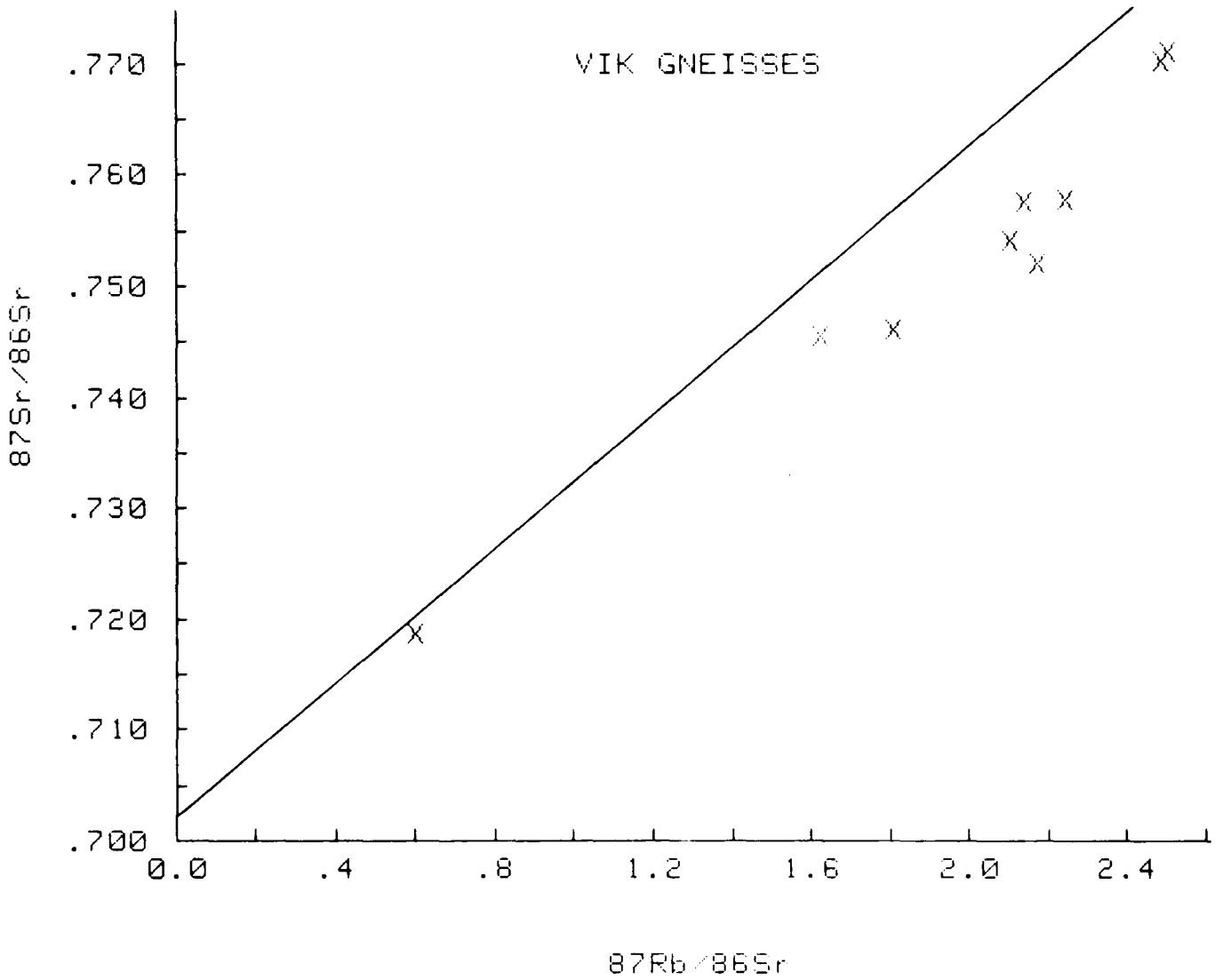

VIK GNEISSES
.770
.760
.750
.740
.730
.720
.710
.700
87Sr/86Sr
0.0
.4
.8
1.2
1.6
2.0
2.4
87Rb/86Sr

Fig. 4.8.

Rb-Sr evolution diagram for the Vik Gneisses, Vestvågøy, showing how the present-day scatter of data-points on the Rb-Sr isochron diagram (Fig. 4.7) can be modelled as due to Rb enrichment in the retrograde metamorphism at 1.1Ga. "Enrichment factors" are listed in Table 4.4.

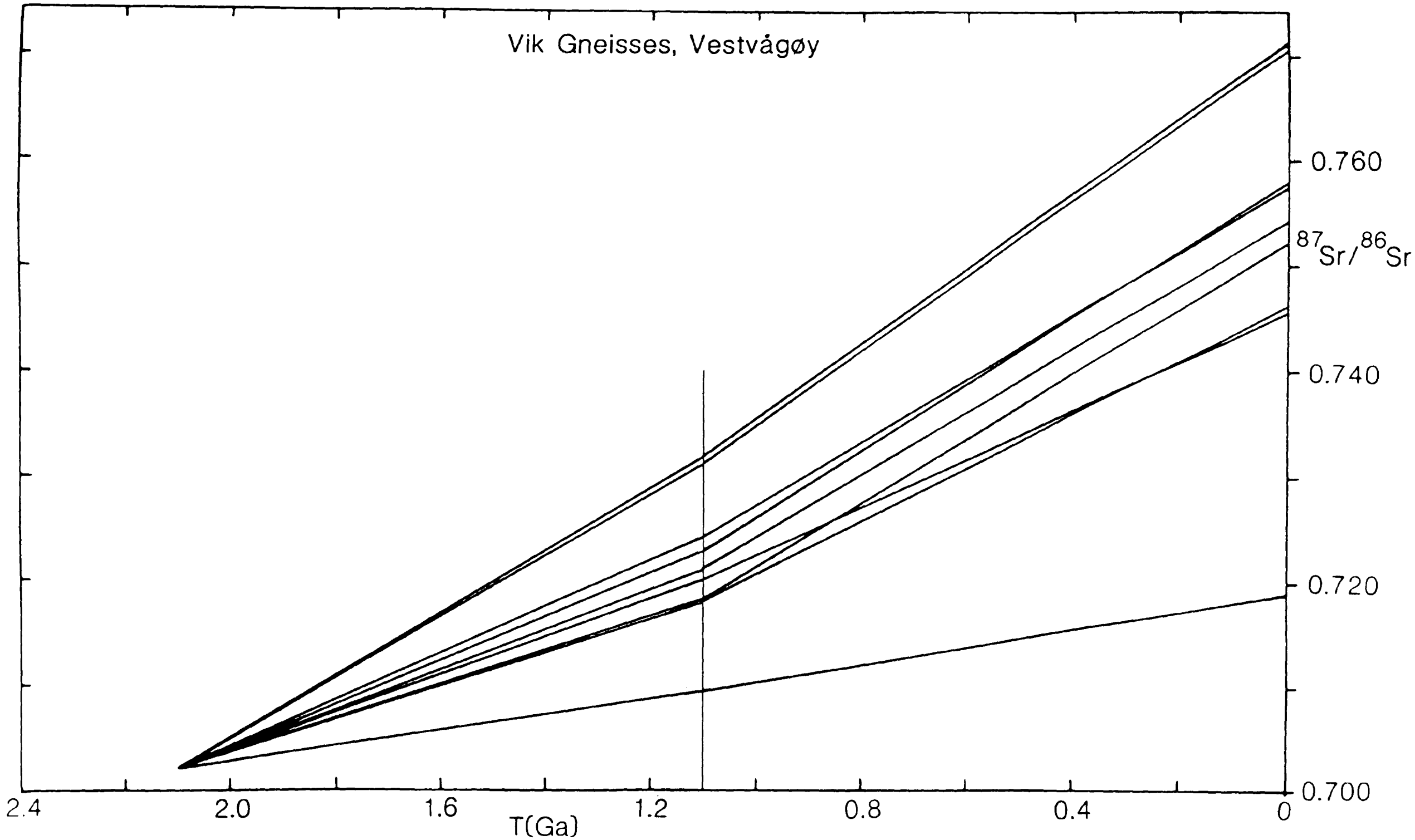

Vik Gneisses, Vestvågøy
0.760
$^{87}Sr/^{86}Sr$
0.740
0.720
0.700
2.4
2.0
1.6
1.2
0.8
0.4
0
T(Ga)

Plate 5.1. Compositional and grain size-layering in the troctolite zone of the Flakstadøy Basic Complex, east of Nesland. Peridotite layers up to 10cm thick grade upwards into more plagioclase-rich layers, often with an accompanying reduction in grain size. The peridotite layers strike 036^{o} and dip 52^{o}E.

Plate 5.2. Very large-scale ophitic texture in the norite zone of the Flakstadøy Basic Complex, west of Nesland. Plagioclase laths are up to 30 x 5cm.



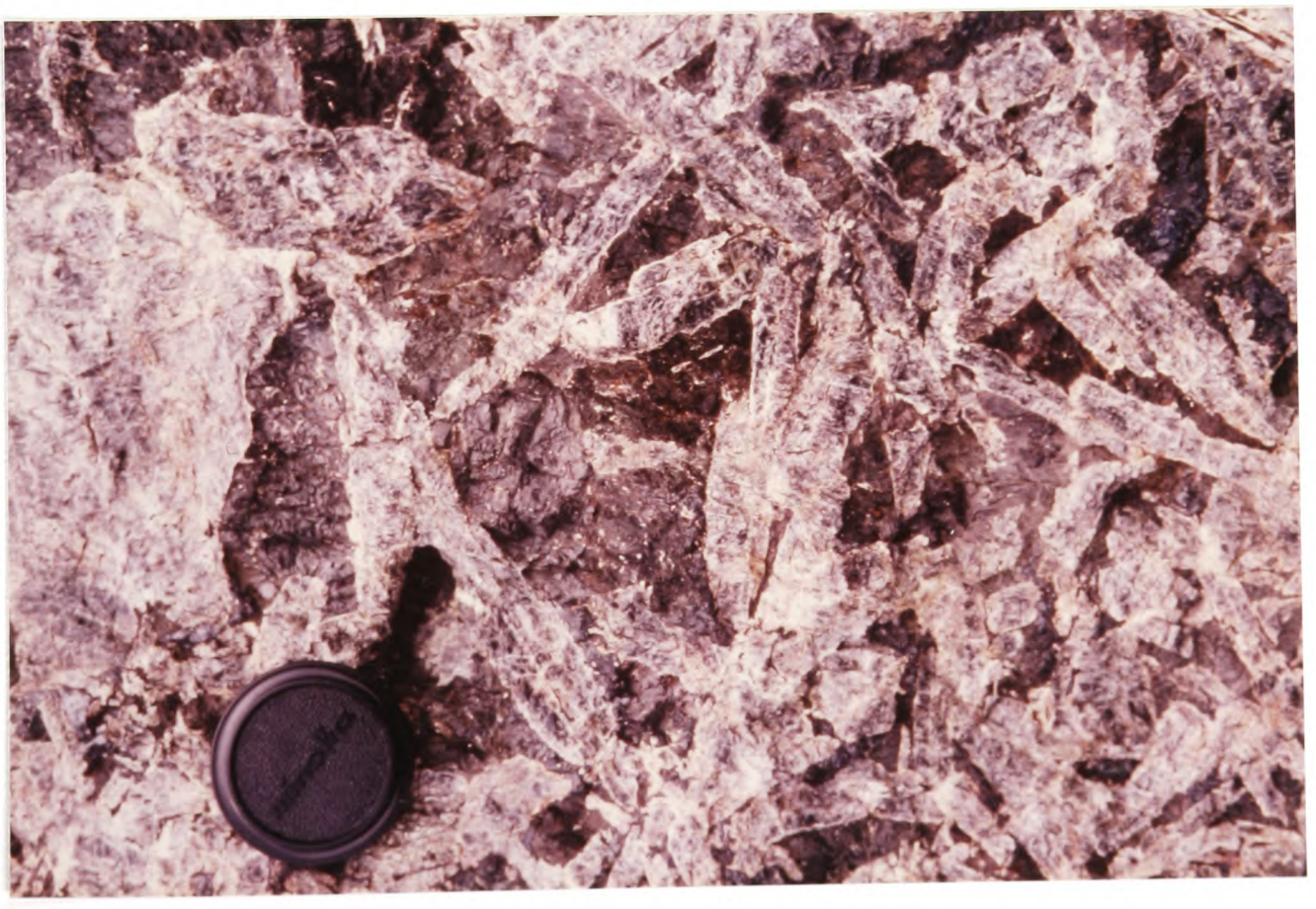
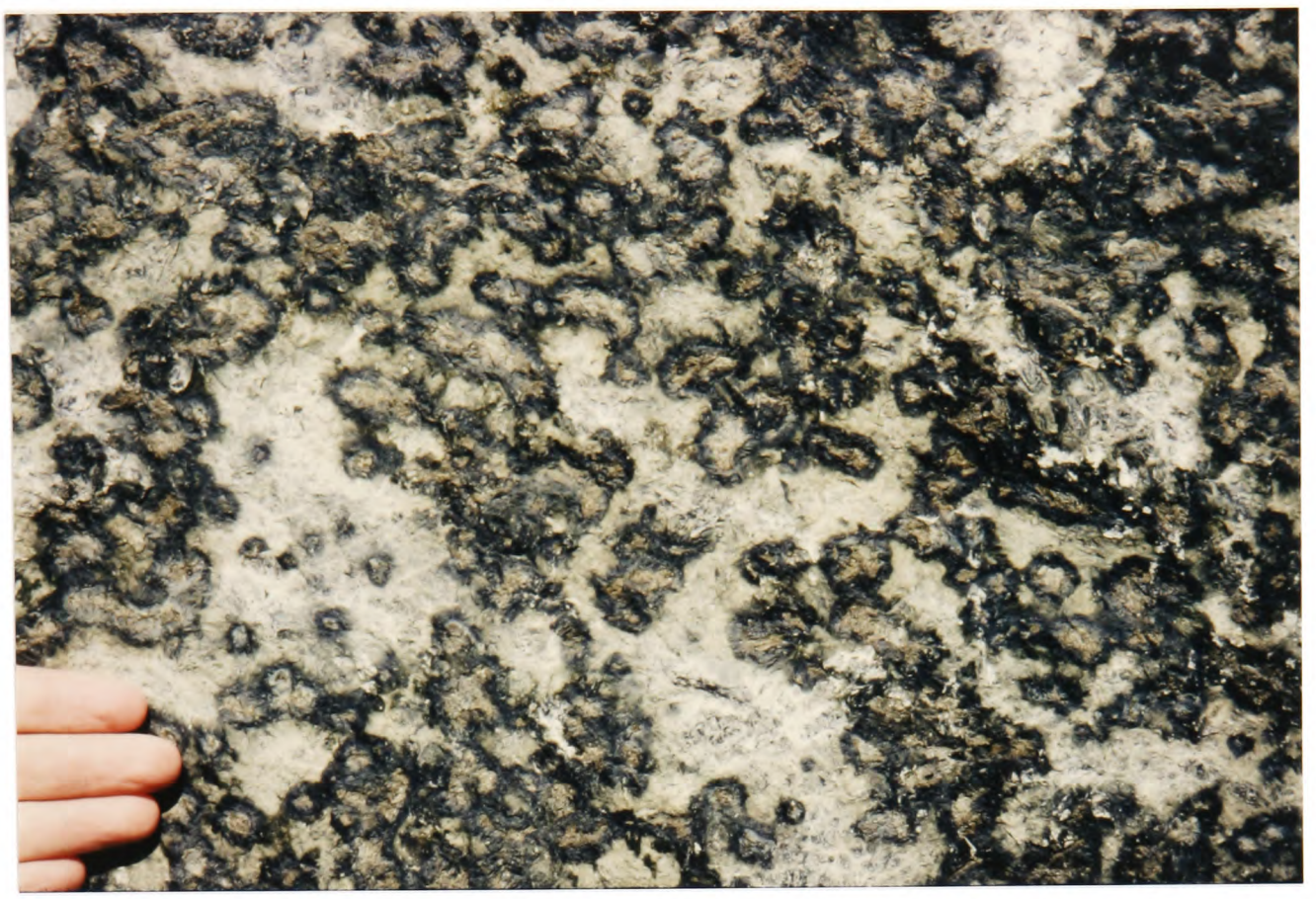


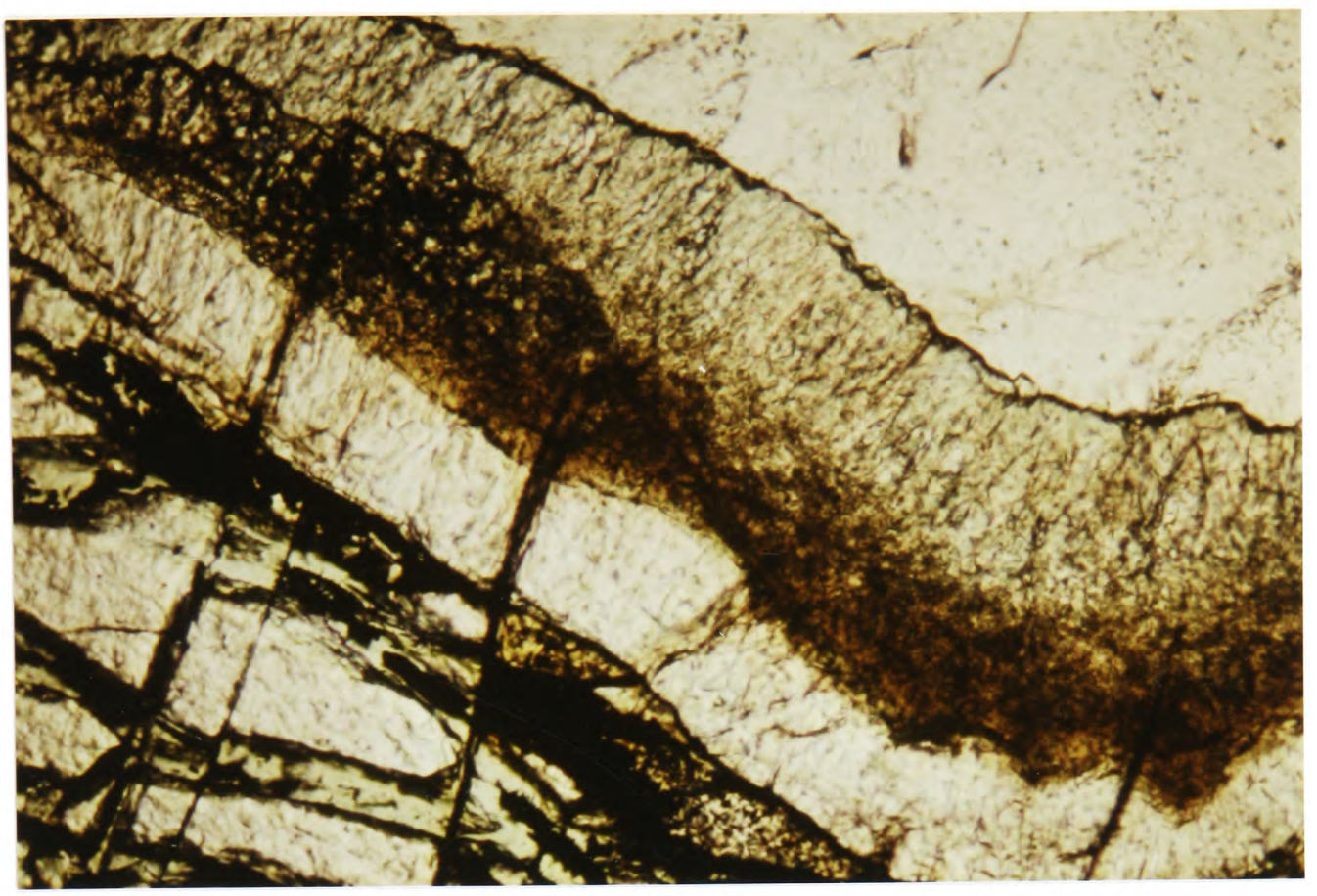
Plate 5.3. Troctolite from the Flakstadøy Basic Complex, north of Nusfjord. Coronas are present between olivine and plagioclase. These are illustrated in thin-section in Plates 5.5 and 5.6.

Plate 5.4. Polished slab of WL326 from the troctolite zone of the Flakstadøy Basic Complex, north of Nusfjord (from the outcrop illustrated in Plate 5.3). Two olivines about 3cm across are mantled by orthopyroxene magmatic reaction rims. The presence of fractures in the same orientation throughout the rock, unrelated to cleavage suggests the rock has been subjected to stress after consolidation of the magma.





Plates 5.5 and 5.6. Corona between olivine and plagioclase in PPL and XPL in WL330, a troctolite sample from the Flakstadøy Basic Complex north of Nusfjord. This is as described for the anorthosites of Flakstadøy by Griffin and Heier (1969). The corona consists of an inner zone of fibrous orthopyroxene adjacent to the olivine, and an outer zone of clinopyroxene with spinel inclusions, oriented perpendicular to the corona boundary; garnet develops as an isotropic brown dust at the contact between the two zones. Assuming $T \approx 850^{o}C$ during corona formation, the appearance of garnet indicates a pressure of about 9kb. The reaction took place with decreasing T at pressures less than 9kb, and was terminated by the fall in temperature. (x160).



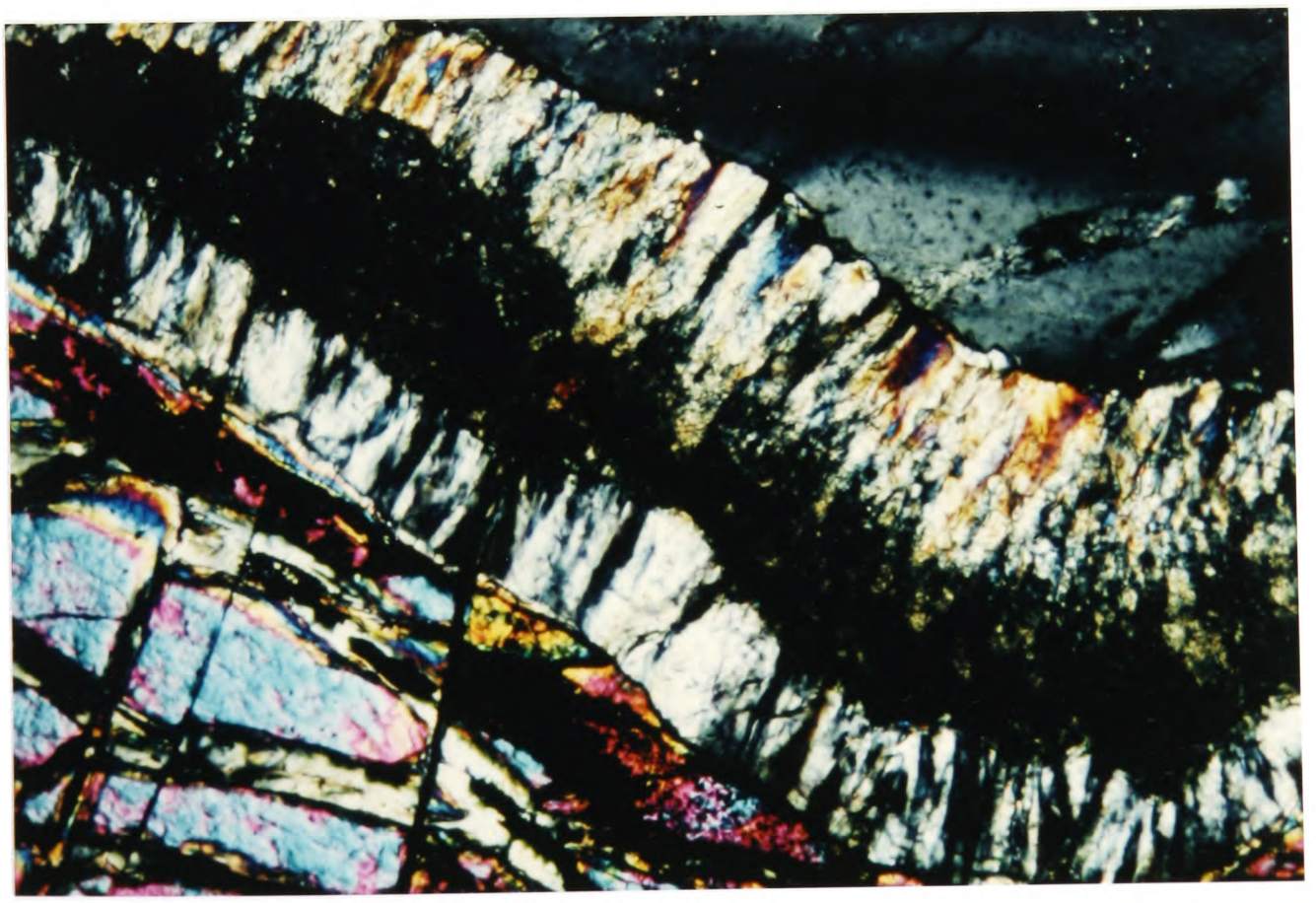


Plate 5.7. Shear zone in the gabbros and norites of the Flakstadøy Basic Complex in Mørkdalen, west of Nusfjord. Two discrete shears are present here; each strikes 126° and dips steeply to the east.

Plate 5.8. Polished slab of WL323 from the Flakstadøy Basic Complex at Mørkdalen, west of Nusfjord. In the shear zones (illustrated in Plate 5.7) eclogite mineralogies have been developed which have subsequently been retrograded to amphibolite facies. The shearing reduced the grain size of the gabbroic rocks facilitating the reactions to produce eclogite-facies mineralogies (Austrheim and Griffin 1982).



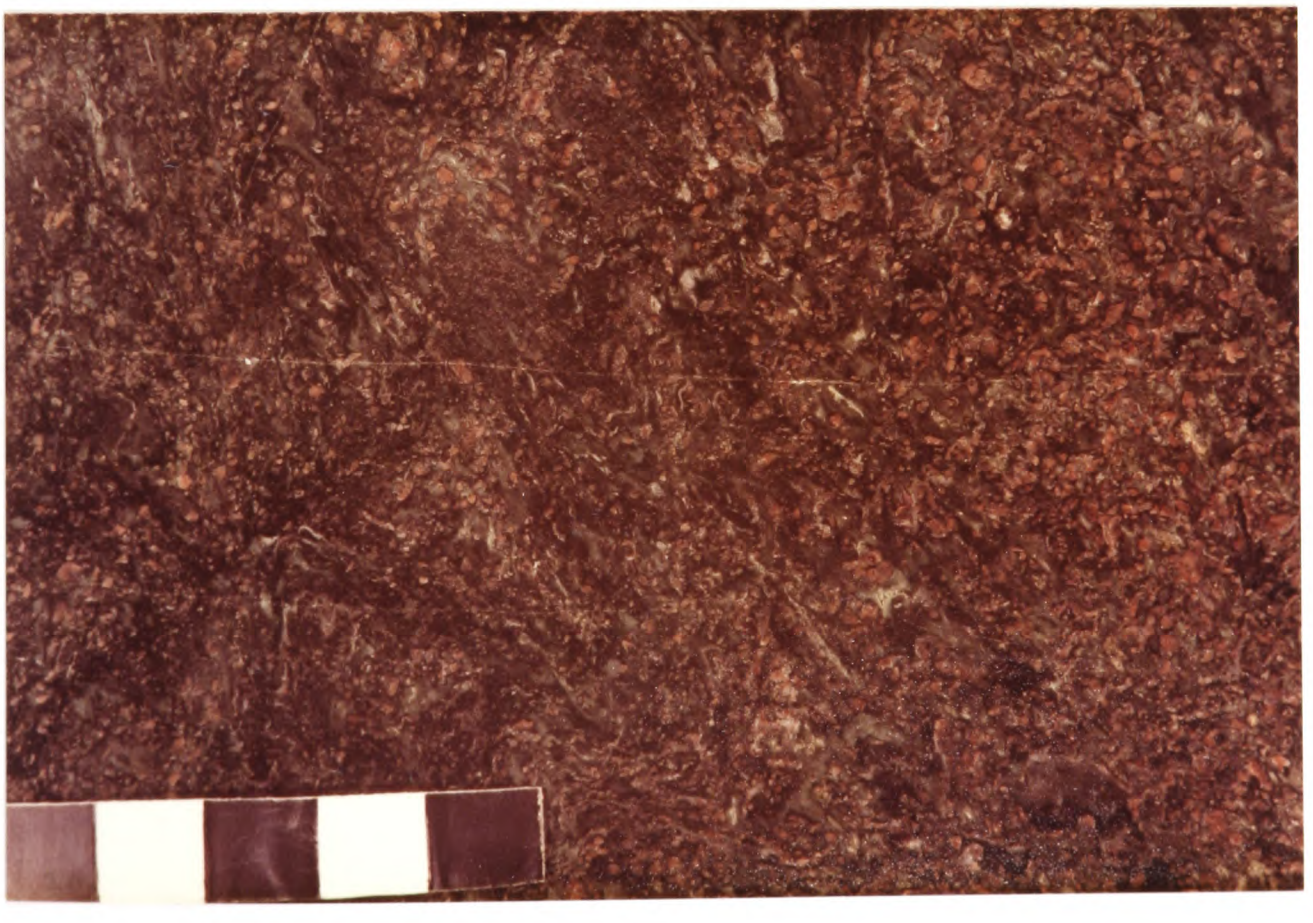
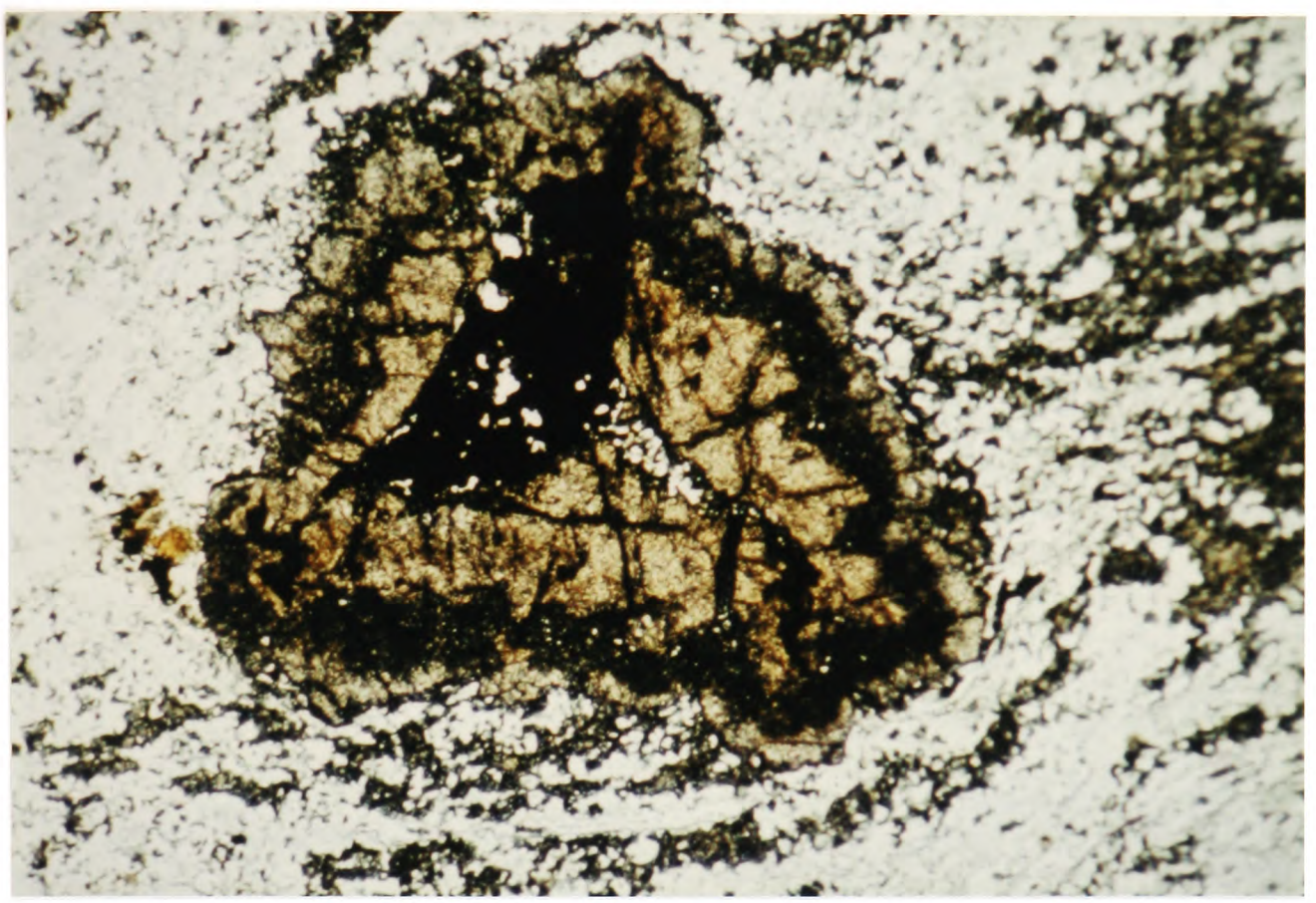


Plate 5.9. Thin-section of a garnet showing multi-stage growth from the Mørkdalen Eclogite, (WL323),west of Nusfjord, Flakstadøy. A pink, inclusion-free core is overgrown by a dusty inner rim and a colourless, inclusion-free outer rim. (×40).

Plate 5.10. Thin-section of typical euhedral garnets with spongy cores in the Mørkdalen Eclogite, (WL323), west of Nusfjord, Flakstadøy. Droop (1983) described similar garnets from the Tauern Window of the Eastern Alps. He described such garnets as growing as rings around omphacite grains which they progressively replace, producing garnets with quartz-filled cores and idiomoprhic rims, in equilibrium with albite and hornblende. (×40).



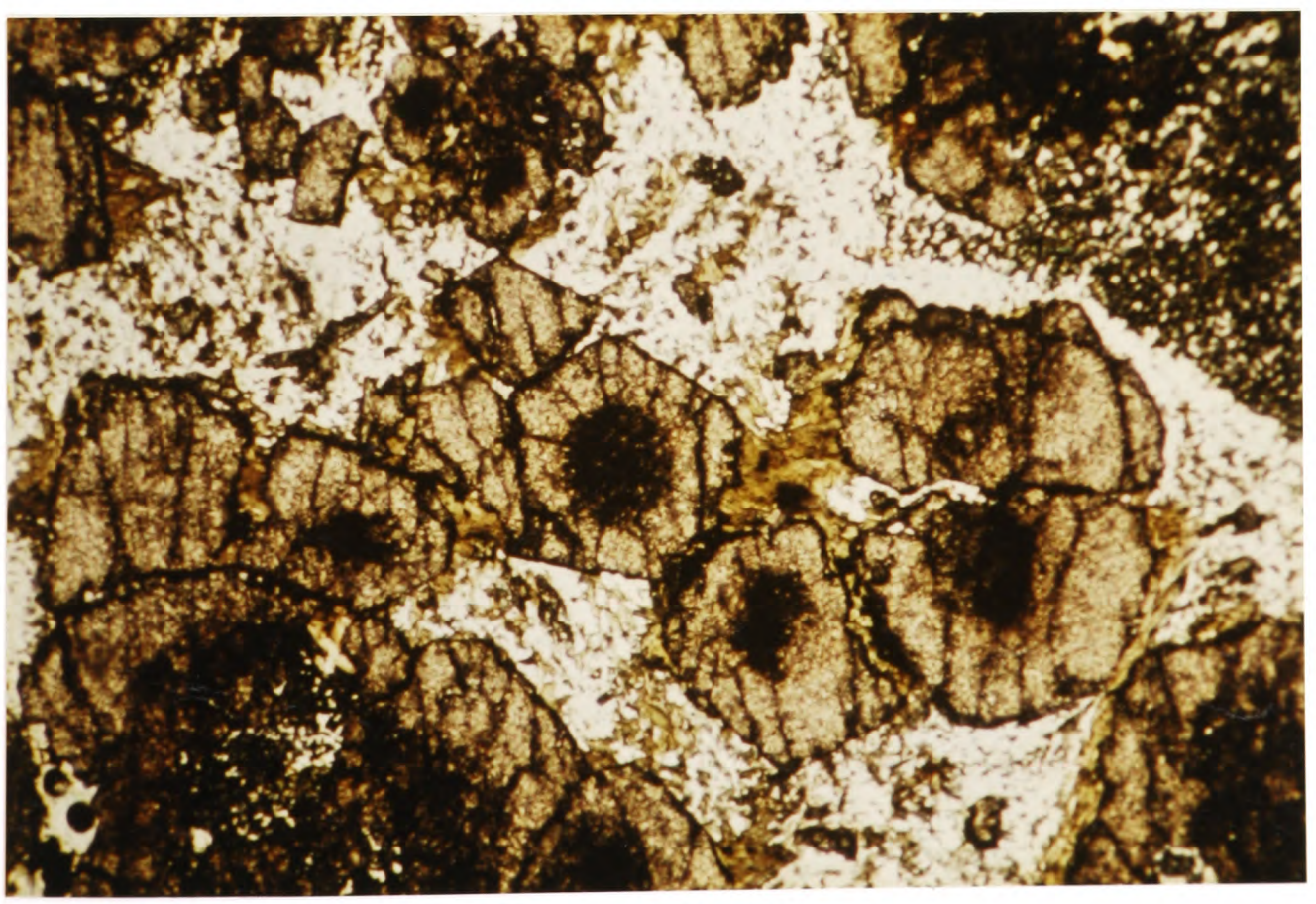


Plate 5.11. Polished slab of WL442 from the gabbro at Våje, West Vestvågøy, showing gabbro to eclogite transition. The gabbro (left) consists of unaltered plagioclase and pyroxenes. Towards the transition the plagioclase has abundant inclusions, and the pyroxenes are extensively altered to hornblende and biotite with fine-grained garnet rims. The eclogite (now retrogressed to amphibolite-facies) (right) consists of pyroxenes pseudomorphed by hornblende, biotite and opaque aggregates, rimmed by euhedral garnets. Plagioclase is altered to fine-grained albite; original grain boundaries are not preserved. White mica is associated with saussuritisation of plagioclase. Most of the opaques have altered to rutile in the eclogite part of WL442.

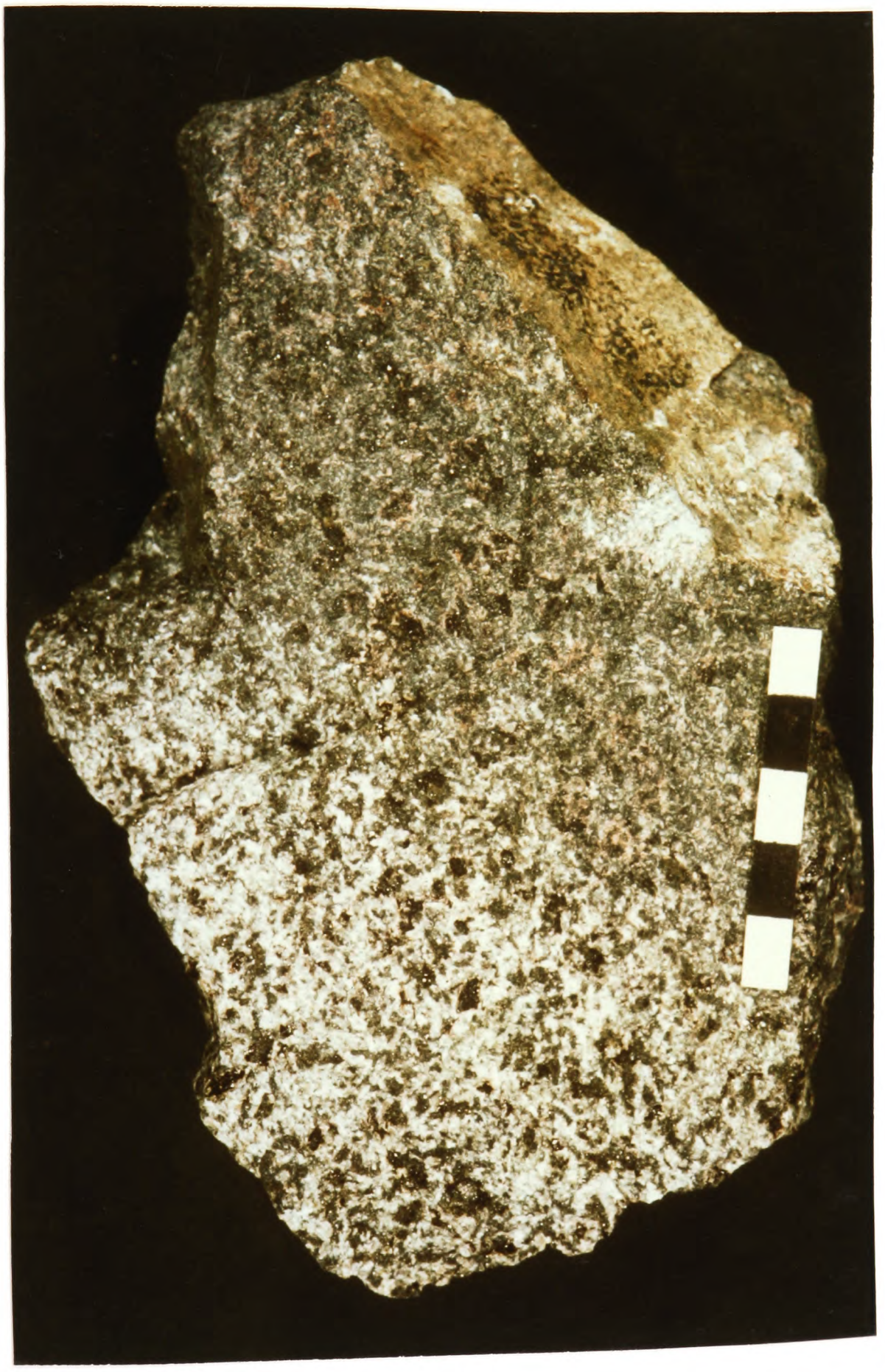


Plate 5.12. Polished slab of WL460 from west of Ramberg Quarry, North Vestvågøy. Augen of garnet amphibolite in sheared charnockite interpreted as a breccia of gabbro in mangeritic rock, in which the gabbro blocks developed eclogite textures and assemblages in response to the deformation. These blocks were subsequently retrogressed to amphibolite-facies parageneses.

Plate 5.13. Layered gabbro in the Eidet-Hovden Gabbro at Hovden Harbour, North-West Langøy. The plagioclase-rich and pyroxene-rich layers are typically 30cm wide and are more evident on a weathered surface than a fresh one.





Table 5.1

Major Element Compositions and CIPW Norms for the Flakstadøy Basic Complex

	WL311	WL314	WL317	WL323	WL325	WL326	WL329	WL346
SiO_2	50.17	49.89	45.38	48.57	50.96	53.09	53.16	51.28
Al_2O_3	21.48	23.38	12.35	17.23	23.78	25.38	27.52	15.50
TiO_2	0.59	0.16	2.40	1.40	0.09	0.13	0.17	1.51
Fe_2O_3	8.47	5.59	19.26	14.50	5.57	2.63	2.23	13.85
MgO	5.07	5.33	6.09	6.25	5.46	2.54	1.12	4.45
CaO	9.18	9.52	9.53	8.08	9.35	9.92	10.38	6.63
Na_2O	3.88	3.86	2.93	2.95	3.97	4.75	4.56	3.82
K_2O	0.64	0.50	1.12	0.61	0.59	0.78	0.65	1.75
MnO	0.11	0.07	0.22	0.18	0.08	0.05	0.03	0.21
P_2O_5	0.07	0.03	0.45	0.02	0.03	0.07	0.03	0.42
LOI	0.39	0.49	0.09	0.23	0.45	0.75	0.28	0.40
Total	100.05	98.80	99.80	100.03	100.33	100.08	100.13	99.82
Norms calculated with $Fe^{3+}/Fe^{3+} + Fe^{2+} = 0.15$								
Q	-	-	-	1.54	-	-	0.31	2.60
Or	3.78	2.95	6.62	3.60	3.49	4.61	3.84	10.34
Ab	32.83	32.66	24.79	24.96	33.59	40.19	38.59	32.33
An	39.31	44.99	17.24	31.97	44.45	45.63	50.22	19.98
C	-	-	-	-	0.32	-	0.91	-
Ci	0.69	0.87	0.16	0.41	0.80	1.33	0.50	0.71
Di	3.42	0.12	21.65	5.71	-	0.19	-	6.99
Hy	7.39	4.79	6.15	19.12	5.65	1.68	3.84	13.48
Ol	5.51	8.20	4.34	-	7.95	4.23	-	-
Mt	1.90	1.25	4.30	3.24	1.25	0.60	0.50	3.11
Il	1.12	0.30	4.55	2.66	0.17	0.25	0.32	2.86
Ap	0.15	0.07	0.98	0.04	0.07	0.15	0.07	0.92
Plag (An_x)	69	72	57	71	71	68	71	54
Mg/Mg + Fe*	0.80	0.85	0.73	0.76	0.85	0.86	0.78	0.72

*for ferromagnesian minerals

Table 5.2

Major Element Compositions and CIPW Norms for other Basic Intrusions

	Vik-Våje		Borge	Eidet-Hovden			Bø
	WL442'G'	WL442'E'	WL465	WL798	WL716	WL718	WL711
SiO_2	51.32	51.29	47.82	47.15	43.08	47.66	49.48
Al_2O_3	19.31	19.22	14.50	16.06	14.88	6.38	16.40
TiO_2	0.90	0.70	0.48	0.59	0.15	0.75	1.43
Fe_2O_3	9.21	9.26	9.43	12.67	10.10	11.85	12.43
MgO	4.93	5.49	12.05	11.78	18.07	13.91	5.27
CaO	8.38	8.08	11.82	6.81	7.50	16.60	8.31
Na_2O	3.84	3.77	2.06	2.89	2.36	1.07	4.07
K_2O	1.17	0.98	0.81	0.68	0.25	0.09	1.22
MnO	0.11	0.14	0.13	0.15	0.12	0.19	0.18
P_2O_5	0.15	0.13	0.10	0.21	0.02	0.03	0.50
LOI	0.38	0.41	0.83	0.52	3.80	0.84	0.35
Total	99.70	99.46	100.04	99.54	100.32	99.37	99.64
Norms calculated with $Fe^{3+}/Fe^{3+} + Fe^{2+} = 0.15$							
Q	-	0.25	-	-	-	-	-
Or	6.91	5.79	4.79	4.02	1.48	0.53	7.21
Ab	32.49	31.90	17.43	24.46	19.97	9.05	34.44
An	32.00	32.63	27.93	28.90	22.41	12.34	22.88
C	-	-	-	-	2.51	-	-
Cc	0.68	0.73	1.48	0.92	6.76	1.49	0.62
Di	5.71	4.02	21.24	1.20	-	52.68	11.04
Hy	13.46	16.13	6.54	15.70	13.52	8.62	6.17
Ol	-	-	12.99	14.00	26.39	4.98	4.84
Mt	2.06	2.08	2.11	2.83	2.26	2.67	2.79
Il	1.71	1.33	0.91	1.12	0.18	1.42	2.71
Ap	0.33	0.28	0.22	0.46	0.04	0.07	1.09
Plag/ (An_x)	65	66	75	69	68	72	56
Mg/Mg+ Fe*	0.80	0.80	0.89	0.85	0.91	0.89	0.77

*for ferromagnesian minerals

Table 5.3

Rb-Sr Data for the Mid Proterozoic Basic Intrusions
(Excluding Flakstadøy)

Sample	Locality and Description	Rb(ppm)	Sr(ppm)	$^{87}Rb/^{86}Sr$	$^{87}Sr/^{86}Sr$
WL440	Vik gabbro	18	612	n.d.	n.d.
WL442'G'	Våje gabbro	26	683	0.1102	0.70610
WL442'E'	Våje 'eclogite'	19	626	0.0880	0.70562
WL462	Borge garnet amphibolite	10	880	n.d.	n.d.
WL467	Borge gabbro	16	825	n.d.	n.d.
WL708	Hovden troctolite	49	625	0.2101	0.70871
WL711	Bø gabbro	22	685	n.d.	n.d.
WL716	Hovden troctolite	2	658	n.d.	n.d.
WL718	Hovden gabbro	3	158	n.d.	n.d.
Errors (2σ)		±5%	±5%	±1%	±0.00005

n.d. = not determined

Table 5.4

Sm-Nd Data for the Mid Proterozoic Basic Intrusions

Sample	Sm(ppm)	Nd(ppm)	$^{147}Sm/^{144}Nd$	$^{143}Nd/^{144}Nd$	T_{CHUR}(Ga)	T_{DM}(Ga)
WL311	1.162	5.687	0.12422	0.511544*	2.26	2.53
WL314	0.404	2.481	0.09899	0.511249	2.14	2.36
WL317	7.543	36.399	0.12595	0.511564	2.27	2.54
WL323	1.070	4.144	0.15690	0.511904	2.73*	3.05*
WL325	0.285	1.997	0.08667	0.511064	2.15	2.35
WL326	0.929	4.960*	0.11384	0.511401*	2.24*	2.48*
WL329	0.481	2.910*	0.10050	0.511253*	2.16*	2.38*
WL442'G'	3.492	16.219	0.13087	0.511737	2.05	2.37
WL442'E'	3.334	15.624	0.12970	0.511676*	2.15*	2.45*
WL465	2.529	12.585	0.12212	0.511579	2.13	2.41
WL711	6.816	35.242	0.11755	0.511541	2.08	2.35
WL716	0.634	3.162	0.12194	0.511582*	2.12*	2.40*
Errors (2σ)	±0.02%	±0.02%	±0.10%	±0.000025	±0.04	±0.04
unless asterisked (*) and stated below						
WL311				±0.000034		
WL323					±0.06	±0.06
WL326		±0.024%		±0.000050	±0.08	±0.08
WL329		±0.037%		±0.000123	±0.12	±0.12
WL442'E'				±0.000027	±0.05	±0.05
WL716				±0.000037	±0.06	±0.06

Table 5.5

Pb Data for the Mid Proterozoic Basic Intrusion

Sample	$^{206}Pb/^{204}Pb$	$^{207}Pb/^{204}Pb$	$^{208}Pb/^{204}Pb$	Apparent μ_1*
WL310	14.957	15.020	35.006	7.69
WL311	15.063	15.049	35.146	7.74
WL314	15.264	15.094	35.298	7.78
WL317	14.813	14.958	34.678	7.62
WL322	15.308	15.083	35.460	7.75
WL323	15.600	15.124	35.191	7.77
WL325	14.794	14.965	34.752	7.64
WL326	15.586	15.139	35.772	7.80
WL329	15.032	15.019	35.028	7.69
WL708	20.852	15.484	39.759	7.39

Errors (2σ) on Pb ratios are better than 0.1%

All samples are from the Flakstadøy Basic Complex except for WL708 which is a troctolite from the Hovden Gabbro, Langøy.

*Calculated assuming intrusion age of 1803Ma (the present study)

Table 5.6

Percentage of Ancient Crustal Material in the Flakstadøy Basic Complex: Nd Isotopic Constraints

Model: the Flakstadøy Basic Complex crystallized under granulite-facies conditions at 1.8Ga from a mantle-derived magma contaminated by 2.7Ga lower crustal material. The percentage of crustal material assimilated is dependent on the Nd concentrations in the components at the time of mixing (Chapter 5.5).

The percentage of late Archaean crustal material for different Nd concentrations:

Nd (ppm) in crust-derived component	Nd(ppm) in mantle-derived component: 6	11.5
9	52%	67%
32	23%	37%
204	5%	8%

6 and 11.5ppm are the lowest and the mean Nd concentrations, respectively in MORB glasses (Cohen et al., 1980).

32ppm is the mean Nd concentration of late Archaean gneisses from Lofoten-Vesterålen (Green et al., 1972; Jacobsen and Wasserburg, 1978; the present study) and from the Lewisian (Hamilton et al., 1979).

9 and 204ppm are the lowest and highest Nd concentrations in anatectic veins in Lofoten-Vesterålen (the present study).

Table 5.7

Percentage of Ancient Crustal Material in the Flakstadøy Basic Complex: Pb Isotopic Constraints

Model: as for Table 5.6. The "crustal Pb column" shows the percentage of Pb in the basic rocks which is derived from a lower crustal source. The other columns show the percentage of the basic rocks by total mass contributed by the lower crustal component, assuming crustal component Pb concentration of 20.2ppm (^{204}Pb = 0.28ppm) (North-West Hinnøy amphibolite-facies gneisses), and using different Pb concentrations for the mantle-derived component:

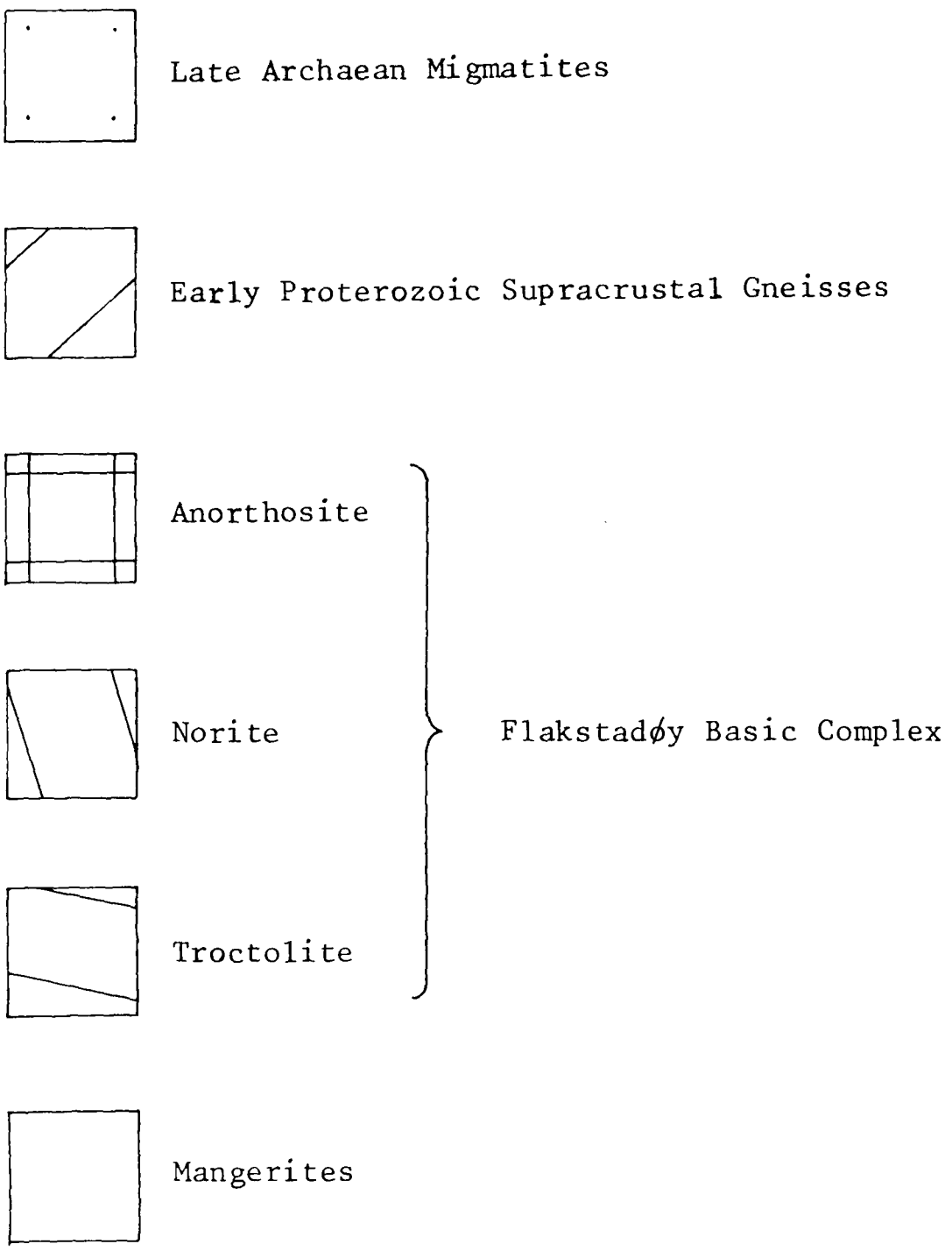
Sample	Crustal Pb	Crustal Contribution Total Pb(ppm) [^{204}Pb(ppm)]		
		0.6[0.008]*	3.2[0.04]†	7.0[0.1]‡
WL310	68%	6%	24%	44%
WL311	57%	4%	16%	32%
WL314	42%	2%	9%	20%
WL317	99%	78%	95%	98%
WL322	52%	3%	13%	28%
WL323	46%	2%	11%	23%
WL325	93%	28%	66%	83%
WL326	35%	2%	7%	16%
WL329	75%	8%	30%	51%

* Mean pristine MORB (Cohen et al., 1980)

† Preshal Mhor Basalt, Isle of Skye, Pb 93% mantle-derived (Dickin, 1981)

‡ Southern Zone Andes Basalt (McHugh, 1980)

Fig. 5.1. Sample Locality Map for Flakstadøy: Flakstadøy Basic Complex



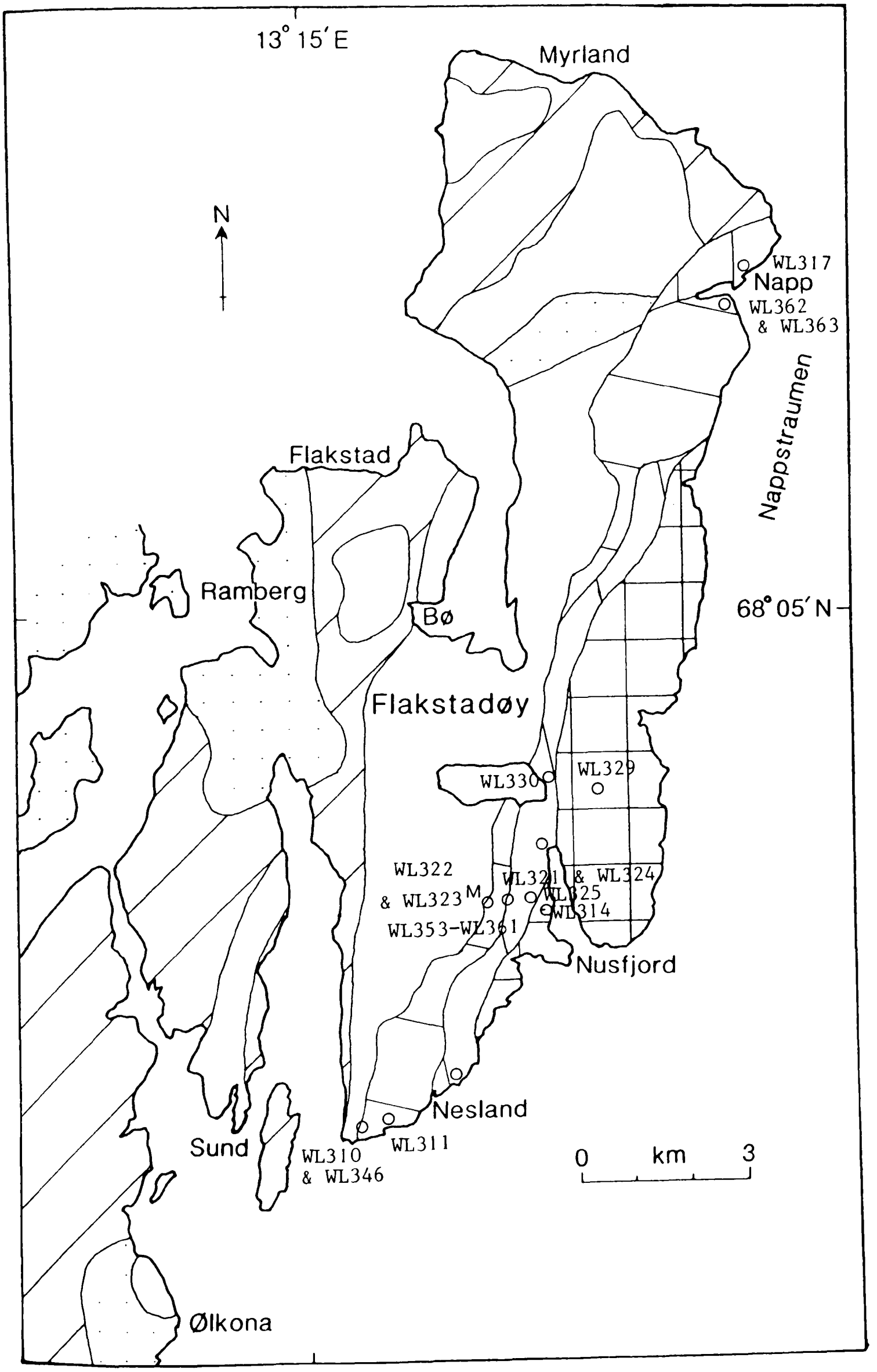
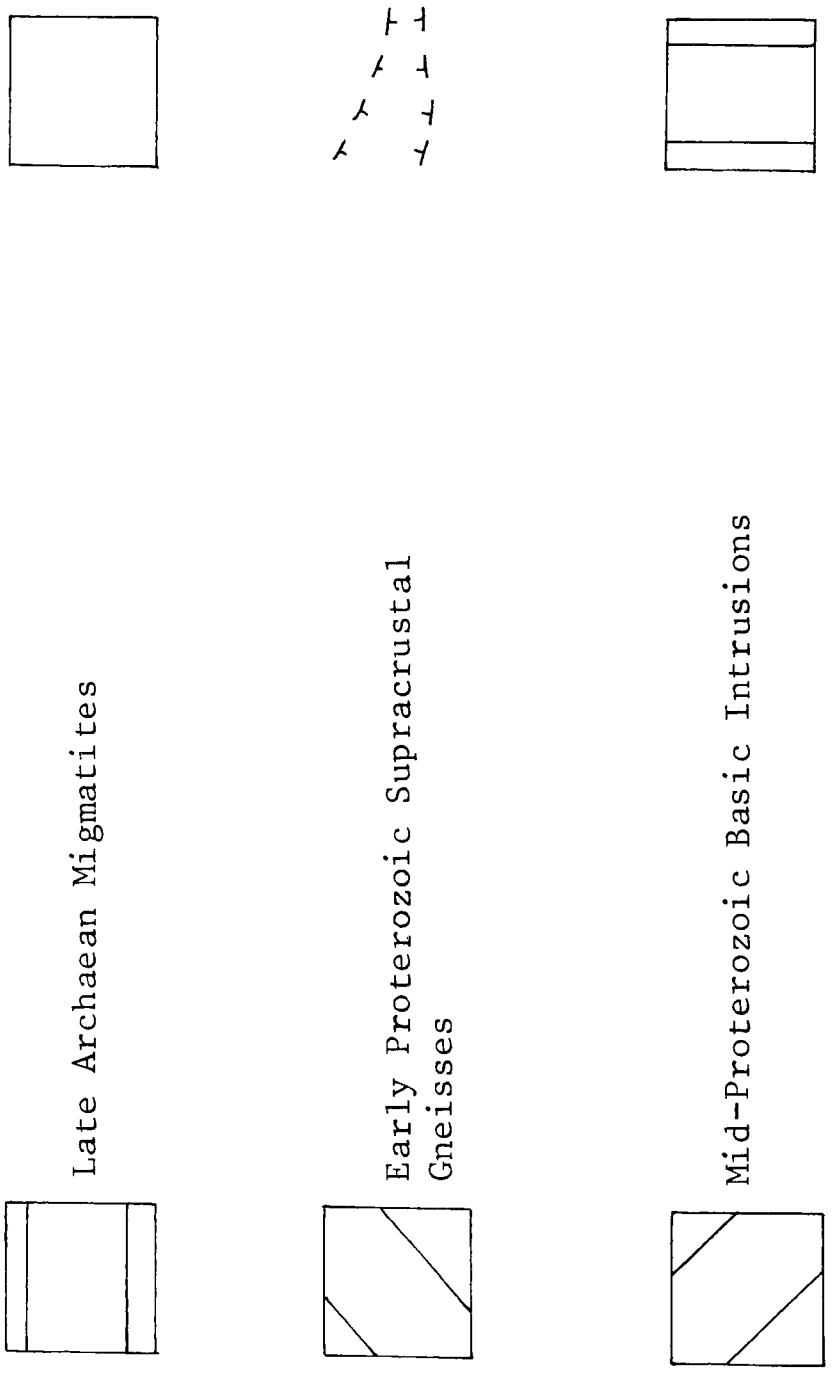

13° 15′ E
Myrland
N
WL317
Napp
WL362
& WL363
Nappstraumen
Flakstad
Ramberg
Bø
68° 05′ N
Flakstadøy
WL330
WL329
WL322
& WL323
M
WL321 & WL324
WL325
WL314
WL353-WL361
Nusfjord
Nesland
Sund
WL310
& WL346
WL311
0 km 3
Ølkona

Fig. 5.2. Sample Locality Map for Flakstadøy and Vestvågøy: Mid-Proterozoic Basic Intrusions



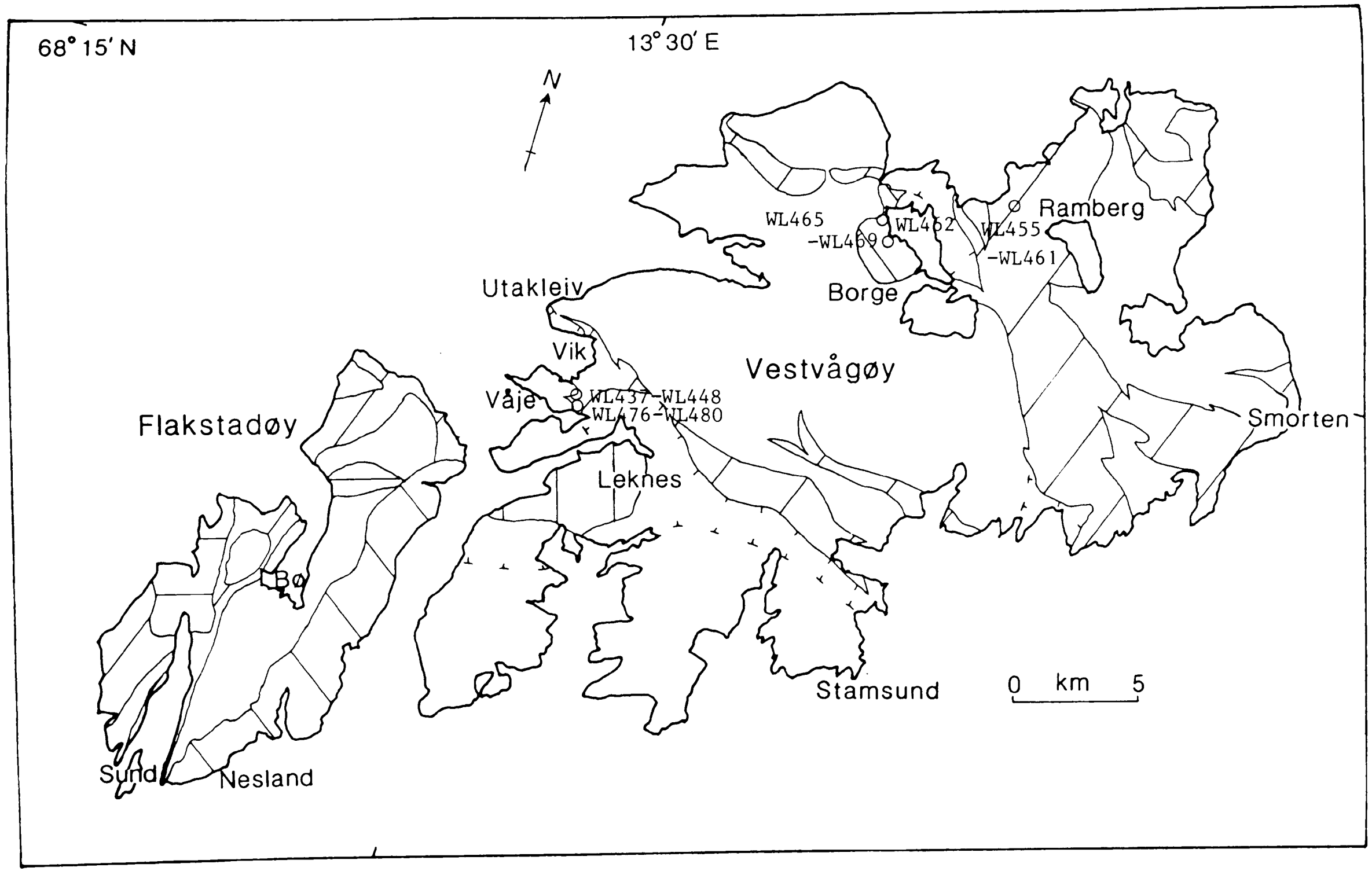
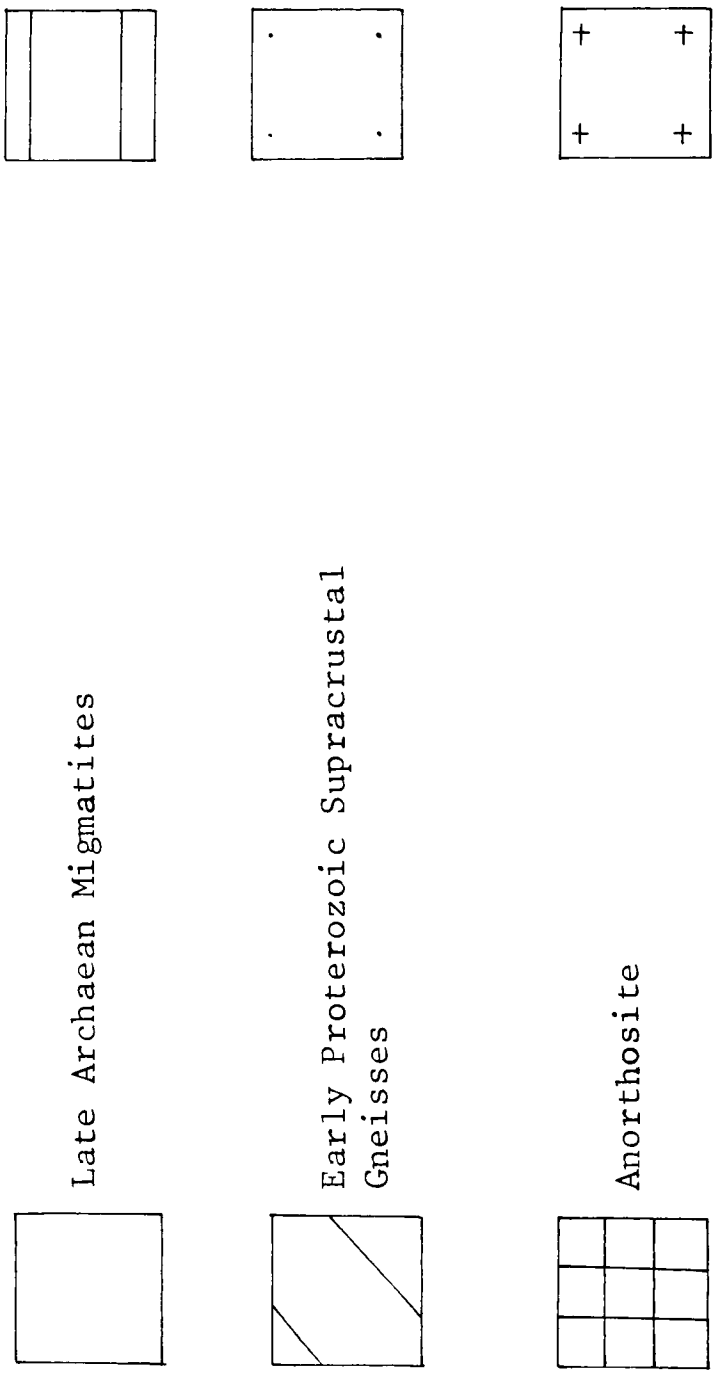

68° 15′ N
13° 30′ E
N
WL465
-WL469
WL462
WL455
-WL461
Ramberg
Borge
Utakleiv
Vik
Vestvågøy
Våje
WL437-WL448
WL476-WL480
Flakstadøy
Smorten
Leknes
Bø
Stamsund
0 km 5
Sund
Nesland

Fig. 5.3. Sample Locality Map for Langøy: Mid-Proterozoic Basic Intrusions



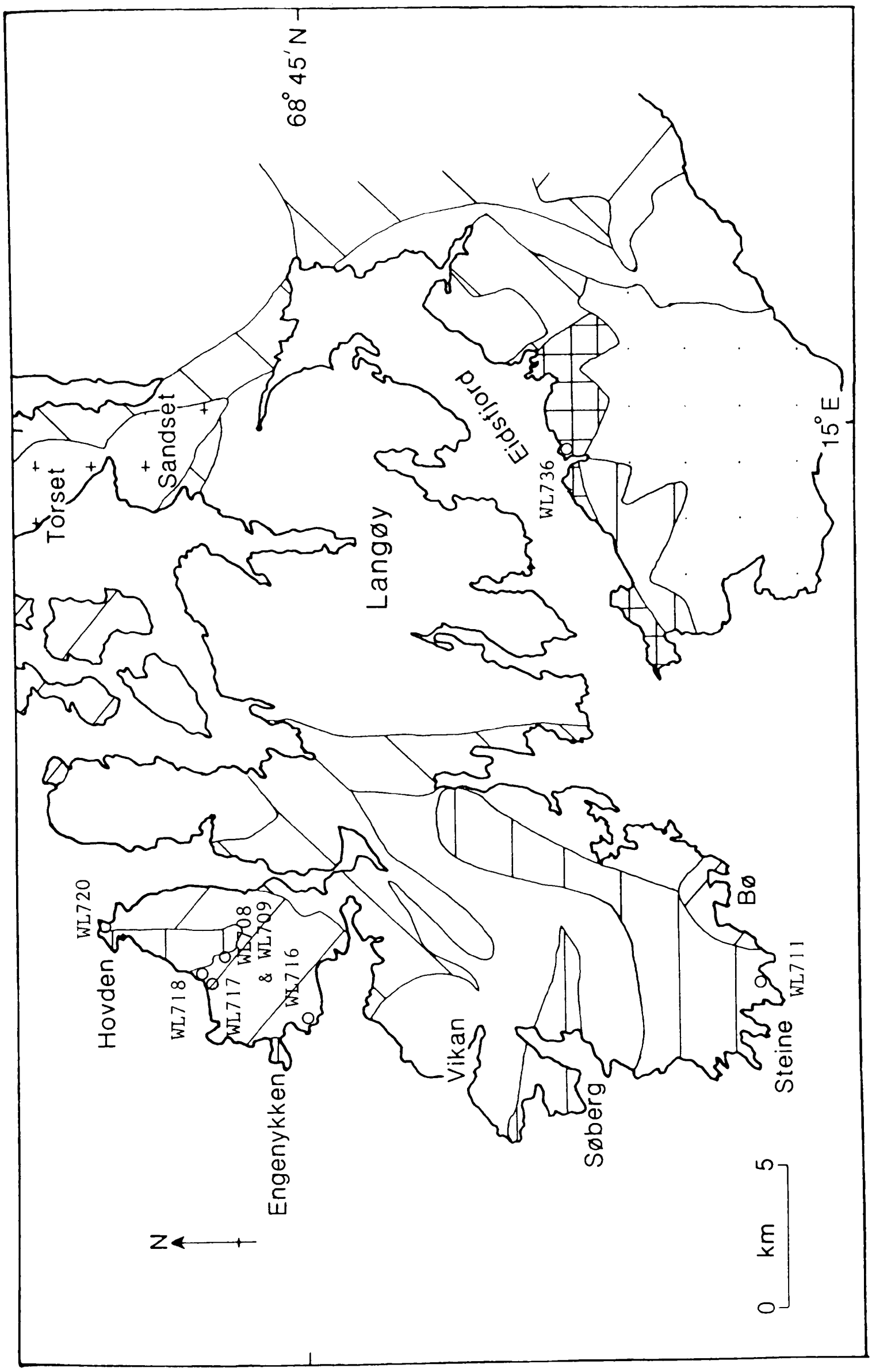

68° 45' N
15° E
Tørset
Sandset
Eidsfjord
WL736
Langøy
WL720
Hovden
WL718
WL717
WL708
& WL709
WL716
Engenykken
Vikan
Søberg
Bø
Steine
WL711
N
0 km 5

Fig. 5.4.

K_2O v. SiO_2 variation diagram for the eight Flakstadøy Basic Complex samples. Possible contaminants of a mantle-derived magma are: (i) late Archaean migmatites (triangle); (ii) early Proterozoic supracrustals (square); and (iii) Flakstadøy Mangerite (star). The Napp gabbro sample, WL317, has lower SiO_2 and higher K_2O than the other basic samples. WL346, from adjacent to the mangerite at Nesland, plots towards the possible contaminants.

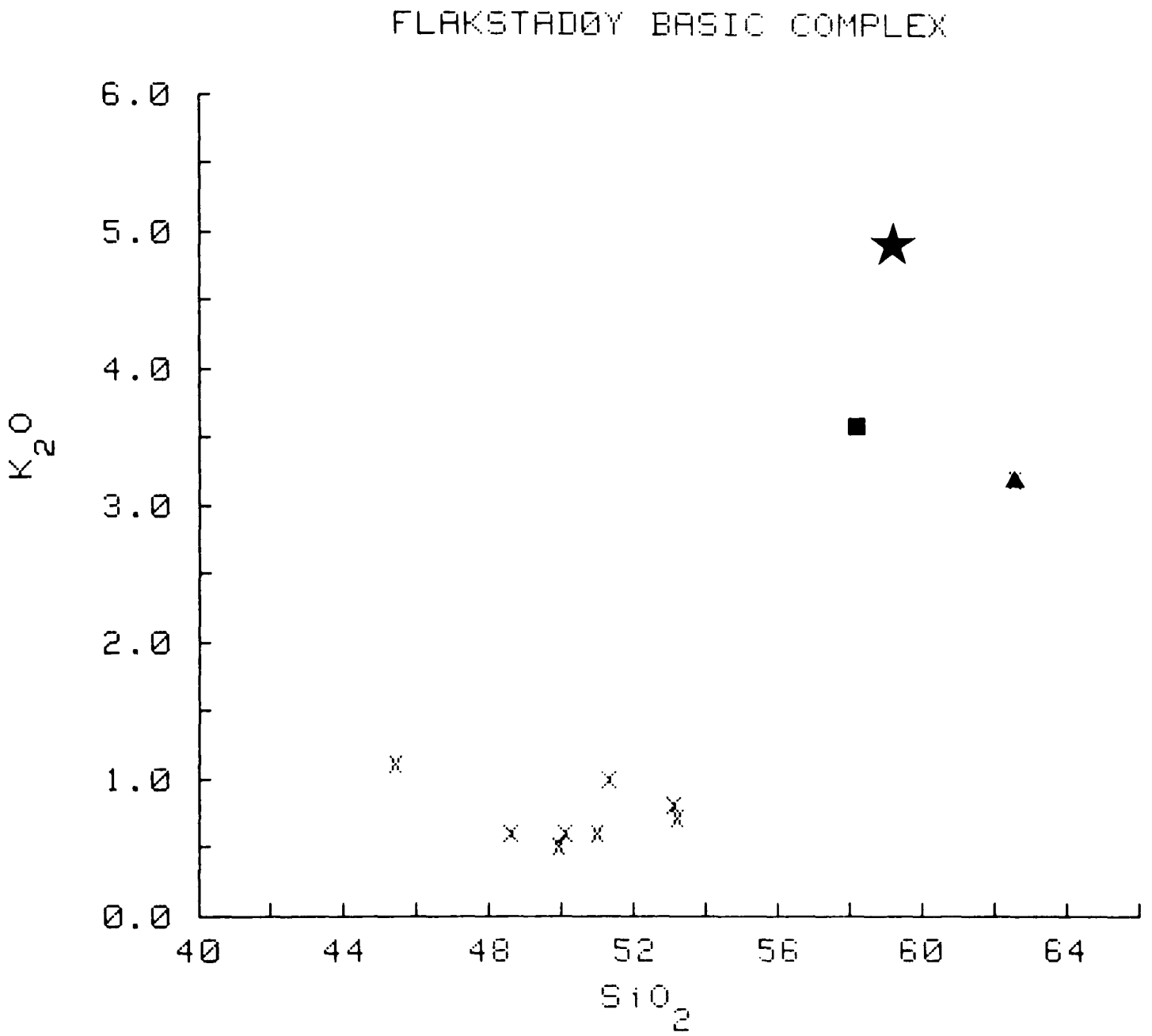

FLAKSTAD0Y BASIC COMPLEX
6.0
5.0
4.0
3.0
2.0
1.0
0.0
K2O
40
44
48
52
56
60
64
SiO2

Fig. 5.5.

CaO v. MgO variation diagram for the eight Flakstadøy Basic Complex samples. Possible contaminants as for Fig. 5.4. WL346 plots towards these contaminants. The wide range in MgO reflects the range in proportions of mafic phases present in the basic rocks.

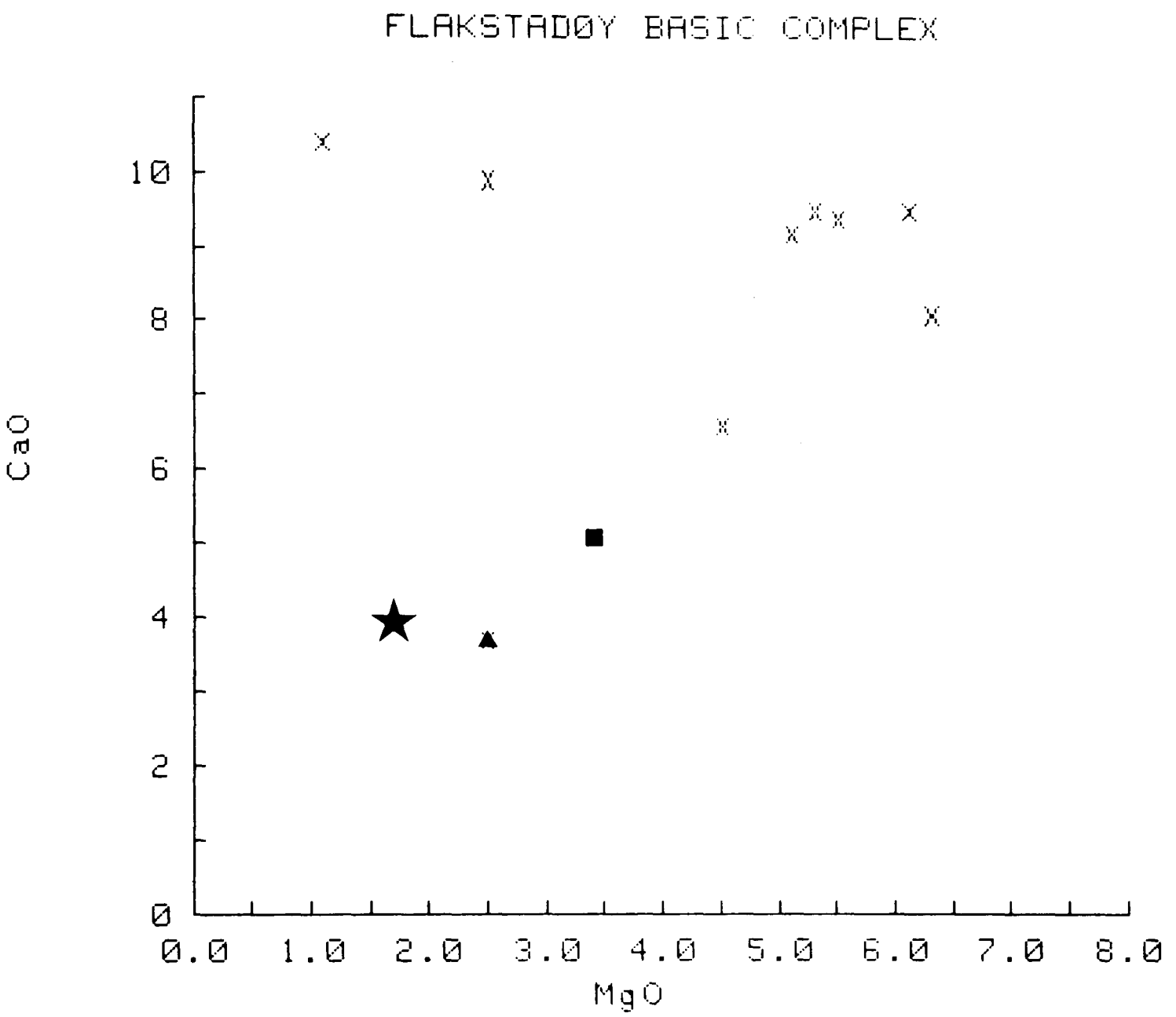

FLAKSTADØY BASIC COMPLEX
CaO
10
8
6
4
2
0
0.0
1.0
2.0
3.0
4.0
5.0
6.0
7.0
8.0
MgO

Fig. 5.6.

P_2O_5 v. TiO_2 variation diagram for the eight Flakstadøy Basic Complex samples. Possible contaminants as for Fig. 5.4. Most of the samples have very low contents of incompatible elements. The Morkdalen eclogite sample, WL323, has high TiO_2 and low P_2O_5, reflected in a high modal content of rutile. WL346, from adjacent to the Flakstadøy Mangerite, plots close to the composition of mean Flakstadøy Mangerite. WL317, from the Napp gabbro, has high P_2O_5 and TiO_2 content and is rich in disseminated ore.

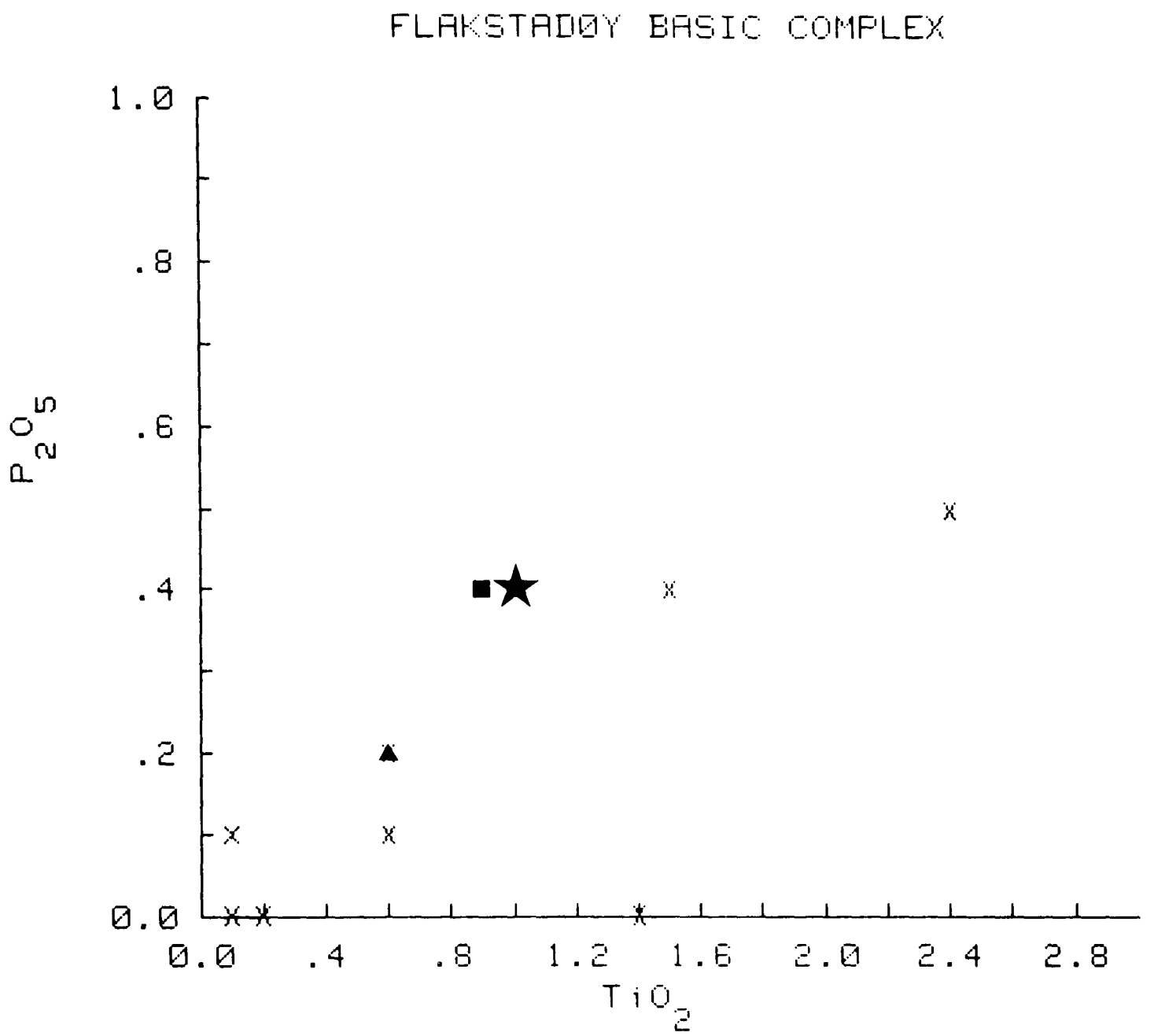

FLAKSTADØY BASIC COMPLEX
1.0
.8
.6
.4
.2
0.0
P_2O_5
0.0
.4
.8
1.2
1.6
2.0
2.4
2.8
TiO_2

Fig. 5.7.

CaO v. TiO_2 variation diagram for the eight Flakstadøy Basic Complex samples. Possible contaminants as for Fig. 5.4. WL317, WL323 and WL346 again plot away from the other samples due to high TiO_2. The low CaO of WL346 can be modelled as due to contamination of a basic magma by any/or a combination of late Archaean gneisses, early Proterozoic supracrustal gneisses and material of similar composition to the Flakstadøy Mangerite.

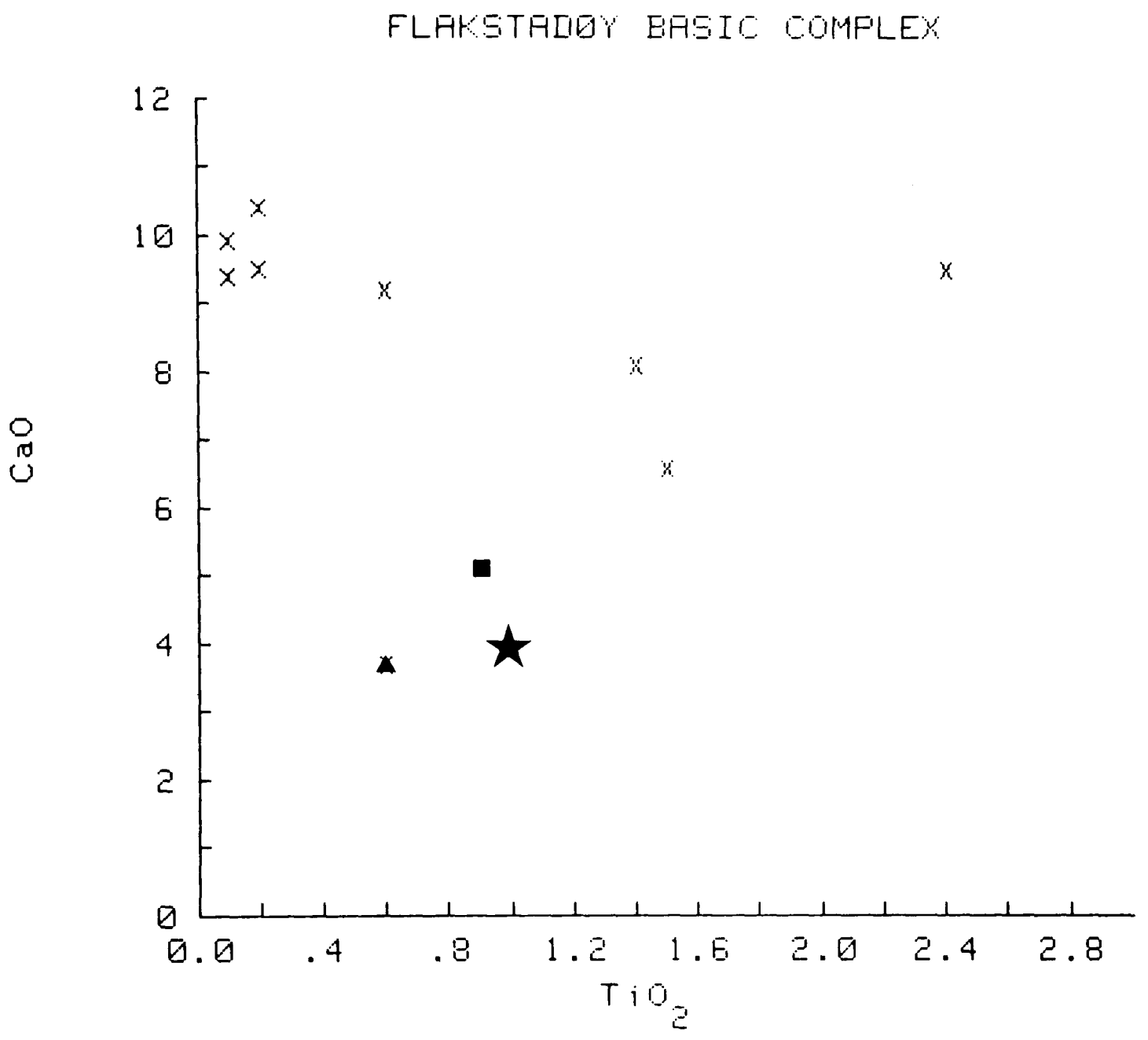

FLAKSTADØY BASIC COMPLEX
CaO
12
10
8
6
4
2
0
0.0
.4
.8
1.2
1.6
2.0
2.4
2.8
TiO2

Fig. 5.8.

Rb-Sr data and whole-rock isochron diagram for the Flakstadøy Basic Complex. The Rb concentration determinations are close to the detection limit for the XRF, hence the Rb-Sr whole-rock isochron age for this intrusion is impressive.

FLAKSTADØY BASIC COMPLEX

SAMPLE NAME	Rb ppm	Sr ppm	87Rb/86Sr	87Sr/86Sr
WL310	11	575	0.0414	0.70504
WL311	5	939	0.0055	0.70422
WL314	3	1041	0.0003	0.70405
WL317	12	521	0.0518	0.70549
WL322	3	849	0.0017	0.70405
WL323	7	635	0.0194	0.70445
WL324	4	979	0.0012	0.70411
WL325	3	1042	0.0003	0.70407
WL326	5	1128	0.0052	0.70429
WL329	4	1190	0.0009	0.70409
WL330	4	968	0.0023	0.70416
WL346	11	633	0.0388	0.70501

Slope	0.025365	Error	0.001128 (1 Sigma)
Intercept	0.704062	Error	0.000026 (1 Sigma)
Centroid	0.013833	0.704413	
Squared residuals	8.880		
M.S.W.D.	0.888		
No. of Cycles	3		

Age 1764.0 +/- 154.8 Ma. (2 sigma)

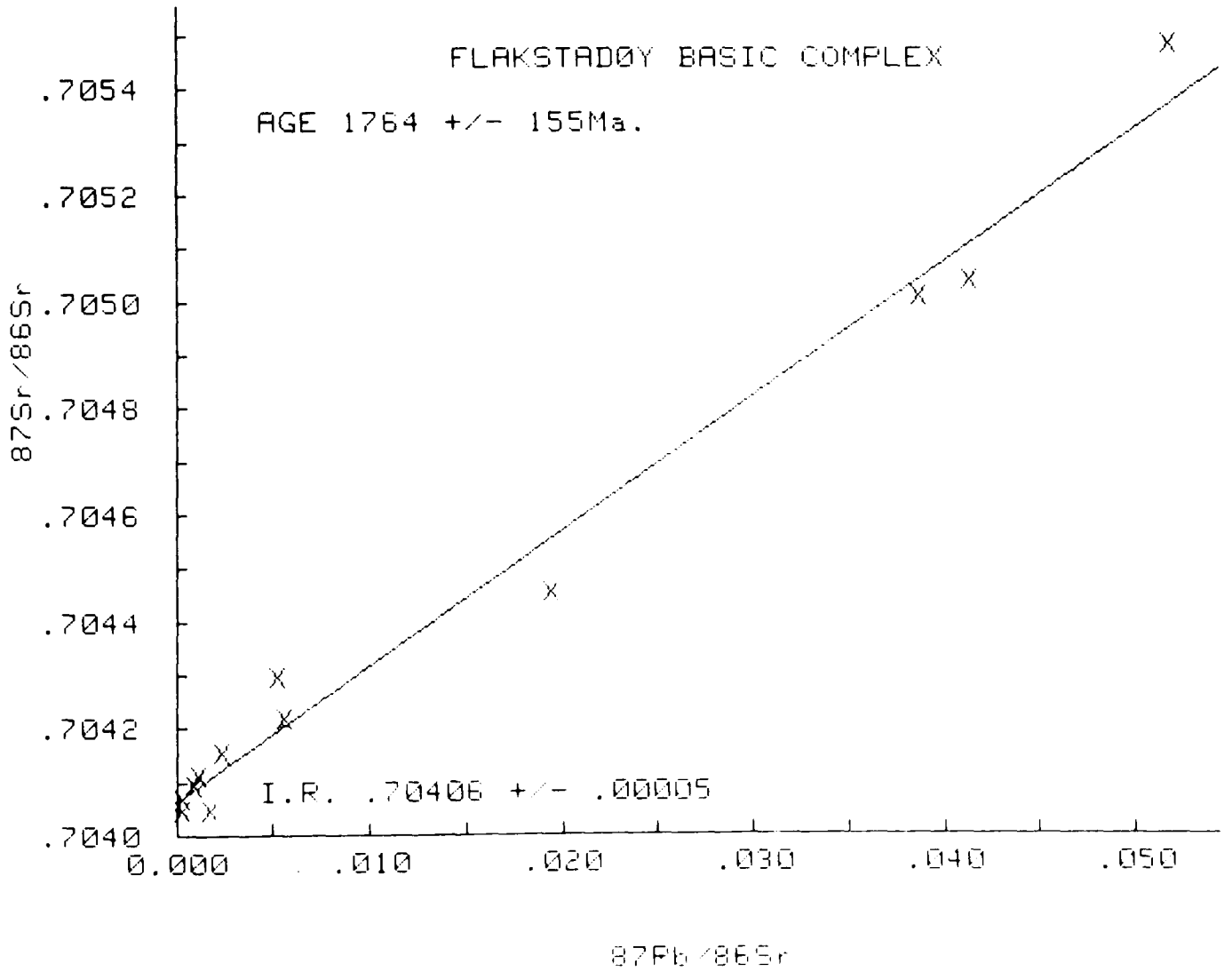


Fig. 5.9.

Sm-Nd data and whole-rock isochron diagram for the Flakstadøy Basic Complex. The Sm-Nd whole-rock isochron age is more precise than the Rb-Sr whole-rock isochron age because of the wide range in Sm/Nd ratios.

FLAKSTADØY BASIC COMPLEX

SAMPLE NAME	Sm ppm	Nd ppm	147Sm/144Nd	143Nd/144Nd
WL314	0.40	2.50	0.0990	0.51125
WL317	7.50	36.00	0.1260	0.51156
WL323	1.10	4.10	0.1569	0.51190
WL326	0.90	5.00	0.1138	0.51140
WL311	1.20	5.70	0.1242	0.51154
WL325	0.30	2.00	0.0867	0.51106
WL329	0.50	2.90	0.1005	0.51125

Slope	0.011864	Error	0.000372 (1 Sigma)
Intercept	0.510057	Error	0.000045 (1 Sigma)
Centroid	0.118805	0.511467	
Squared residuals	3.018		
M.S.W.D.	0.604		
No. of Cycles	2		

Age 1803.3 +/- 112.3 Ma. (2 sigma)

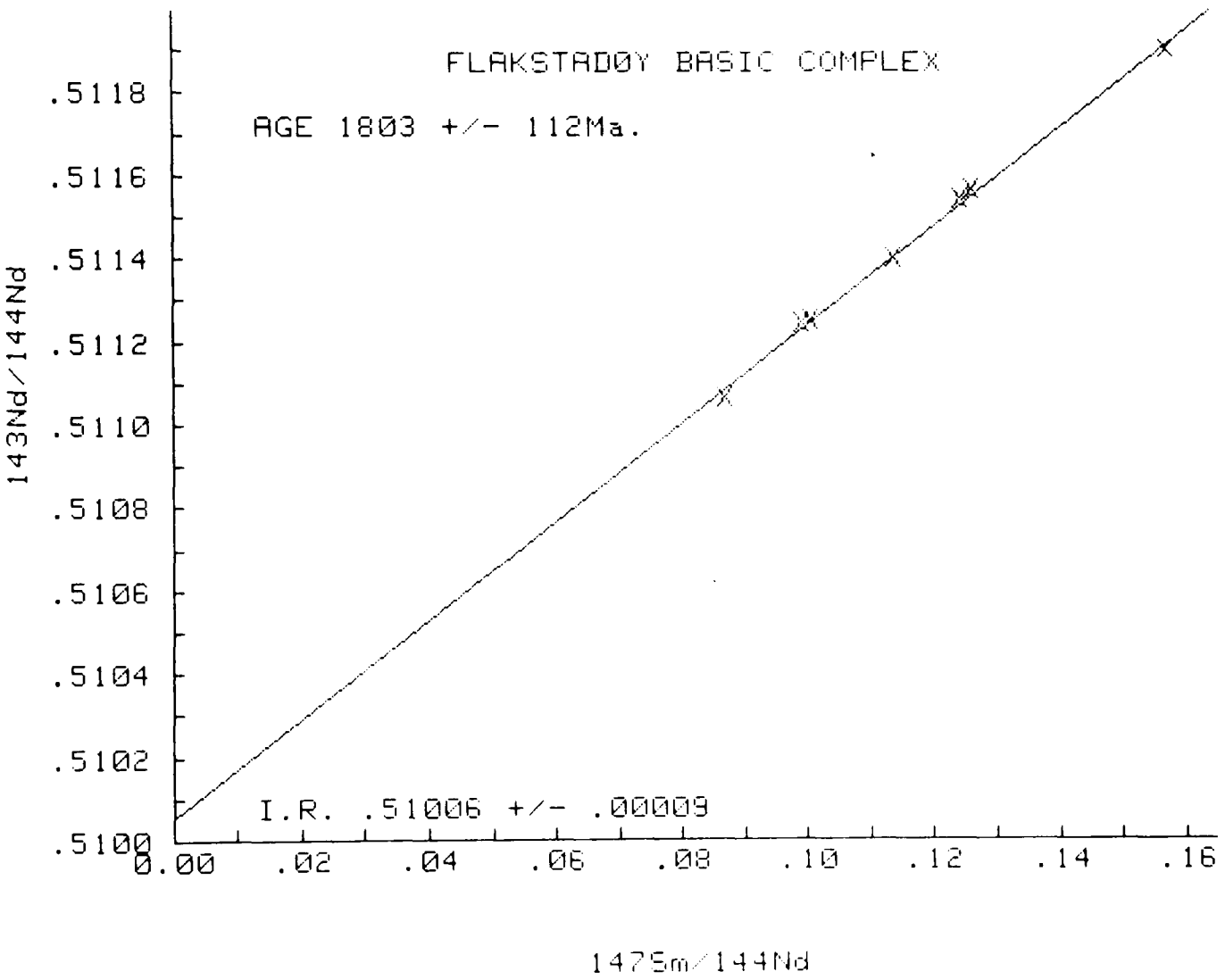
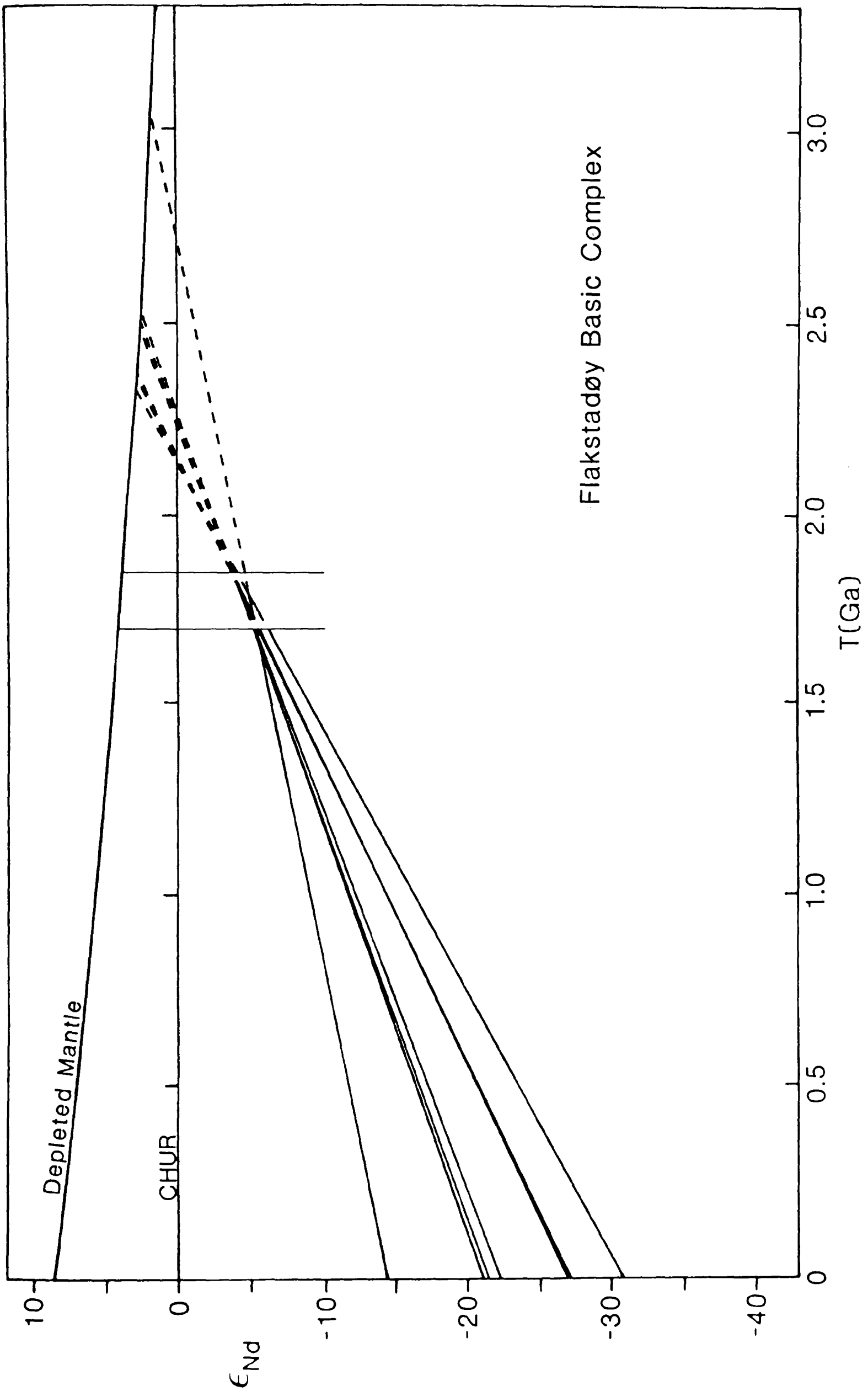


Fig. 5.10.

Sm-Nd evolution diagram for the Flakstadøy Basic Complex. The narrow range of individual ε_{Nd} values at 1.8Ga (-4.3 to -5.1) is a consequence of the homogeneity of $^{143}Nd/^{144}Nd$ through the intrusion at thattime. The ε_{Nd} values indicate the necessity for an ancient crustal component in the basic magma. The wide range of Sm/Nd ratios, which enable the determination of the Sm-Nd whole-rock isochron age, is shown by the different slopes of the evolution lines. The vertical lines define the age range 1.7 - 1.85Ga.


Flakstadøy Basic Complex
Depleted Mantle
CHUR
ϵ_{Nd}
10
0
-10
-20
-30
-40
0
0.5
1.0
1.5
2.0
2.5
3.0
T(Ga)

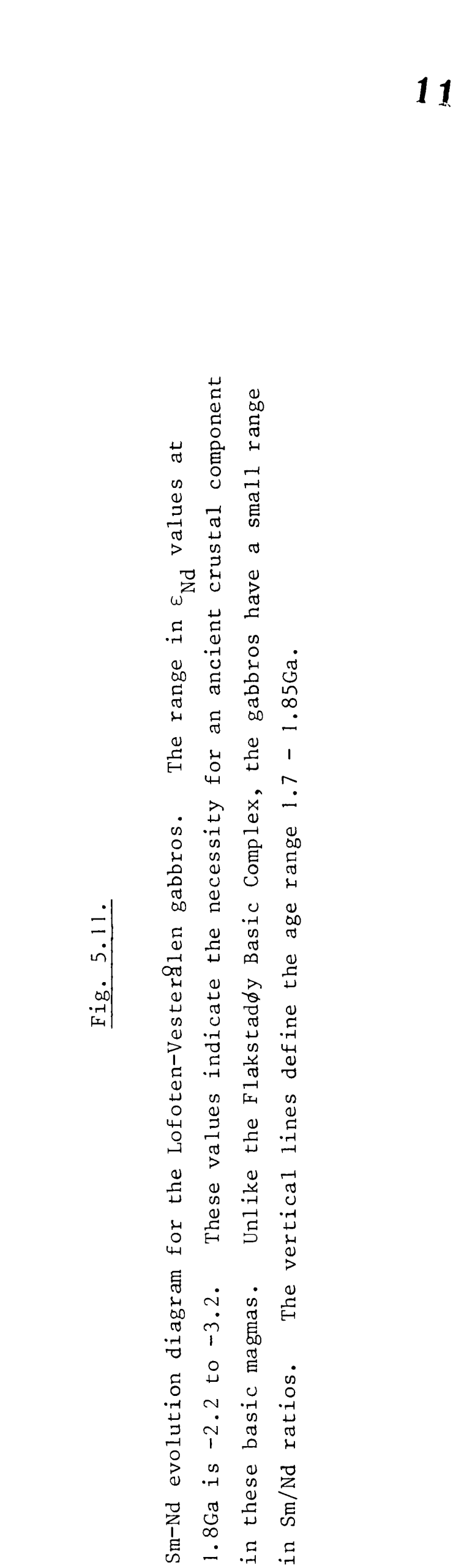


Fig. 5.11. Sm-Nd evolution diagram for the Lofoten-Vesterålen gabbros. The range in ε_{Nd} values at 1.8Ga is -2.2 to -3.2. These values indicate the necessity for an ancient crustal component in these basic magmas. Unlike the Flakstadøy Basic Complex, the gabbros have a small range in Sm/Nd ratios. The vertical lines define the age range 1.7 - 1.85Ga.

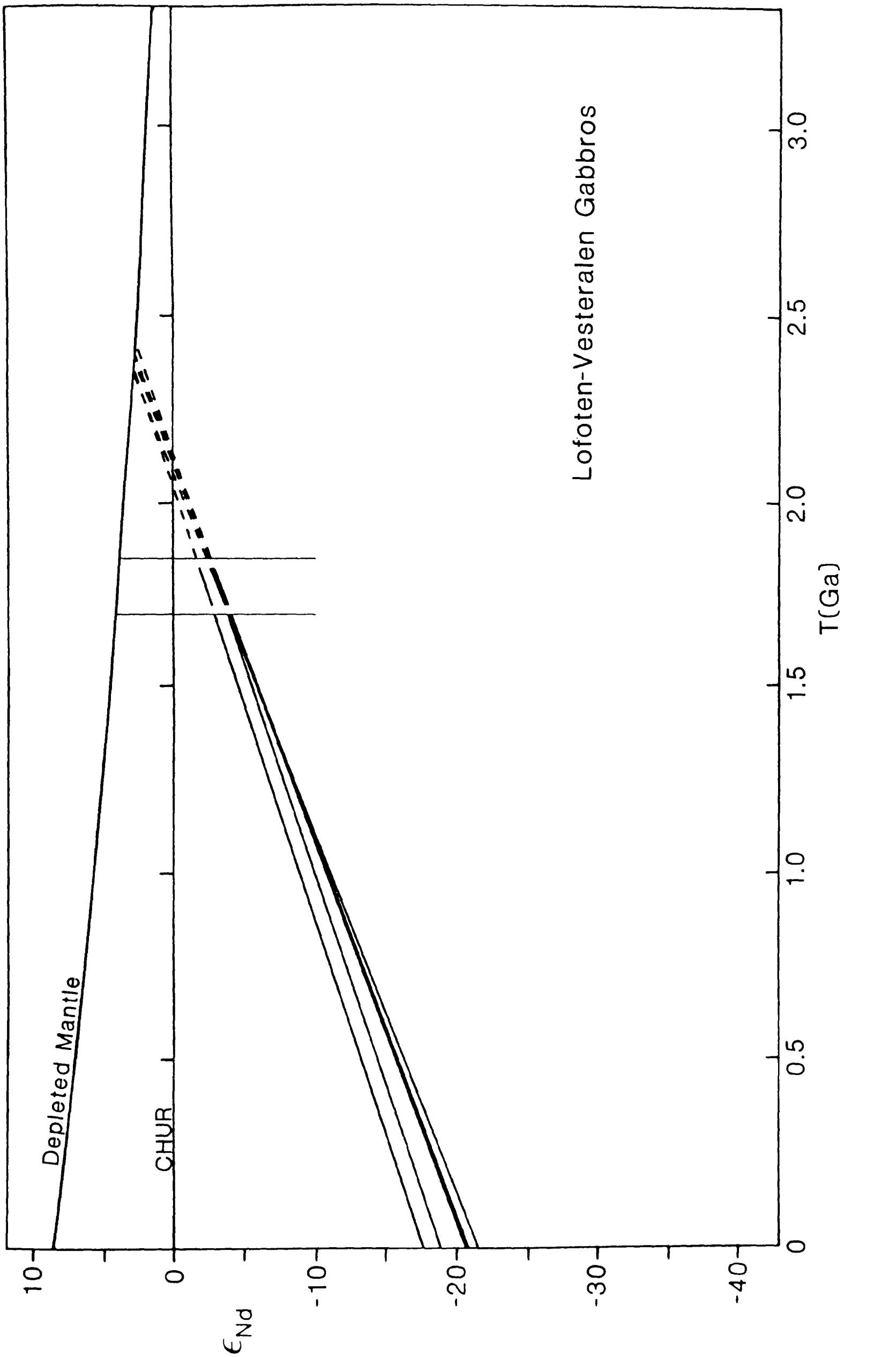

Lofoten-Vesteralen Gabbros
Depleted Mantle
CHUR
ϵ_{Nd}
10
0
-10
-20
-30
-40
0
0.5
1.0
1.5
2.0
2.5
3.0
T(Ga)

Fig. 5.12.

$^{207}Pb/^{204}Pb$ v. $^{206}Pb/^{204}Pb$ diagram for the Flakstadøy Basic Complex showing two samples plotting very close to the 1.8Ga first-stage isochron. Any finite μ value for these samples would rule out their formation by simple extraction from the mantle at 1.8Ga. The data-points are consistent with the formation of the basic magmas by extraction from the mantle at 1.8Ga and contaminated by late Archaean migmatitic gneisses. The two parallel 1.8Ga model isochrons are for melting of mean North-West Hinnøy amphibolite-facies gneisses and for rocks derived from the mantle $\mu_1 = 7.9$) at 1.8Ga.

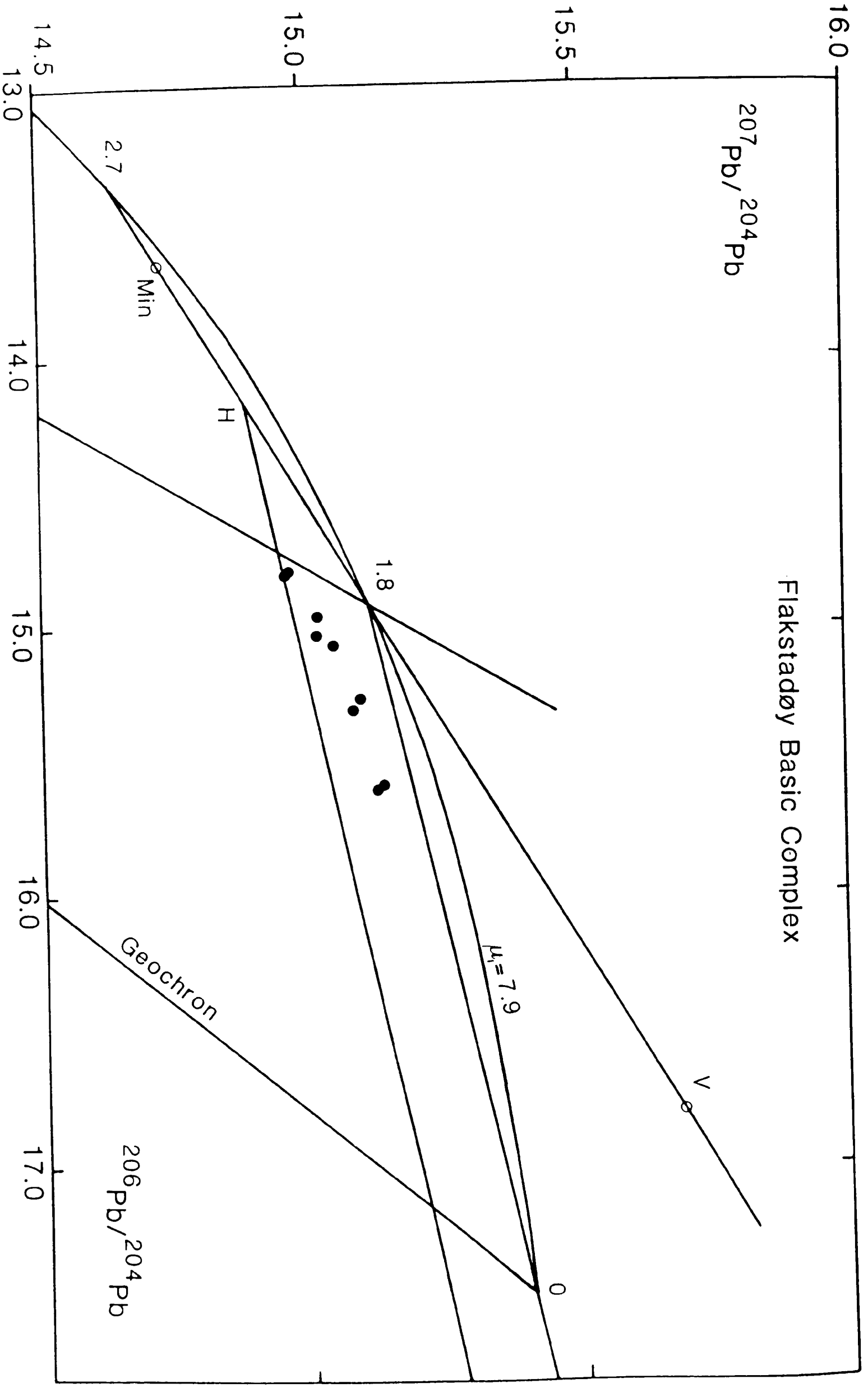
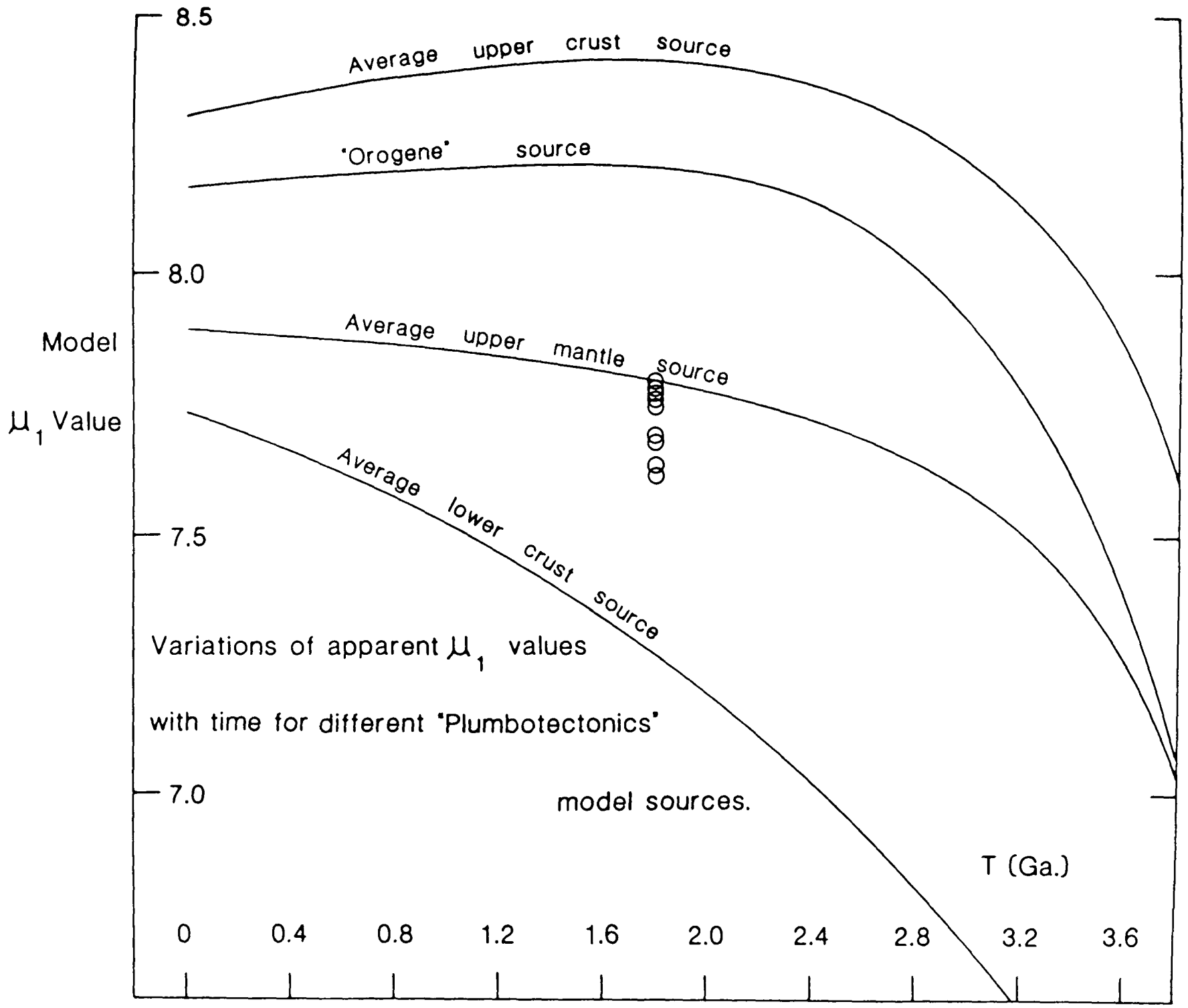

Flakstadøy Basic Complex
$^{207}Pb/^{204}Pb$
$^{206}Pb/^{204}Pb$
16.0
15.5
15.0
14.5
13.0
14.0
15.0
16.0
17.0
2.7
Min
H
1.8
μ_1=7.9
V
0
Geochron

Fig. 5.13.

Model μ_1 v. T for the Flakstadøy Basic Complex showing the evolution of model μ_1 with time in "orogene", upper crust, lower crust and upper mantle (Plumbotectonics model of Zartman and Doe (1981)). This model confirms that the rocks of the Flakstadøy Basic Complex were derived from an upper mantle source and contaminated with different amounts of material from a lower crustal source. The Napp gabbro sample, WL317, has the greater lower crustal component in this model.


8.5
8.0
7.5
7.0
Model
μ_1 Value
Average upper crust source
"Orogene" source
Average upper mantle source
Average lower crust source
Variations of apparent μ_1 values
with time for different "Plumbotectonics"
model sources.
T (Ga.)
0
0.4
0.8
1.2
1.6
2.0
2.4
2.8
3.2
3.6

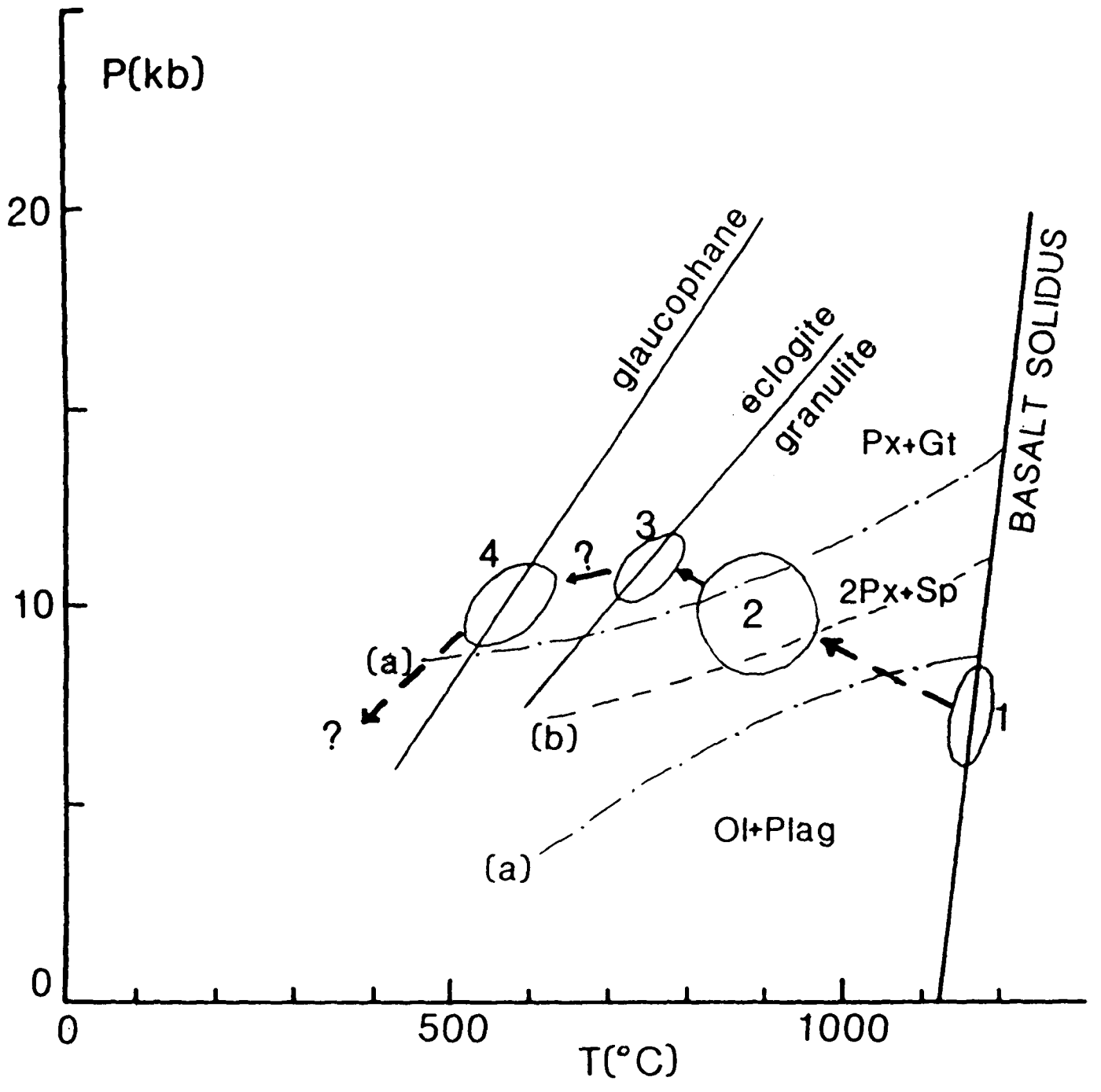


Fig. 5.14. Possible P,T, t path (arrows) for the basic rocks of the Lofoten-Vesterålen province, based upon (see Section 5.5.2):

1. Primary magmatic mineral assemblages;
2. Corona development;
3. Eclogite-facies Assemblages in shear zones;
4. Presence of glaucophane.

Phase boundaries (a) from Herzberg (1978) separate fields of Px + Gt, 2Px + Sp and Ol + Plag. Curve (t) suggests displacement of 2Px + Sp = Px + Gt equilibrium to lower P in Fe-rich compositions. The glaucophane stability field is for a water-deficient system (Maresch, 1977). (After Austrheim and Griffin, 1982).

Plate 6.1. Ultramylonite breccia in the Ølkona Mangerite, Moskenesøy. Ultramylonites are also common in the migmatites adjacent to the mangerite.

Plate 6.2. 80 x 35cm xenolith in the Ølkona Mangerite, Moskenesøy. Xenoliths of material more mafic than the mangerite host, possibly from the dioritic parts of the late Archaean migmatites, are quite common in this mangerite; they are typically well-rounded and have diffuse margins.





Plate 6.3. Orthopyroxene + plagioclase → garnet + quartz (x 40); from WL303 from the Sund Mangerite, South-West Flakstadøy. The garnet corona-forming reactions have been interpreted by Griffin and Heier (1969) as retrograde reactions occurring with falling T at constant P.

Plate 6.4. Exsolution/unmixing of mesoperthite (x 40) to plagioclase and orthoclase domains during recrystallization to amphibolite-facies assemblages as described by Griffin and Heier (1969). From WL403, a sample from the South-West Lofoten Mangerite on Vestvågøy. (See also Plate 6.21).

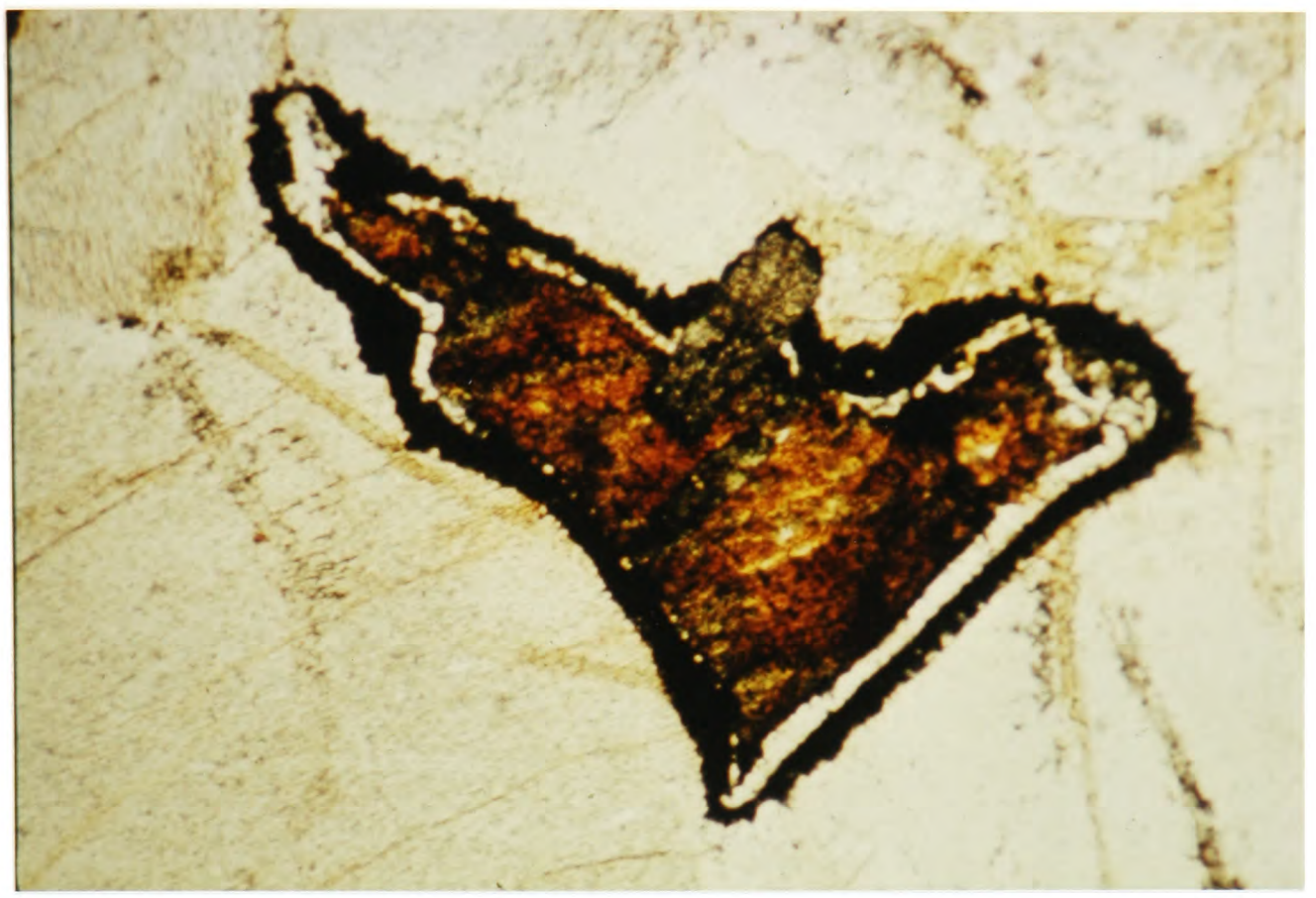
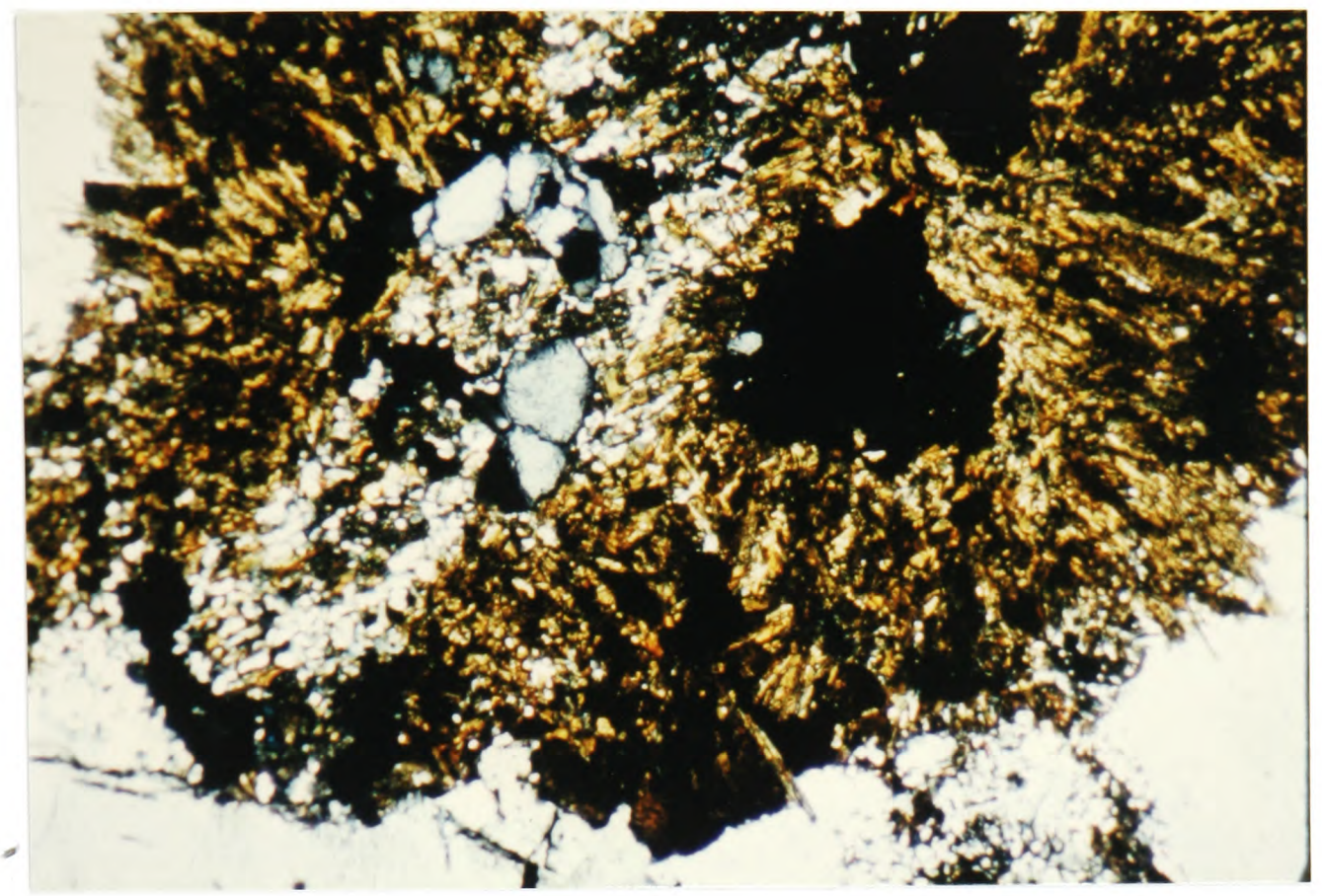




Plate 6.5. Hornblende-quartz-biotite pseudomorph after pyroxene (x 40) from WL404 from the South-West Lofoten Mangerite on Vestvågøy. This reaction involves hydration-retrogression.

Plate 6.6. Orthopyroxene + plagioclase → hornblende and quartz (x 40); from WL410 from the South-West Lofoten Mangerite on Vestvågøy. This reaction involves hydration-retrogression.



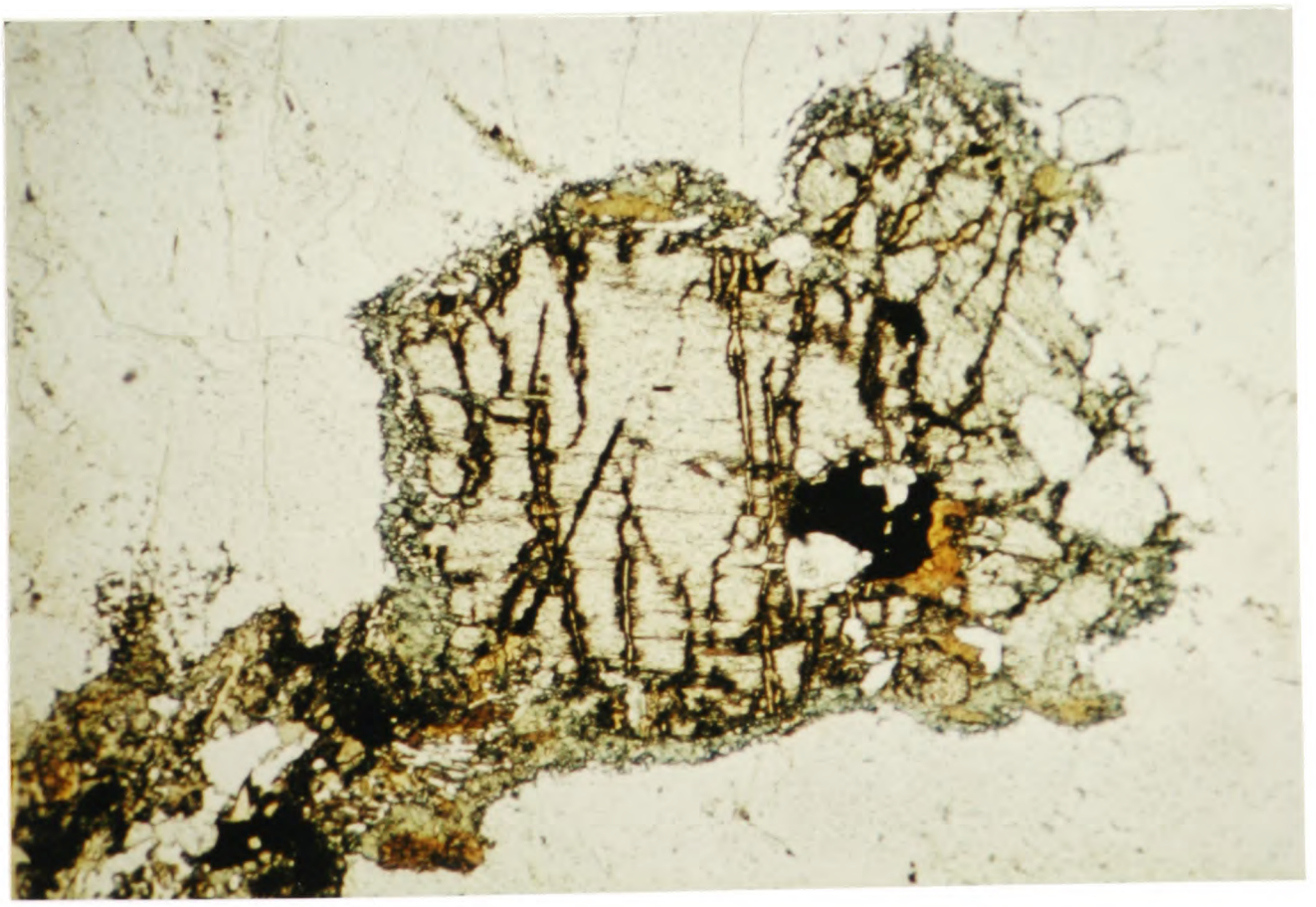


Plate 6.7. Opaques + plagioclase → biotite (x 60); from WL401 from the South-West Lofoten Mangerite on Vestvågøy. Biotite plates up to 0.1mm long growing perpendicular to the margin of an opaque crystal.

Plate 6.8. 50 x 25cm xenolith (WL471) in the South-West Lofoten Mangerite near Stamsund, Vestvågøy. The only xenoliths observed in this mangerite are present near Stamsund. They are typically well-rounded, fine-grained and darker than the mangerite host rock. The xenolith illustrated may belong to the early Proterozoic supracrustal gneisses.

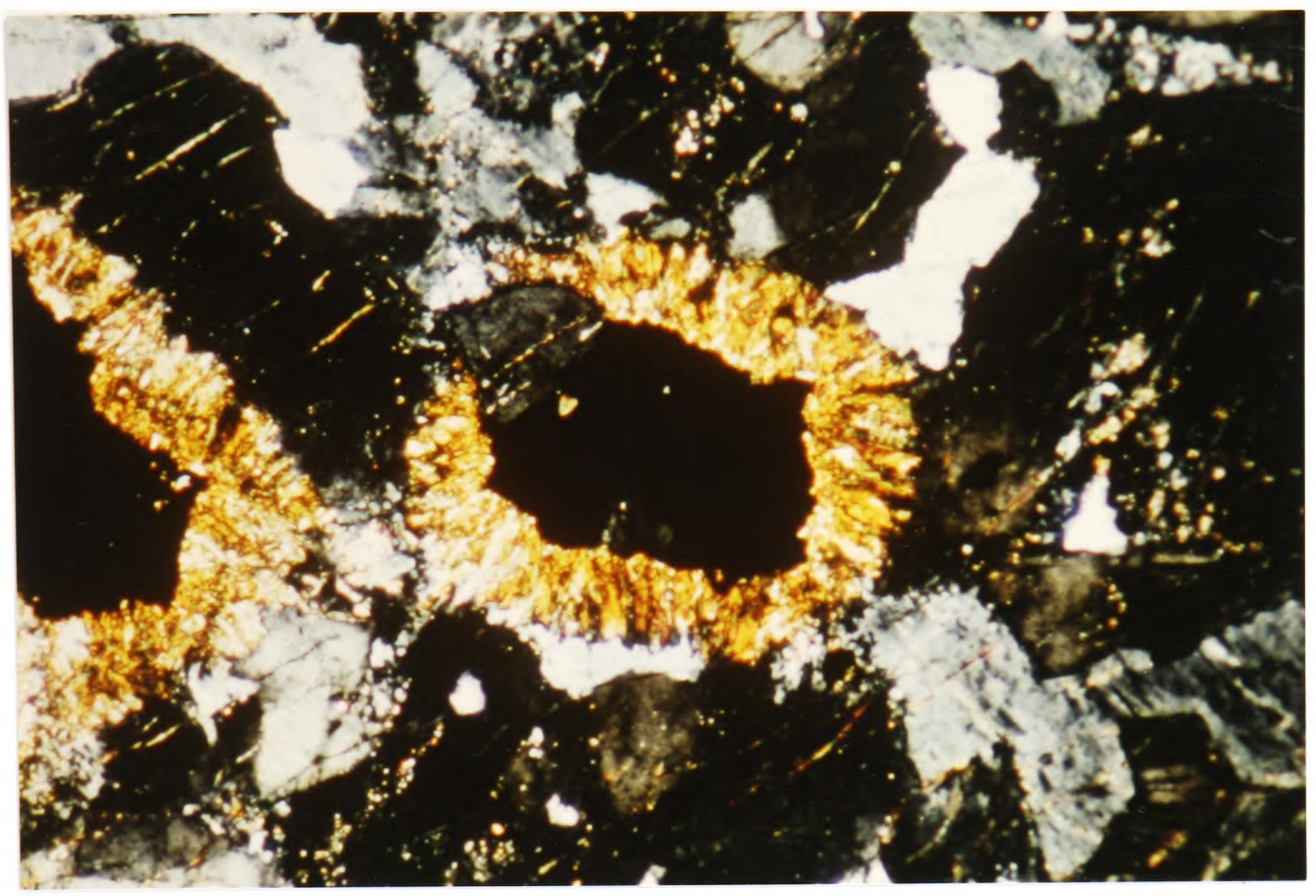




Plate 6.9. Pyroxenite and magnetite-rich layers up to 40cm thick which dip steeply north towards the centre of the Hopen Mangerite/Charnockite. These rocks are typically gabbroic in composition and are marginal to the Hopen intrusion against the Festvåg Migmatites, South-West Austvågøy. Apatite, ilmenite and magnetite are cumulus phases in these rocks as well as pyroxenite phases.

Plate 6.10. Erosional unconformity in the layered marginal gabbro to the Hopen Mangerite/Charnockite, near Festvåg, South-West Austvågøy.





Plate 6.11. Breccia of gabbro in mangerite (gabbroic blocks up to 1m across) presumed to have fallen from the mountains to the south-east, south of Rørvik. This may represent a northern marginal gabbroic series to the Hopen intrusion similar to that on the southern margin of the intrusion near Festvåg (Plates 6.9 and 6.10).

Plate 6.12. Polished slab of WL565, a charnockite from the Hopen intrusion with a granular texture of green feldspars, blue-grey quartz and minor opaques and pyroxenes.





Plates 6.13 and 6.14 A large block of mafic rock being broken up by the Hopen Mangerite/Charnockite, 2km north of Festvåg, South-West Austvågøy. Plate 6.14 is a close-up of part of Plate 6.13 and shows how slivers of the xenolith are in the process of incorporation into the mangerite, which is foliated parallel to the margin of the xenolith (see Plate 6.15).





Plate 6.15. Polished slab of WL567, a sample from the mangerite-xenolith margin (Plates 6.13 and 6.14) in the Hopen intrusion, north of Festvåg. Note the foliation in the mangerite which is parallel to the contact with the xenolith. The xenolith is similar to the amphibolites in the Festvåg Migmatites.

Plate 6.16. 25 x 20cm xenolith in the Hopen Mangerite/Charnockite. It is rounded and darker than the host mangeritic rock which has no foliation. It is located 1km north of Festvåg, South-West Austvågøy.



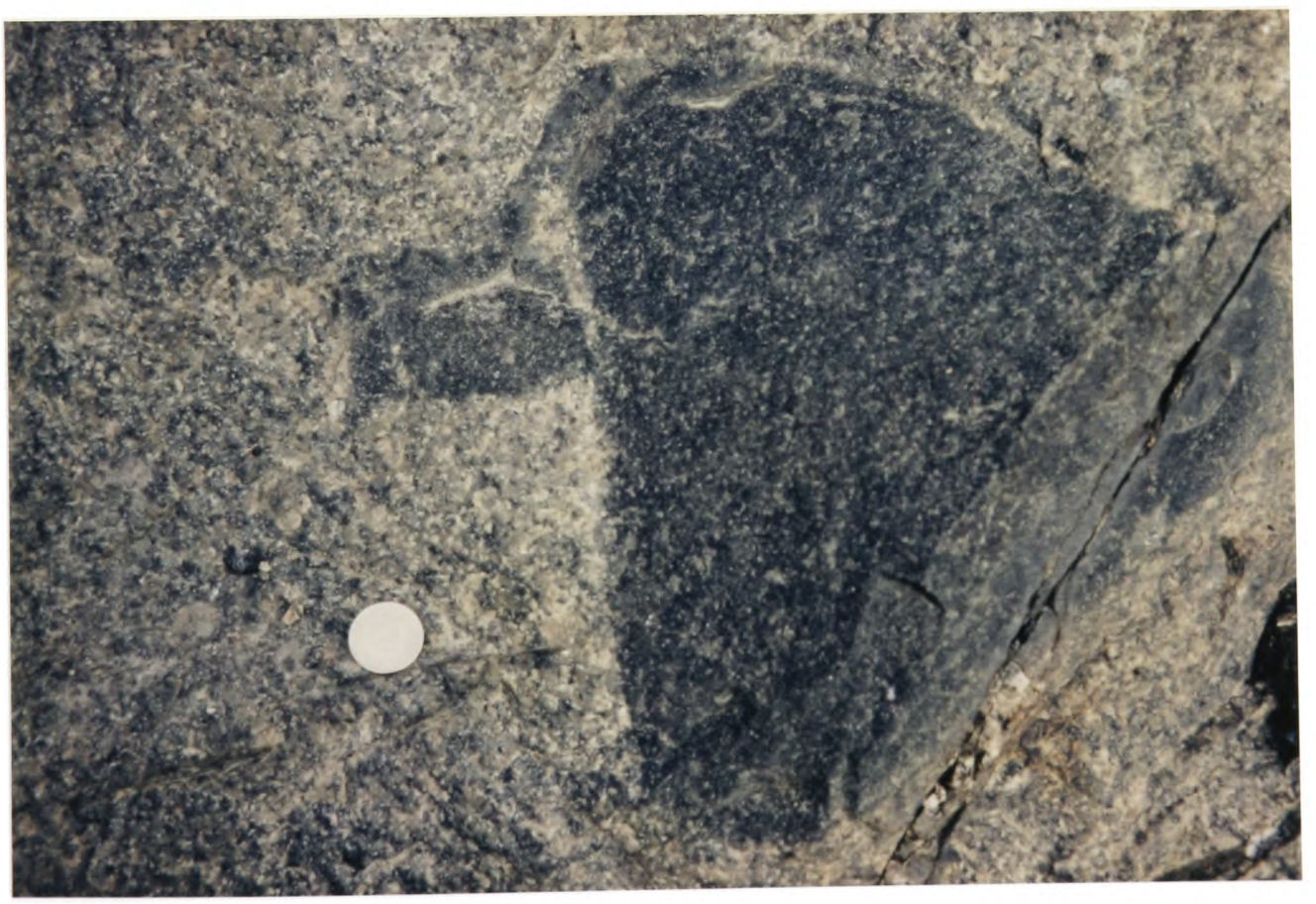
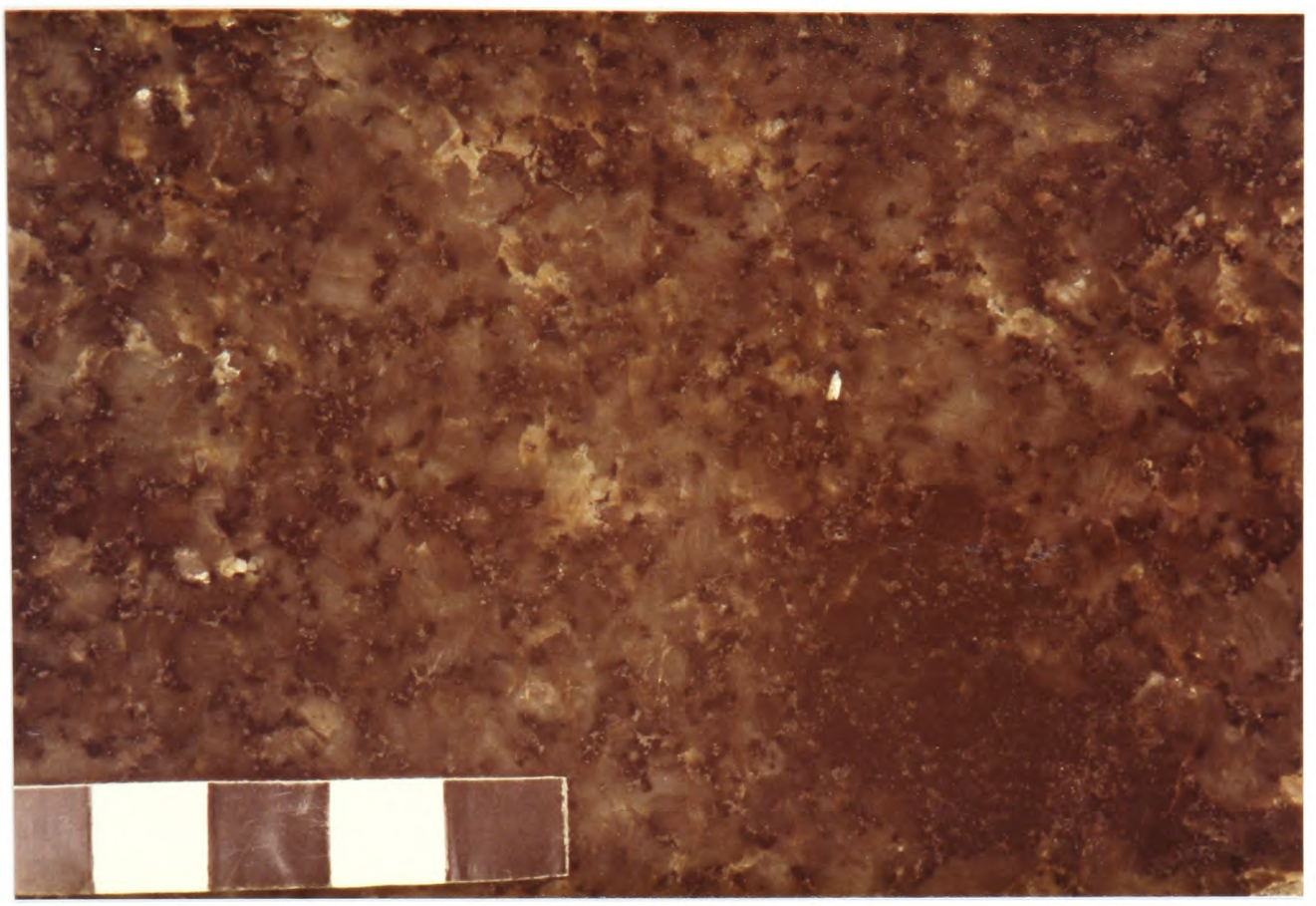


Plate 6.17. Polished slab of WL628, a sample from near Offersøy, Hinnøy, which is typical of the Raftsund Mangerite as a whole. It is dark brown/green, granular, and composed chiefly of blocky mesoperthite crystals with plagioclase and pyroxenes.

Plate 6.18. Polished slab of WL610, a sample from near Tennstrand, Hinnøy, which is typical of the retrograded parts of the Raftsund Mangerite. The feldspars are pale grey or white, and the pyroxenes are altered to hornblende and biotite which occur in aggregates with opaques and garnets, giving the rock a spotted appearance similar to the retrograded mangerites on Vestvågøy and Austvågøy.



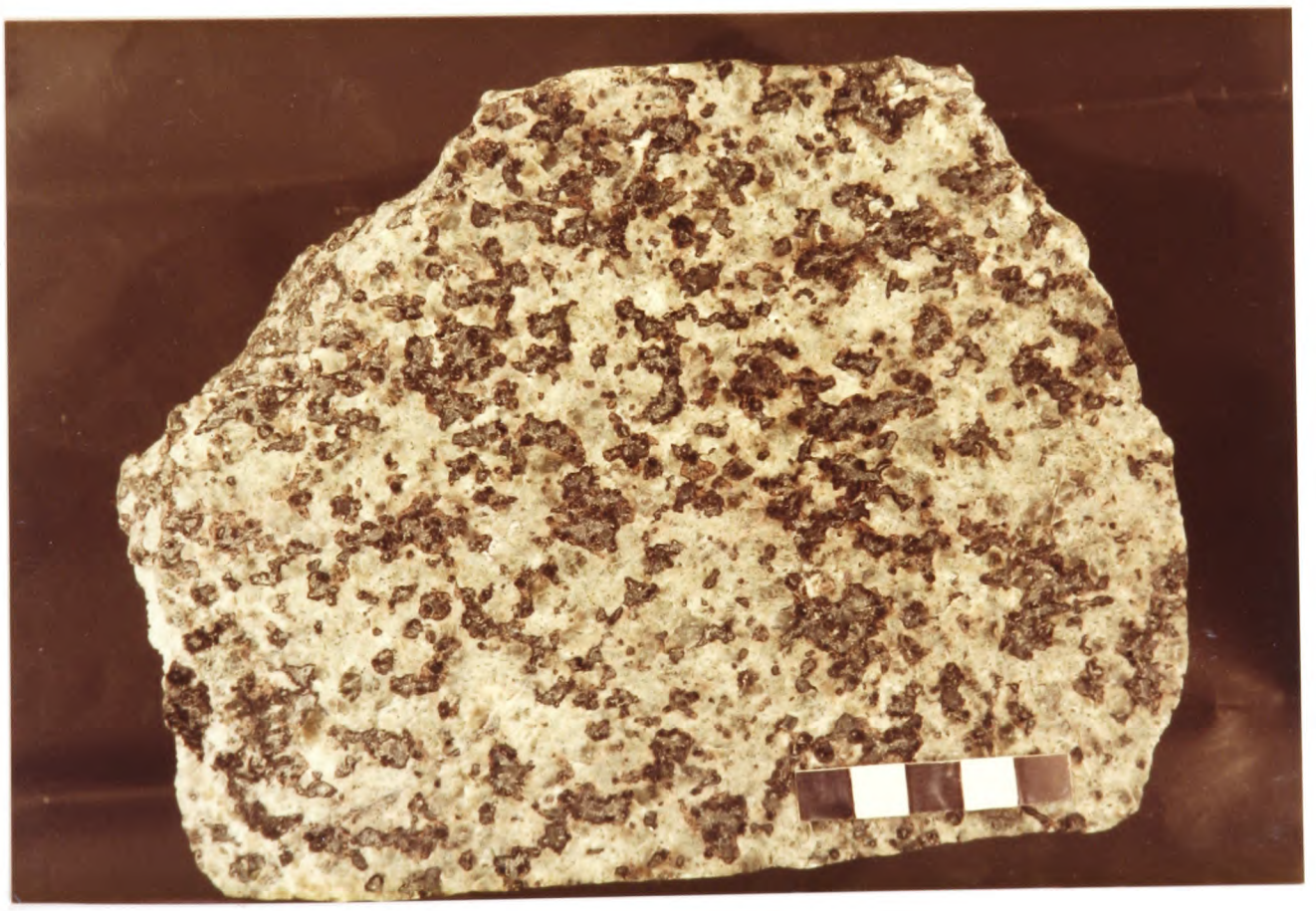


Plate 6.19. A graded channel which scours into homogeneous mangerite on the north side of Tenfjord, Hinnøy. Magmatic-sedimentary features are well-developed in the central parts of the intrusion.

Plate 6.20. Polished slab of WL618, (the top is to the right), a graded mangerite from near Digermulen, Hinnøy, similar to that illustrated in Plate 6.19. This has features in common with the "fine-grained layering" of Griffin et al. (1974).



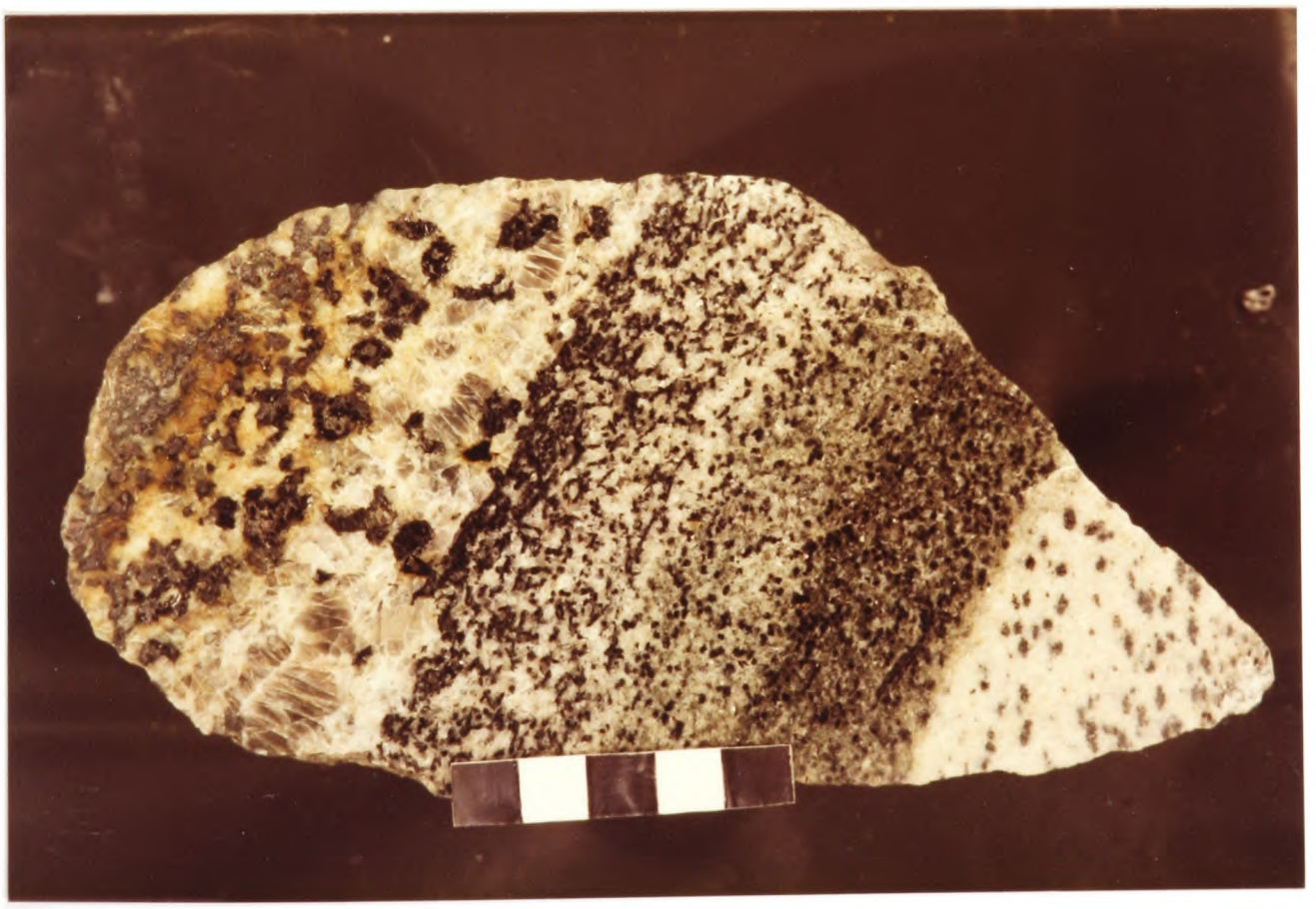
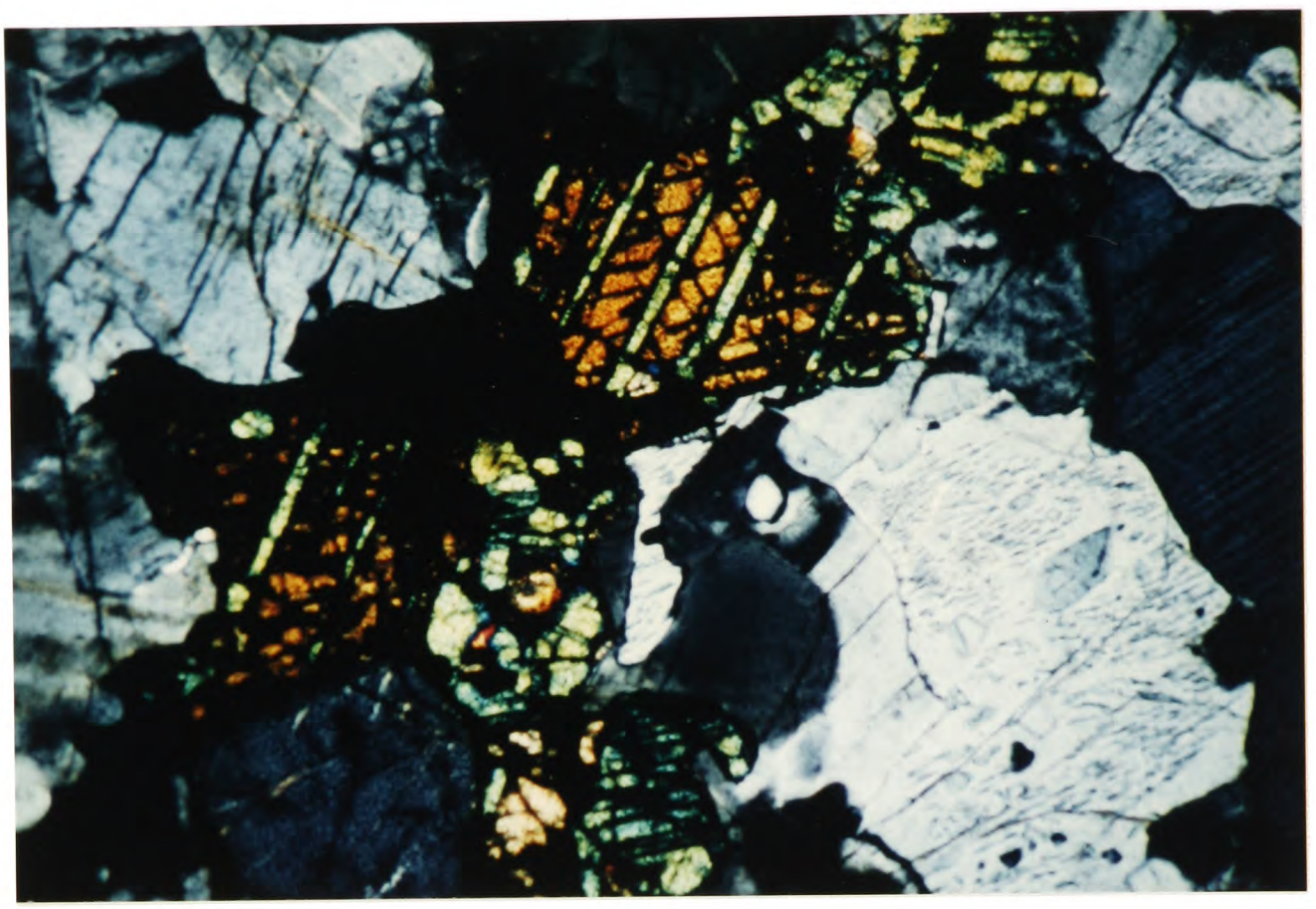


Plate 6.21. Exsolution/unmixing of mesoperthite (x 60) to plagioclase and orthoclase domains during recrystallization to amphibolite-facies assemblages as described by Griffin and Heier (1969). From WL538, a sample from the Raftsund Mangerite on Austvågøy, south of Fiskebøl. (See also Plate 6.4).

Plate 6.22. Broad exsolution lamellae of clinopyroxene in orthopyroxene (x 40) in WL605 from Raften, Hinnøy.



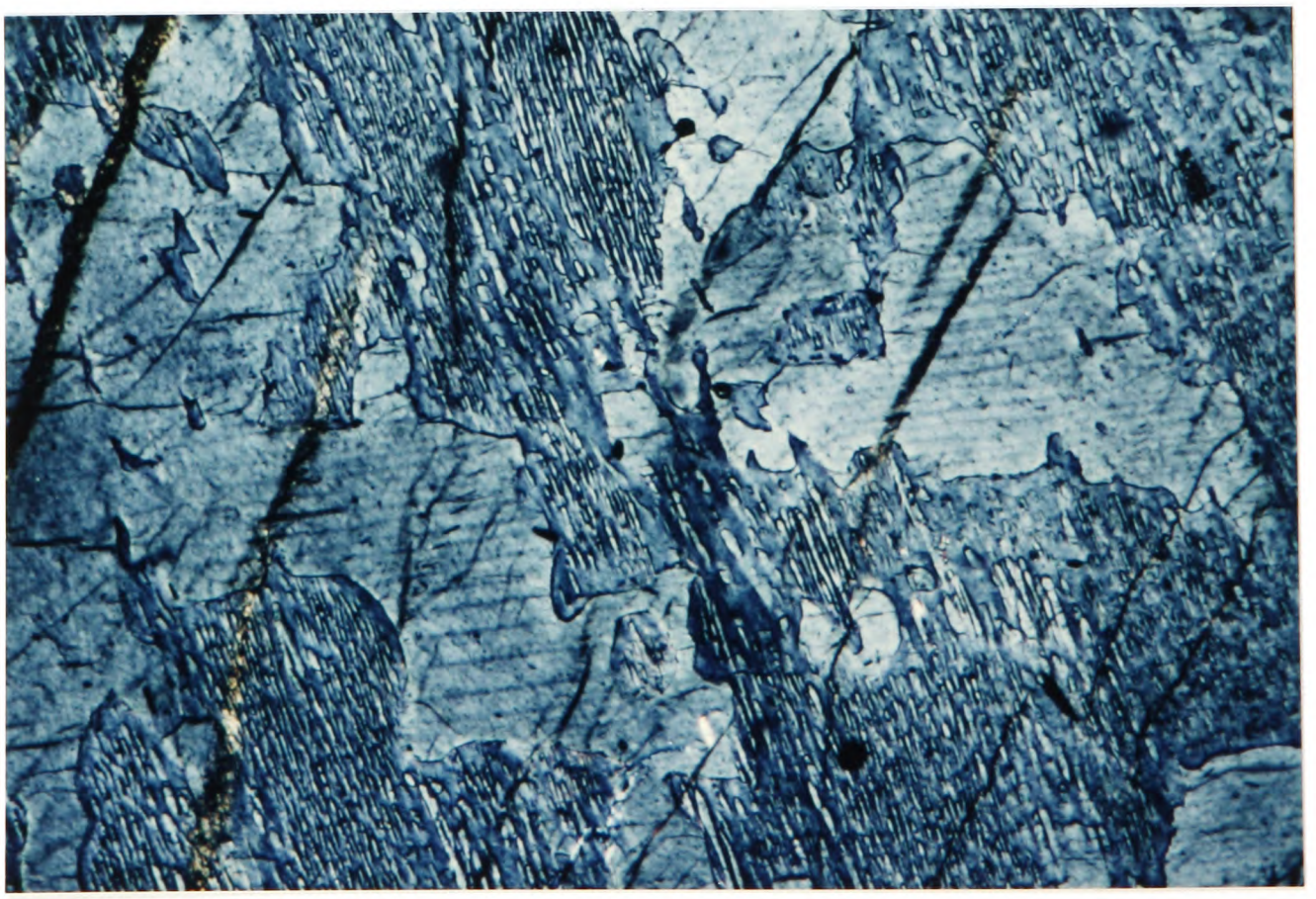


Plate 6.23. Orthopyroxene occurring as a magmatic overgrowth to pale-green clinopyroxene, which contains earlier-formed opaques. From WL538, south of Fiskebøl, Austvågøy. Magmatic hornblende overgrows earlier-formed pyroxenes in some Raftsund Mangerite samples.

Plate 6.24. 5 x 4cm xenolith in the Raftsund Mangerite near Kongsmarken, Hinnøy. The only mangerites with more abundant xenoliths than the Raftsund Mangerite are the Sund Mangerite, the Hopen Mangerite/Charnockite and the Engenykken Mangerite on Langøy. The xenoliths near Kongsmarken are typically well-rounded, some are zoned, some have reaction rims and most are less than 10cm across, all suggesting that the xenoliths have undergone partial assimilation by the mangerite.

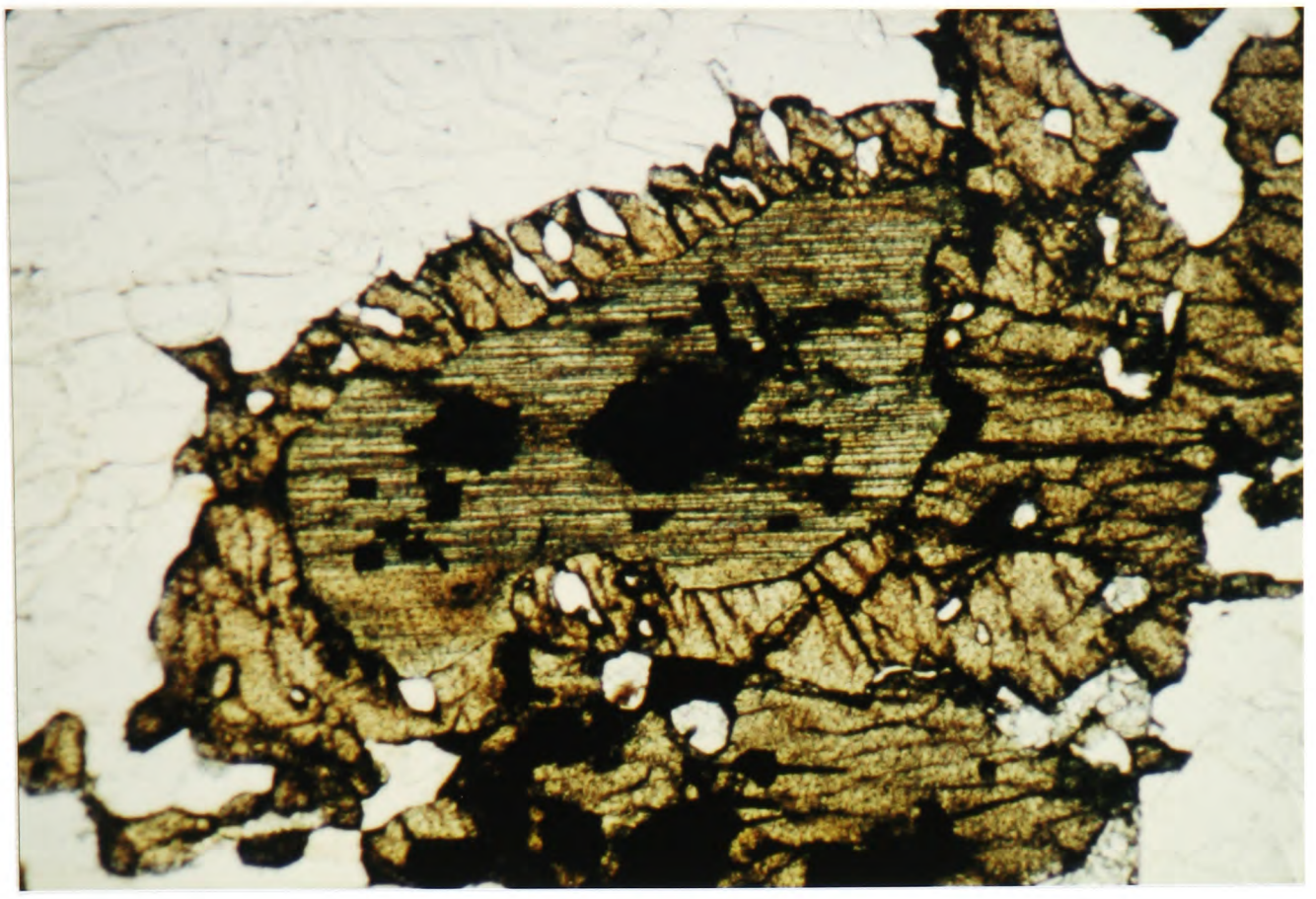




Plate 6.25. Polished slab of a coarsely granophyric charnockite vein (WL720) which is 20cm wide and intrudes the Eidet-Hovden Gabbro at Hovden Harbour, only a few tens of metres from the Hovden Mangerite. These veins suggest that the mangerite post-dates the gabbro, as is also the case on Vestvågøy.



Table 6.1

Major Element Compositions and CIPW Norms for the Sund-Ølkona Mangerite

	Ølkona, Moskenesøy			Sund, Flakstadøy	
	WL202	WL204	WL219	WL302	WL335
SiO_2	61.40	61.90	62.77	70.16	65.20
Al_2O_3	20.73	17.60	16.95	14.10	15.75
TiO_2	0.04	1.04	0.30	0.31	0.39
Fe_2O_3	1.53	3.62	2.91	3.49	6.41
MgO	0.97	0.76	1.45	0.06	0.60
CaO	5.27	2.47	2.79	0.86	1.15
Na_2O	7.68	4.45	3.28	4.87	4.30
K_2O	1.73	7.50	8.96	5.28	5.66
MnO	0.06	0.09	0.09	0.10	0.16
P_2O_5	0.10	0.22	0.24	0.02	0.05
LOI	0.49	0.31	0.60	0.66	0.28
Total	99.99	99.98	100.34	99.90	99.95
Norms calculated with $Fe^{3+}/Fe^{3+} + Fe^{2+} = 0.10$					
Q	-	2.46	3.28	20.08	14.03
Or	10.22	44.32	52.95	31.20	33.45
Ab	64.52	37.66	27.76	41.21	36.39
An	16.98	5.90	5.06	1.02	4.30
Ne	0.25	-	-	-	-
C	-	-	-	-	0.97
Cc	0.87	0.55	1.07	1.17	0.50
Di	5.34	3.00	3.95	0.50	-
Hy	-	1.25	3.27	1.83	5.32
Ol	0.63	-	-	-	-
Mt	0.24	0.55	0.45	0.54	0.98
Il	0.08	1.97	0.57	0.59	0.74
Ap	0.22	0.48	0.52	0.04	0.11
Plag(An_x)	33	23	26	4	18
Mg/Mg+Fe*	0.75	0.75	0.75	0.09	0.34

*for ferromagnesian minerals

Table 6.2

Major Element Compositions and CIPW Norms for the Flakstadøy Charnockite and for the South-West Lofoten Mangerite on Flakstadøy

	Flakstadøy Charnockite	South-West Lofoten Mangerite					
	WL306	WL307	WL309	WL315	WL316	WL319	WL331
SiO_2	73.34	55.99	54.06	52.24	55.62	62.67	59.03
Al_2O_3	14.11	16.42	15.37	15.94	18.68	18.44	17.93
TiO_2	0.24	1.65	1.92	1.10	0.96	0.63	1.13
Fe_2O3	1.87	8.70	10.65	11.44	7.49	3.41	5.53
MgO	0.38	2.21	2.72	5.11	2.65	0.69	1.28
CaO	1.35	4.59	5.22	7.75	6.12	1.73	3.46
Na_2O	3.75	4.94	4.59	3.86	4.65	5.48	5.25
K_2O	4.94	4.28	3.64	1.59	2.85	6.18	5.00
MnO	0.05	0.18	0.22	0.18	0.13	0.12	0.15
P_2O_5	0.05	0.83	1.19	0.55	0.42	0.25	0.45
LOI	0.24	0.24	0.26	0.36	0.41	0.33	0.14
Total	100.32	100.01	99.84	100.12	99.98	99.94	99.35
Norms calculated with $Fe^{3+}/Fe^{3+} + Fe^{2+} = 0.10$							
Q	29.28	0.37	1.48	1.48	1.79	3.02	1.29
Or	29.19	25.29	21.51	9.40	16.84	36.52	29.55
Ab	31.73	41.80	38.84	32.66	39.35	46.37	44.43
An	5.44	9.99	10.59	21.48	21.68	5.68	10.59
C	0.60	-	-	-	-	0.66	-
Cc	0.43	0.43	0.46	0.64	0.73	0.59	0.25
Di	-	5.24	5.33	9.70	3.53	-	2.52
Hy	1.86	6.25	8.37	14.05	8.44	3.11	3.97
Ol	-	-	-	-	-	-	-
Mt	0.29	1.32	1.62	1.72	1.13	0.53	0.85
Il	0.46	3.13	3.64	2.09	1.82	1.20	2.14
Ap	0.11	1.81	2.60	1.20	0.92	0.55	0.98
Plag(An_x)	24	31	34	55	51	19	31
Mg/Mg+Fe*	0.58	0.69	0.68	0.74	0.71	0.62	0.68

*for ferromagnesian minerals

Table 6.3

Major Element Compositions and CIPW Norms for the South-West Lofoten Mangerite on Vestvågøy

	WL401	WL404	WL405	WL410	WL416
SiO_2	59.12	61.08	57.72	54.46	56.17
Al_2O_3	18.22	17.93	16.57	18.18	18.79
TiO_2	1.23	0.93	1.43	0.73	1.09
Fe_2O_3	5.21	4.21	7.41	8.12	6.84
MgO	1.32	0.99	1.78	3.92	2.14
CaO	3.70	2.21	3.78	7.64	4.44
Na_2O	5.20	5.18	4.96	4.30	5.07
K_2O	4.66	6.16	5.05	1.63	4.34
MnO	0.11	0.11	0.17	0.14	0.12
P_2O_5	0.52	0.30	0.73	0.30	0.43
LOI	0.78	0.95	0.30	0.28	0.53
Total	100.08	100.05	99.89	99.70	99.95
	Norms calculated with $Fe^{3+}/Fe^{3+} + Fe^{2+} = 0.10$				
Q	3.19	2.95	1.11	2.34	-
Or	27.54	36.40	29.84	9.63	25.65
Ab	44.00	43.83	41.97	36.39	42.90
An	11.95	5.34	8.03	25.49	15.70
C	0.24	0.78	-	-	-
Cc	1.39	1.69	0.53	0.50	0.94
Di	-	-	3.91	7.57	1.20
Hy	4.86	3.88	5.32	10.48	2.02
Ol	-	-	-	-	4.09
Mt	0.79	0.65	1.13	1.22	1.03
Il	2.33	1.76	2.71	1.38	2.07
Ap	1.14	0.66	1.60	0.66	0.94
Plag(An_x)	34	19	27	57	41
Mg/Mg+Fe*	0.73	0.70	0.68	0.75	0.71

*for ferromagnesian minerals

Table 6.4

Major Element Compositions and CIPW Norms for the Hopen Mangerite/Charnockite

	WL508	WL514	WL516	WL517	WL570	WL575
SiO_2	67.94	72.71	65.41	62.79	72.28	76.62
Al_2O_3	13.86	12.87	16.80	17.82	12.55	11.02
TiO_2	0.63	0.42	0.52	0.61	0.43	0.32
Fe_2O_3	5.04	3.67	4.02	4.34	4.37	2.95
MgO	0.63	0.23	0.37	0.37	0.07	0.13
CaO	1.68	0.85	1.83	2.52	0.82	0.89
Na_2O	4.47	4.14	5.01	6.43	4.19	3.50
K_2O	4.91	5.04	5.85	4.17	5.15	4.39
MnO	0.09	0.09	0.09	0.06	0.08	0.05
P_2O5	0.16	0.05	0.09	0.08	0.01	0.00
LOI	0.45	0.34	0.45	0.54	0.17	0.50
Total	99.85	100.41	100.44	99.73	100.12	100.38
Norms calculated with $Fe^{3+}/Fe^{3+} + Fe^{2+} = 0.05$						
Q	19.00	27.09	9.50	4.07	26.10	37.63
Or	29.02	29.79	34.57	24.64	30.44	25.94
Ab	37.83	35.03	42.40	54.41	35.46	29.62
An	3.25	1.65	6.08	7.45	0.23	1.39
C	-	-	-	-	-	-
Cc	0.80	0.60	0.80	0.96	0.30	0.89
Do	1.94	0.80	0.63	2.09	2.75	0.95
Hy	3.45	2.35	2.88	2.18	1.40	1.58
Ol	-	-	-	-	-	-
Mt	0.38	0.28	0.31	0.32	0.33	0.22
Il	1.20	0.80	0.99	1.16	0.82	0.61
Ap	0.35	0.11	0.17	0.17	0.02	-
Plag(An_X)	14	8	21	21	1	8
Mg/Mg+Fe*	0.42	0.26	0.35	0.34	0.08	0.20

*for ferromagnesian minerals

Table 6.5

Major Element Compositions and CIPW Norms for the Austvågøy Grey Mangerite

	WL522	WL526	WL533
SiO_2	62.58	71.60	59.57
Al_2O3	16.30	13.48	16.21
TiO_2	0.66	0.34	0.98
Fe_2O_3	6.06	3.48	7.68
MgO	0.32	0.19	1.71
CaO	1.75	0.85	3.78
Na_2O	4.78	4.47	4.40
K_2O	6.63	5.03	4.69
MnO	0.08	0.05	0.11
P_2O_5	0.09	0.04	0.40
LOI	0.37	0.56	0.42
Total	99.60	100.09	99.95
Norms calculated with $Fe^{3+}/Fe^{3+} + Fe^{2+} = 0.10$			
Q	5.36	24.46	6.39
Or	39.18	29.73	27.72
Ab	40.45	37.83	37.23
An	3.44	1.79	10.63
C	-	0.02	-
Cc	0.66	1.00	0.75
Di	2.78	-	3.20
Hy	2.40	2.29	6.30
Ol	-	-	-
Mt	0.90	0.52	1.15
Il	1.25	0.64	1.86
Ap	0.20	0.09	0.87
Plag(An_x)	14	8	35
Mg/Mg+Fe*	0.26	0.26	0.61

*for ferromagnesian minerals

Table 6.6

Major Element Compositions and CIPW Norms for the Raftsund Mangerite

	Hamarøy	Austvågøy	Hinnøy			
	WL101	WL539	WL604	WL606	WL607	WL628
SiO_2	58.63	60.05	57.61	59.78	51.52	60.40
Al_2O_3	16.27	18.24	17.88	18.57	14.28	15.59
TiO_2	1.16	0.78	1.31	0.81	2.42	0.90
Fe_2O_3	8.23	5.20	7.19	4.91	13.63	8.69
MgO	0.77	0.58	1.08	0.65	2.81	0.47
CaO	3.51	3.01	4.09	3.22	5.50	2.58
Na_2O	5.09	5.55	4.79	5.36	4.21	4.77
K_2O	4.76	5.40	4.85	5.44	3.56	5.96
MnO	0.22	0.13	0.14	0.11	0.27	0.28
P_2O_5	0.39	0.29	0.67	0.36	1.47	0.20
LOI	0.45	0.24	0.04	0.22	0.20	0.04
Total	99.49	99.47	99.66	99.44	99.86	99.88
Norms calculated with $Fe^{3+}/Fe^{3+} + Fe^{2+} = 0.05$						
Q	3.12	0.42	1.81	0.64	0.50	3.45
Or	28.13	31.91	28.66	32.15	21.04	35.22
Ab	43.07	46.96	40.53	45.36	35.63	40.36
An	7.49	8.91	12.96	10.54	9.55	3.53
C	-	-	-	-	-	-
Cc	0.80	0.43	0.07	0.39	0.36	0.07
Di	4.80	2.71	2.34	1.87	6.08	6.77
Hy	4.04	2.87	4.94	3.17	10.58	3.10
Ol	-	-	-	-	-	-
Mt	0.63	0.40	0.54	0.37	1.03	0.68
Il	2.20	1.48	2.49	1.54	4.59	1.71
Ap	0.85	0.63	1.46	0.79	3.21	0.44
Plag(An_x)	25	26	38	30	34	14
Mg/Mg+Fe*	0.36	0.40	0.46	0.46	0.58	0.22

*for ferromagnesian minerals

Table 6.7

Major Element Compositions and CIPW Norms for the Langøy Mangerites

	Hovden		Steine		Søberg	Eidsfjord
	WL703	WL707	WL713	WL714	WL715	WL732
SiO_2	60.67	60.87	57.98	58.24	56.97	51.55
Al_2O_3	19.52	19.03	19.71	19.87	18.54	16.12
TiO_2	0.65	0.78	0.79	0.77	0.95	2.10
Fe_2O_3	3.37	3.96	5.21	4.79	6.79	12.36
MgO	0.66	0.74	1.47	1.44	1.83	3.10
CaO	3.31	3.00	4.53	4.16	5.06	6.43
Na_2O	5.76	5.48	5.44	5.48	5.28	4.28
K_2O	5.15	5.82	4.08	4.18	3.11	2.37
MnO	0.07	0.07	0.09	0.10	0.07	0.18
P_2O_5	0.28	0.29	0.26	0.22	0.37	1.08
LOI	0.41	0.40	0.55	0.49	1.48	0.09
Total	99.87	100.45	100.10	99.74	100.45	99.66
Norms calculated with $Fe^{3+}/Fe^{3+} + Fe^{2+} = 0.10$						
Q	0.45	0.30	-	-	2.92	1.57
Or	30.44	34.39	24.11	24.70	18.38	14.01
Ab	48.74	46.37	46.03	46.37	44.68	36.22
An	12.20	10.14	17.31	17.27	16.98	17.77
C	-	-	-	-	0.27	-
Cc	0.73	0.71	0.98	0.87	2.63	0.17
Do	0.67	1.07	1.09	0.03	-	5.49
Hy	2.57	2.75	4.39	4.95	7.58	10.01
Ol	-	-	0.74	0.49	-	-
Mt	0.51	0.60	0.78	0.73	1.01	1.85
Il	1.23	1.48	1.50	1.46	1.80	3.98
Ap	0.61	0.63	0.57	0.48	0.81	2.36
Plag(An_x)*	32	29	41	41	42	48
Mg/Mg+Fe	0.63	0.63	0.68	0.70	0.66	0.67

*for ferromagnesian minerals

Table 6.8

Major Element Compositions and CIPW Norms for Xenoliths in Mangerites

	Sund, Flakstadøy WL332	Djupfjord, Hopen, Austvågøy WL568	Eidsfjord, Langøy WL733
SiO_2	55.05	48.35	49.55
Al_2O_3	17.66	15.36	14.31
TiO_2	0.87	1.92	2.23
Fe_2O_3	8.03	12.94	14.97
MgO	3.82	5.65	4.23
CaO	6.19	8.12	7.48
Na_2O	6.28	4.18	3.60
K_2O	1.47	1.47	1.93
MnO	0.12	0.16	0.23
P_2O_5	0.33	0.60	1.35
LOI	0.38	1.42	0.01
Total	100.22	100.14	99.88
Norms calculated with $Fe^{3+}/Fe^{3+} + Fe^{2+} = 0.20$			
Q	-	-	3.28
Or	8.69	8.69	11.41
Ab	53.14	35.37	30.46
An	15.66	18.81	17.19
C	-	-	-
Cc	0.68	2.52	0.02
Di	9.13	9.62	8.90
Hy	3.64	4.84	10.25
Ol	8.22	5.78	-
Mt	2.41	3.86	4.49
Il	1.65	3.64	4.23
Ap	0.72	1.31	2.95
Plag(An_x)	36	50	52
Mg/Mg+Fe*	0.82	0.84	0.78

* for ferromagnesian minerals

Table 6.9

Rb-Sr Data for the Langøy Mangerites

Sample	Mangerite	Rb(ppm)	Sr(ppm)	$^{87}Rb/^{86}Sr$	$^{87}Sr/^{86}Sr$
WL703	Hovden	26	526	0.1360	0.70704
WL707	Hovden	30	440	0.1774	0.70819
WL713	Steine	64	836	0.2144	0.70822
WL714	Steine	50	734	0.1907	0.70764
WL715	Søberg	30	874	0.0908	0.70546
WL732	Eidsfjord	13	758	0.0437	0.70645
Errors (2σ)		±5%	±5%	±1%	±0.00005

Table 6.10

Rb-Sr Data for Xenoliths in Mangerites

Sample	Mangerite	Rb(ppm)	Sr(ppm)	$^{87}Rb/^{86}Sr$	$^{87}Sr/^{86}Sr$
WL332	Sund	32	854	0.1050	0.70619
WL568	Hopen	17	1016	0.0417	0.70479
WL733	Eidsfjord	11	687	0.0402	0.70645
Errors (2σ)		±5%	±5%	±1%	±0.00005

Table 6.11

Sm-Nd Data for the Mid Proterozoic Mangeritic Intrusions

Sample	Sm(ppm)	Nd(ppm)	$^{147}Sm/^{144}Nd$	$^{143}Nd/^{144}Nd$	T_{CHUR}(Ga)	T_{DM}(Ga)
	The Sund-Ølkona Mangerite					
WL202	3.177	17.602	0.10970	0.511264	2.37	2.58
WL204	3.797	22.632	0.10198	0.511209	2.27	2.48
WL302	9.594	60.764	0.09597	0.511206	2.14	2.35
WL335	4.248	24.978	0.10336	0.511315	2.13	2.36
	The Flakstadøy Charnockite					
WL306	3.407	29.417	0.07040	0.510843	2.14	2.32
	The South-West Lofoten Mangerite					
WL307	12.857	71.743	0.10892	0.511344	2.21	2.44
WL315	7.540	39.333*	0.11651	0.511688	1.78	2.09
WL316	6.345	34.671	0.11122	0.511640	1.75	2.06
WL319	9.073	50.485	0.10922	0.511399	2.13	2.37
WL331	9.635	50.231	0.11659	0.511407	2.30	2.54
WL401	7.055	40.287	0.10643	0.511328	2.18	2.41
WL404	4.849	26.842	0.10980	0.511352	2.22	2.45
WL405	9.377	59.887	0.11200	0.511387	2.22	2.45
WL410	5.768	29.483	0.11891	0.511719	1.77	2.10
WL416	7.355	41.615	0.10743	0.511457	1.99	2.25
	The Hopen Mangerite/Charnockite					
WL508	10.415	55.929	0.11318	0.511296	2.42	2.62
WL510	10.331	54.599	0.11500	0.511361	2.34	2.57
WL514	10.928	71.409	0.09301	0.511113	2.21	2.41
WL516	6.519	34.338	0.11539	0.511334	2.40	2.62
WL517	4.824	26.990	0.10863	0.511255	2.36	2.57
WL570	9.782	56.245	0.10570	0.511204	2.37	2.57
WL575	11.322	73.009	0.09426	0.511089	2.27	2.47
	The Austvågøy Grey Mangerite					
WL522	7.664	43.091	0.10810	0.511195	2.44	2.64
WL526	7.573	42.586	0.10808	0.511222	2.40	2.60
WL533	7.655	42.355	0.10985	0.511379*	2.18	2.41

Table 6.11 (continued)

Sample	Sm(ppm)	Nd(ppm)	$^{147}Sm/^{144}Nd$	$^{143}Nd/^{144}Nd$	T_{CHUR}(Ga)	T_{DM}(Ga)
	The Raftsund Mangerite					
WL101	19.176	111.288	0.10473	0.511291	2.20	2.42
WL539	5.789	31.200	0.11276	0.511386	2.24	2.47
WL604	6.915	36.243	0.11597	0.511423	2.26	2.50
WL606	5.745	31.022	0.11255	0.511374	2.25	2.49
WL607	19.161	106.208	0.10965	0.511317	2.28	2.50
WL628	10.755	55.475	0.11783	0.511429	2.30	2.54
	The Hovden Mangerite					
WL703	2.721	14.434	0.11457	0.511498	2.08	2.35
WL707	2.619	13.726	0.11600	0.511525	2.07	2.32
	The Steine Mangerite					
WL713	5.365	30.041	0.10855	0.511543	1.87	2.15
	The Eidsfjord Mangerite					
WL732	14.057	79.586	0.10735	0.511221	2.38	2.59
Errors (2)	±0.02%	±0.02%	±0.10%	±0.000025	±0.04	±0.04
	unless asterisked (*) and stated below					
WL315		±0.027%				
WL533				±0.000029		

Table 6.12

Pb Data for the Mid Proterozoic Mangeritic Intrusions

Sample	$^{206}Pb/^{204}Pb$	$^{207}Pb/^{204}Pb$	$^{208}Pb/^{204}Pb$	Apparent μ_1 †
	The Sund-Ølkona Mangerite			
WL202	14.581	14.900	34.489	7.56
WL204	14.383	14.931	34.388	7.66
WL204*	14.358	14.881	34.269	
WL302	17.620	15.307	38.044	7.70
WL302*	16.031	15.154	36.931	
WL303	15.216	15.009	34.699	7.63
	The Flakstadøy Charnockite			
WL306	15.176	14.972	36.193	7.56
	The South-West Lofoten Mangerite			
WL307	14.903	15.004	34.860	7.67
WL307*	14.907	15.029	34.921	
WL315	16.038	15.225	35.382	7.86
WL315*	15.622	15.165	35.095	
WL316	15.642	15.159	35.090	7.81
WL319	15.686	15.095	35.121	7.69
WL331	15.170	15.071	34.992	7.74
WL331*	15.001	15.041	34.856	
WL401	15.046	15.013	34.944	7.66
WL401*	14.840	14.995	34.783	
WL402	15.129	15.046	35.096	7.66
WL403	14.878	15.037	34.824	7.74
WL404	14.792	14.963	34.748	7.62
WL405	14.899	14.983	34.839	7.63
WL405*	14.844	14.997	34.819	
WL410	16.176	15.223	35.344	7.83
WL410*	15.901	15.213	35.219	
WL416	16.007	15.204	35.520	7.83
WL417	15.218	15.033	35.057	7.66

Table 6.12 (continued)

Pb Data for the Mid Proterozoic Mangeritic Intrusions

Sample	$^{206}Pb/^{204}Pb$	$^{207}Pb/^{204}Pb$	$^{208}Pb/^{204}Pb$	Apparent μ_1 †
	The Hopen Mangeritic/Charnockite			
WL508	15.036	14.976	34.857	7.61
WL510	15.091	14.971	35.337	7.59
WL510*	14.591	14.927	34.765	
WL514	14.925	14.949	37.415	7.59
WL516	14.396	14.864	34.520	7.54
WL516*	14.280	14.867	34.463	
WL517	14.752	14.922	34.641	7.57
WL518	14.667	14.894	34.659	7.54
WL518*	14.347	14.864	34.476	
	The Austvågøy Grey Mangerite			
WL522	15.410	15.009	34.649	7.59
WL525	14.996	14.967	34.526	7.60
WL526	16.186	15.109	36.189	7.62
WL529	15.144	15.028	35.217	7.68
WL530	14.820	14.971	34.832	7.64
WL533	14.573	14.952	34.742	7.66
	The Raftsund Mangerite			
WL101	15.615	15.130	35.715	7.76
WL538	15.132	15.040	35.333	7.69
WL539	14.852	14.978	35.014	7.63
WL540	15.015	15.015	34.103	7.67
WL602	15.097	15.031	35.378	7.68
WL603	15.144	15.032	35.345	7.68
WL604	15.311	15.046	35.535	7.67
WL605	15.078	15.011	35.325	7.65
WL606	15.306	15.072	35.749	7.72
WL607	14.862	14.998	35.056	7.67
WL617	15.026	15.017	35.172	7.67

Table 6.12 (continued)

Sample	$^{206}Pb/^{204}Pb$	$^{207}Pb/^{204}Pb$	$^{208}Pb/^{204}Pb$	Apparent μ_1 †
	The Raftsund Mangerite			
WL620	15.118	15.020	35.363	7.66
WL625	15.049	15.030	35.160	7.69
WL626	14.931	15.011	35.095	7.68
WL628	15.070	15.018	35.233	7.66
	The Hovden Mangerite			
WL703	15.540	15.098	35.123	7.72
WL707	15.538	15.101	35.175	7.73

Errors (2σ) on Pb ratios are better than 0.1%

*All asterisked data are for alkali feldspar spearates; all other data are for whole rocks.

†Calculated assuming intrusion ages of:

Sund-Ølkona Mangerite	=	1800 Ma (Griffin et al., 1978)
Flakstadøy Charnockite	=	1735 Ma‡
South-West Lofoten Mangerite	=	1735 Ma (Griffin et al., 1978)
Hopen Mangerite/Charnockite	=	1822 Ma (the present study)
Austvågøy Grey Mangerite	=	1796 Ma (the present study)
Raftsund Mangerite	=	1733 Ma (the present study)
Hovden Mangerite	=	1730 Ma‡

‡Assumed to be the same age as South-West Lofoten Mangerite and Steine Mangerite (Griffin et al., 1978) respectively.

Table 6.13

Percentage of Ancient Crustal Material in the Mangerites: Nd Isotopic Constraints

Model: the mangerites crystallized under granulite-facies conditions at 1.8Ga from magmas derived from the anatexis of 2.7Ga lower crust and from the mantle. Assuming that the original mantle-derived component contained 11.5ppm Nd (the mean Nd concentration in MORB glasses, Cohen et al., 1980) and for different Nd concentrations in the crustal component the percentage of late Archaean material contributed is calculated for mangerites with the lowest, mean and highest ε_{Nd} values at 1.8Ga.

Nd (ppm) in crust-derived component	ε_{Nd} at 1.8Ga: +0.5	-4.8	-7.5
15	19%	56%	78%
32	10%	38%	62%
40	8%	33%	57%

32ppm is the mean Nd concentration of late Archaean gneisses from Lofoten-Vesterålen (Green et al., 1972; Jacobsen and Wasserburg, 1978; the present study) and from the Lewisian (Hamilton et al., 1979).

15ppm is the value for the 2.7Ga gneisses at Sandset, Central Langøy (the present study).

40ppm is an assumed upper limit for Nd concentration in crustal melts.

Table 6.14

Percentage of Ancient Crustal Material in the Mangerites: Pb Isotopic Constraints

Model: as for Table 6.13. The "crustal Pb column" shows the percentage of Pb in the mangerites which is derived from a lower crustal source. The other columns show the percentage of the mangerites by total mass contributed by the lower crustal component assuming crustal component Pb concentration of 20.2ppm (^{204}Pb = 0.28ppm) (North-West Hinnøy amphibolite-facies gneisses), and using different Pb concentrations for the mantle-derived component:

Sample	Crustal Pb	Crustal Contribution Total Pb (ppm [^{204}Pb (ppm)] 0.6[0.008]*	3.2[0.04]+	7.0[0.1]†	20[0.28]‡
	The Sund-Ølkona Mangerite				
WL202	121%	-	-	-	-
WL204	86%	18%	46%	68%	86%
WL302	72%	7%	27%	48%	72%
WL303	95%	34%	72%	87%	95%
	The Flakstadøy Charnockite				
WL306	117%	-	-	-	-

Sample	Crustal Pb	Crustal Contribution Total Pb (ppm) [^{204}Pb (ppm)] 0.6[0.08]*	3.2[0.04]+	7.0[0.1]‡	20[0.28]ǂ
	The South-West Lofoten Mangerite				
WL307	75%	8%	30%	52%	75%
WL315	11%	0%	2%	4%	11%
WL316	26%	1%	5%	11%	26%
WL319	72%	7%	27%	48%	72%
WL331	50%	3%	13%	26%	50%
WL401	80%	10%	36%	58%	80%
WL402	64%	5%	20%	39%	64%
WL403	51%	3%	13%	27%	51%
WL404	94%	32%	71%	86%	94%
WL405	89%	19%	53%	74%	89%
WL410	23%	1%	4%	9%	23%
WL416	23%	1%	4%	9%	23%
WL417	79%	10%	35%	57%	79%
	The Hopen Mangerite/Charnockite				
WL508	104%	-	-	-	-
WL510	111%	-	-	-	-
WL514	113%	-	-	-	-
WL516	131%	-	-	-	-

Sample	Crustal Pb	Crustal Contribution Total Pb (ppm) [^{204}Pb (ppm)]			
		0.6[0.08]	3.2[0.04]+	7.0[0.1]†	20[0.28]‡
WL517	119%	-	-	-	-
WL518	131%	-	-	-	-
	The Austvågøy Grey Mangerite				
WL522	109%	-	-	-	-
WL525	107%	-	-	-	-
WL526	99%	81%	96%	98%	99%
WL529	77%	9%	32%	54%	77%
WL530	91%	23%	59%	78%	91%
WL533	86%	15%	46%	68%	86%
	The Raftsund Mangerite				
WL101	43%	2%	10%	21%	43%
WL538	68%	6%	23%	43%	68%
WL539	89%	18%	53%	74%	89%
WL540	76%	8%	31%	53%	76%
WL602	71%	7%	26%	47%	71%
WL603	74%	8%	29%	51%	74%
WL604	77%	9%	32%	55%	77%
WL605	83%	13%	42%	64%	83%

Sample	Crustal Pb	Crustal Contribution Total Pb (ppm) [^{204}Pb (ppm)] 0.6[0.08]	3.2[0.04]+	7.0[0.1]†	20[0.28]‡
WL606	59%	4%	17%	34%	59%
WL607	76%	8%	31%	53%	76%
WL617	76%	8%	31%	53%	76%
WL620	80%	10%	37%	59%	80%
WL625	69%	6%	24%	44%	69%
WL626	73%	7%	27%	49%	73%
WL628	78%	9%	34%	56%	78%
	The Hovden Mangerite				
WL703	59%	4%	17%	34%	59%
WL707	57%	4%	16%	32%	57%

* mean pristine MORB (Cohen et al., 1980)

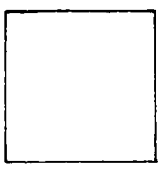
\+ Preshal Mhor Basalt, Isle of Skye, Pb 93% mantle-derived (Dickin, 1981)

† Southern Zone Andes Basalt (McHugh, 1980)

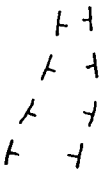
‡ Pb-enriched magma, evolved from an original basaltic parent liquid by extensive crsytal fractionation.

Fig. 6.1. Sample Locality Map for Flakstadøy and Vestvagøy: Mid-Proterozoic

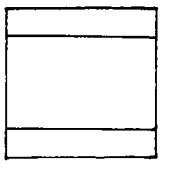
Mangeritic Intrusions



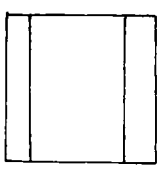
Mangerites



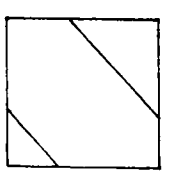
Retrograded Mangerites



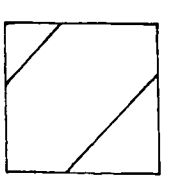
Leknes Metasediments



Late Archaean Migmatites Gneisses



Early Proterozoic Supracrustal Gneisses



Mid-Proterozoic Basic Intrusions

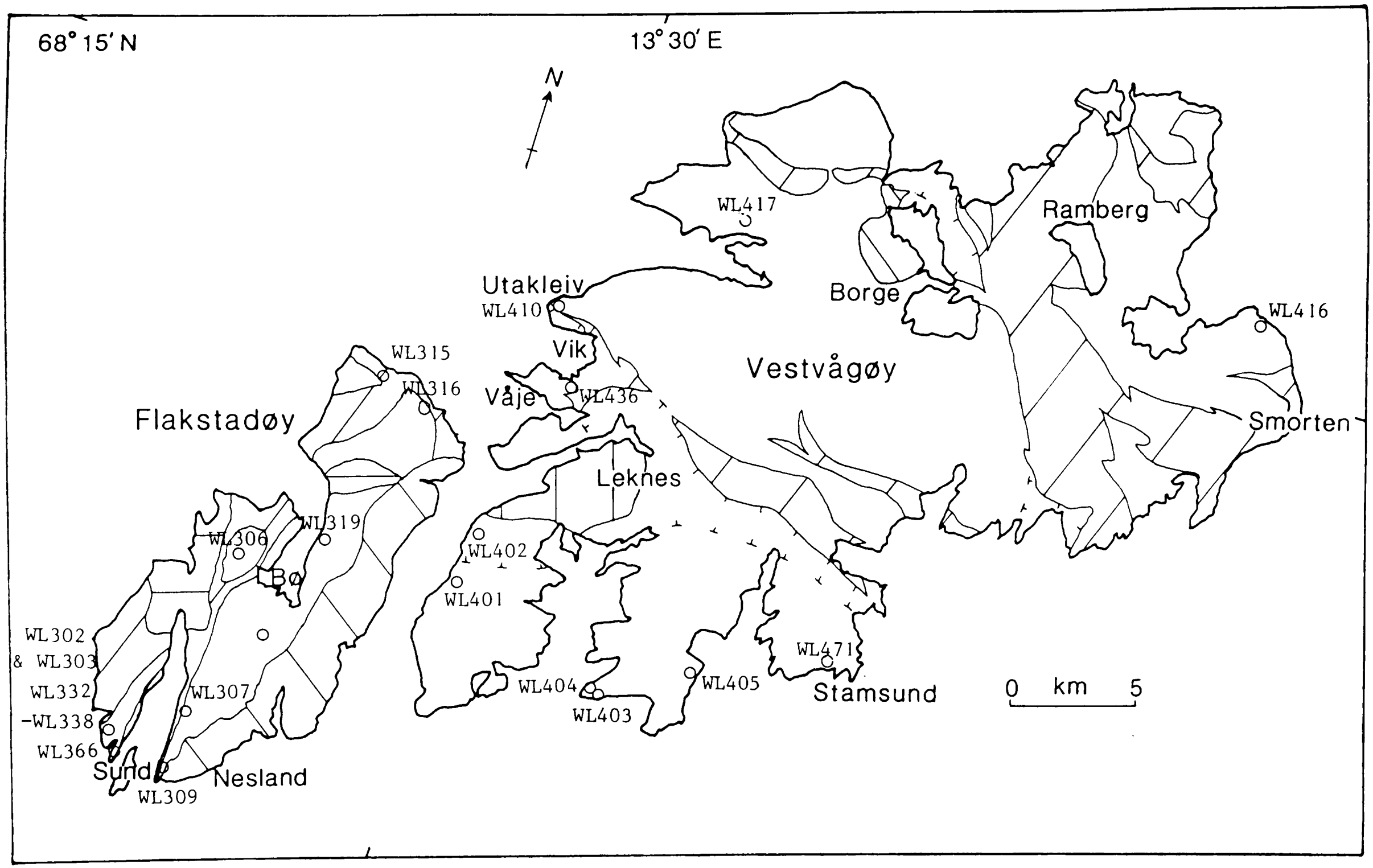
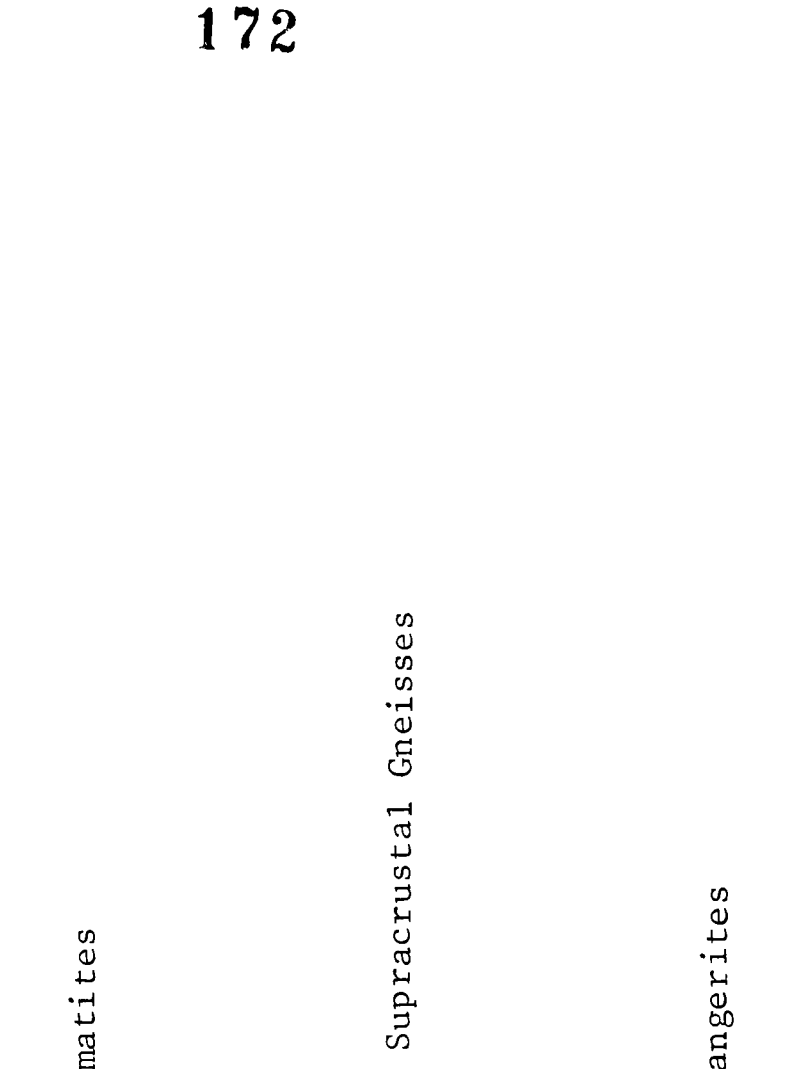

68° 15' N
13° 30' E
N
WL417
Ramberg
Utakleiv
WL410
Borge
WL416
Vik
WL315
WL316
Vestvågøy
Våje
WL436
Flakstadøy
Smorten
Leknes
WL319
WL306
WL402
Bø
WL401
WL302
& WL303
WL471
WL332
WL307
WL404
WL405
-WL338
WL403
Stamsund
0 km 5
WL366
Sund
Nesland
WL309

Fig. 6.2. Sample Locality Map of South-West Austvågøy: Mid-Proterozoic Mangeritic Intrusions



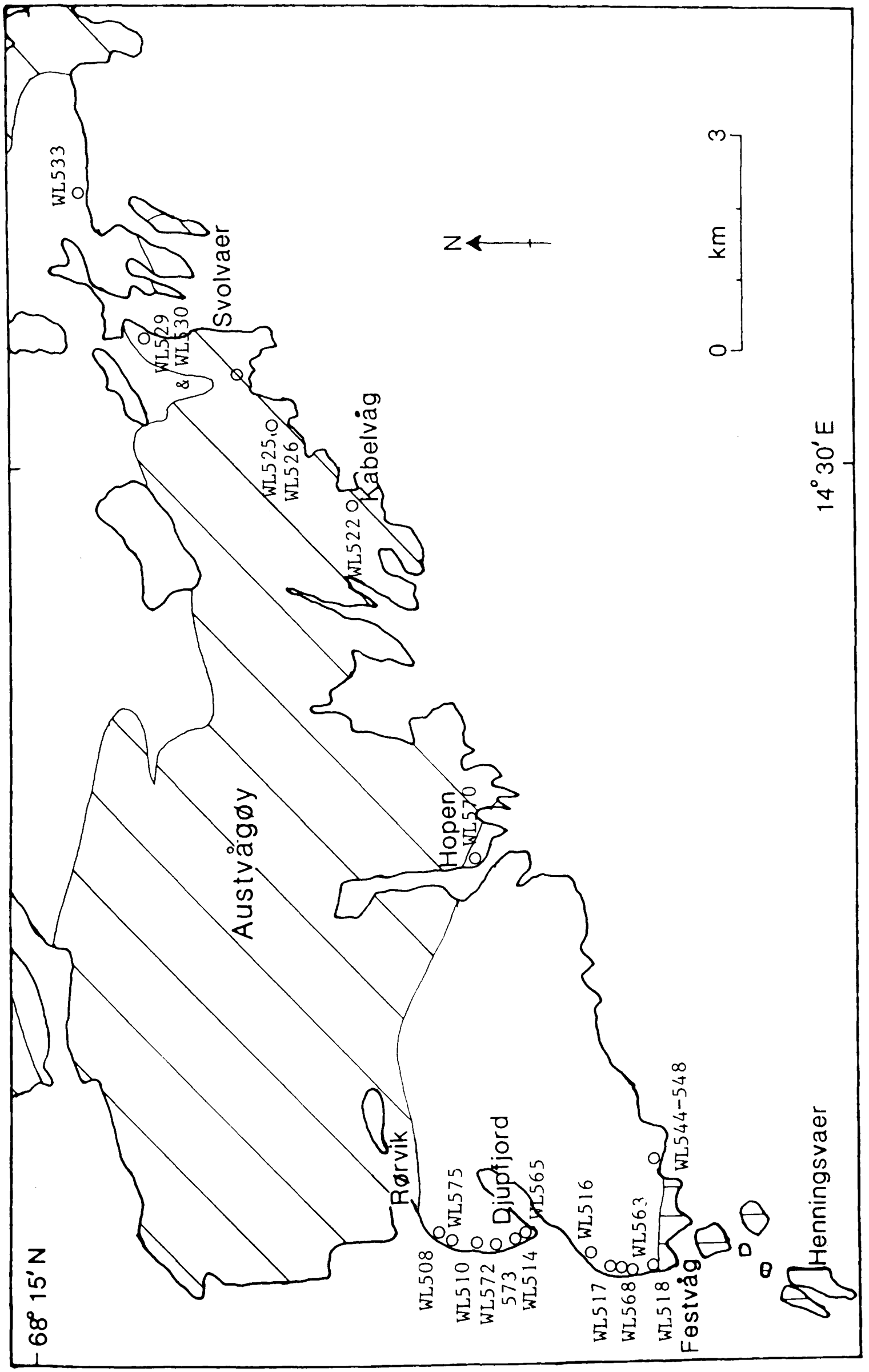
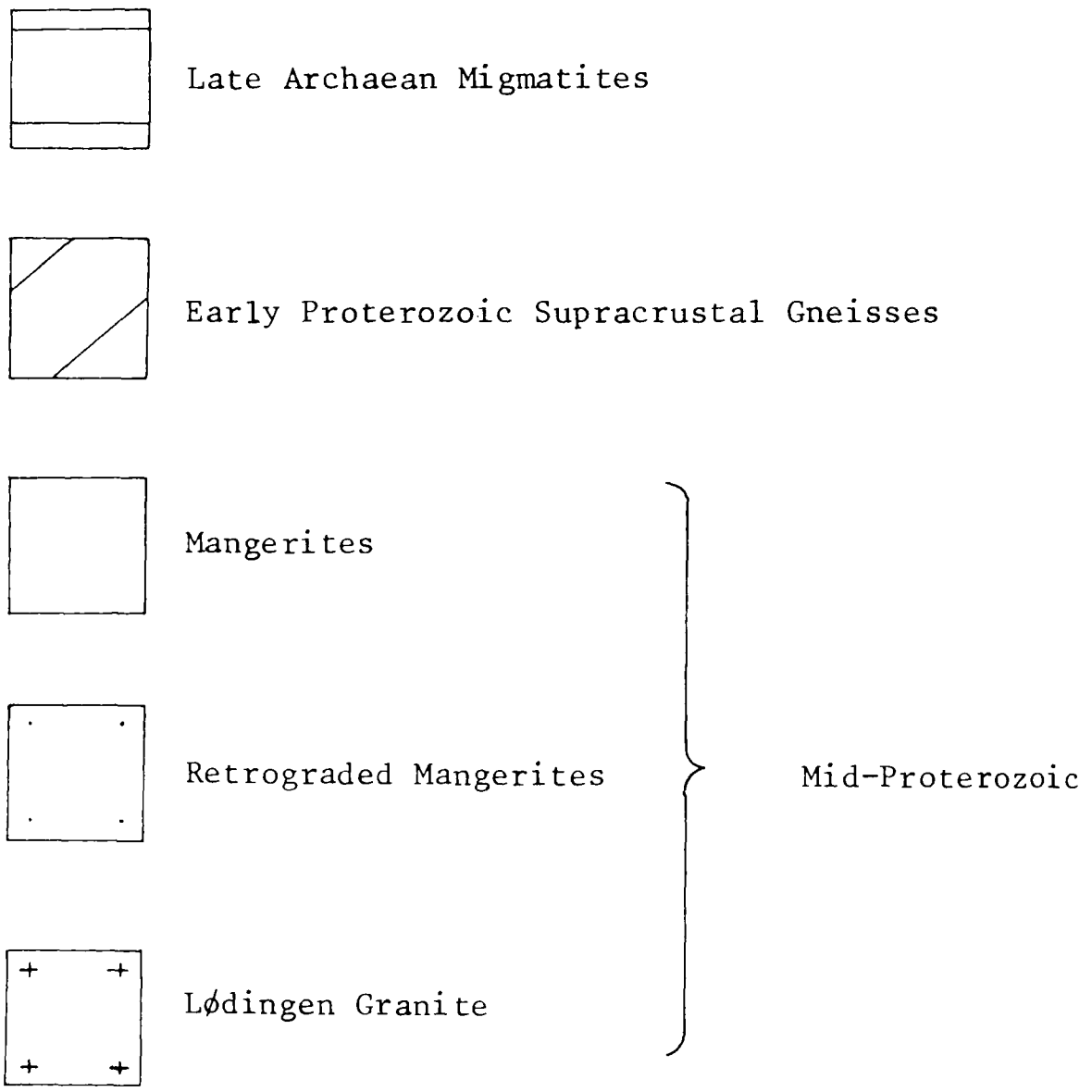

68° 15' N
14° 30' E
N
0
km
3
WL533
Svolvaer
WL529
& WL530
WL525
WL526
Kabelvåg
WL522
Austvågøy
Hopen
WL570
Rørvik
WL508
WL575
WL510
WL572
573
WL514
Djupfjord
WL565
WL516
WL517
WL568
WL563
WL518
WL544-548
Festvåg
Henningsvaer

Fig. 6.3. Sample Locality Map for the Mid-Proterozoic Raftsund Mangerite



△ cpx - opx zone

□ cpx - opx - ol zone

○ cpx - ol zone

▲ other samples

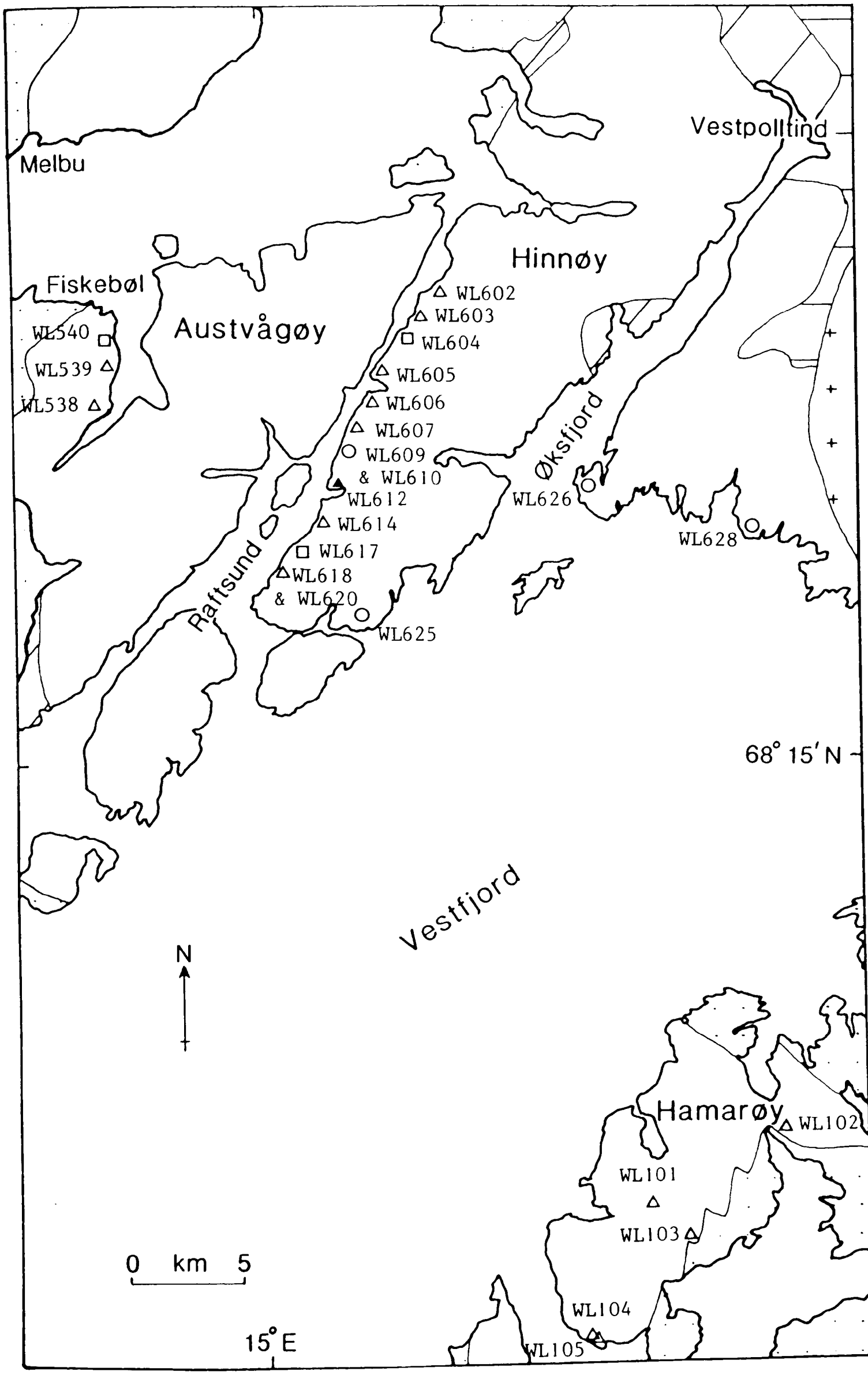
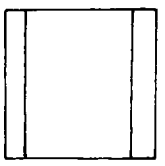
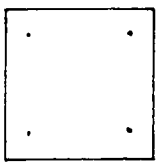

Melbu
Vestpolltind
Hinnøy
Fiskebøl
Austvågøy
WL602
WL603
WL604
WL605
WL606
WL607
WL609
& WL610
WL612
WL614
WL617
WL618
& WL620
WL625
WL540
WL539
WL538
Raftsund
Øksfjord
WL626
WL628
68° 15' N
Vestfjord
N
Hamarøy
WL102
WL101
WL103
WL104
WL105
0 km 5
15° E

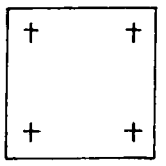
Fig. 6.4. Sample Locality Map for Langøy: Mid-Proterozoic Mangeritic Intrusions



Mangerite



Retrograded Mangerite



Torset Granite

Late Archaean Migmatites



Early Proterozoic Supracrustal Gneisses

Anorthosite

Gabbro

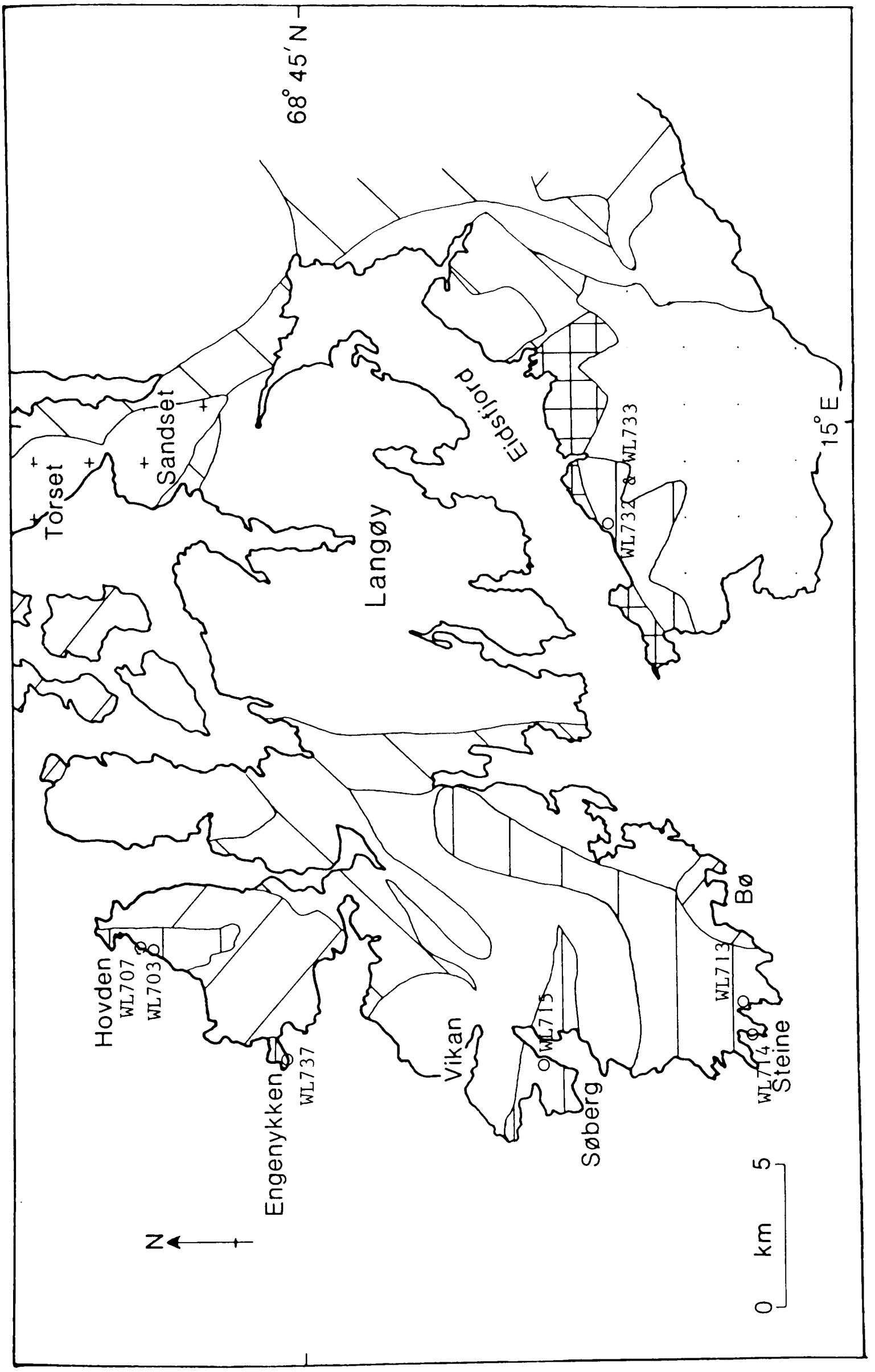

68° 45′ N
15° E
Eidsfjord
Langøy
Sandset
Torset
WL732
WL733
Hovden
WL707
WL703
Engenykken
WL737
Vikan
WL715
Søberg
WL713
Bø
WL714
Steine
N
0 km 5

Fig. 6.5.

Na_2O v. SiO_2 variation diagram for the thirty-eight mangerite samples analysed. The four possible source compositions considered are: (i) late Archaean migmatites (triangle); (ii) early Proterozoic supracrustals (square); (iii) the early Proterozoic Vik Gneisses (rhyolitic composition), Vestvågøy (inverted triangle); and (iv) the Flakstadøy Basic Complex (circle). The mangerites could have formed by mixing of varying proportions of these components followed by crystal fractionation of mafic phases. Diamond symbol represents average pyroxenite composition, formation of which may have controlled the evolution of the mangeritic magmas. Samples from Ølkona and Hopen have the highest Na_2O content and in that respect are the most fractionated mangerites.

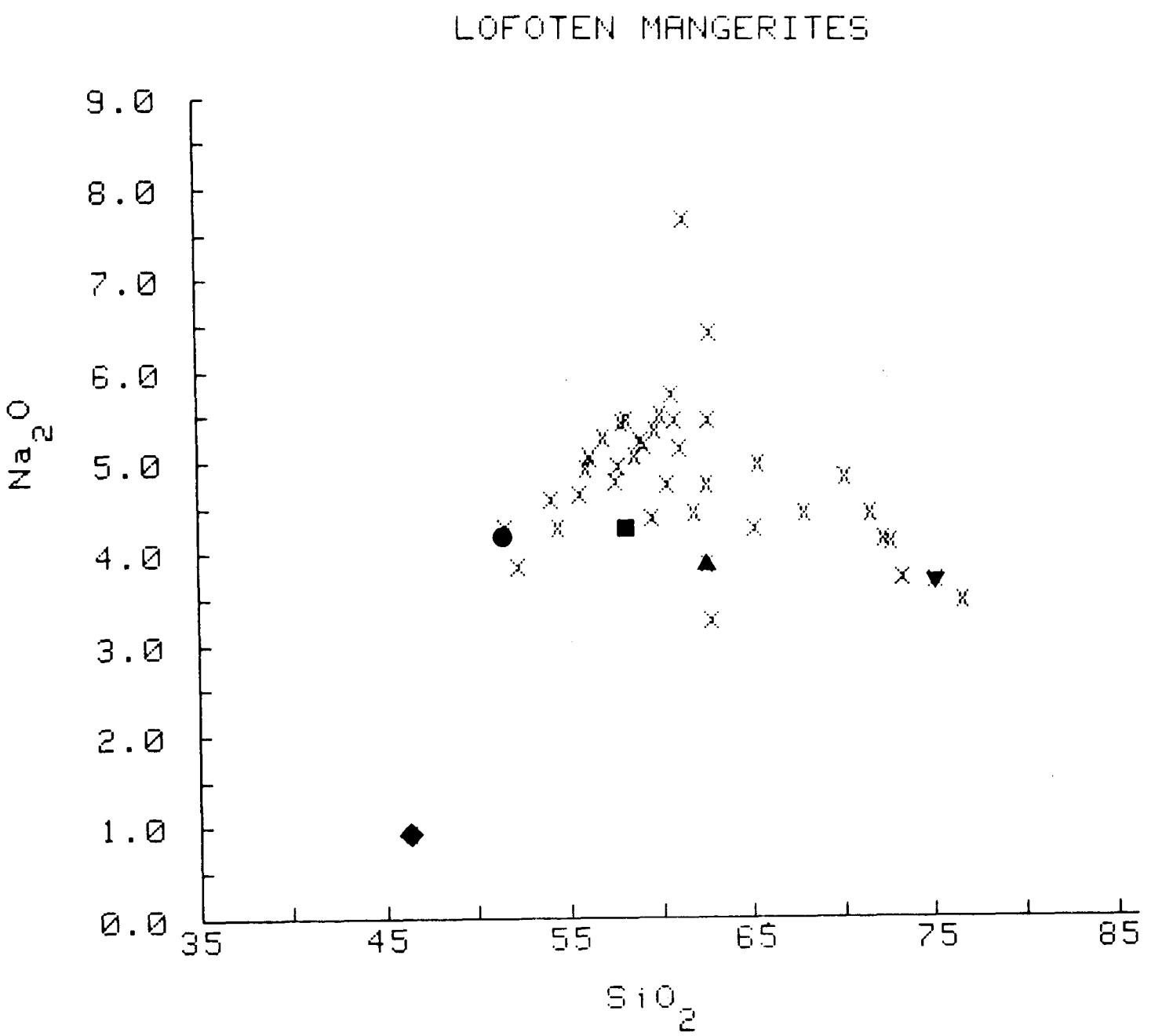

LOFOTEN MANGERITES
9.0
8.0
7.0
6.0
5.0
4.0
3.0
2.0
1.0
0.0
Na2O
35
45
55
65
75
85
SiO2

Fig. 6.6.

K_2O v. SiO_2 variation diagram for the thirty-eight mangerite samples analysed. Symbols as for Fig. 6.5. Similar to Na_2O v. SiO_2 plot (Fig. 6.5) except the "end-member mixing line" has a steep positive slope. Magma compositions evolve away from the average pyroxenite composition. Two samples from Ølkona have the highest K_2O content and in that respect are the most evolved of the mangerites. Note the generally very high K_2O contents of the mangerites.

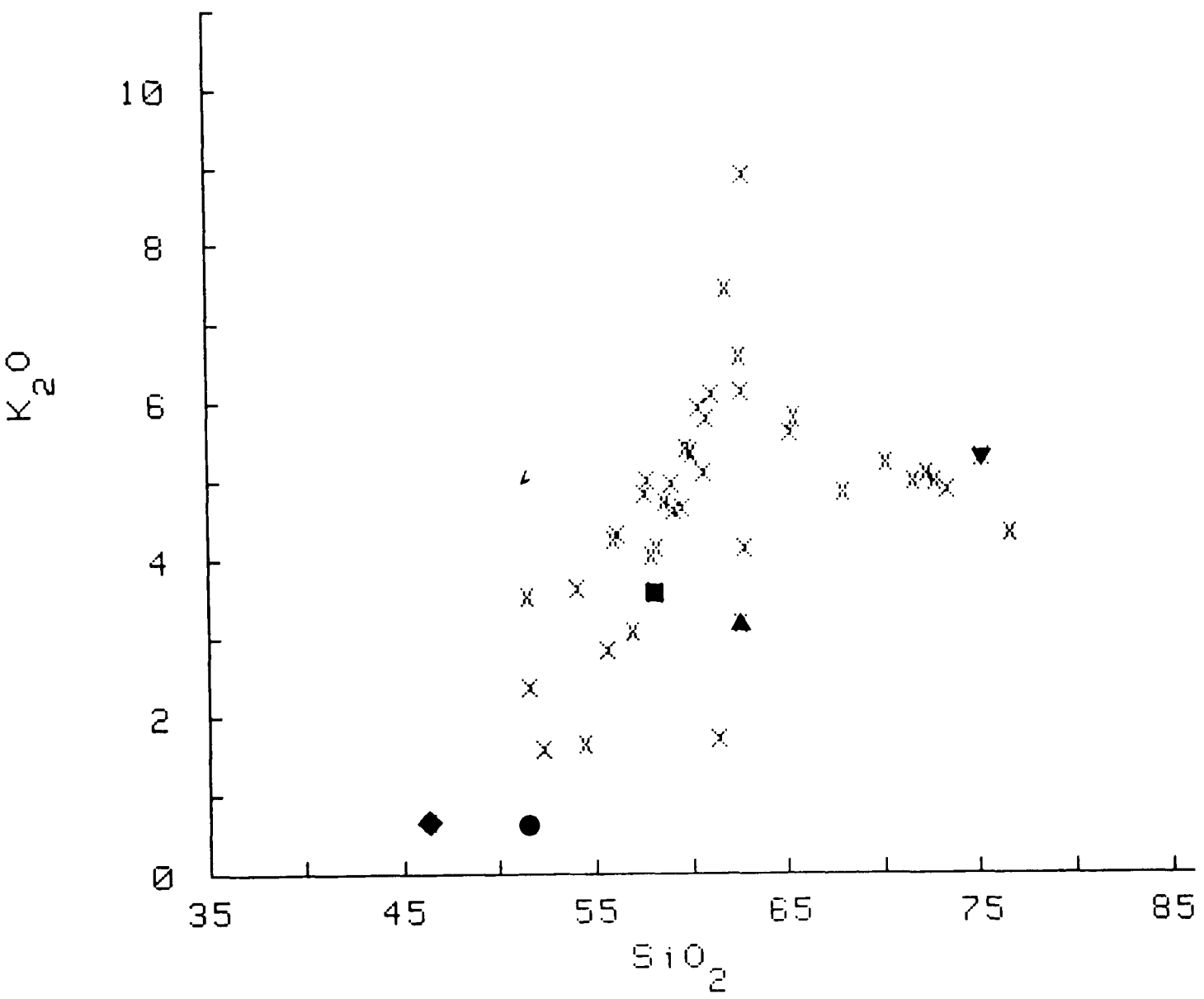

LOFOTEN MANGERITES
K2O
10
8
6
4
2
0
35
45
55
65
75
85
SiO2

Fig. 6.7.

CaO v. SiO_2 variation diagram for the thirty-eight mangerite samples analysed. Symbols as for Fig. 6.5. There is a good negative correlation between these two oxides for the mangerites. The samples plot on a vector away from the average pyroxenite composition. This implies that the mangerite magmas evolved by early crystallization of pyroxenite phases. The least evolved samples (high CaO, low SiO_2), from the South-West Lofoten Mangerite, require a large component of mantle-derived material since they are less-evolved than the crustal components.

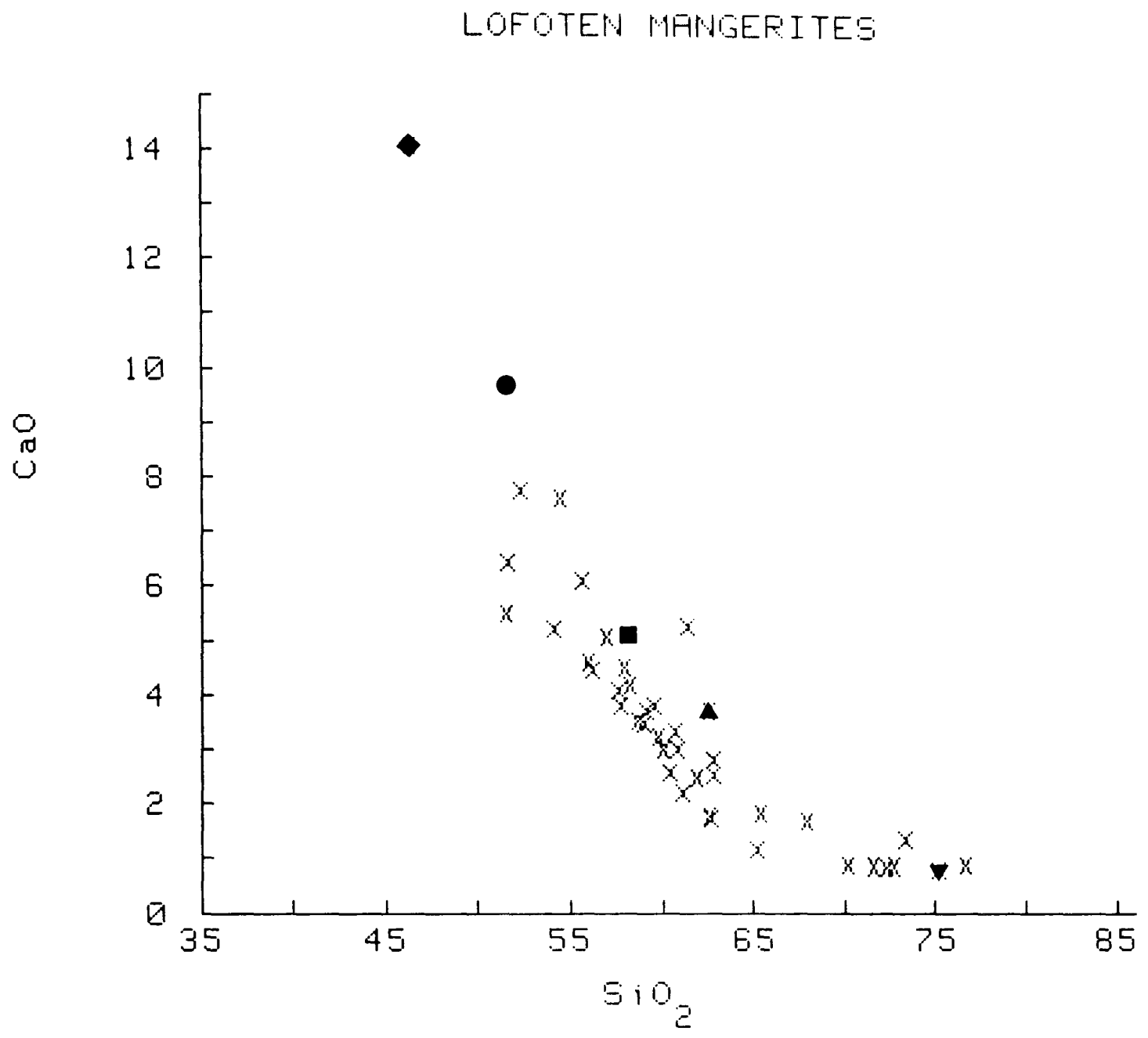

LOFOTEN MANGERITES
CaO
14
12
10
8
6
4
2
0
35
45
55
65
75
85
SiO2

Fig. 6.8.

MgO v. SiO_2 variation diagram for the thirty-eight mangerite samples analysed. Symbols as for Fig. 6.5. As for the CaO v. SiO_2 plot (Fig. 6.7), these two oxides have a negative correlation. The trend is convex towards the origin implying that MgO-rich phases, probably olivine, are fractionated early from the mangeritic magmas. MgO is $\leq$1% for all mangeritic rocks with SiO_2 $\geq$63%. WL315, a sample from the South-West Lofoten Mangerite is the least evolved sample on this variation diagram.

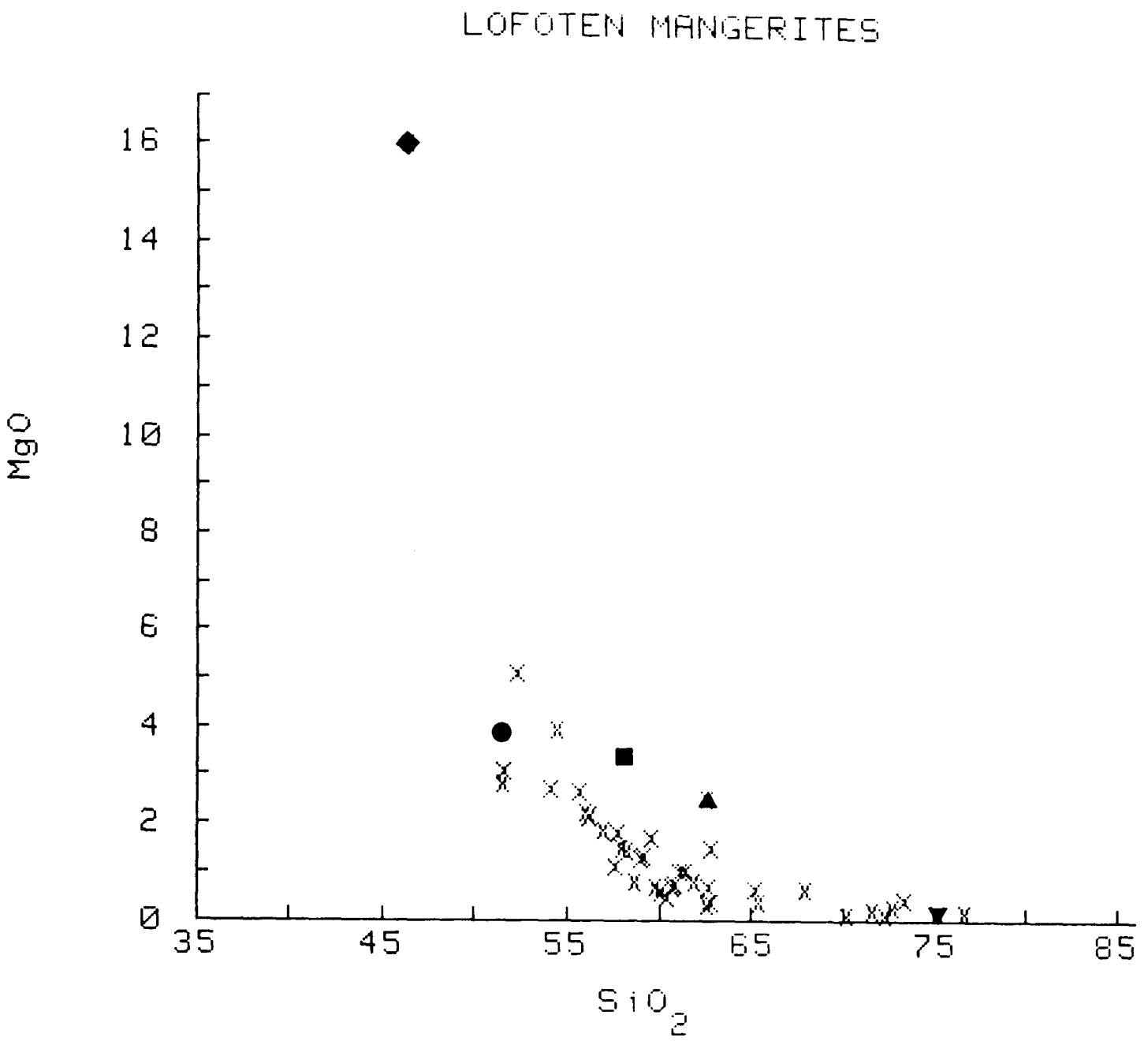

LOFOTEN MANGERITES
MgO
16
14
12
10
8
6
4
2
0
35
45
55
65
75
85
SiO2

Fig. 6.9.

Fe_2O_3 v. SiO_2 variation diagram for the thirty-eight mangerite samples analysed. Symbols as for Fig. 6.5. There is a negative correlation between these two oxides. Samples less evolved (high Fe_2O_3 , low SiO_2) than all of the mean crustal components must have a large component of high Fe_2O_3 - low SiO_2 material. The Flakstadøy Basic Complex has low Fe_2O_3 (4.9%) but this may have been higher prior to fractionation; the gabbros of Vestvågøy and Langøy have an average Fe_2O_3 content of 10.7% and hence would be a suitable high Fe_2O_3 - low SiO_2 end-member for the mangeritic magmas.

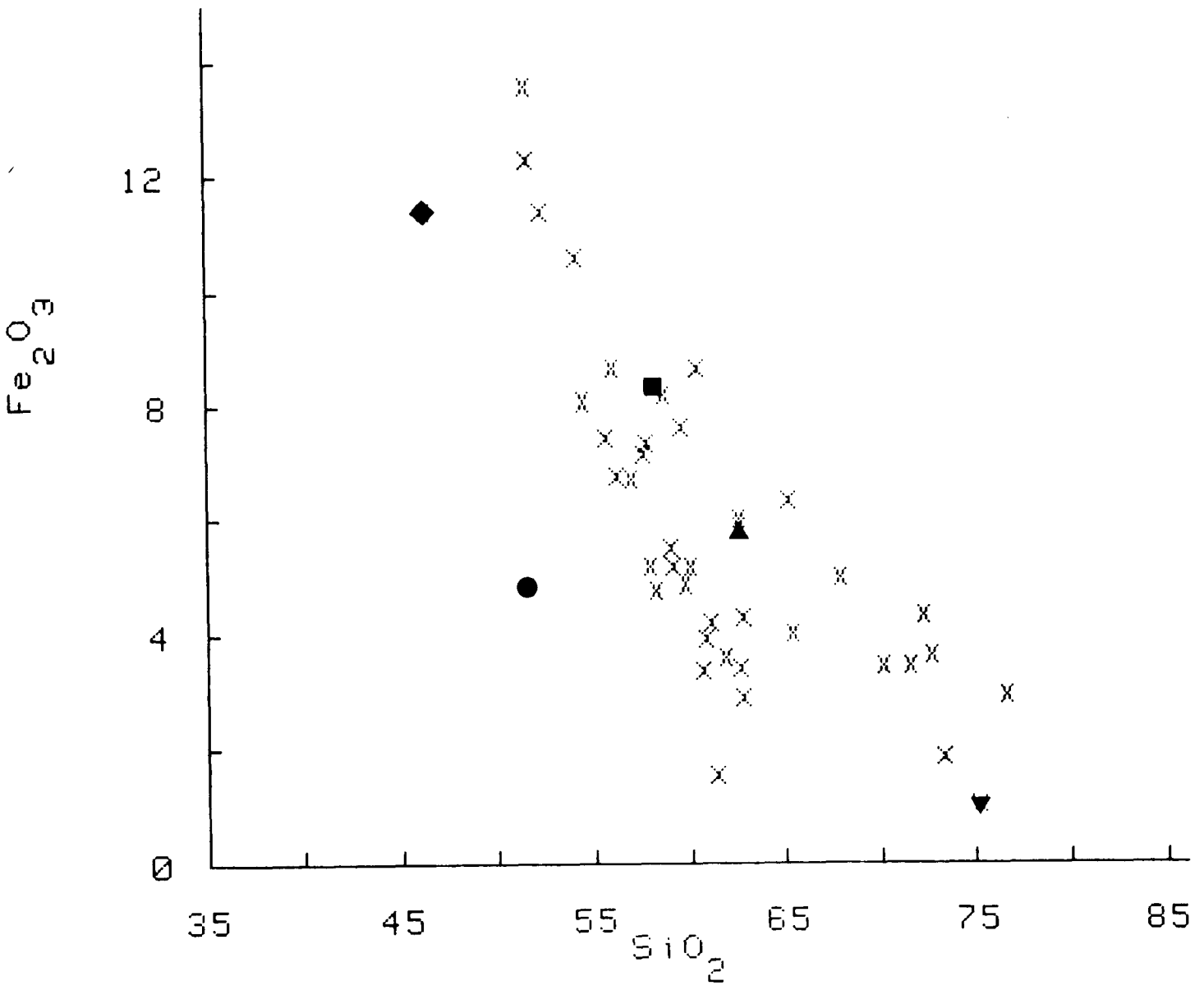

LOFOTEN MANGERITES
Fe2O3
12
8
4
0
35
45
55
65
75
85
SiO2

Fig. 6.10.

Fe_2O_3 v. TiO_2 variation diagram for the thirty-eight mangerite samples analysed. Symbols as for Fig. 6.5. There is a good positive correlation through the origin for these two oxides. Since Fe is a compatible element (shown by decrease in Fe_2O_3 with increase in SiO_2, Fig. 6.9) Ti is also compatible, more evolved magmas having lower TiO_2 contents. This is compatible with the observation that opaques (probably ilmenite and magnetite) occur with cumulus pyroxenes and olivines in the mangeritic rocks.

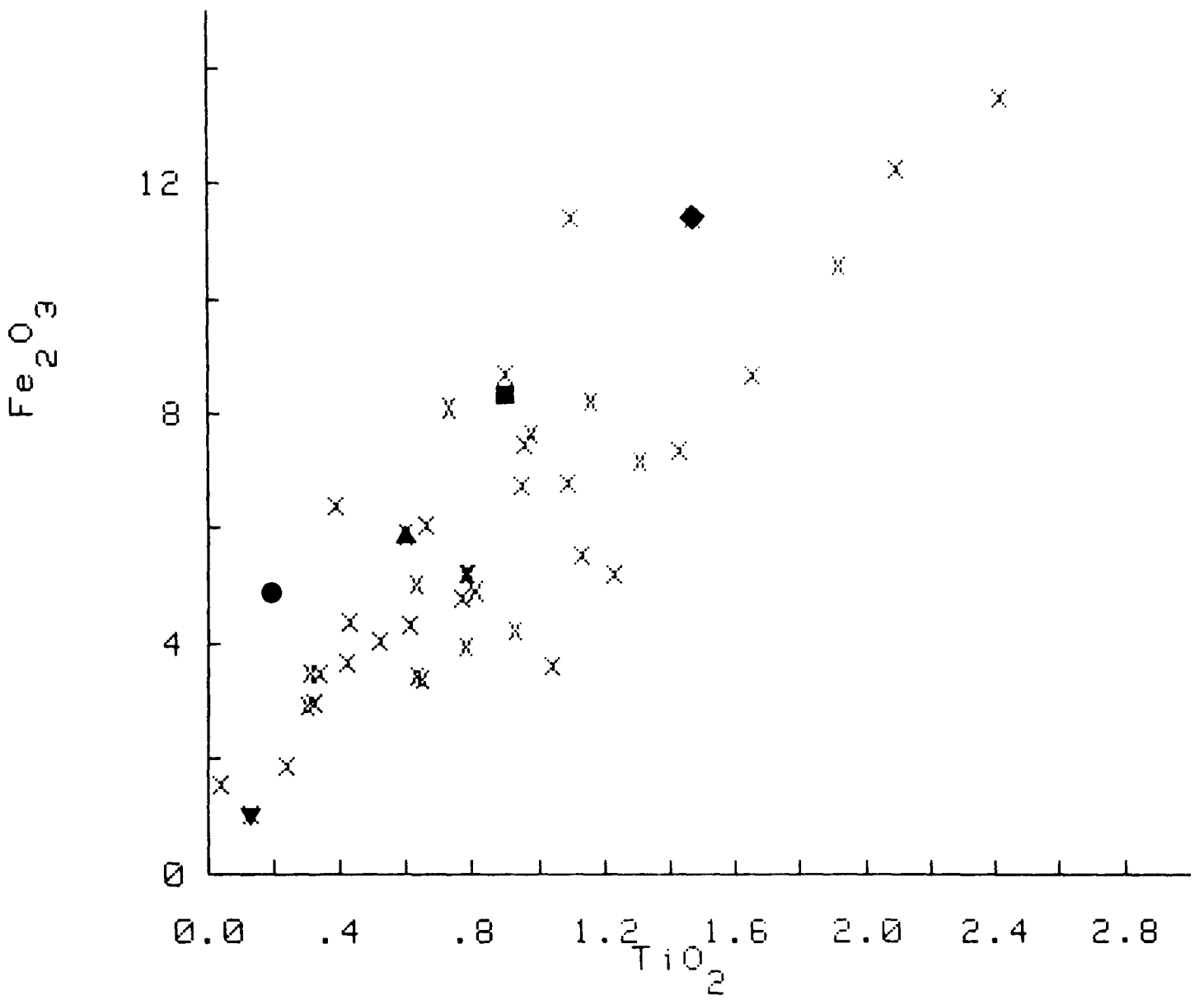

LOFOTEN MANGERITES
Fe2O3
12
8
4
0
0.0
.4
.8
1.2
1.6
2.0
2.4
2.8
TiO2

Fig. 6.11.

P_2O_5 v. TiO_2 variation diagram for the thirty-eight mangerite samples analysed. Symbols as for Fig. 6.5. There is a strong positive correlation between these two oxides which indicates that P, like Ti, is a compatible element, i.e. P-bearing phases are fractionated from the magma. This is in accord with the occurrence of early-crystallized (? cumulus) apatite within pyroxenes and olivine, and with the high abundance of apatite in the marginal gabbroic series to the Hopen intrusion.

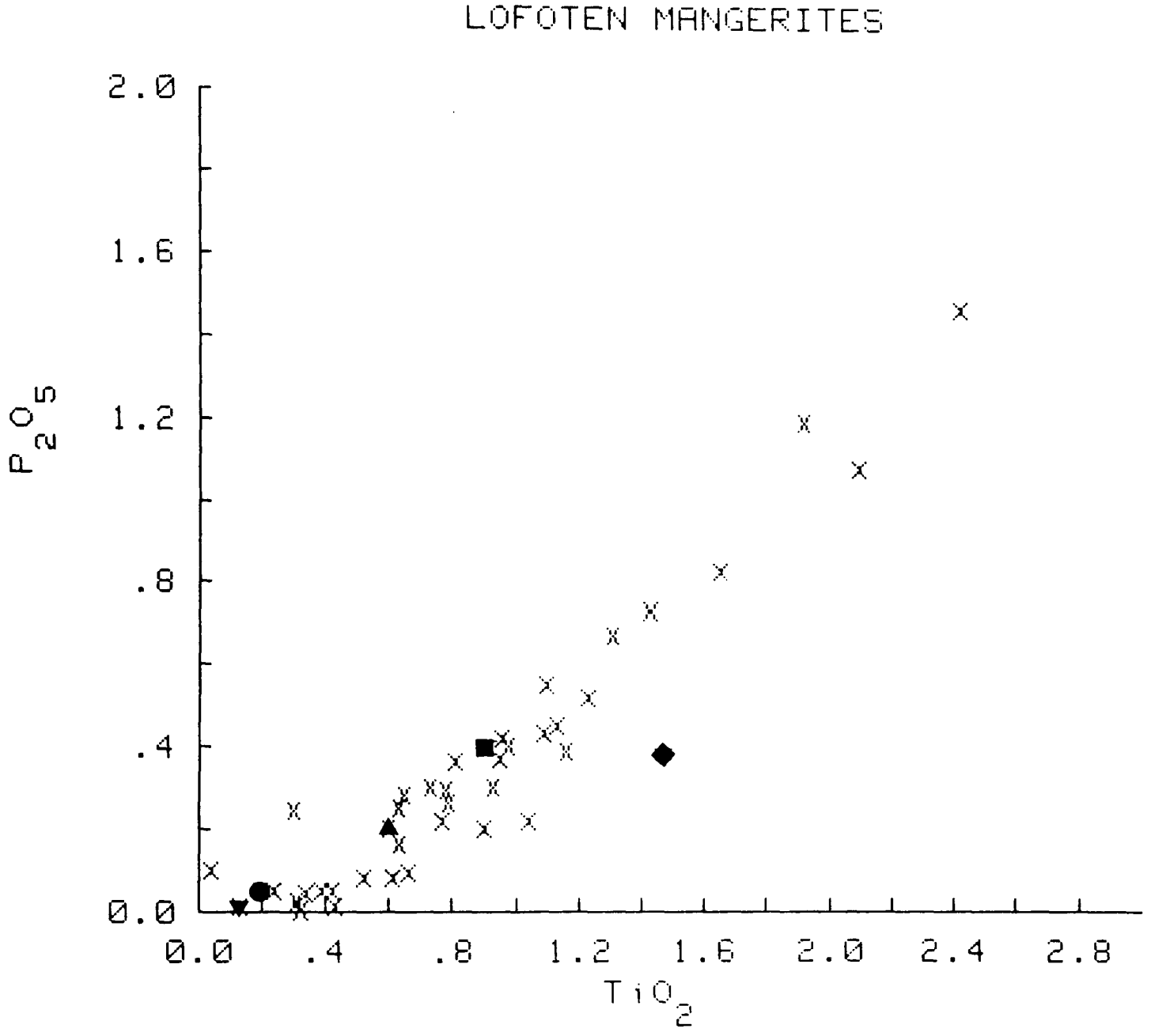

LOFOTEN MANGERITES
2.0
1.6
1.2
.8
.4
0.0
P_2O_5
0.0
.4
.8
1.2
1.6
2.0
2.4
2.8
TiO_2

Fig. 6.12.

CaO v. MgO variation diagram for the thirty-eight mangerite samples analysed. Symbols as for Fig. 6.5. These two oxides are positively correlated with the trend convex towards the CaO axis. Progressive removal of pyroxenite phases from the mangerite magmas would produce an evolution trend with positive slope towards the origin from the original magma composition. The curvature of the trend can be explained by the early crystallization of olivine and plagioclase which causes a marked decrease in MgO in the residual liquid, but less markedly so in CaO. Subsequently, as clinopyroxene begins to crystallize, the CaO content of the magmas decreases markedly.

LOFOTEN MANGERITES

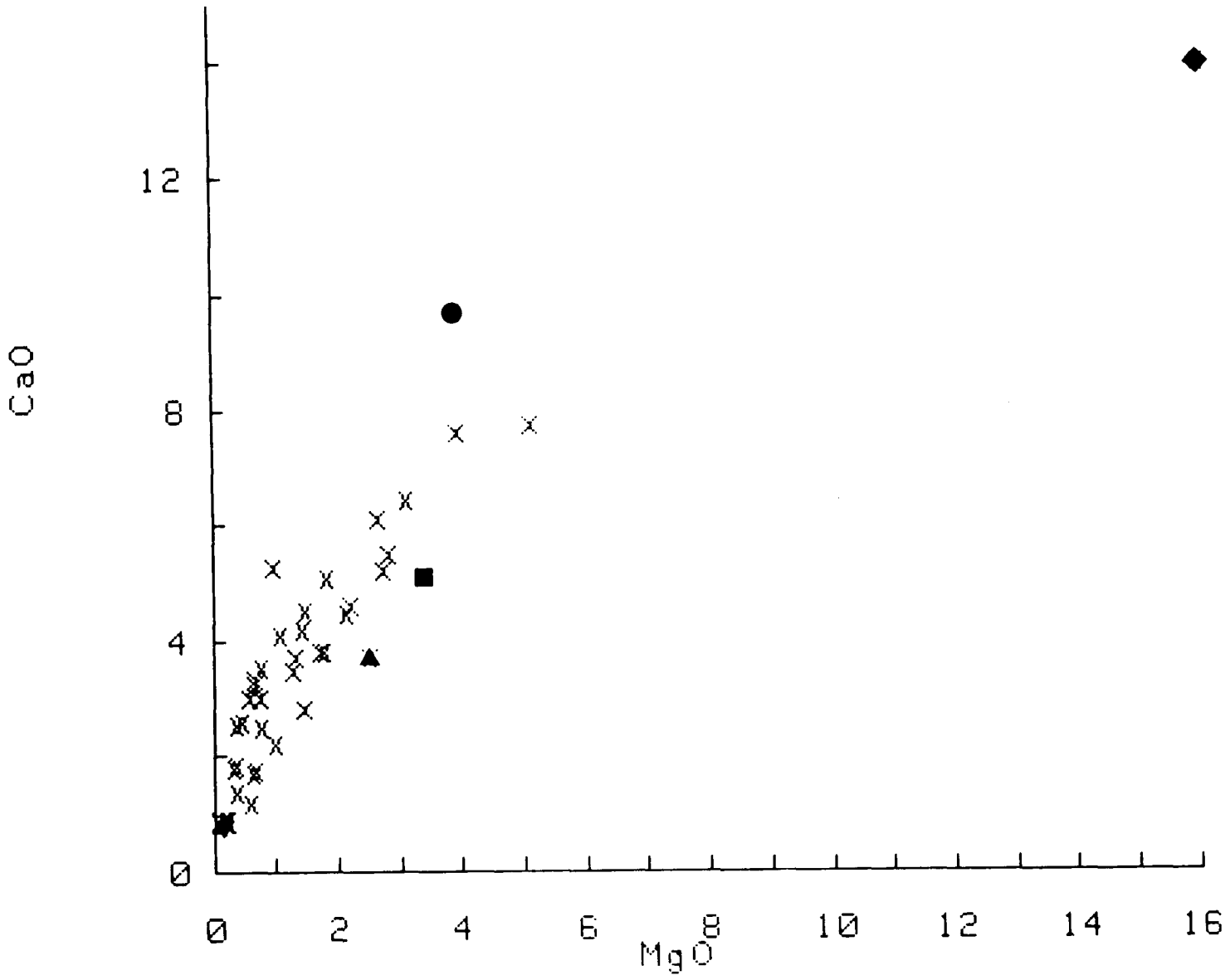


Fig. 6.13.

CaO v. MgO variation diagram for the six Raftsund Mangerite samples analysed. Symbols as for Fig. 6.5. The curved positive trend recognised for all the mangerite samples in Fig. 6.12 is shown very clearly for the mangerite intrusion with the best-developed cumulate features and in which olivine is an important primary phase. Olivine is overgrown by clinopyroxene in some Raftsund Mangerite samples (see Section 6.2.6), supporting the sequence of crystallization offered in explanation of the curvature in Fig. 6.12.

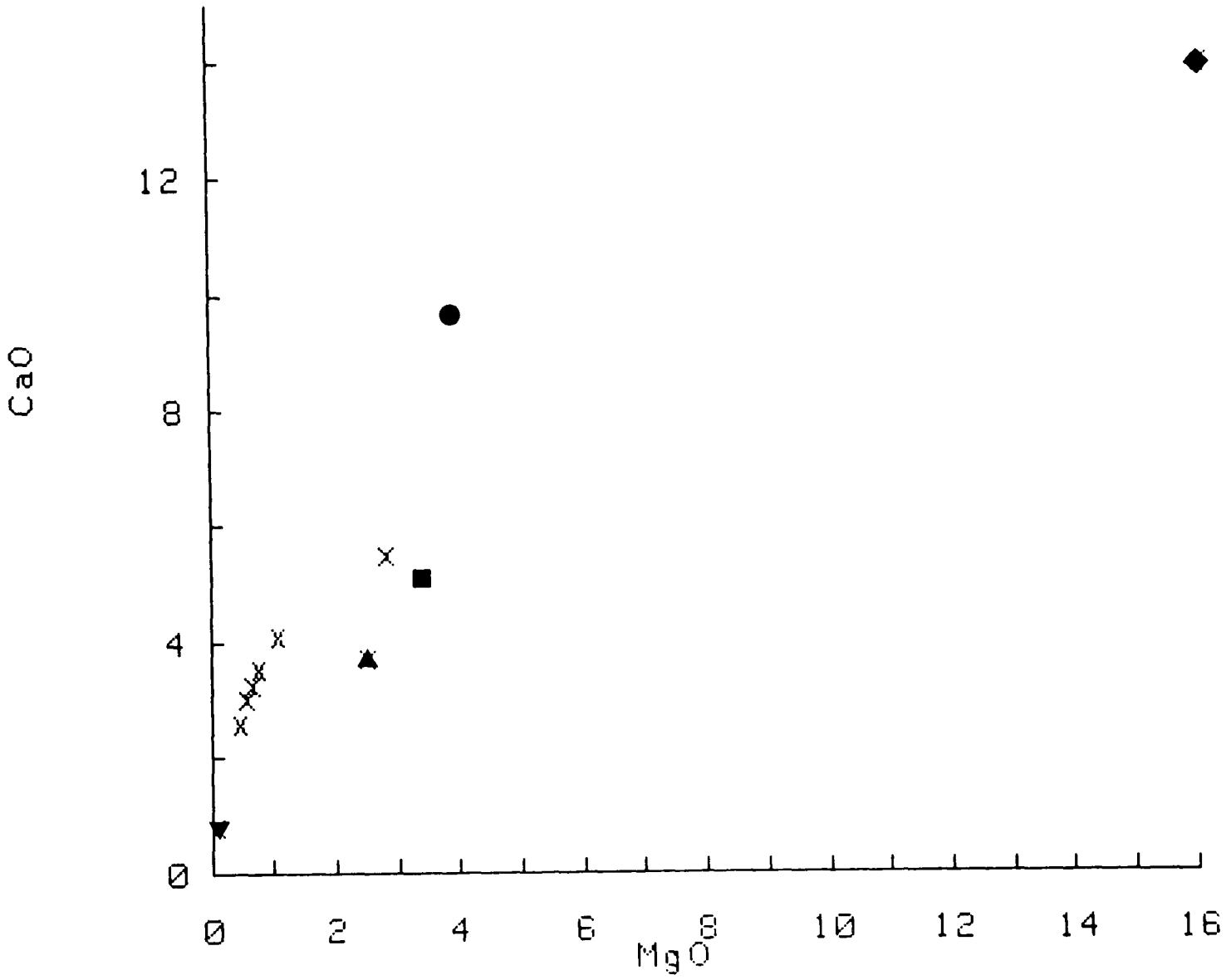

RAFTSUND MANGERITE
CaO
12
8
4
0
0
2
4
6
8
10
12
14
16
MgO

Fig. 6.14.

Rb-Sr isotope data and whole-rock isochron for five samples from the Sund-Ølkona Mangerite. This intrusion has one of the greatest ranges in Rb/Sr ratios since it contains charnockites which tend to have high Rb/Sr ratios. The seven-point isochron age for this intrusion published in Griffin et al. (1978) is 1800 ± 50Ma (2σ) and $(^{87}Sr/^{86}Sr)_o$ is 0.70333 ± 58.

SAMPLE NAME	Rb ppm	Sr ppm	87Rb 86Sr	87Sr/86Sr
SUND-ØLKONA MANGERITE				
WL202	9	572	0.0324	0.70511
WL204	83	426	0.5613	0.71816
WL303	68	57	4.4249	0.81974
WL335	58	72	2.8504	0.77645
WL337	42	222	0.5570	0.71849

Slope	0.025515	Error	0.000152 (1 Sigma)
Intercept	0.704222	Error	0.000068 (1 Sigma)
Centroid	0.211275	0.709612	
Squared residuals	12.310		
M.S.W.D.	4.103		
No. of Cycles	3		

Slope	0.025515	Error	0.000308 (1 Sigma)
Inter ept	0.704222	Error	0.000137 (1 Sigma)
Centroid	0.211275	0.709612	
Squared residuals	3.000		
M.S.W.D.	1.000		
No. of Cycles	3		

Age 1774.3 +/- 42.2 Ma. (2 sigma)

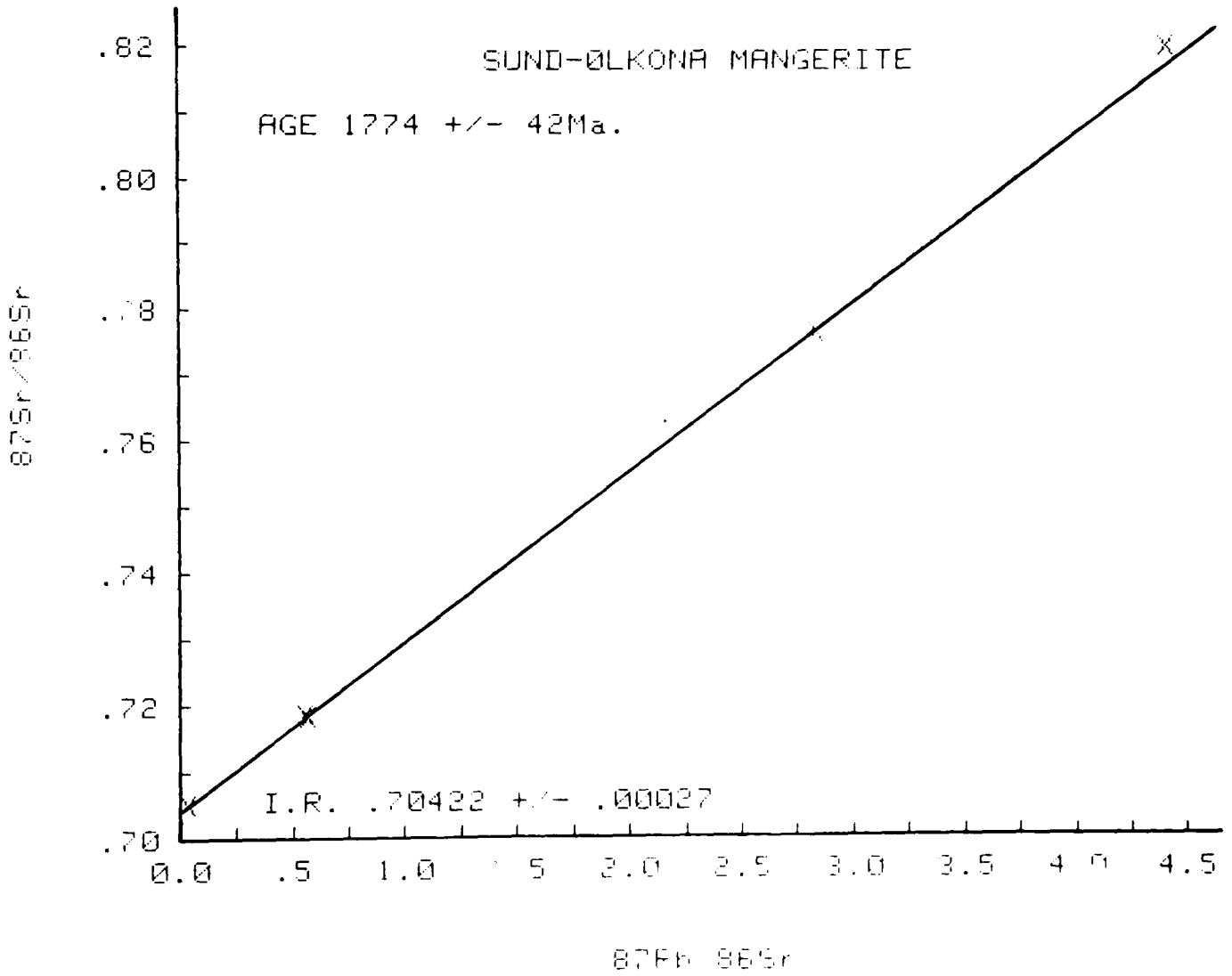


Fig. 6.15.

Rb-Sr isotope data and whole-rock isochron for fourteen samples from the South-West Lofoten Mangerite (six from Flakstadøy, eight from Vestvågøy). The scatter about the isochron could be due to either subsequent disturbance of the Sr isotopes by metamorphism (as suggested for the migmatites at Festvåg and Sandset and for the Vik gneisses) or by variations in initial $^{87}Sr/^{86}Sr$ ratios. The wide ranges in petrography and chemistry for this mangerite suggests that the latter explanation may be valid. The fourteen point isochron age for this intrusion published in Griffin et ao. (1978) is 1735 ± 25Ma (2σ) and $(^{87}Sr/^{86}Sr)_0$ is 0.70411 ± 16.

SOUTH-WEST LOFOTEN MANGERITE

SAMPLE NAME	Rb ppm	Sr ppm	87Rb/86Sr	87Sr/86Sr
WL307	33	565	0.1609	0.70819
WL309	28	594	0.1285	0.70721
WL315	24	843	0.0752	0.70499
WL316	34	919	0.0995	0.70558
WL319	155	263	1.7784	0.74887
WL331	42	495	0.2292	0.71002
WL401	42	639	0.1742	0.70873
WL402	53	371	0.3995	0.71434
WL403	47	396	0.3717	0.71323
WL404	54	422	0.3885	0.71407
WL405	40	461	0.2648	0.71095
WL410	20	973	0.0521	0.70447
WL416	79	826	0.2431	0.70959
WL417	77	384	0.6057	0.71951

Slope	0.027252	Error	0.000189 (1 Sigma)
Intercept	0.703356	Error	0.000044 (1 Sigma)
Centroid	0.185430	0.708409	
Squared residuals	291.783		
M.S.W.D.	24.315		
No. of Cycles	5		

Slope	0.027252	Error	0.000933 (1 Sigma)
Intercept	0.703356	Error	0.000216 (1 Sigma)
Centroid	0.185430	0.708409	
Squared residuals	12.000		
M.S.W.D.	1.000		
No. of Cycles	5		

Age 1893.5 +/- 127.9 Ma. (2 sigma)

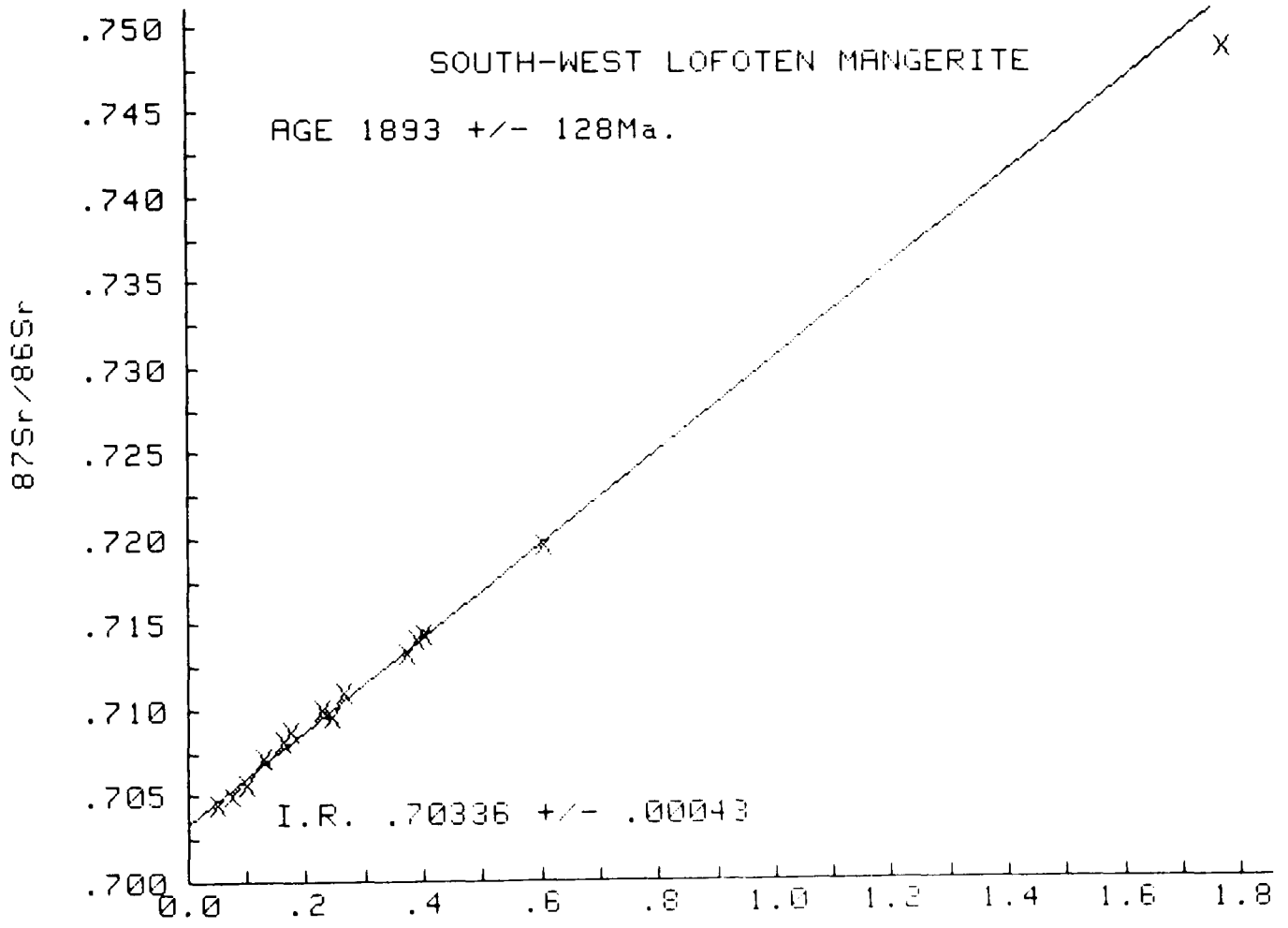


Fig. 6.16.

Rb-Sr isotope data and whole-rock isochron for nine samples from the Hopen Mangerite/Charnockite. The charnockite sample, WL575, has the highest Rb/Sr and $^{87}Sr/^{86}Sr$ ratios of any mangeritic rock analysed. The nine-point isochron age for this intrusion published in Griffin et al. (1978) is 1790 ± 50 Ma (2σ) and $(^{87}Sr/^{86}Sr)_0$ is 0.70456 ± 72.

HOPEN MANGERITE/CHARNOCKITE

SAMPLE NAME	Rb ppm	Sr ppm	87Rb/86Sr	87Sr/86Sr
WL508	88	192	2.0585	0.75960
WL510	71	220	1.3031	0.73901
WL514	83	72	3.9962	0.81012
WL516	78	254	1.1173	0.73385
WL517	40	326	0.4155	0.71581
WL518	38	202	0.5608	0.71899
WL565	54	44	4.1661	0.81413
WL573	93	104	2.7373	0.77507
WL575	93	39	11.4930	0.99700

Slope	0.026045	Error	0.000131 (1 Sigma)
Intercept	0.704801	Error	0.000131 (1 Sigma)
Centroid	0.726091	0.723712	
Squared residuals	23.562		
M.S.W.D.	3.366		
No. of Cycles	2		

Slope	0.026045	Error	0.000241 (1 Sigma)
Intercept	0.704801	Error	0.000240 (1 Sigma)
Centroid	0.726091	0.723712	
Squared residuals	7.000		
M.S.W.D.	1.000		
No. of Cycles	2		

Age 1810.7 +/- 33.1 Ma. (2 sigma)

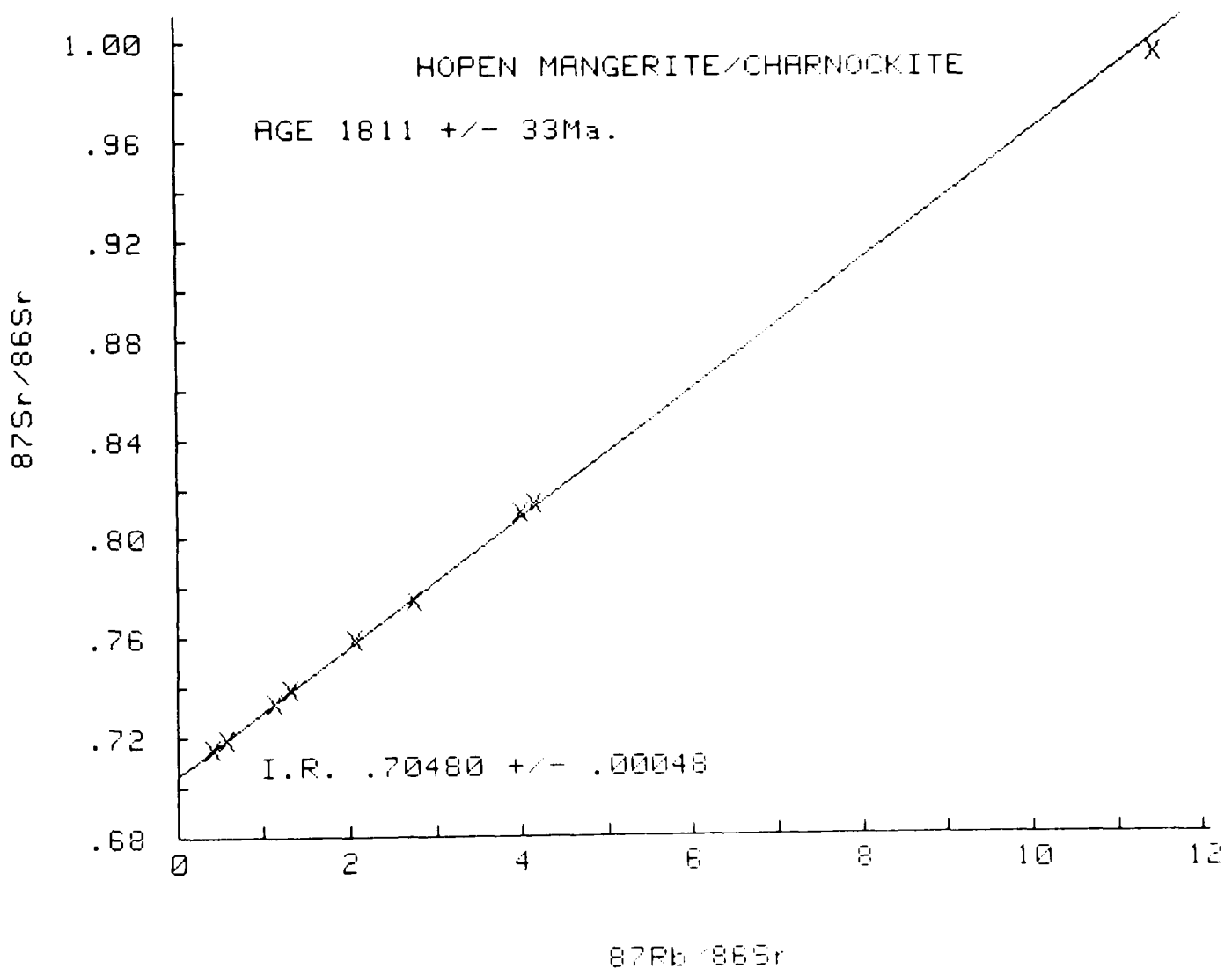


Fig. 6.17.

Rb-Sr isotope data and whole-rock isochron for six samples from the Austvågøy Grey Mangerite. The nine-point isochron age for this intrusion published in Griffin et al. (1978) is 1805 ± 20Ma (2σ) and $(^{87}Sr/^{86}Sr)_0$ is 0.70318 ± 32.

AUSTVAGØY GREY MANGERITE

SAMPLE NAME	Rb ppm	Sr ppm	87Rb/86Sr	87Sr/86Sr
WL522	115	169	3.4365	0.79414
WL525	85	216	1.5860	0.74633
WL526	98	106	3.1114	0.78638
WL529	149	382	1.1538	0.73338
WL530	30	362	0.2199	0.71005
WL533	94	454	0.6074	0.71907

Slope	0.026000	Error	0.000153 (1 Sigma)
Intercept	0.704106	Error	0.000102 (1 Sigma)
Centroid	0.444994	0.715675	
Squared residuals	43.596		
M.S.W.D.	10.899		
No. of Cycles	3		

Slope	0.026000	Error	0.000507 (1 Sigma)
Intercept	0.704106	Error	0.000335 (1 Sigma)
Centroid	0.444994	0.715675	
Squared residuals	4.000		
M.S.W.D.	1.000		
No. of Cycles	3		

Age 1807.6 +/- 69.5 Ma. (2 sigma)

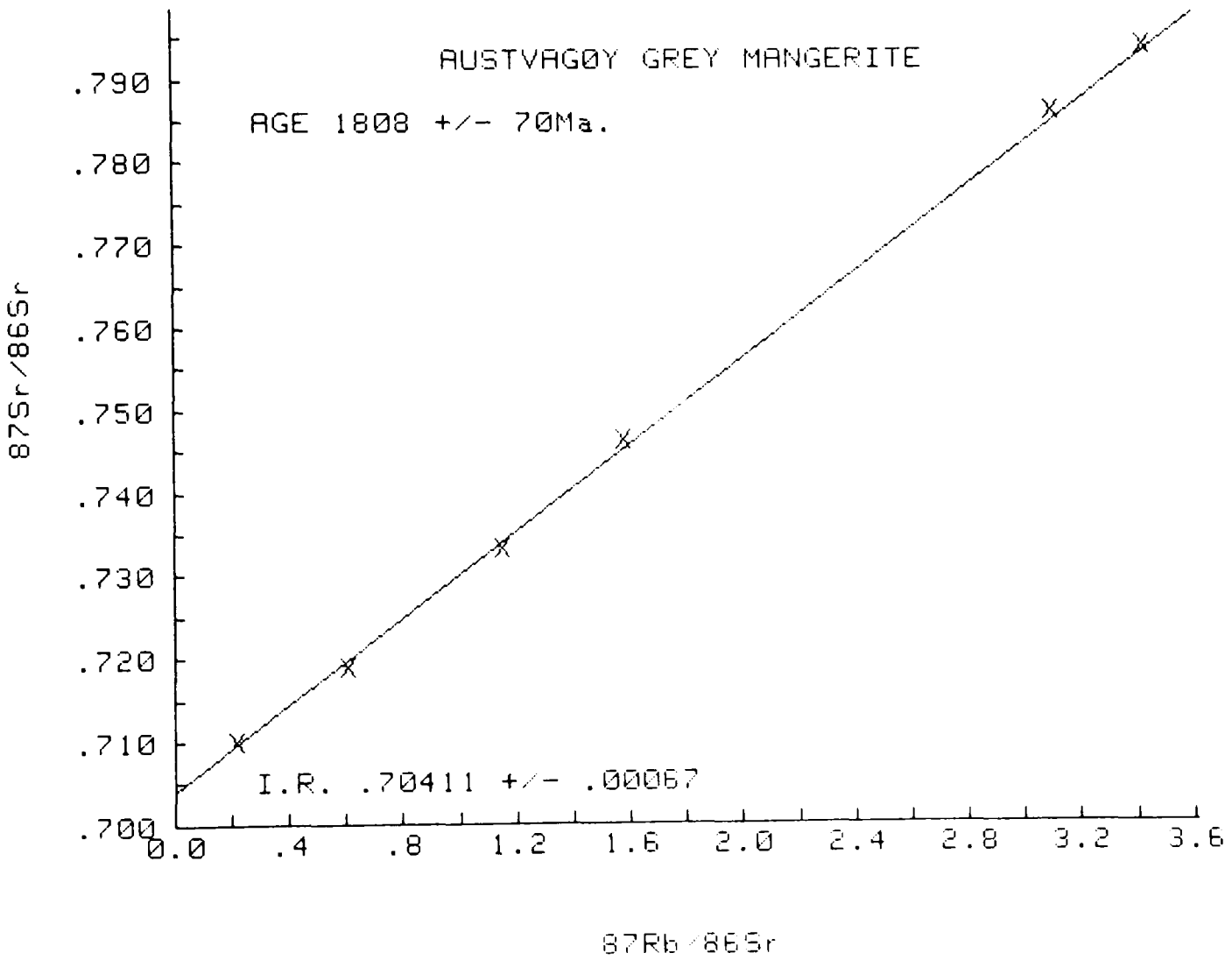


Fig. 6.18.

Rb-Sr isotope data and whole-rock isochron for twenty-one samples from the Raftsund Mangerite. This confirms that this is the youngest mangerite intrusion in the Lofoten-Vesterålen province. The Raftsund Mangerite has a small range of Rb/Sr ratios, just as it also shows little chemical variation. The twelve-point isochron age for the main (Austvågøy and Hinnøy) part of this intrusion published in Griffin et al. (1978) is 1705 ± 30Ma (2σ) and $(^{87}Sr/^{86}Sr)_0$ is 0.70513 ± 34.

RAFTSUND MANGERITE

SAMPLE NAME	Rb ppm	Sr ppm	87Rb/86Sr	87Sr/86Sr
WL101	55	398	0.3891	0.71428
WL102	60	329	0.5294	0.71777
WL103	52	355	0.4227	0.71552
WL104	52	359	0.4190	0.71560
WL105	53	345	0.4451	0.71600
WL538	48	271	0.5193	0.71759
WL539	59	273	0.6182	0.72016
WL540	49	272	0.5120	0.71743
WL602	45	424	0.2906	0.71196
WL603	37	401	0.2521	0.71090
WL604	42	359	0.3204	0.71256
WL605	48	398	0.3320	0.71283
WL606	58	299	0.5590	0.71856
WL607	27	346	0.2043	0.71007
WL609	61	134	1.3769	0.73974
WL614	59	216	0.8193	0.72492
WL617	56	243	0.6782	0.72156
WL620	63	173	1.1065	0.73250
WL625	72	120	1.9231	0.75232
WL626	54	242	0.6538	0.72077
WL628	75	55	5.0953	0.83162

Slope	0.024890	Error	0.000129 (1 Sigma)
Intercept	0.704750	Error	0.000062 (1 Sigma)
Centroid	0.419212	0.715184	
Squared residuals	42.636		
M.S.W.D.	2.244		
No. of Cycles	3		

Age 1731.3 +/- 17.8 Ma. (2 sigma)

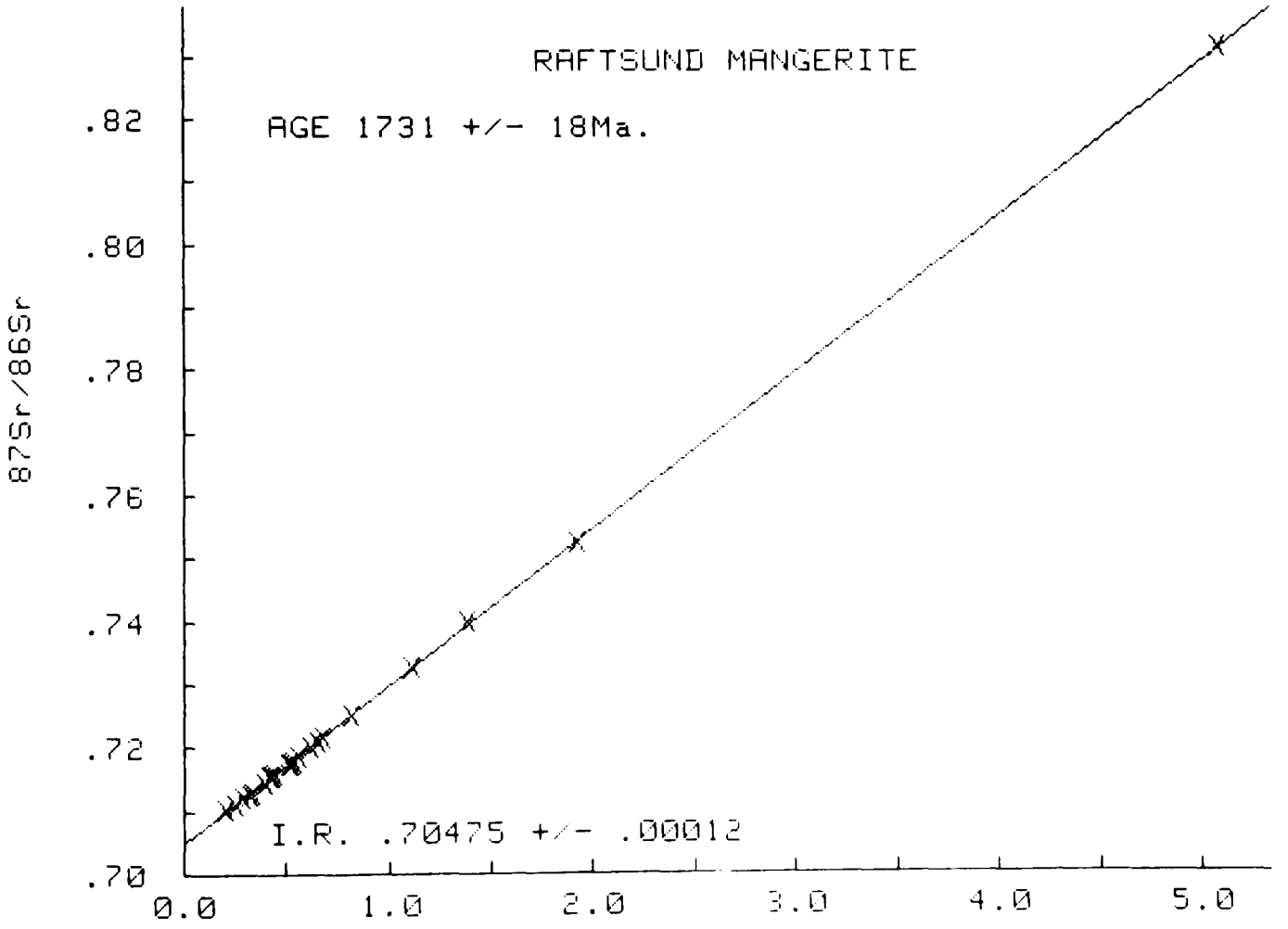
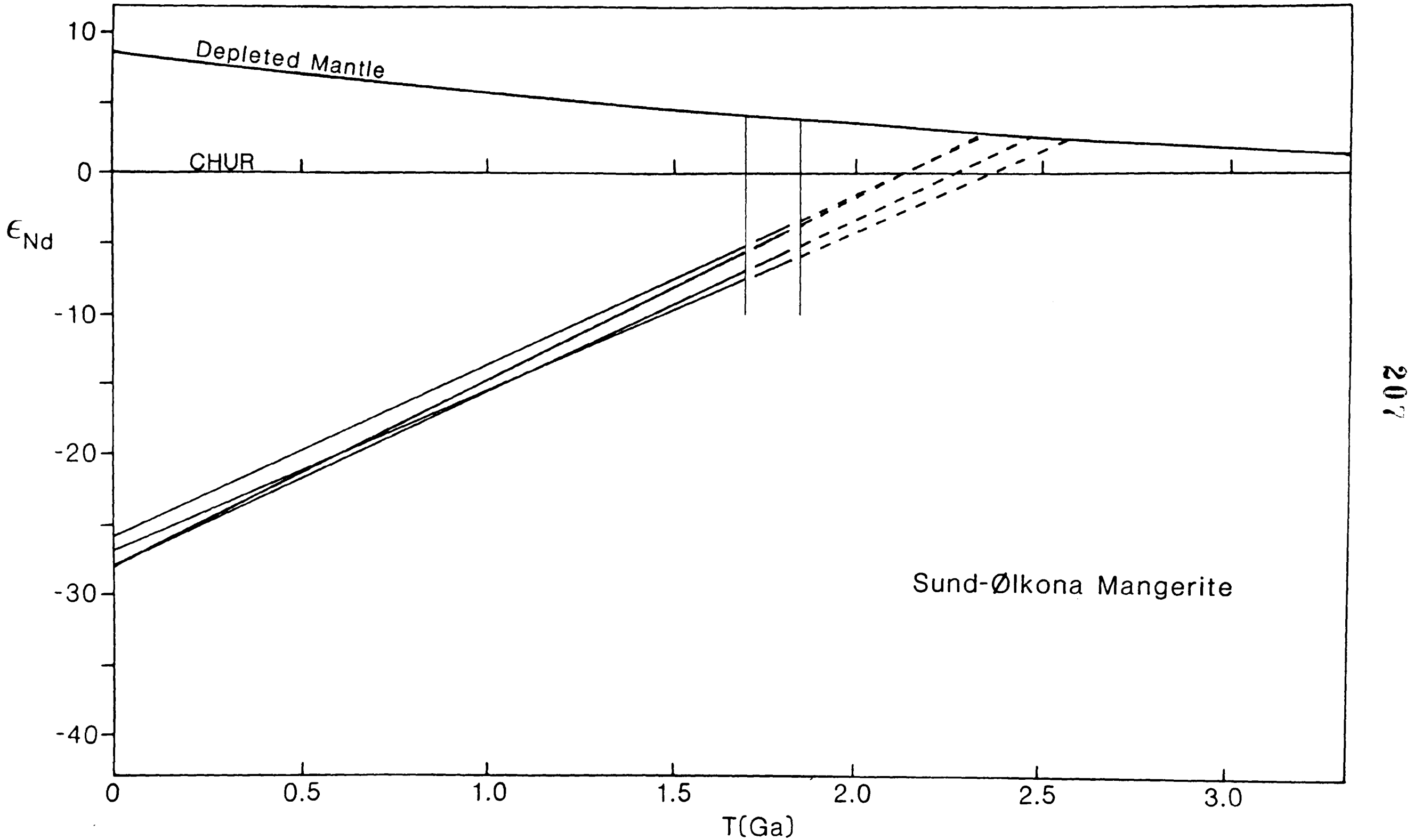


Fig. 6.19.

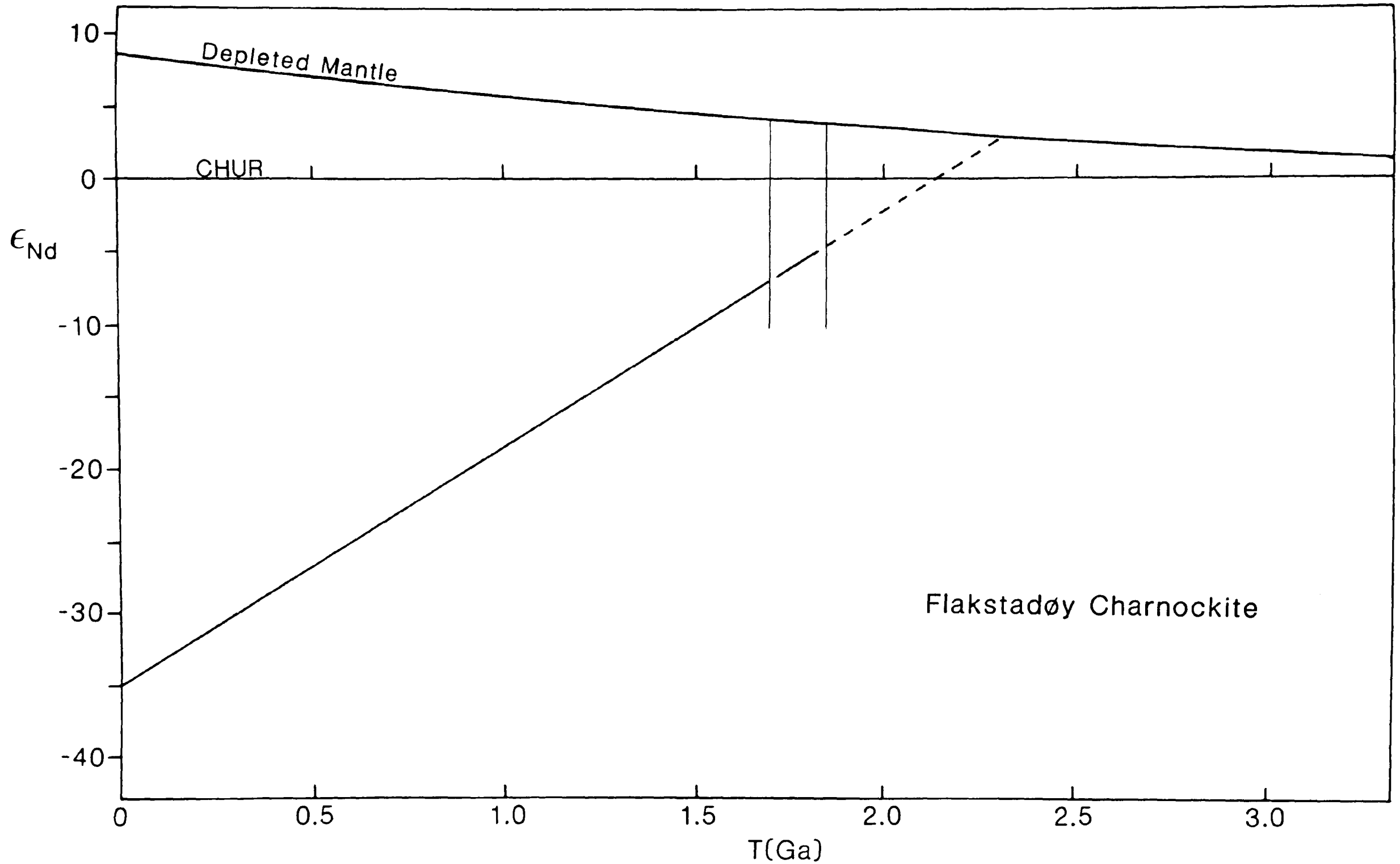
Sm-Nd evolution diagram for the Sund-Ølkona Mangerite. The narrow range of $^{147}Sm/^{144}Nd$ values effectively rules out Sm-Nd whole-rock isochron dating for this, and the other, mangerite intrusions. Sm-Nd data are tabulated in Table 6.11. ε_{Nd} values were not homogeneous for the Sund-Ølkona Mangerite at the time of intrusion. (The vertical lines define the age range 1.7 - 1.85Ga). These values are all negative showing that the mangerites cannot have formed by simple extraction of magma from depleted (or undepleted mantle) at 1.8Ga. For the mangerites, the interpretation of a T_{DM} model age as approximating rock-formation age is manifestly inappropriate, rather, T_{DM} is a composite age, averaging the crustal residence age of all the components sampled in the mangerite-forming magmatic processes. The oldest source available is the 2.7Ga migmatitic gneisses and the youngest is 1.8Ga mantle-derived magmas. T_{DM} model ages falling outside this age range would invalidate the model.


10
0
-10
-20
-30
-40
ϵ_{Nd}
Depleted Mantle
CHUR
Sund-Ølkona Mangerite
0
0.5
1.0
1.5
2.0
2.5
3.0
T(Ga)

202

Fig. 6.20.

Sm-Nd evolution diagram for the Flakstadøy Charnockite. This sample, WL306, has the lowest $^{147}Sm/^{144}Nd$ ratio and most negative present-day ε_{Nd} value (Table 6.11) of any mangeritic sample analysed excluding anatectic veins and dykes (see Chapter 7). The vertical lines define the age range 1.7 - 1.85Ga.


10
0
-10
-20
-30
-40
ϵ_{Nd}
Depleted Mantle
CHUR
Flakstadøy Charnockite
0
0.5
1.0
1.5
2.0
2.5
3.0
T(Ga)

203

Fig. 6.21.

Sm-Nd evolution diagram for the South-West Lofoten Mangerite. This intrusion has the widest chemical range of the mangerites (Tables 6.2 and 6.3), scatter of data-points about its Rb-Sr whole-rock isochron and the widest range in ε_{Nd} values at the time of intrusion. (The vertical lines define the age range 1.7 - 1.85Ga). This suggests that the possibility of real heterogeneities in the Sr and Nd isotopic compositions of parent magmas is an issue worthy of serious consideration. The very narrow range of $^{147}Sm/^{144}Nd$ ratios for the intrusion is shown by the parallelism of the evolution lines. The youngest T_{DM} value (2.06Ga) is for a sample from this intrusion (Table 6.11).

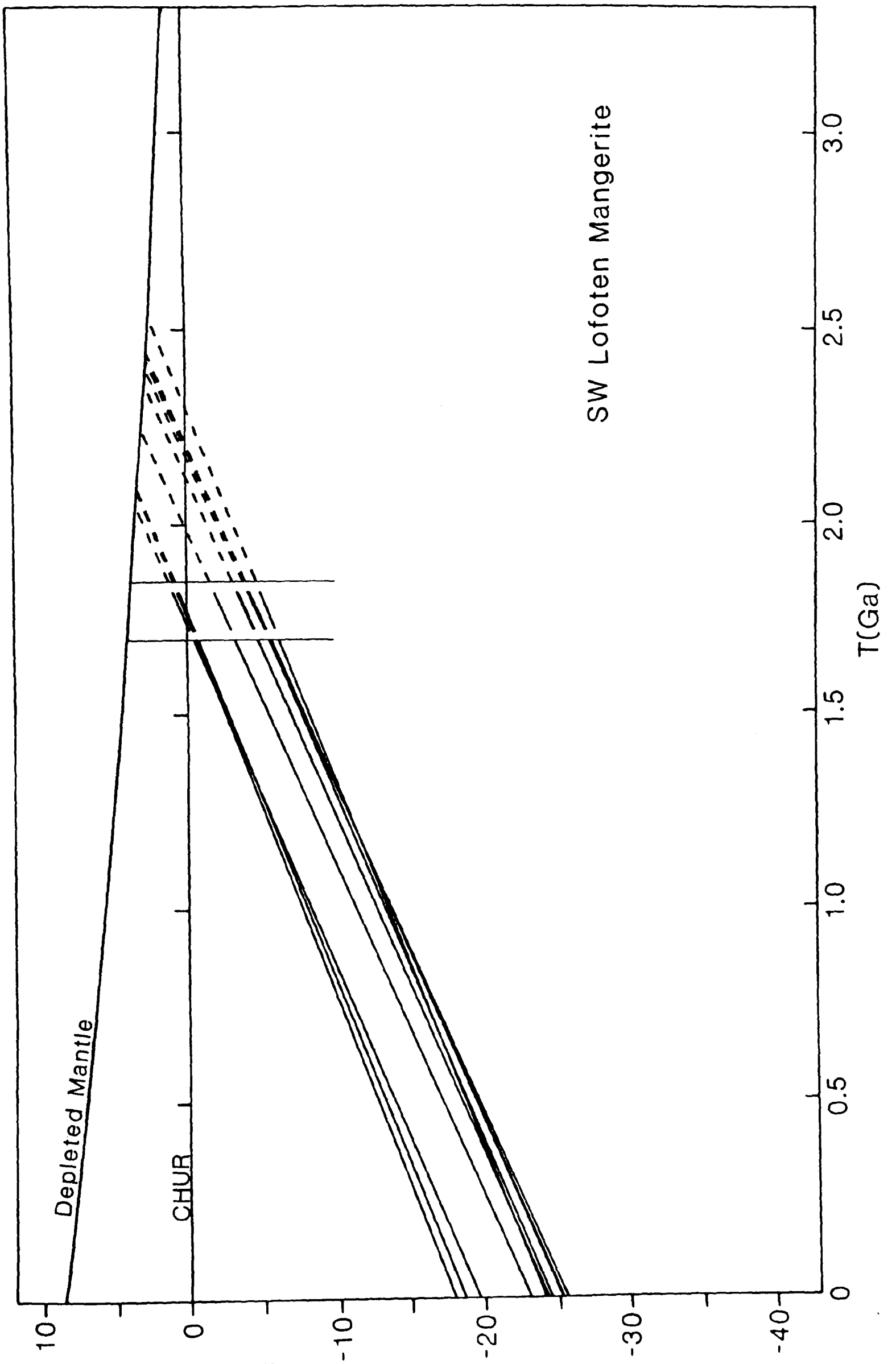

SW Lofoten Mangerite
Depleted Mantle
CHUR
ϵ_{Nd}
10
0
-10
-20
-30
-40
0
0.5
1.0
1.5
2.0
2.5
3.0
T(Ga)

Fig. 6.22.

Sm-Nd evolution diagram for the Hopen Mangerite/Charnockite. This intrusion shows slight convergence of Nd evolution lines at about 1.7Ga (the vertical lines define the age range 1.7 - 1.85Ga) but the range of $^{147}Sm/^{144}Nd$ ratios is still too small for effective Sm-Nd whole-rock isochron dating. The charnockite samples have lower $^{147}Sm/^{144}Nd$ ratios than the mangerites. Sm-Nd data tabulated in Table 6.11.

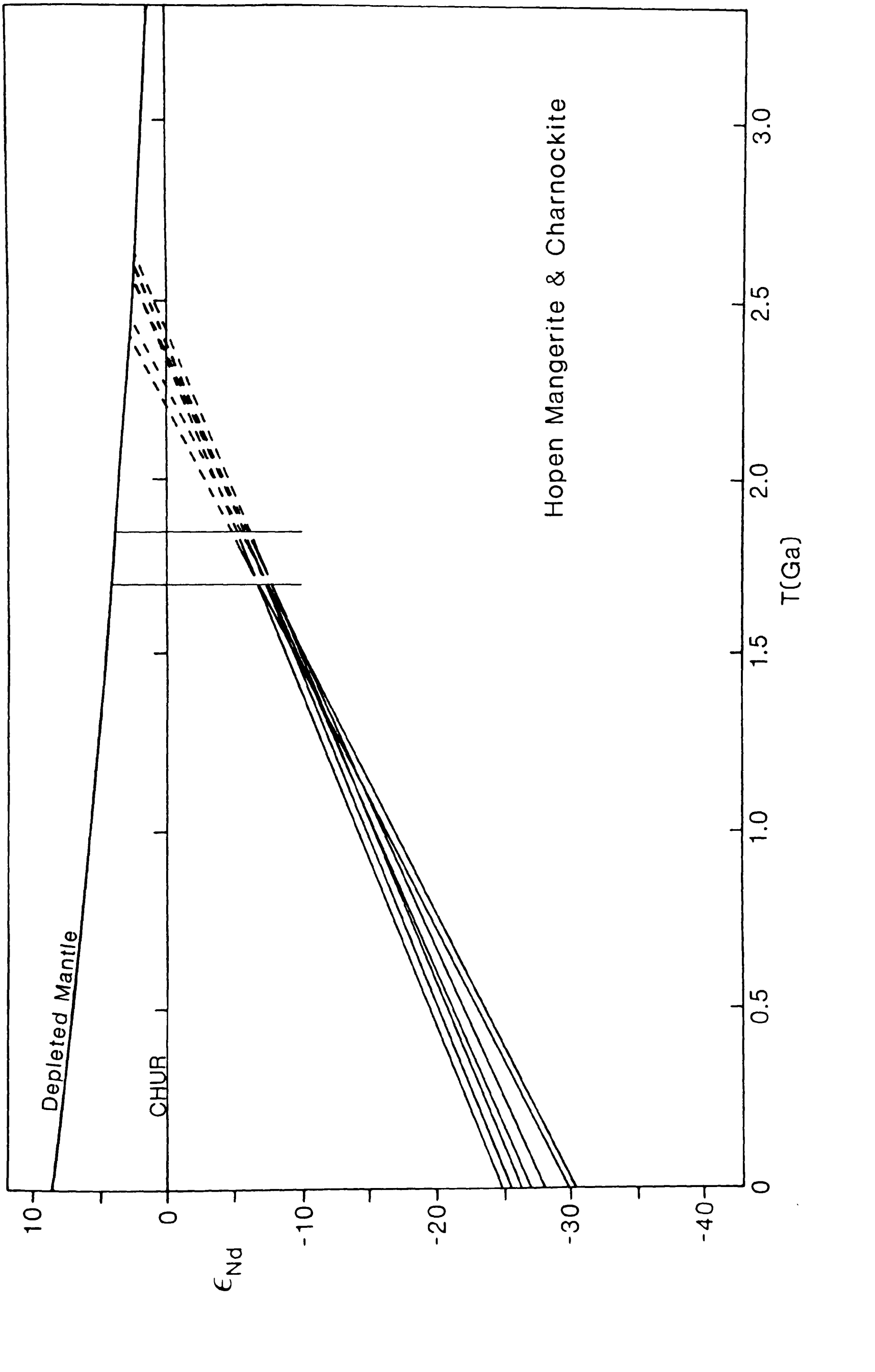

Hopen Mangerite & Charnockite
Depleted Mantle
CHUR
10
0
-10
-20
-30
-40
ϵ_{Nd}
0
0.5
1.0
1.5
2.0
2.5
3.0
T(Ga)

Fig. 6.23.

Sm-Nd evolution diagram for the Austvågøy Grey Mangerite. The oldest T_{DM} value (2.64Ga) is for a sample from this intrusion (Table 6.11). The verticallines define the age range 1.7 - 1.85Ga.

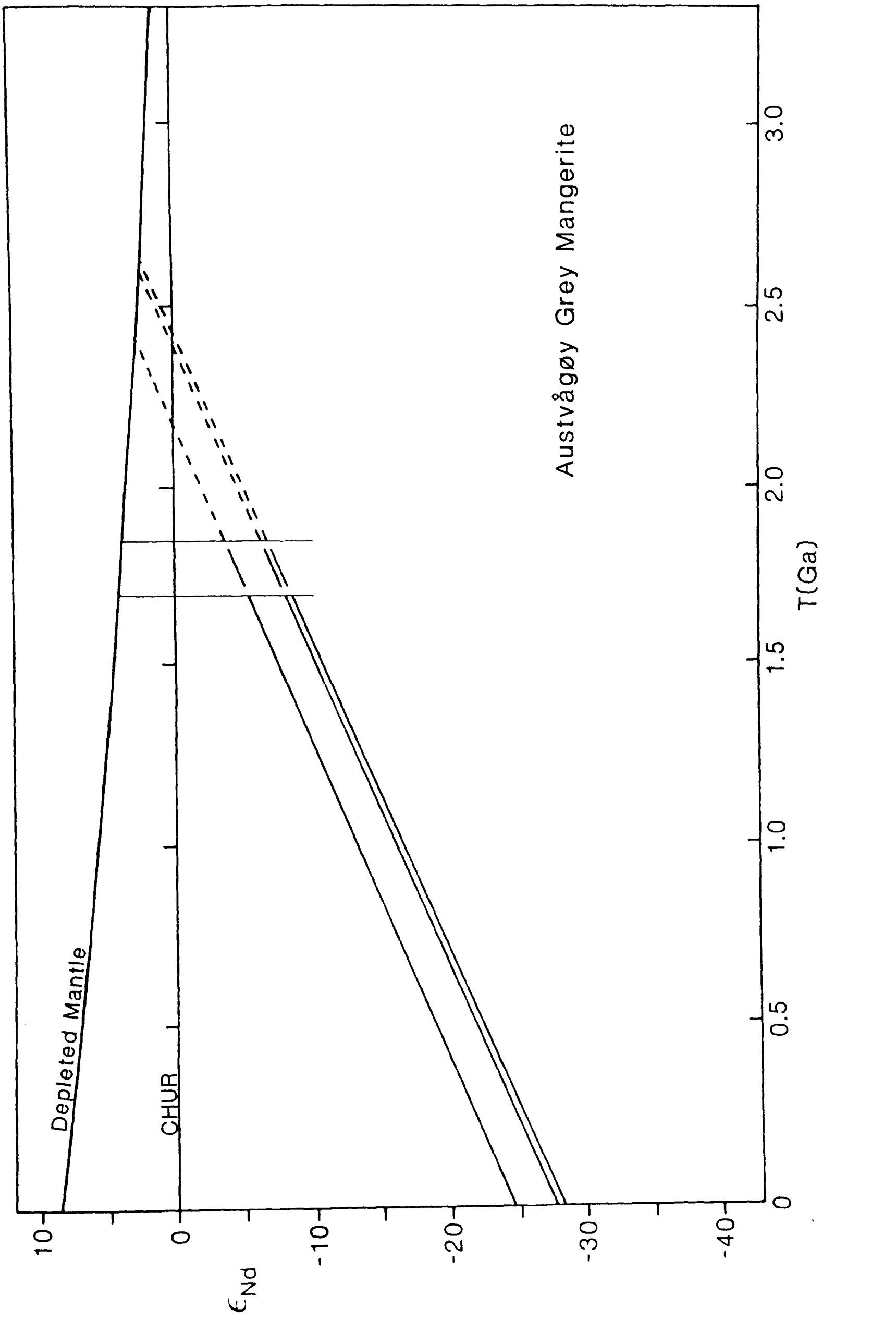

Austvågøy Grey Mangerite
Depleted Mantle
CHUR
10
0
-10
-20
-30
-40
ϵ_{Nd}
0
0.5
1.0
1.5
2.0
2.5
3.0
T(Ga)

Fig. 6.24.

Sm-Nd evolution diagram for the Raftsund Mangerite. As for the Hopen intrusion (Fig. 6.22) the Raftsund Mangerite shows slight convergence at 1.7 - 1.85Ga (the age range defined by the vertical lines) but the range of $^{147}Sm/^{144}Nd$ values is too small for effective Sm-Nd whole-rock isochron dating. The Raftsund Mangerite has the narrowest range of T_{DM} values of the mangerite intrusions, which, using this model, would indicate that it is a very homogeneous body. This is in agreement with the narrow range in major element compositions (Table 6.6).

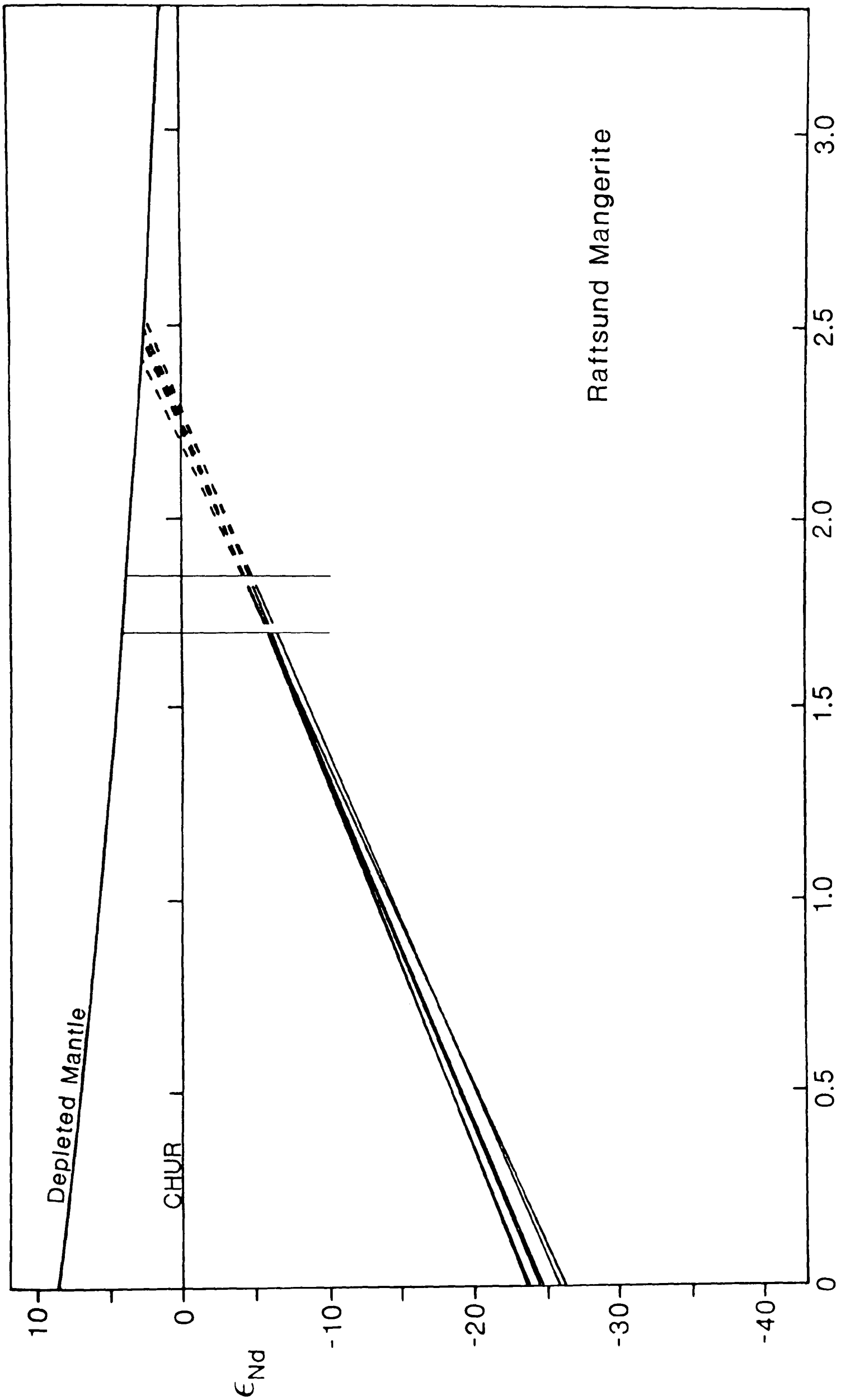

Raftsund Mangerite
Depleted Mantle
CHUR
10
0
-10
-20
-30
-40
ϵ_{Nd}
0
0.5
1.0
1.5
2.0
2.5
3.0
T(Ga)

Fig. 6.25.

Sm-Nd evolution diagram for the Langøy Mangerites. Two samples are from the Hovden Mangerite, one from the Steine Mangerite and one from the Eidsfjord Mangerite (Table 6.11).

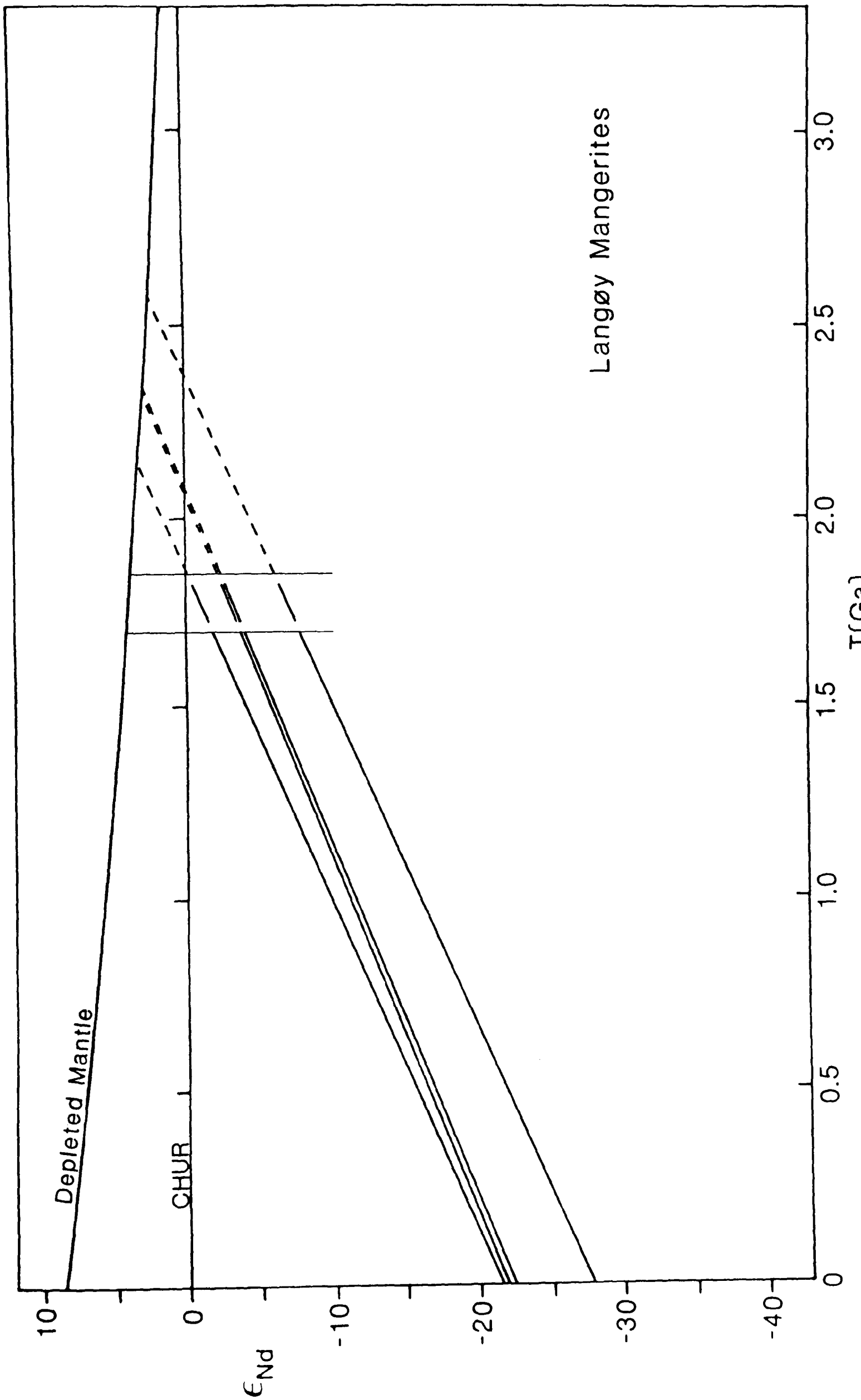
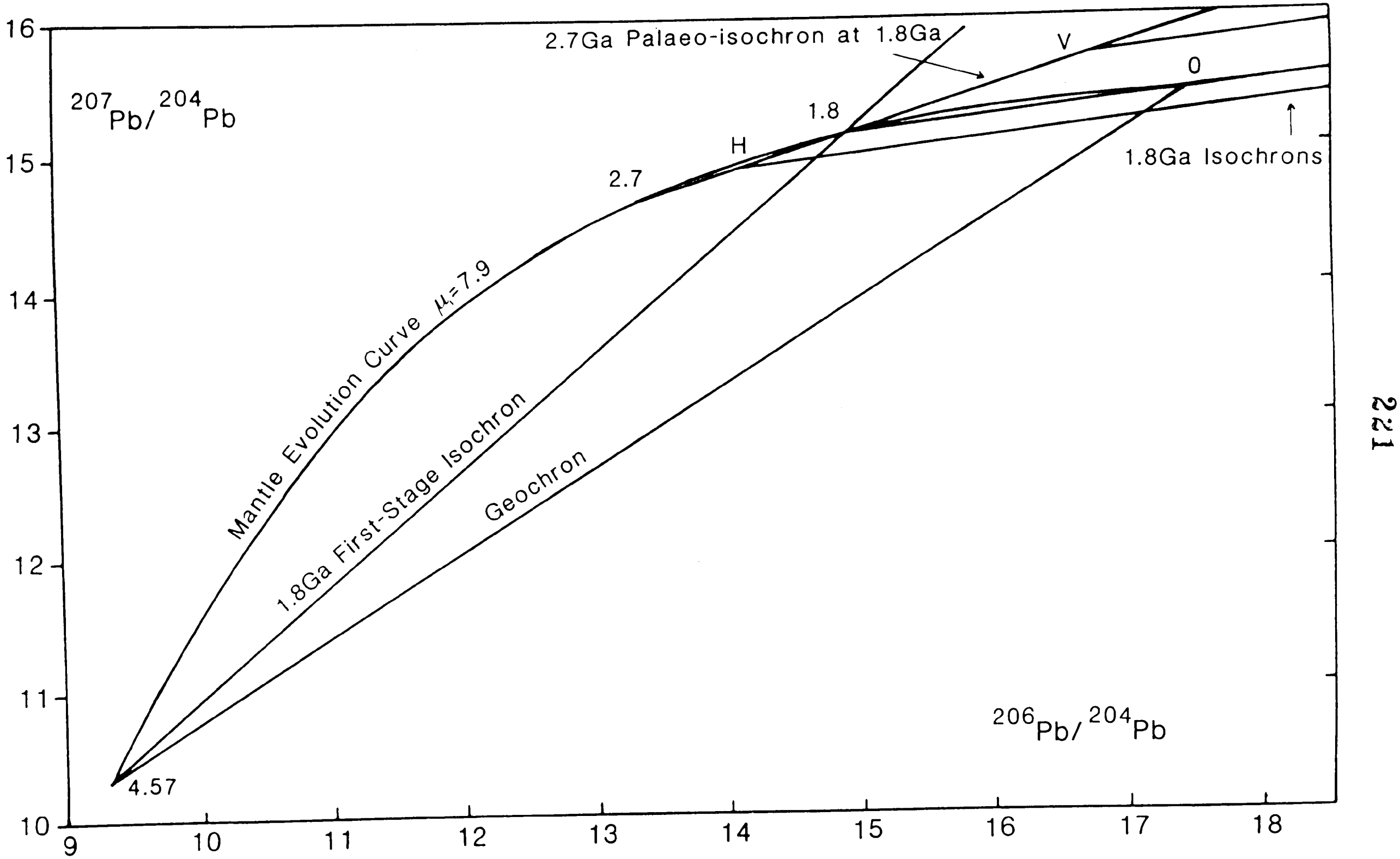

Langøy Mangerites
Depleted Mantle
CHUR
ϵ_{Nd}
10
0
-10
-20
-30
-40
0
0.5
1.0
1.5
2.0
2.5
3.0
T(Ga)

Fig. 6.26.

The interpretational model for the mangerites in the $^{207}Pb/^{204}Pb$ v. $^{206}Pb/^{204}Pb$ diagram. The diagram shows a mantle evolution curve with $\mu_1 = 7.9$ (constrained by the unradiogenic compositions of some alkali feldspar separates) between 4.57Ga and 0Ga; a 2.7Ga palaeo-isochron at 1.8Ga represents the position of the isochron for 2.7Ga gneisses i.e. at the time of emplacement of the mangerites. The Vikan (V) and North-West Hinnøy (H) gneiss Pb/Pb palaeo-isochron centroids are shown, and the upper and lower limits for the spread of the North-West Hinnøy data. The 1.8Ga first-stage isochron and the Geochron are plotted from the Bulk-earth or primordial Pb isotopic composition at 4.57Ga to 1.8Ga and 0Ga respectively. Parallel 1.8Ga isochrons are shown for rock suites hypothetically derived from single-stage mantle with $\mu_1 = 7.9$ at 1.8Ga, and from melting of Vikan, and North-West Hinnøy gneisses of mean Pb isotope composition at 1.8Ga. The Pb isotope compositions of the mangerites are seen related to this model in Figs. 6.27 to 6.32.


16
15
14
13
12
11
10
9
10
11
12
13
14
15
16
17
18
$^{207}Pb/^{204}Pb$
$^{206}Pb/^{204}Pb$
2.7Ga Palaeo-isochron at 1.8Ga
V
0
1.8
H
2.7
1.8Ga Isochrons
Mantle Evolution Curve μ_1=7.9
1.8Ga First-Stage Isochron
Geochron
4.57

2.21

Fig. 6.27.

$^{207}Pb/^{204}Pb$ v. $^{206}Pb/^{204}Pb$ diagram for the Sund-Ølkona Mangerite shows two whole-rock (circles) and one alkali feldspar mineral separate (triangles) data-point less radiogenic than the 1.8Ga first-stage isochron, demonstrating that these rocks must contain a component derived from U-depleted crust older than 1.8Ga. The Sund-Ølkona Mangerite includes the most radiogenic mangeritic rock from the Lofoten-Vesterålen province: WL302. Vikan (V) and North-West Hinnøy (H) 1.8Ga palaeo-centroids are shown and the lower limit for the North-West Hinnøy gneisses at 1.8Ga.

Sund-Ølkona Mangerite

$^{207}Pb/^{204}Pb$

16.0
15.5
15.0
14.5

13.0
14.0
15.0
16.0
17.0

$^{206}Pb/^{204}Pb$

V
0
μ_1=7.9
1.8
H
Min
2.7
Geochron

223

Fig. 6.28.

$^{207}Pb/^{204}Pb$ v. $^{206}Pb/^{204}Pb$ diagram for the South-West Lofoten Mangerite (whole rock analyses: circles; alkali feldspar separates: triangle) and the Flakstadøy Charnockite (square). On geochemical, and Sr and Nd isotopic grounds, the South-West Lofoten Mangerite is the most heterogeneous of the mangerites. It also has the widest range of Pb isotope compositions for any mangerite (excluding WL302 from Sund-Ølkona). The most basic samples have the most radiogenic Pb isotopic compositions for this mangerite and plot close to the 1.8Ga isochron for rocks derived from the mantle, implying that they have a smaller crustal component than the other samples in this mangerite body.

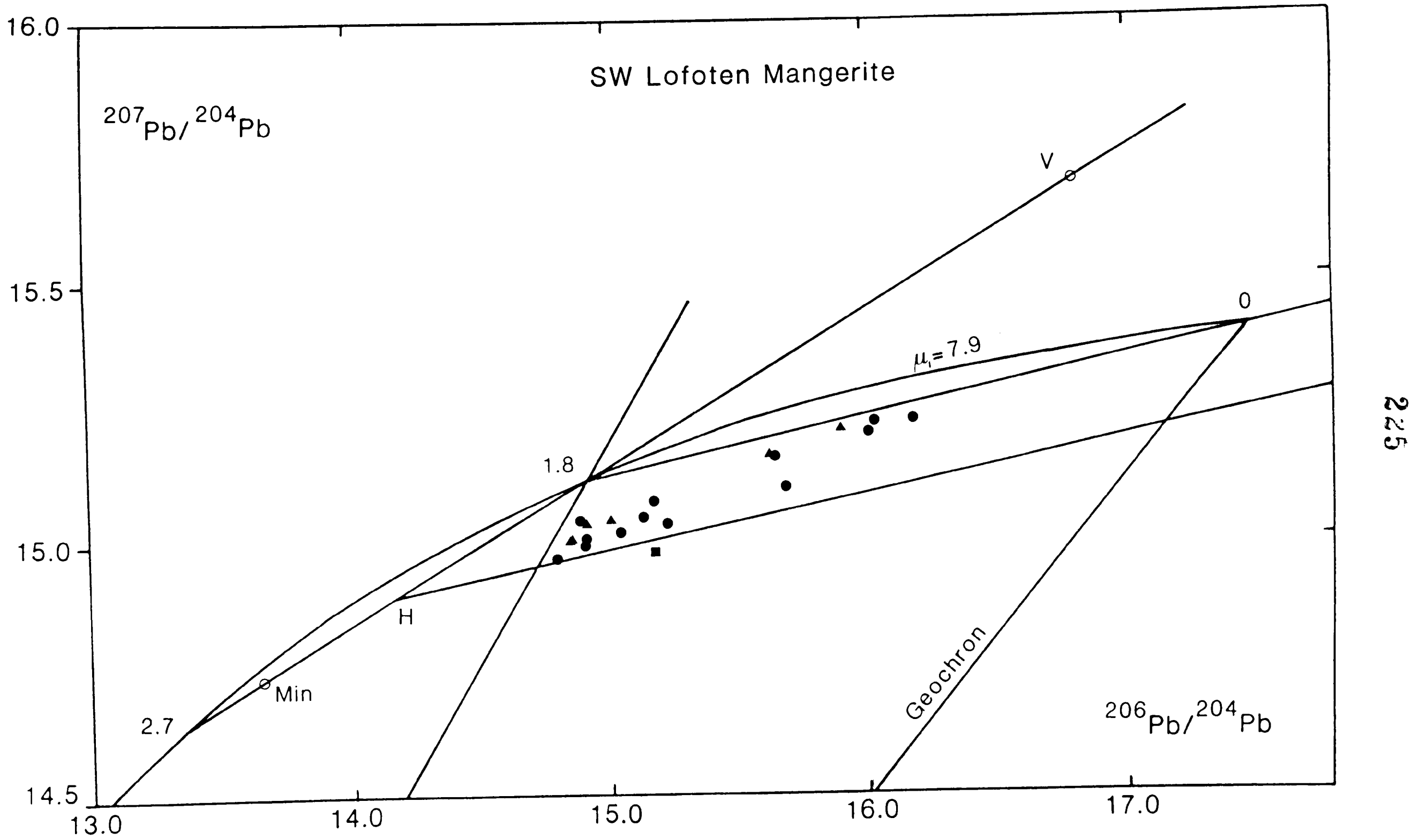

SW Lofoten Mangerite
$^{207}Pb/^{204}Pb$
$^{206}Pb/^{204}Pb$
16.0
15.5
15.0
14.5
13.0
14.0
15.0
16.0
17.0
V
0
μ_1=7.9
1.8
H
Min
2.7
Geochron

Fig. 6.29.

$^{207}Pb/^{204}Pb$ v. $^{206}Pb/^{204}Pb$ diagram for the Hopen Mangerite/Charnockite which has the least radiogenic average Pb isotope composition of the mangerites. One whole-rock (circle) and three alkali feldspar (triangles) data-points are less radiogenic than the 1.8Ga first-stage isochron, demanding an ancient crustal component for these rocks. The data-points plot on or below 1.8Ga "mean crustal isochron" suggesting that the lower crustal component for these rocks was extremely depleted in uranium.

Hopen Mangerite & Charnockite

$^{207}Pb/^{204}Pb$

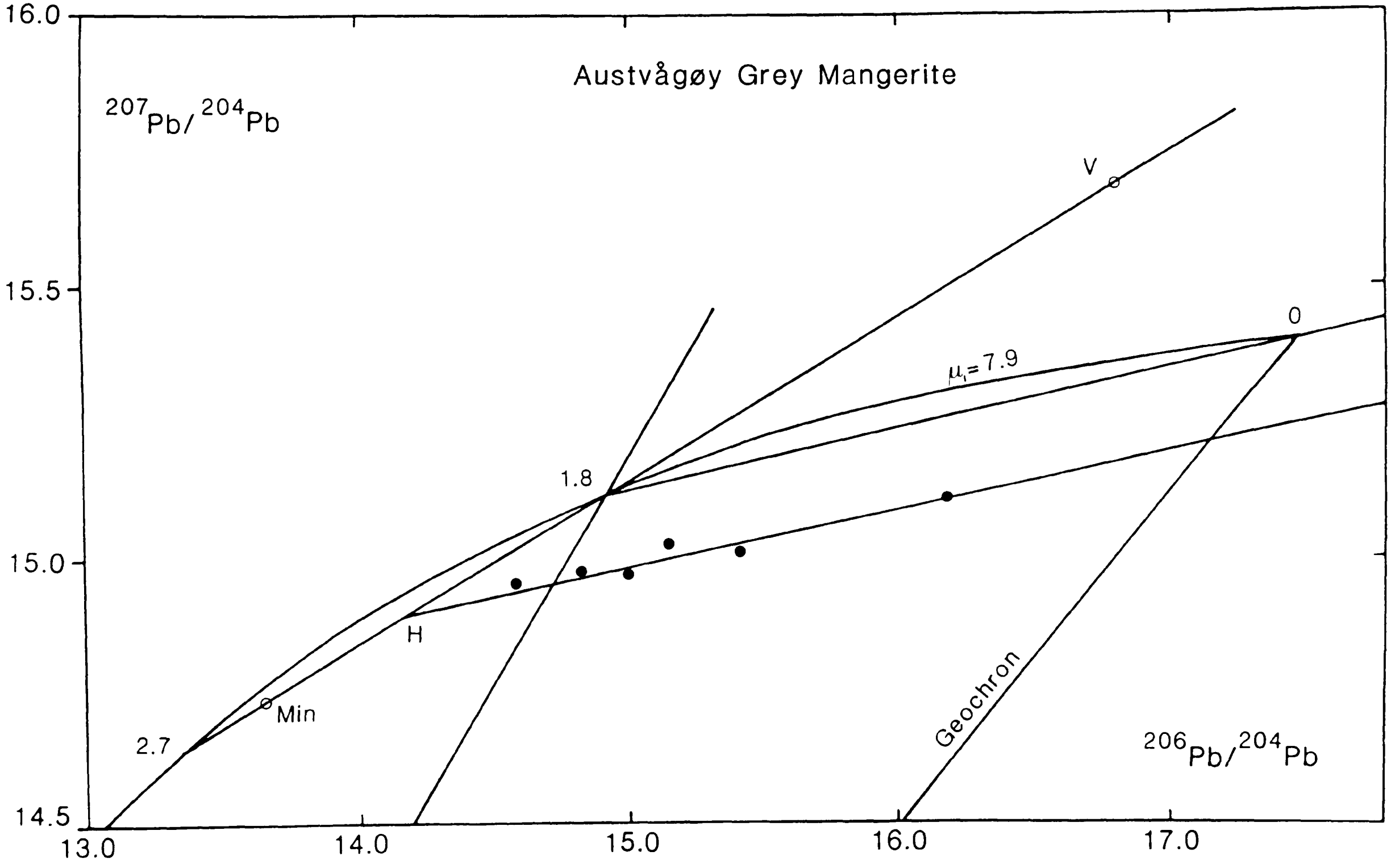
$^{206}Pb/^{204}Pb$

16.0
15.5
15.0
14.5
13.0
14.0
15.0
16.0
17.0

V
O
$\mu_1 = 7.9$
1.8
2.7
H
Min
Geochron

Fig. 6.30.

$^{207}Pb/^{204}Pb$ v. $^{206}Pb/^{204}Pb$ diagram for the Austvågøy Grey Mangerite for which one whole-rock data-point is less radiogenic than the 1.8Ga first-stage isochron, hence this intrusion requires an ancient crustal component. The data-points for the Austvågøy Grey Mangerite form an array parallel to the data for the Hopen intrusion (Fig. 6.29) but plotting higher on the diagram; this suggests that the crustal component for the Austvågøy Grey Mangerite was less strongly depleted in uranium than the crustal source of the Hopen intrusion, and consequently the former may have been derived from a higher crustal level than the latter.


Austvågøy Grey Mangerite
$^{207}Pb/^{204}Pb$
$^{206}Pb/^{204}Pb$
16.0
15.5
15.0
14.5
13.0
14.0
15.0
16.0
17.0
V
0
$\mu_1 = 7.9$
1.8
H
Min
2.7
Geochron

672

Fig. 6.31.

$^{207}Pb/^{204}Pb$ v. $^{206}Pb/^{204}Pb$ diagram for the Raftsund Mangerite, which is the largest intrusion in the Lofoten-Vesterålen province, but shows the smallest range in geochemistry and Sr and Nd isotopes of any of the mangerites. This figure demonstrates that, except for WL101, the sample from Hamarøy, the Raftsund Mangerites has the smallest range in Pb isotope compositions of any mangerite. The sample from the mangerite on Hamarøy is much more radiogenic than any of the other fourteen samples from the main body of the Raftsund Mangerite, on Austvågøy and Hinnøy. This casts some doubt on the theory that the Hamarøy Mangerite is part of the Raftsund Mangerite.

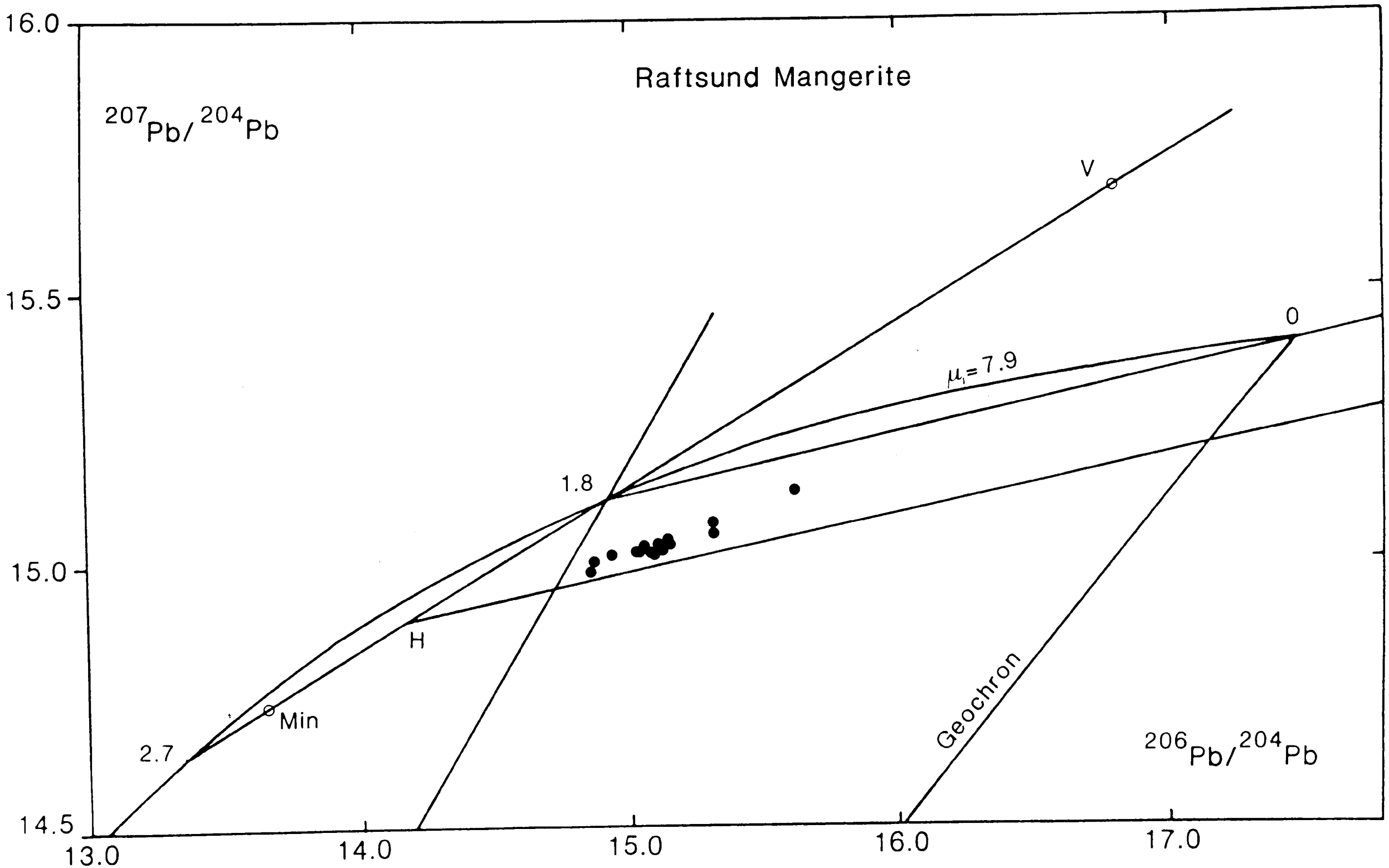

Raftsund Mangerite
$^{207}Pb/^{204}Pb$
$^{206}Pb/^{204}Pb$
16.0
15.5
15.0
14.5
13.0
14.0
15.0
16.0
17.0
V
0
μ_1=7.9
1.8
H
Min
2.7
Geochron

Fig. 6.32.

$^{207}Pb/^{204}Pb$ v. $^{206}Pb/^{204}Pb$ diagram for the Hovden Mangerite. The two samples analysed have Pb isotopic compositions within analytical error of each other, and more radiogenic than the majority of the mangerites.

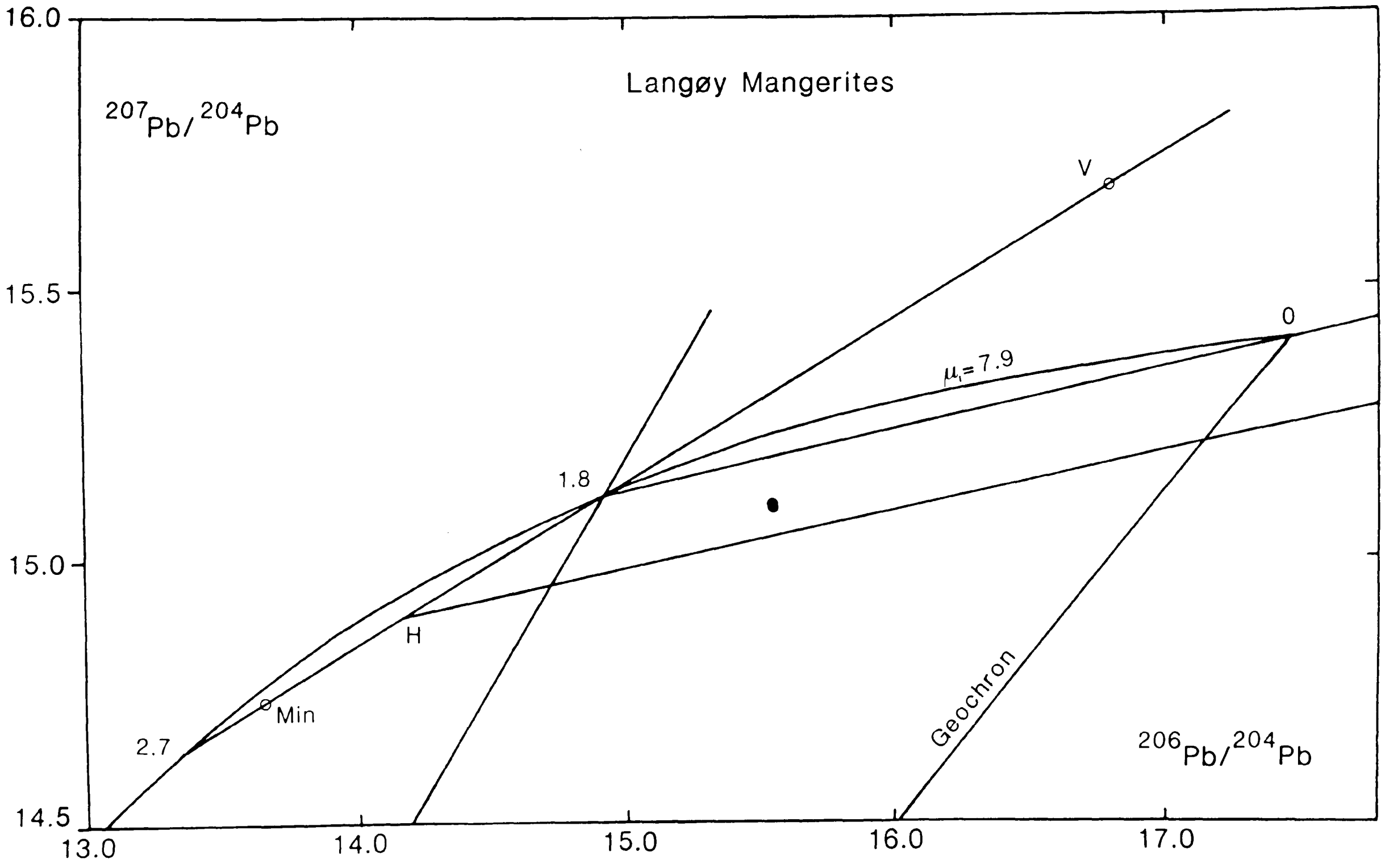

Langøy Mangerites
$^{207}Pb/^{204}Pb$
$^{206}Pb/^{204}Pb$
16.0
15.5
15.0
14.5
13.0
14.0
15.0
16.0
17.0
V
0
$\mu_1 = 7.9$
1.8
H
Min
2.7
Geochron

Fig. 6.33.

Model μ_1 v. T for the mangeritic intrusions showing the evolution of model μ_1 with time in "orogene", upper crust, lower crust and upper mantle (Plumbotectonics model of Zartman and Doe (1981)). The model μ_1 values cover a slightly wider range than those for the Flakstadøy Basic Complex (Fig. 5.13), but this diagram, nonetheless confirms that the mangerites were derived in part from a lower crustal source. The model requires a small component from the "orogene" or from "Plumbotectonics" upper crust source for the more basic rocks from the South-West Lofoten Mangerite which have high μ_1 values.

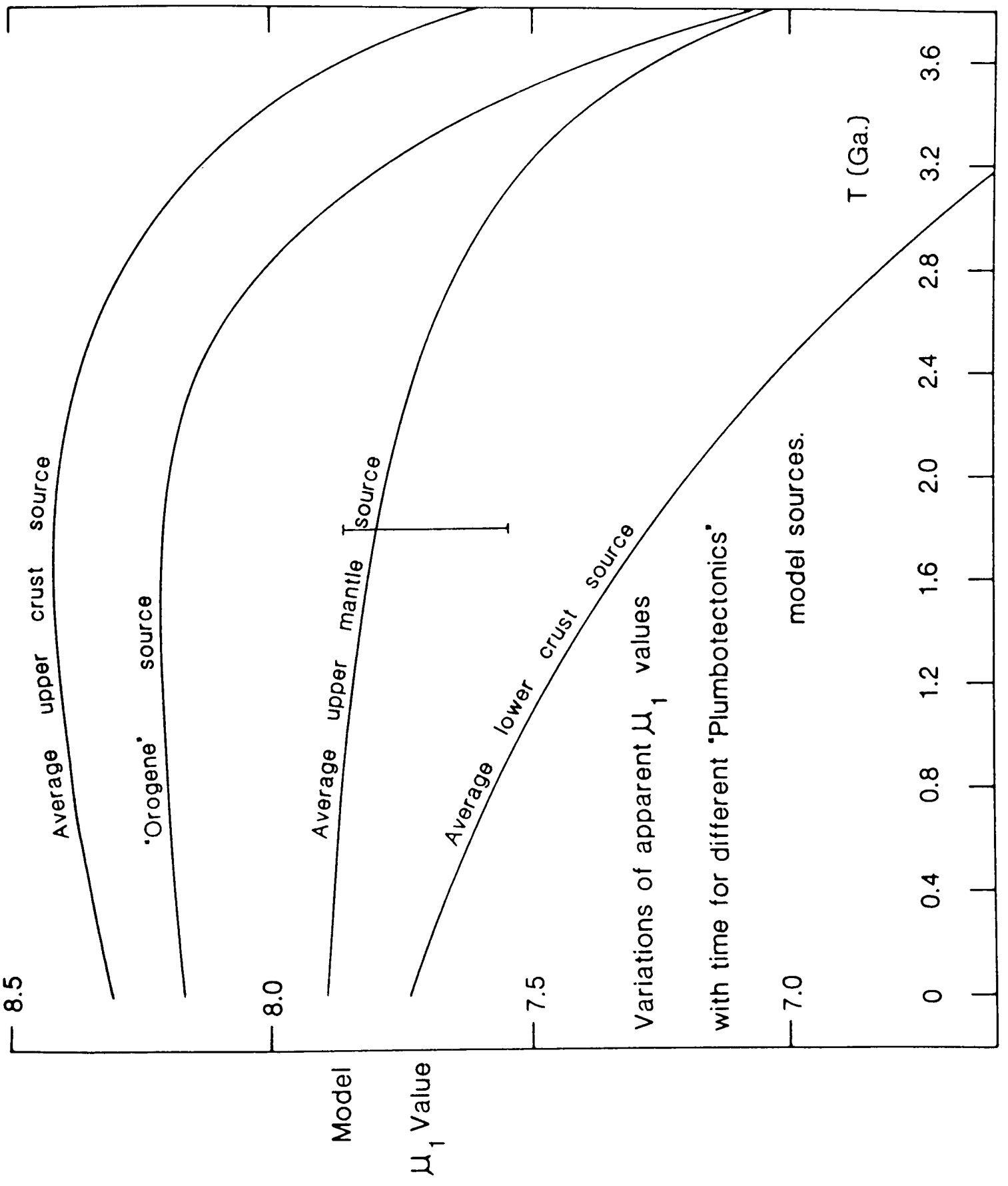

Variations of apparent μ_1 values with time for different 'Plumbotectonics' model sources.
Model μ_1 Value
8.5
8.0
7.5
7.0
Average upper crust source
'Orogene' source
Average upper mantle source
Average lower crust source
0
0.4
0.8
1.2
1.6
2.0
2.4
2.8
3.2
3.6
T (Ga.)

Fig. 6.34.

Apparent $(^{87}Sr/^{86}Sr)_{1.8}$ v. T_{DM} for mangerites (circles) and basic rocks (open triangles). There is a positive correlation between these parameters for the mangerites as predicted by the model (the higher the T_{DM} model age, the larger the proportion of material from 2.7Ga crust; and the higher the apparent $(^{87}Sr/^{86}Sr)_{1.8}$ the greater the proportion of the magma that was derived from a crustal source). The $(^{87}Sr/^{86}Sr)_{1.8}$ values for the Flakstadøy Basic Complex show very little variation due to the very low Rb concentrations. The sense of curvature of the correlation trend for the mangerites suggests that the mantle-derived component has a higher Sr/Nd ratio than the crust-derived end-member (see Section 6.5.1).

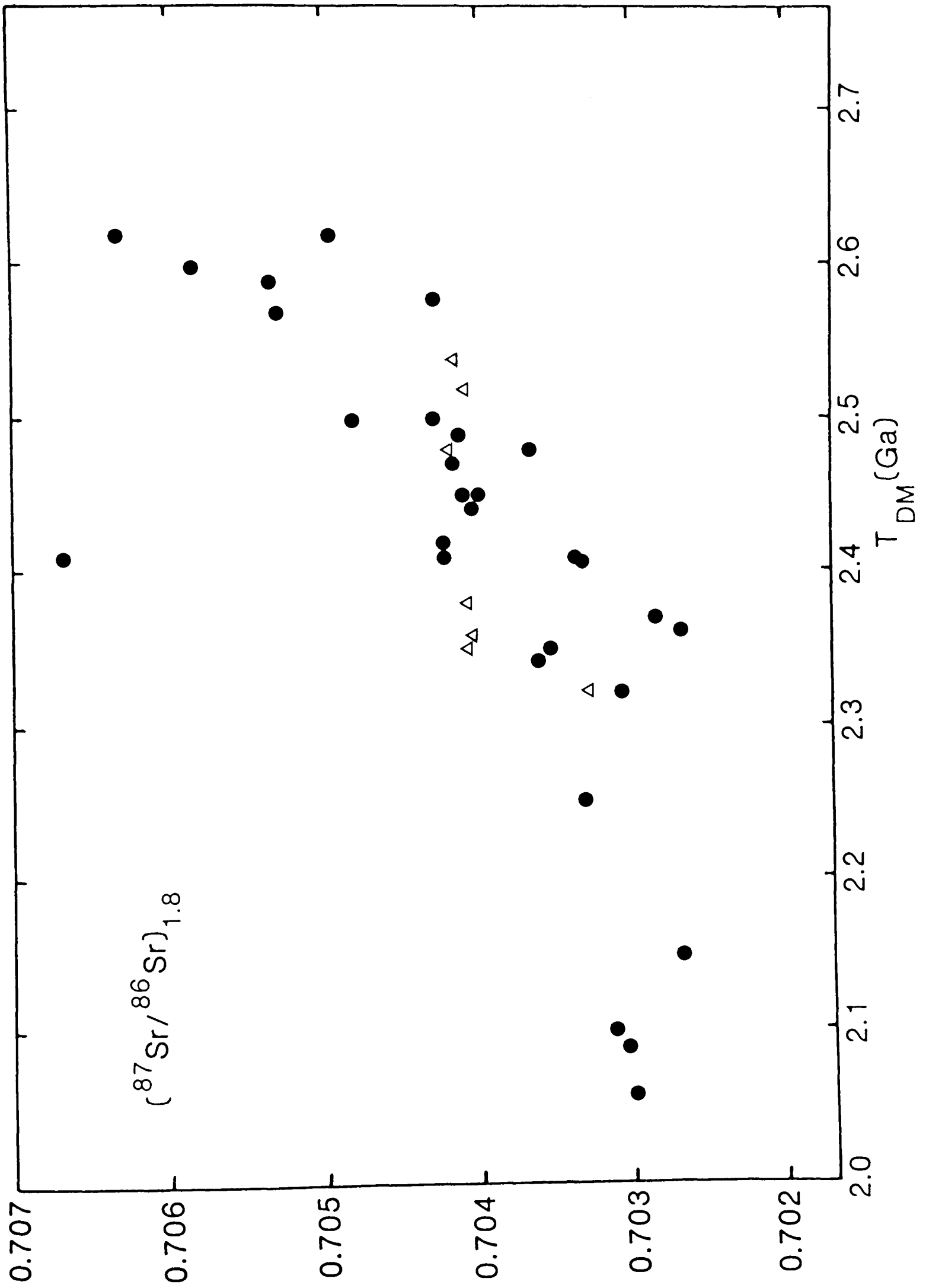

0.707
0.706
0.705
0.704
0.703
0.702
$(^{87}Sr/^{86}Sr)_{1.8}$
2.0
2.1
2.2
2.3
2.4
2.5
2.6
2.7
T_{DM}(Ga)

Fig. 6.35.

Model μ_1 v. T_{DM} for mangerites (circles) and basic rocks (open triangles). There is a negative correlation between the parameters for the mangerites as predicted by the model (the higher the apparent μ_1, the greater the proportion of the high-μ component, i.e. mantle-derived magma). There is no correlation for the Flakstadøy Basic Complex since its Nd isotopes were homogenized at 1.8Ga so that its T_{DM} values do not indicate relative crust and mantle contributions to the magma. The sense of curvature of the correlation trend for the mangerites suggests that the mantle-derived component may have a rather high Pb concentration (see Section 6.5.1).

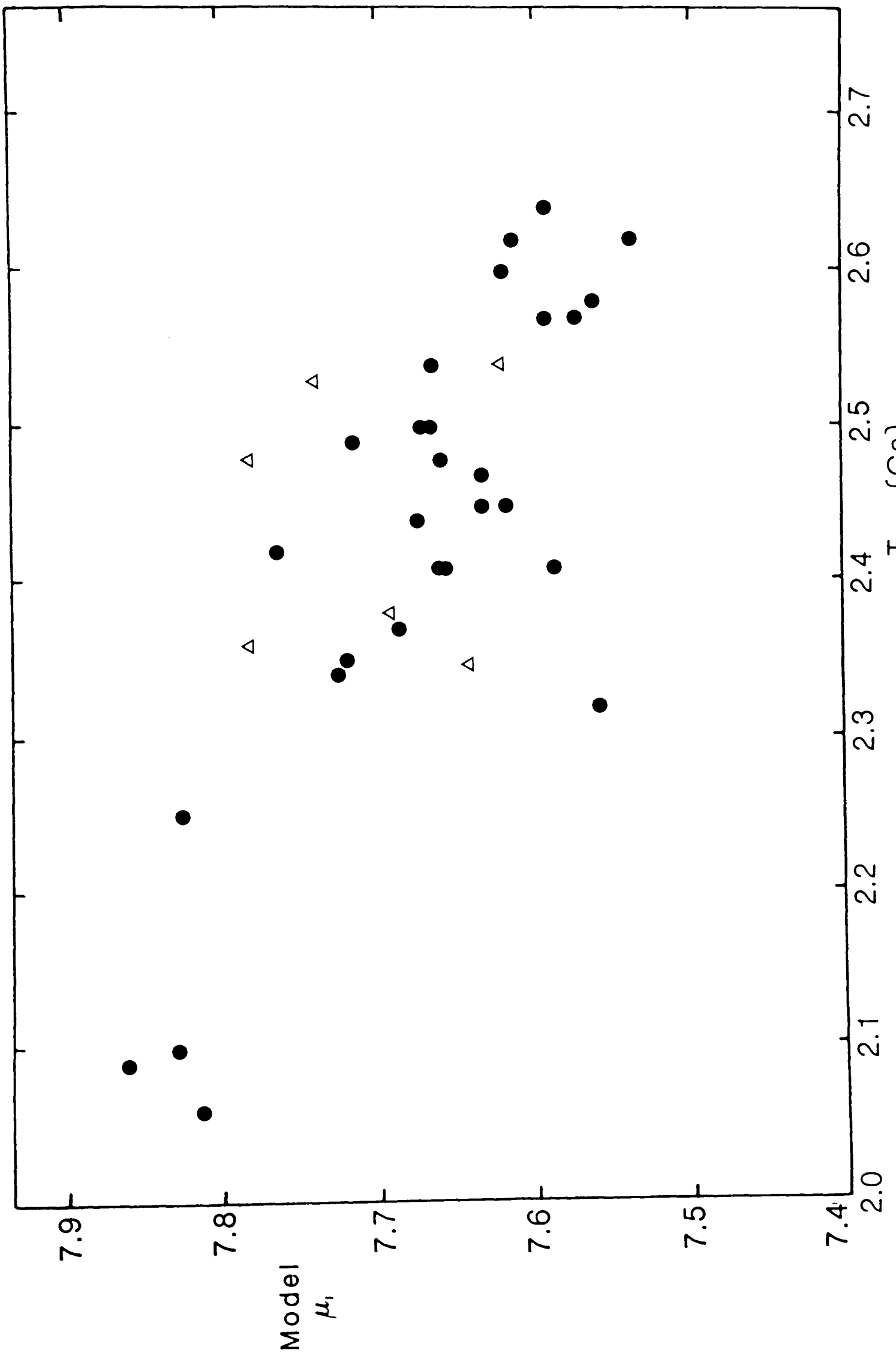

Model μ_1
7.9
7.8
7.7
7.6
7.5
7.4
T_{DM}(Ga)
2.0
2.1
2.2
2.3
2.4
2.5
2.6
2.7

Fig. 6.36.

Apparent $(^{87}Sr/^{86}Sr)_{1.8}$ v. T_{DM} for the South-West Lofoten Mangerite. WL315, WL316 and WL410 (squares) are from the north-west side of Flakstadøy and Vestvågøy and have a large mantle-derived component (low apparent $(^{87}Sr/^{86}Sr)_{1.8}$ and young T_{DM} model age) compared to the samples from the south side of the islands: WL307, WL319, WL331, WL401, WL404 and WL405 (circles). WL416 (triangle), from north-east Vestvågøy is intermediate between these two groups both geographically and on this diagram. WL319 has anomalously low $(^{87}Sr/^{86}Sr)_{1.8}$.

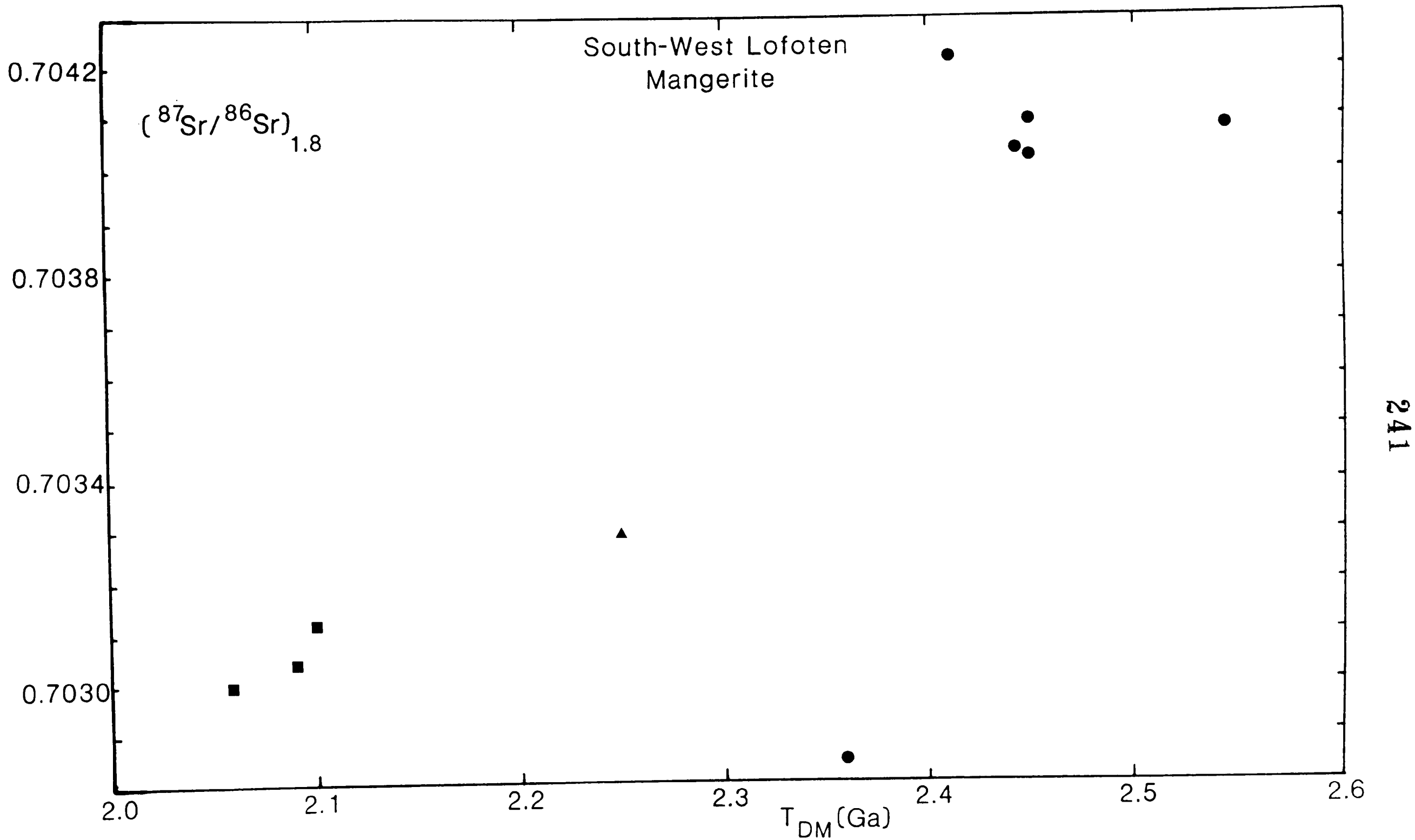

South-West Lofoten
Mangerite
$(^{87}Sr/^{86}Sr)_{1.8}$
0.7042
0.7038
0.7034
0.7030
2.0
2.1
2.2
2.3
2.4
2.5
2.6
T_{DM}(Ga)

Fig. 6.37.

Model μ_1 v. T_{DM} for the South-West Lofoten Mangerite. Symbols as for Fig. 6.36.
The samples from the north-west side of the islands have Sr and Nd isotope characteristics suggesting that they contain a large mantle-derived component (Fig. 6.36); their high model μ_1 values support this conclusion.

South-West Lofoten
Mangerite

Model μ_1

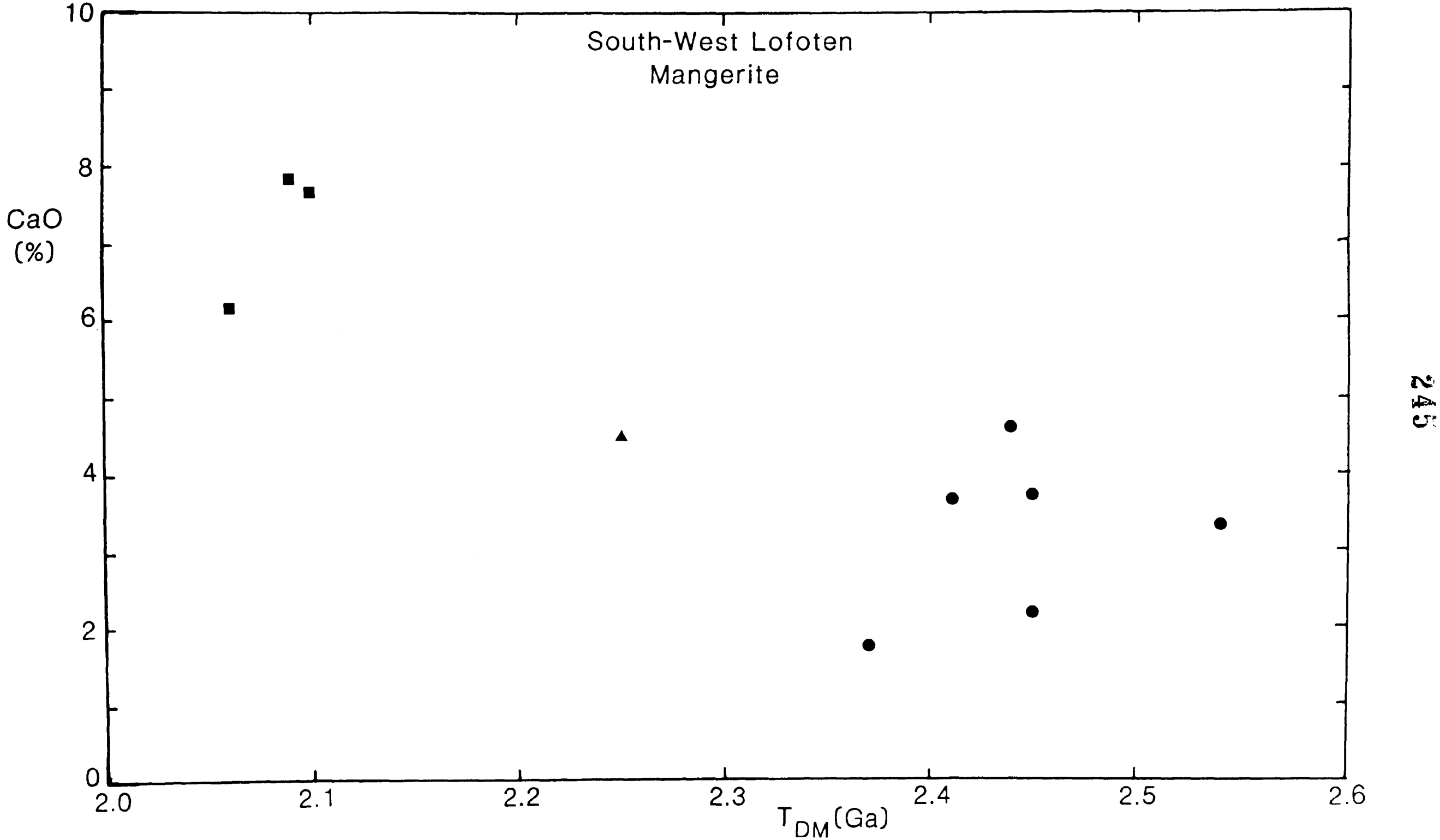
7.9
7.8
7.7
7.6

2.0 2.1 2.2 2.3 2.4 2.5 2.6

T_{DM} (Ga)

Fig. 6.38.

CaO% v. T_{DM} for the South-West Lofoten Mangerite. Symbols as for Fig. 6.36. The samples from the north-west side of the islands have Sr, Nd and Pb isotope characteristics suggesting that they contain a large mantle-derived component (Figs. 6.36 and 6.37); their high CaO CaO concentration supports this conclusion. Thus there is correlation between Sr, Nd and Pb isotopes and chemical composition for this intrusion and possibly geographical location since those samples with large mantle-derived components are from the north-west side of the islands, closest to the axis of the upwarping of the Moho and hence to the mantle source. These correlations demonstrate that the scatter of data-points about the Rb-Sr whole-rock isochron of this intrusion (Fig. 6.15) is not random but, rather, is due to real initial $^{87}Sr/^{86}Sr$ ratio variations, and further, that the South-West Lofoten Mangerite did not crystallize from a single, homogeneous magma.


South-West Lofoten
Mangerite
CaO
(%)
10
8
6
4
2
0
2.0
2.1
2.2
2.3
2.4
2.5
2.6
T_{DM}(Ga)

245

Plate 7.1. Red monzonite sheets at Å, Moskenesøy, as described by Green and Jorde (1971). They are up to 2m wide and discordant to the foliation of the supracrustal gneisses and have mangeritic compositions. These sheets are cross-cut by a minor set of later charnockite veins.

Plate 7.2. Anatectic vein of mangeritic composition in the early Proterozoic supracrustal gneisses at Hamnøy Bridge, Moskenesøy, discordant to the gneiss foliation and with thin mafic selvages.





Plates 7.3. and 7.4. Polished slab of WL247, a sample of early Proterozoic supracrustal gneisses from Hamnøy Bridge, Moskenesøy. Fine-grained, quartzo-feldspathic gneiss contain mafic lenses and coarse-grained pinkish-grey melts. The melts consist of perthitic feldspar with minor orthopyroxene and clinopyroxene, opaques and biotite, and accessory apatite and calcite. Plate 7.4 is a detail from Plate 7.3.





Plates 7.5. and 7.6. A pinkish-grey anatectic melt of mangeritic composition in early Proterozoic supracrustal gneisses at Hamnøy Bridge, Moskenesøy. The anatectic dyke is 2m wide and 8m long, concordant to the gneiss foliation. It interfingers with the gneiss at either end and it contains slivers of the gneiss.





Plate 7.7. Anatectic melts in early Proterozoic supracrustal gneisses at Ølkona, Moskenesøy. These leucocratic melts are developed concordant to the gneiss foliae and cut across the gneiss and coalesce with each other. This represents one of the best examples of in-situ anatexis in the Lofoten-Vesterålen province.

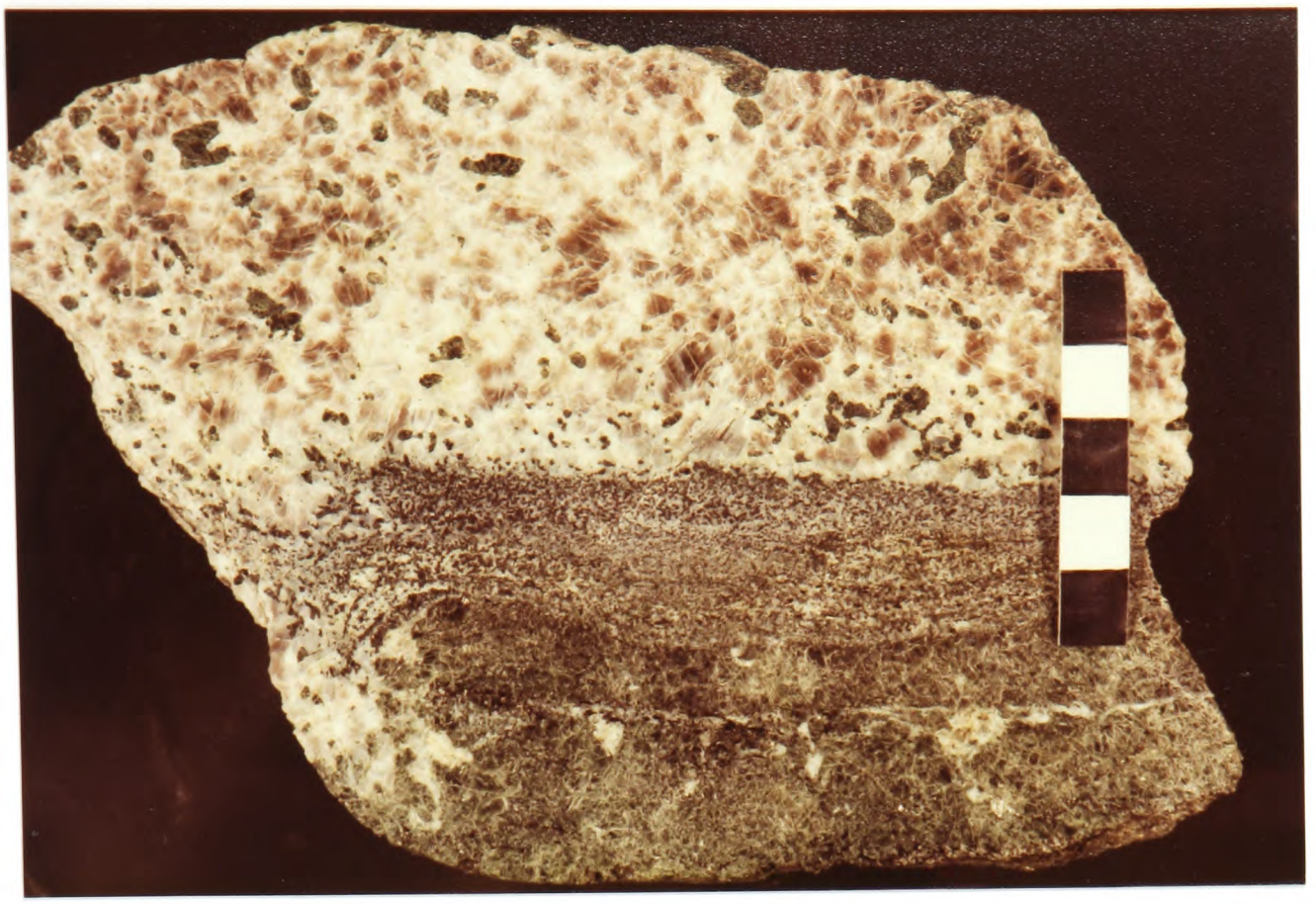
Plate 7.8 . Leucocratic melt, 2m wide, with rounded blocks of pyroxenite, in the quartzo-feldspathic early Proterozoic supracrustal gneisses, the marble layer and its surrounding pyroxenite layer, at Ølkona, Moskenesøy.





Plate 7.9. Polished slab of WL217, a sample from the leucocratic melt illustrated in Plate 7.8. It is mangeritic in composition and contains a pyroxenite xenolith. The pyroxenite is largely monomineralic pale-green clinopyroxene, but also contains a biotite and plagioclase-bearing band with very rare calcite and opaque phases.

Plate 7.10. Two generations of leucocratic melt veins in early Proterozoic supracr ustal gneisses near Nesland, Flakstadøy. The 2m wide red monzonite dyke is very similar to those at Å, Mosekenesøy, and is discordant to the foliation of the gneisses at a small angle. The 0.2m wide charnockite dyke (bottom of plate) cross-cuts the monzonite dyke.



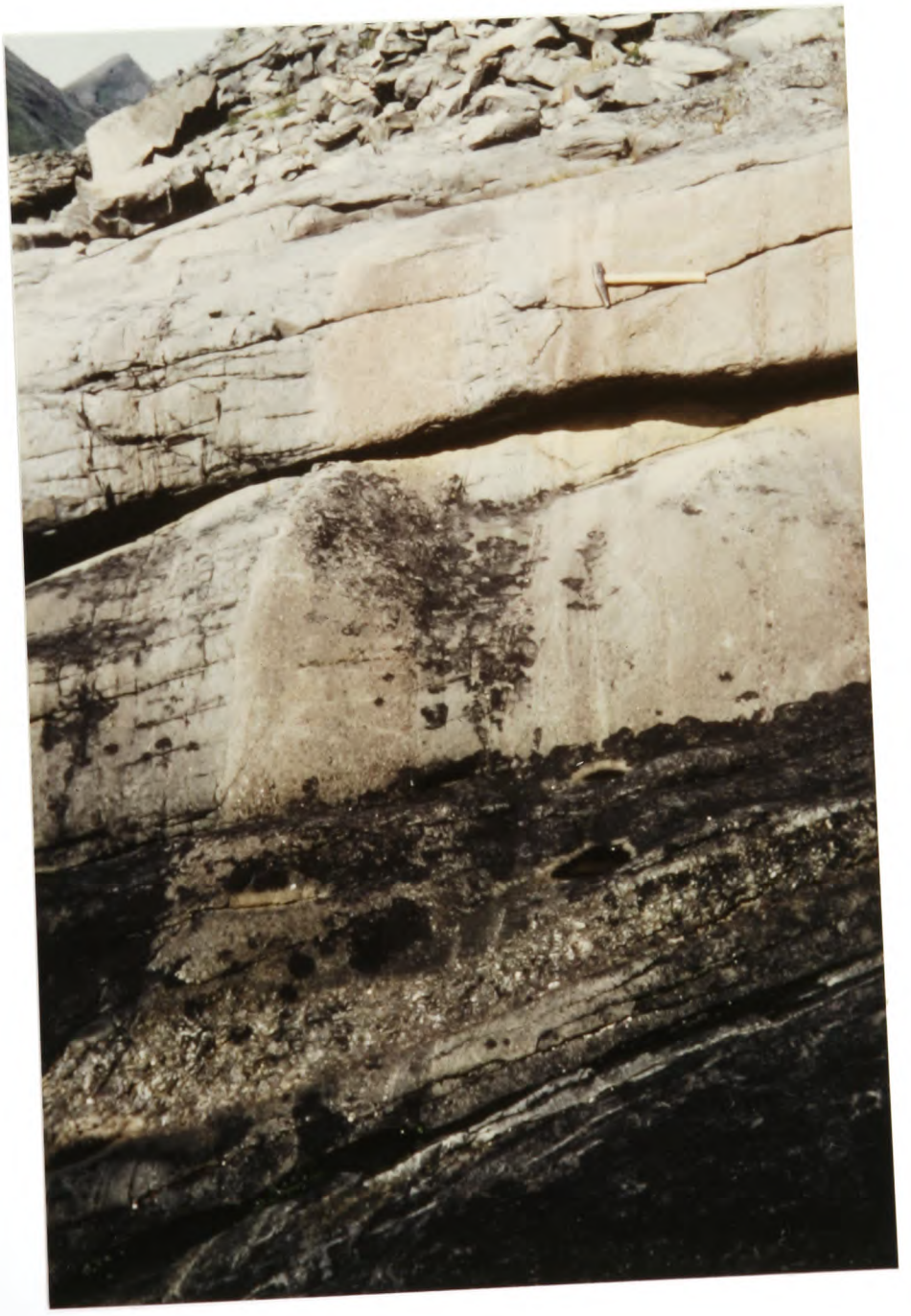


Plate 7.11. Two generations of leucocratic dykes in the Borge Gabbro, Vestvågøy. The earlier, sub-vertical mangeritic dyke is cross-cut by two sub-horizontal charnockite sills, 0.2m wide.



Table 7.1

Major Element Compositions and CIPW Norms for the Mangeritic and Charnockitic Anatectic Melts

	Moskenesøy				Flakstadøy		Vestvågøy	
	WL212	WL216	WL230	WL232	WL340	WL341	WL441	WL467
SiO_2	61.29	63.19	56.55	64.25	54.72	69.36	74.96	72.06
Al_2O_3	20.70	17.14	17.50	18.17	15.94	17.05	13.60	14.10
TiO_2	0.39	0.08	0.82	0.10	1.81	0.05	0.14	0.21
Fe_2O_3	2.84	1.25	9.19	1.13	9.92	0.58	0.79	2.53
MgO	0.51	0.93	1.22	0.67	2.49	0.14	0.19	0.14
CaO	2.48	2.29	4.67	2.19	4.81	0.71	0.58	0.54
Na_2O	5.37	1.59	5.72	5.01	4.73	4.15	2.48	3.76
K_2O	6.25	12.77	3.28	7.42	4.23	7.97	7.45	6.38
MnO	0.02	0.05	1.10	0.04	0.22	0.03	0.00	0.01
P_2O_5	0.02	0.27	0.61	0.62	0.96	0.02	0.00	0.02
LOI	0.32	0.51	0.31	0.38	0.06	0.24	0.19	0.39
Total	100.20	100.07	99.98	99.98	99.90	100.31	100.38	100.14
Norms calculated with $Fe^{3+}/Fe^{3+} + Fe^{2+} = 0.10$								
Q	0.07	1.27	0.13	3.14	-	13.28	30.68	24.50
Or	36.94	75.47	19.38	43.85	25.00	47.10	44.03	37.70
Ab	45.44	13.45	48.40	42.40	40.03	35.12	20.99	31.82
An	10.94	1.92	12.39	5.18	9.77	2.47	2.14	1.04
C	1.09	-	-	-	-	0.69	0.67	0.63
Cc	0.57	0.91	0.55	0.68	0.11	0.43	0.34	0.69
Di	-	4.58	4.71	0.14	6.19	-	-	-
Hy	2.53	0.89	5.54	2.24	5.86	0.69	0.76	1.69
Ol	-	-	-	-	0.89	-	-	-
Mt	0.42	0.20	1.37	0.18	1.51	0.09	0.11	0.37
Il	0.74	0.15	1.56	0.19	3.43	0.09	0.27	0.40
Ap	0.04	0.59	1.33	1.35	2.10	0.04	-	0.04
Plag (An_x)	31	21	33	19	32	12	16	6
Mg/Mg +Fe*	0.57	0.80	0.45	0.77	0.68	0.57	0.68	0.25

*for ferromagnesian minerals

Table 7.2

Rb-Sr Data for the Mangeritic and Charnockitic Anatectic Veins

Sample	Locality	Rb(ppm)	Sr(ppm)	$^{87}Rb/^{86}Sr$	$^{87}Sr/^{86}Sr$
WL212	Ølkona, Moskenesøy	87	711	0.3493	0.71276
WL216	Ølkona, Moskenesøy	196	604	0.9626	0.72914
WL230	Å, Moskenesøy	15	638	0.0584	0.70618
WL232	Å, Moskenesøy	57	802	0.2028	0.70812
WL340	Nesland, Flakstadøy	35	530	0.1876	0.70882
WL341	Nesland, Flakstadøy	89	305	0.8605	0.72499
WL441	Våje, Vestvågøy	125	354	1.0442	0.73027
WL467	Borge, Vestvågøy	274	48	n.d.	n.d.
Errors (2σ)		±5%	±5%	±1%	±0.00005

Table 7.3

Sm-Nd Data for the Mangeritic and Charnockitic Anatectic Veins

Sample	Sm(ppm)	Nd(ppm)	$^{147}Sm/^{144}Nd$	$^{143}Nd/^{144}Nd$	T_{CHUR}(Ga)	T_{DM}(Ga)
WL212	1.366	21.200	0.03916	0.510549	2.00	2.16
WL216	4.493	25.522	0.10701	0.511189	2.42	2.62
WL230	7.877	42.629	0.11230	0.511360	2.27	2.50
WL232	5.675	34.332	0.10046	0.511331	2.04	2.28
WL340	14.687	83.465	0.10695	0.511310	2.22	2.45
WL341	0.997	8.710	0.06957	0.510737*	2.25	2.42
WL467	26.638	203.977*	0.07937	0.510797	2.36	2.53
Errors (2σ)	±0.02%	±0.02%	±0.10%	±0.000025	±0.04	±0.04

unless asterisked (*) and stated below

WL341				±0.000029		
WL467		±0.044%				

Table 7.4

Pb Data for the Mangeritic and Charnockitic Anatectic Melts

Sample	$^{206}Pb/^{204}Pb$	$^{207}Pb/^{204}Pb$	$^{208}Pb/^{204}Pb$	Apparent μ_1*
WL212	15.290	15.025	34.797	7.65
WL216	15.170	15.045	35.223	7.71
WL230	14.825	15.030	34.719	7.75
WL340	14.938	15.015	34.858	7.70
WL341	16.421	15.295	36.289	7.92

Errors (2σ) on Pb ratios are better than 0.1%

*Calculated assuming intrusion age = 1800Ma

Table 7.5

Percentage of Ancient Crustal Material in the Mangeritic and Charnockitic Anatectic Melts: Nd Isotopic Constraints

Model: the anatectic melts formed by anatexis of the 2.7Ga granulite-facies gneisses caused by a rise in temperature due to the emplacement of basaltic magmas. The anatectic melts contain a juvenile component, derived from the supracrustal gneisses and/or mantle-derived magmas, as well as ancient crust-derived material. Assuming that the juvenile component contained 11.5ppm Nd (the mean Nd concentration in MORB glasses, Cohen et al., 1980) and for different Nd concentrations in the crustal component the percentage of late Archaean material contributed is calculated for anatectic melts with the lowest, mean and highest values at 1.8Ga.

Nd(ppm) in crust-derived component	ε_{Nd} at 1.8Ga		
	-3.1	-5.9	-8.6
15	44%	65%	87%
32	26%	46%	76%
40	22%	41%	72%

The Nd concentrations used for the crust-derived component are explained in Table 6.13.

Table 7.6

Percentage of Ancient Crustal Material in the Mangeritic and Charnockitic Anatectic Melts: Pb Isotopic Constraints

Model: as for Table 7.5. The "crustal Pb column" shows the percentage of Pb in the anatectic melts which is derived from an ancient lower crustal source. The other columns show the percentage of the anatectic melts by total mass contributed by the lower crustal component assuming crustal component Pb concentration of 20.2ppm (^{204}Pb = 0.28ppm) (North-West Hinnøy amphibolite-facies gneisses), and using different Pb concentrations for the juvenile crust/mantle-derived component:

Sample	Crustal Pb	Crustal Contribution Total Pb(ppm) [^{204}Pb (ppm)] 0.06[0.008]*	3.2[0.04]+	7.0[0.1]†	20[0.28]ǂ
WL212	90%	20%	55%	75%	90%
WL216	67%	6%	23%	42%	67%
WL239	52%	3%	13%	28%	52%
WL340	70%	6%	25%	46%	70%
WL341	-7%	-	-	-	-

* mean pristine MORB (Cohen et al., 1980

\+ Preshal Mhor Basalt, Isle of Skye, Pb 93% mantle-derived (Dickin, 1981)

† Southern Zone Andes Basalt (McHugh, 1980)

ǂ Pb-enriched residual basaltic magma

Fig. 7.1.

Sm-Nd evolution diagram for the mangeritic and charnockitic veins on Moskenesøy (data in Table 7.3). The range of the evolution lines for the Sund-Ølkona Mangerite (from Fig. 6.19) is shown for comparison. Three of the four anatectic melts have evolution lines parallel to the Nd evolution lines for the Sund-Ølkona Mangerite. They have a wider range in ε_{Nd} values and T_{DM} model ages than this intrusion: this is to be expected since veins derived from localised volumes of gneiss would have greater isotopic diversity than larger mangerite intrusions formed by the coalescing of melts from many anatectic veins and dykes. The mangerite vein from Ølkona, WL212 (Plate 7.7), has the lowest $^{147}Sm/^{144}Nd$ ratio of any mangeritic rock or anatectic vein analysed. This melt is the most convincing in-situ anatectic melt analysed. Its Nd model age of 2.16 Ga supports the field observation that this melt vein could be totally derived from the early Proterozoic supracrustal gneisses in which it occurs. The vertical lines define the age range 1.7 - 1.85Ga.

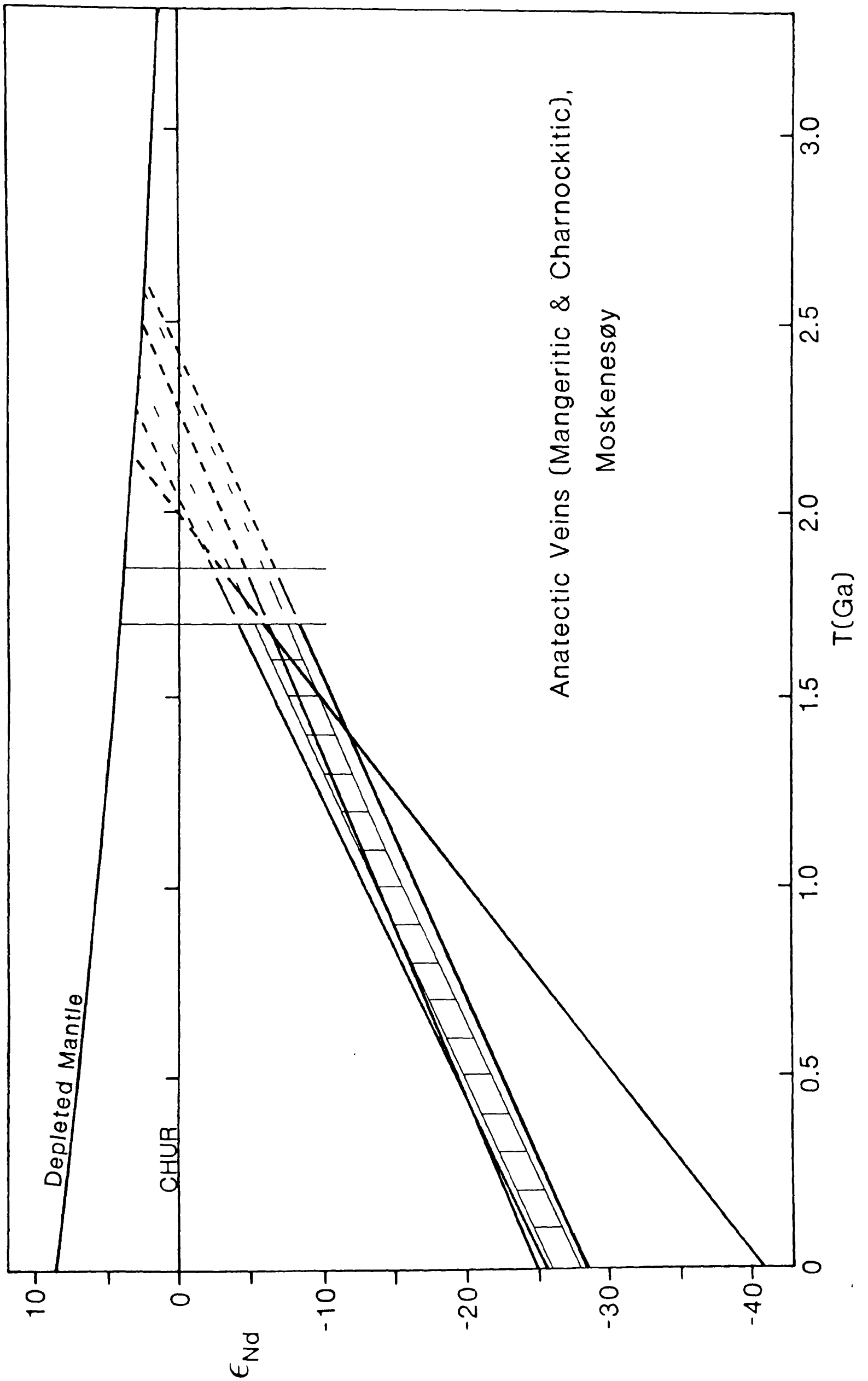

Anatectic Veins (Mangeritic & Charnockitic),
Moskenesøy
Depleted Mantle
CHUR
ϵ_{Nd}
10
0
-10
-20
-30
-40
0
0.5
1.0
1.5
2.0
2.5
3.0
T(Ga)

Fig. 7.2.

Sm-Nd evolution diagram for the mangeritic and charnockitic veins on Flakstadøy and Vestvågøy (data in Table 7.3). The range of the evolution lines for the South-West Lofoten Mangerite (from Fig. 6.21) and the evolution line for the Flakstadøy Charnockite (Fig. 6.20) are shown for comparison. The evolution line for WL340, the mangerite dyke from Nesland, is parallel to the evolution lines for the South-West Lofoten Mangerite. It is difficult to see how an apophysis from this intrusion could have a Sm-Nd isotope composition outside the full range for the intrusion but small melts with a wide range of Sm-Nd isotope compositions could have been combined into the South-West Lofoten Mangerite to produce the present range of evolution lines. The charnockites from Nesland and Borge have substantially more negative ε_{Nd} values than the South-West Lofoten Mangerite both at 0Ga and at 1.8Ga, but their Sm-Nd isotopic evolution lines are close and parallel to that for the Flakstadøy Charnockite. Rb and Sr concentrations also suggest a strong similarity between the Flakstadøy Charnockite and the charnockite vein intruding the gabbro at Borge, Vestvågøy. The vertical lines define the age range 1.7 - 1.85Ga.

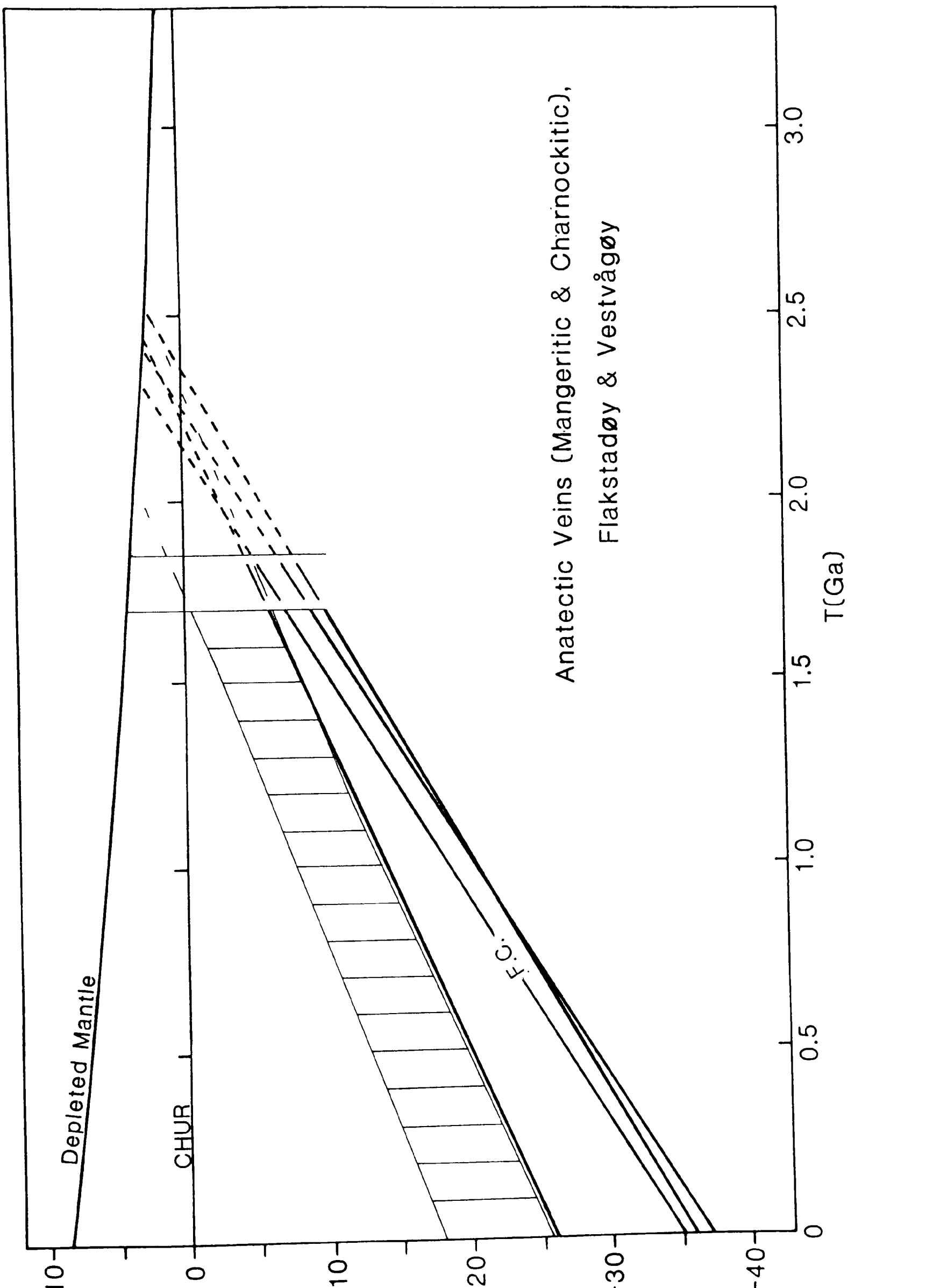

Anatectic Veins (Mangeritic & Charnockitic),
Flakstadøy & Vestvågøy
Depleted Mantle
CHUR
F.G.
ϵ_{Nd}
10
0
-10
-20
-30
-40
0
0.5
1.0
1.5
2.0
2.5
3.0
T(Ga)

Fig. 7.3.

$^{207}Pb/^{204}Pb$ v. $^{206}Pb/^{204}Pb$ diagram for the mangerite and charnockite anatectic veins (data in Table 7.4) using the same interpretational model as for the mangerites (Fig. 6.26). All of the data-points (except for WL341, the charnockite vein from Nesland), plot just above the 1.8Ga model isochron for derivation from average lower crust, and just to the right of the 1.8Ga first-stage isochron. Any finite μ at the present day for the sample from the monzonite sheet at Å, WL230, would imply that at 1.8Ga this data-point plotted to the left of this isochron, and hence a single-stage evolution in the mantle up to 1.8Ga for this rock is not possible. Apart from WL341, which plots slightly above the 1.8Ga model isochron for rocks derived from mantle with $\mu_1 = 7.9$, the anatectic melts have Nd (Figs. 7.1 and 7.2) and Pb isotopic compositions consistent with their formation from different proportions of material derived from 2.7Ga lower crust and material derived from mantle with $\mu_1 = 7.9$ at 1.8Ga.

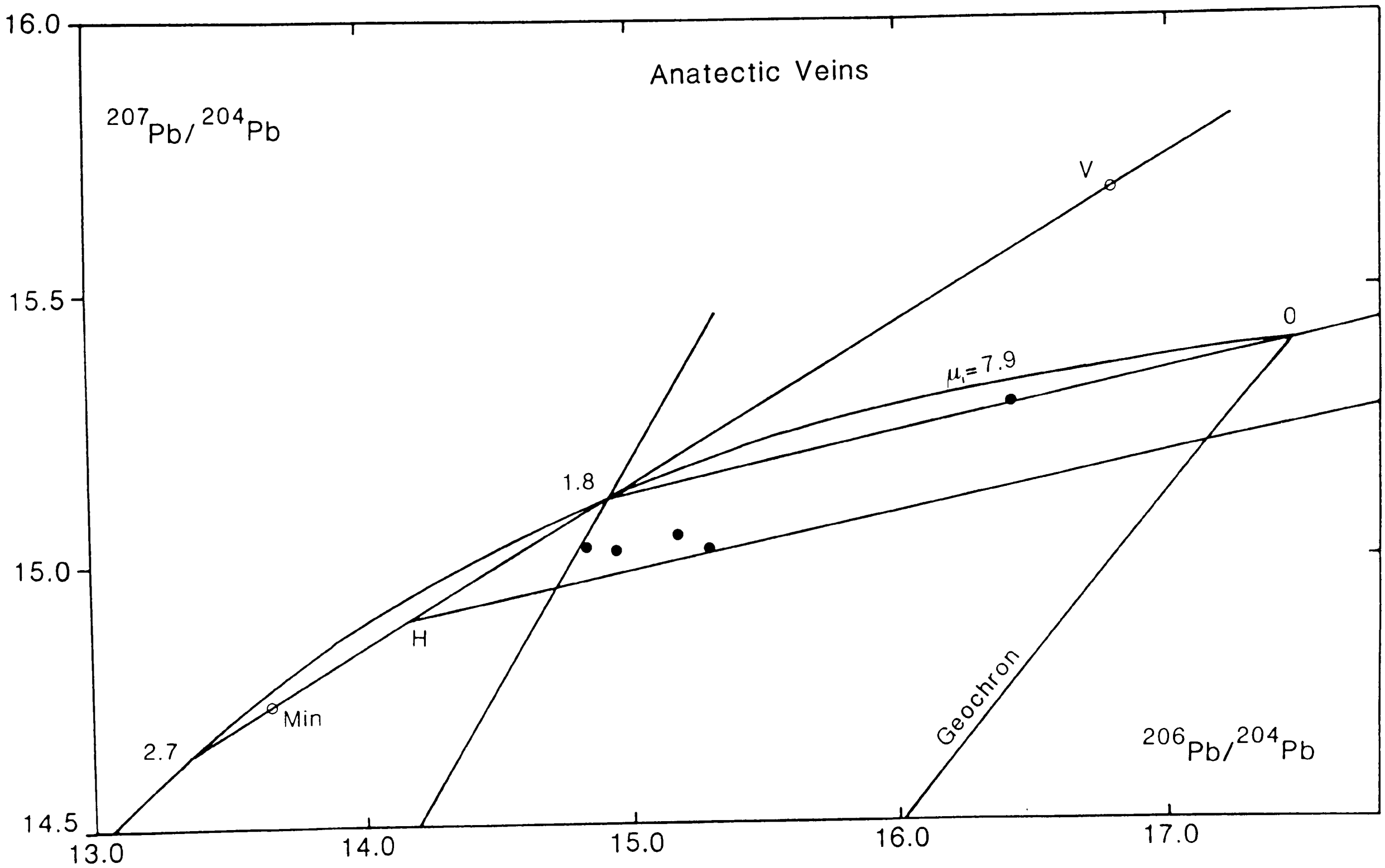

Anatectic Veins
$^{207}Pb/^{204}Pb$
$^{206}Pb/^{204}Pb$
16.0
15.5
15.0
14.5
13.0
14.0
15.0
16.0
17.0
V
0
μ_1=7.9
1.8
H
Min
2.7
Geochron

Fig. 7.4.

Model μ_1 v. T for the mangeritic and charnockitic anatectic melts showing the evolution of model μ_1 v. T with time in "orogene", upper crust, lower crust and upper mantle (Plumbotectonics model of Zartman and Doe, (1981)). The four mangerite samples are confirmed as being derived from lower crustal and upper mantle sources. The Nesland charnockite, WL341, apparently requires an "orogene" or upper crust component added to material derived from an upper mantle source.

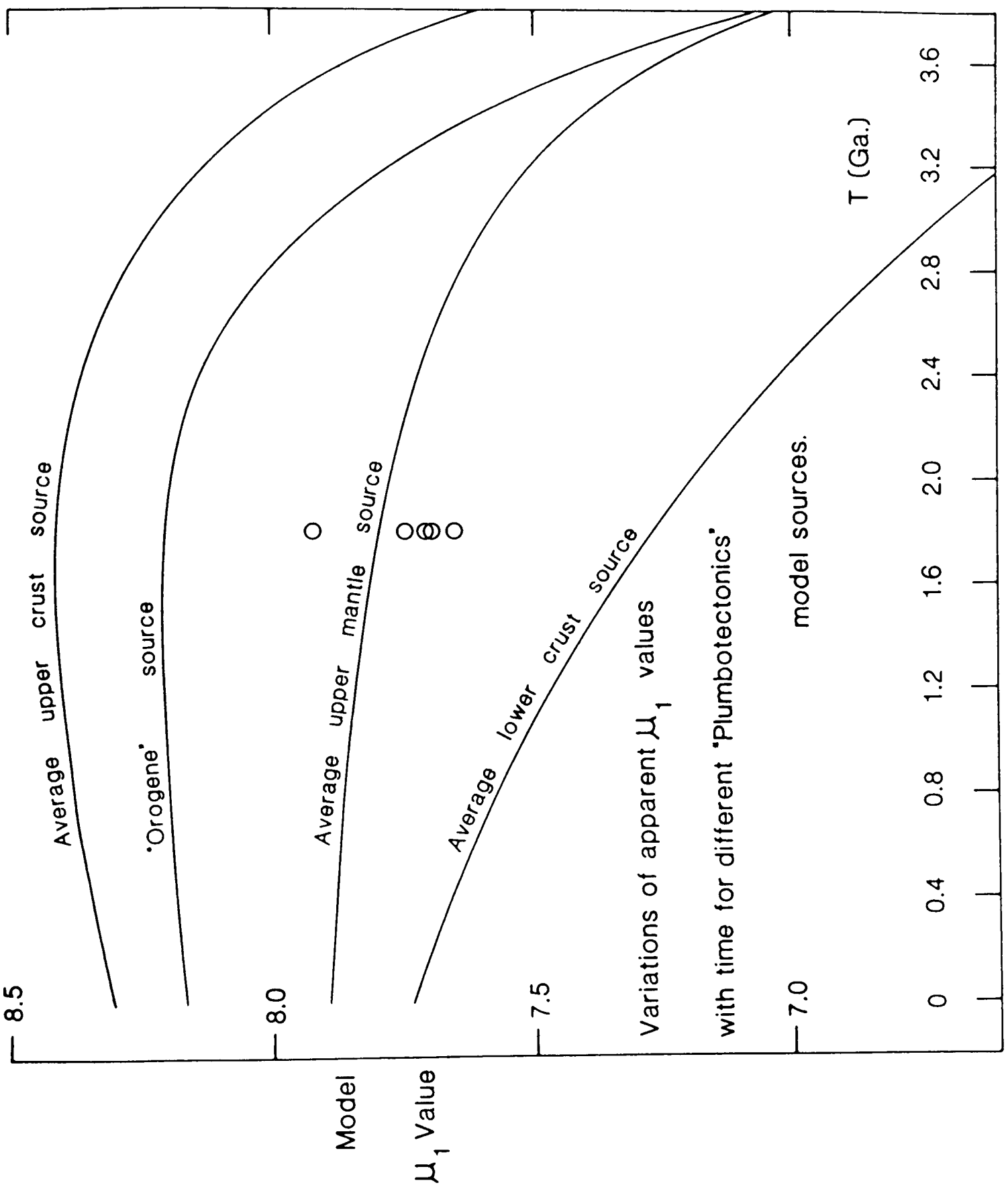

Average upper crust source
'Orogene' source
Average upper mantle source
Average lower crust source
Variations of apparent μ_1 values
with time for different 'Plumbotectonics'
model sources.
Model μ_1 Value
8.5
8.0
7.5
7.0
0
0.4
0.8
1.2
1.6
2.0
2.4
2.8
3.2
3.6
T (Ga.)

Fig. 7.5.

Apparent $(^{87}Sr/^{86}Sr)_{1.8}$ v. T_{DM} for the mangeritic and charnockitic anatectic melts (squares) showing mangerites (open circles) (from Fig. 6.34) for comparison. There is no clear correlation for the melts since they are derived from small areas of gneisses and hence have isotopes characteristic of those gneisses. In a large magma, coalescence reduces extreme, local isotopic variations.

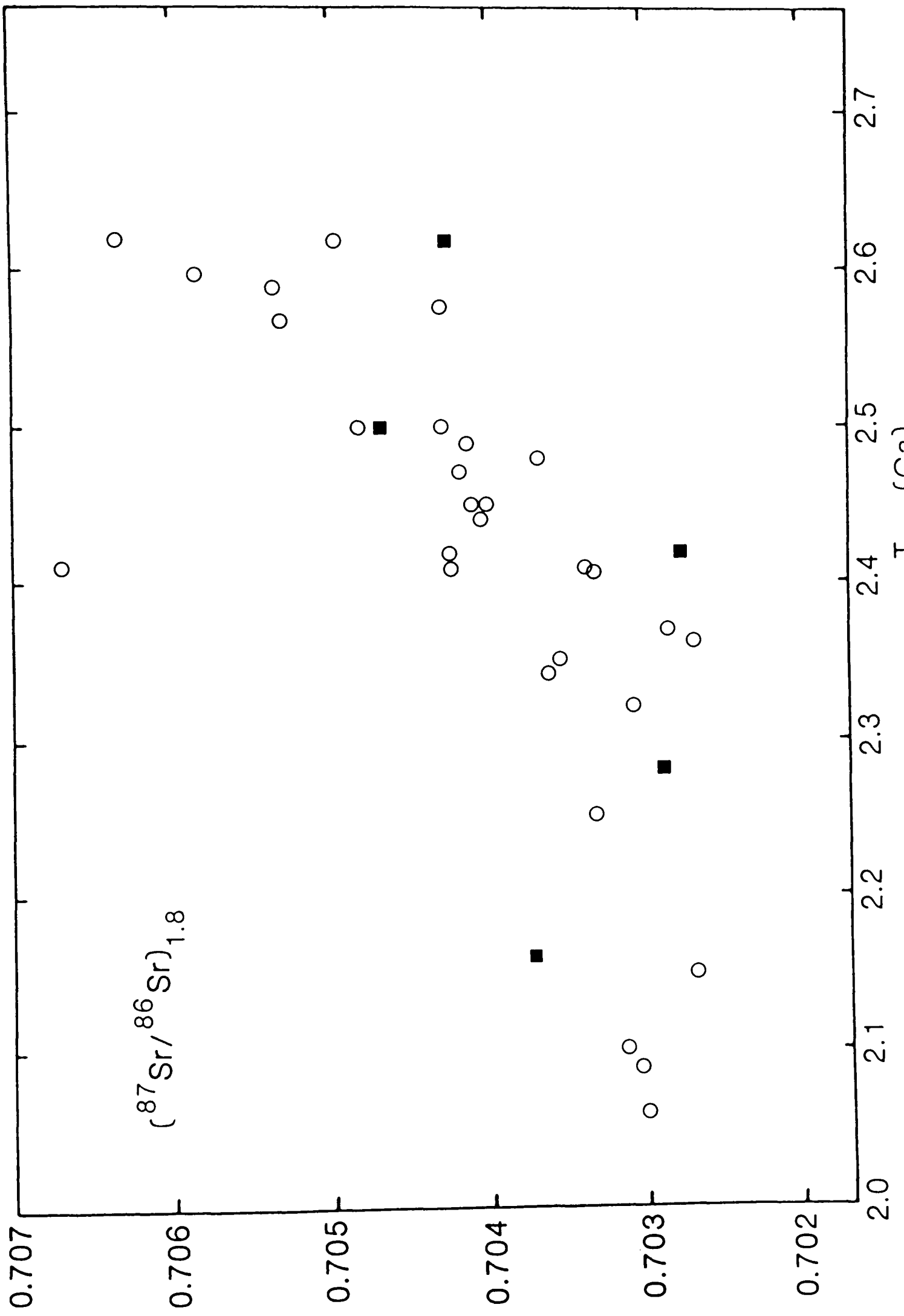

0.707
0.706
0.705
0.704
0.703
0.702
$(^{87}Sr/^{86}Sr)_{1.8}$
2.0
2.1
2.2
2.3
2.4
2.5
2.6
2.7
T_{DM}(Ga)

Fig. 7.6.

Model μ_1 v. T_{DM} for the mangeritic and charnockitic anatectic melts (squares) showing mangerites (open circles) (from Fig. 6.35) for comparison. There is no clear correlation for the melts since they are derived from small areas of gneisses and hence have isotopes characteristic of those gneisses. In a large magma, coalescence reduces extreme, local isotopic variations.

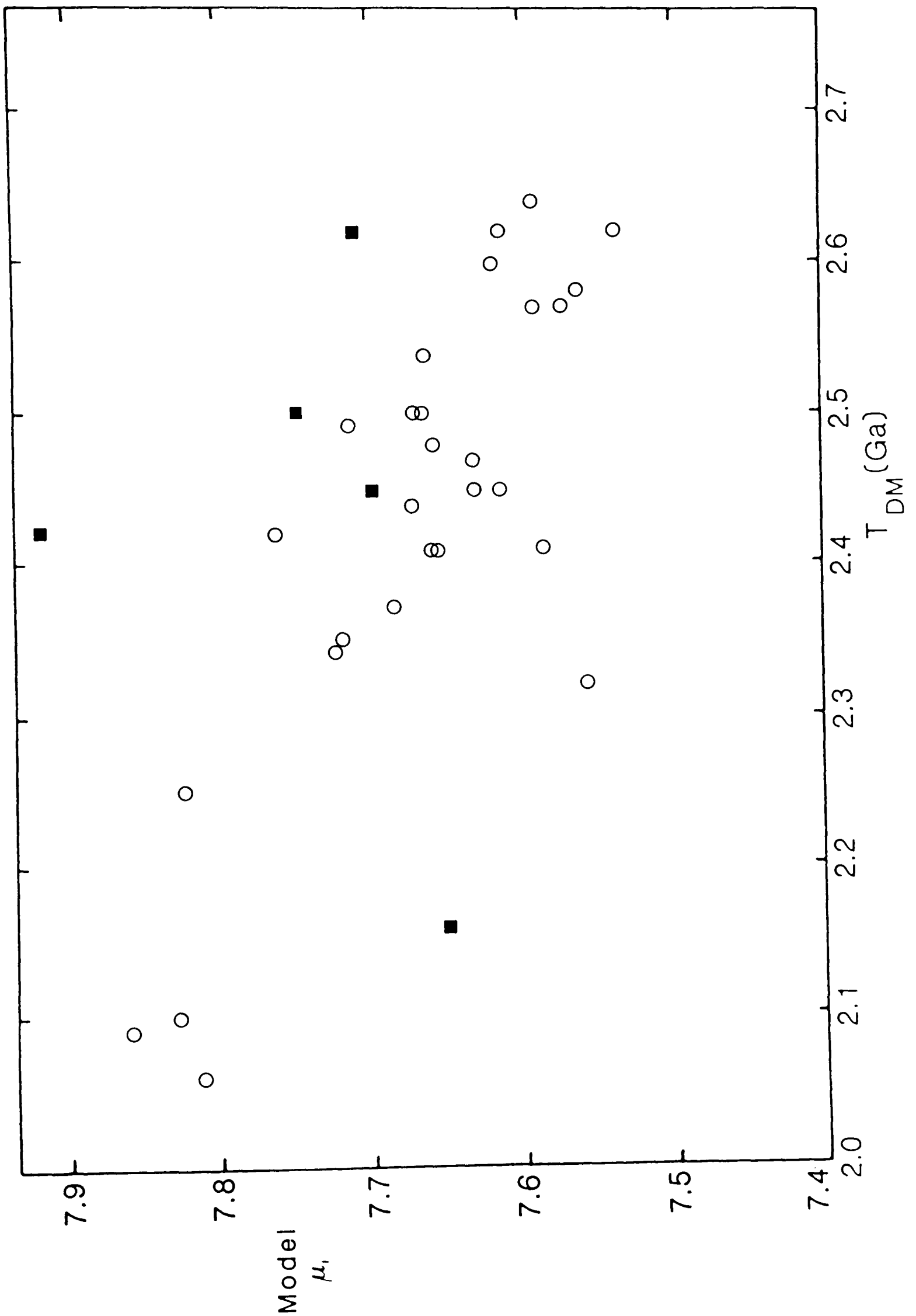

Model μ_1
7.9
7.8
7.7
7.6
7.5
7.4
T_{DM}(Ga)
2.0
2.1
2.2
2.3
2.4
2.5
2.6
2.7

Plate 8.1. East-west trending dolerite dykes in the Hopen Mangerite/Charnockite, South-West Austvågøy. The plate shows a number of dykes up to 4m wide and parallel to the foliation of the charnockite.

Plate 8.2. The margin between the dolerite dykes and the Hopen Mangerite/Charnockite. The charnockite back-veins the the dolerite, demonstrating that the dolerites were intruded into the charnockite when it was still hot and hence that the dolerites post-date the mangeritic rocks by only a short period of time.





Plate 8.3. Polished slab of WL613, a dyke from the north side of Tenfjord, Raftsund, Hinnøy. It strikes 015°, dips 82°W and is up to 5m wide. It is a plagioclase-phyric lamprophyre. Plagioclase phenocrysts are up to 45 x 22mm and are extensively sericitized. The groundmass is fine-grained biotite and plagioclase and a minor carbonate phase.

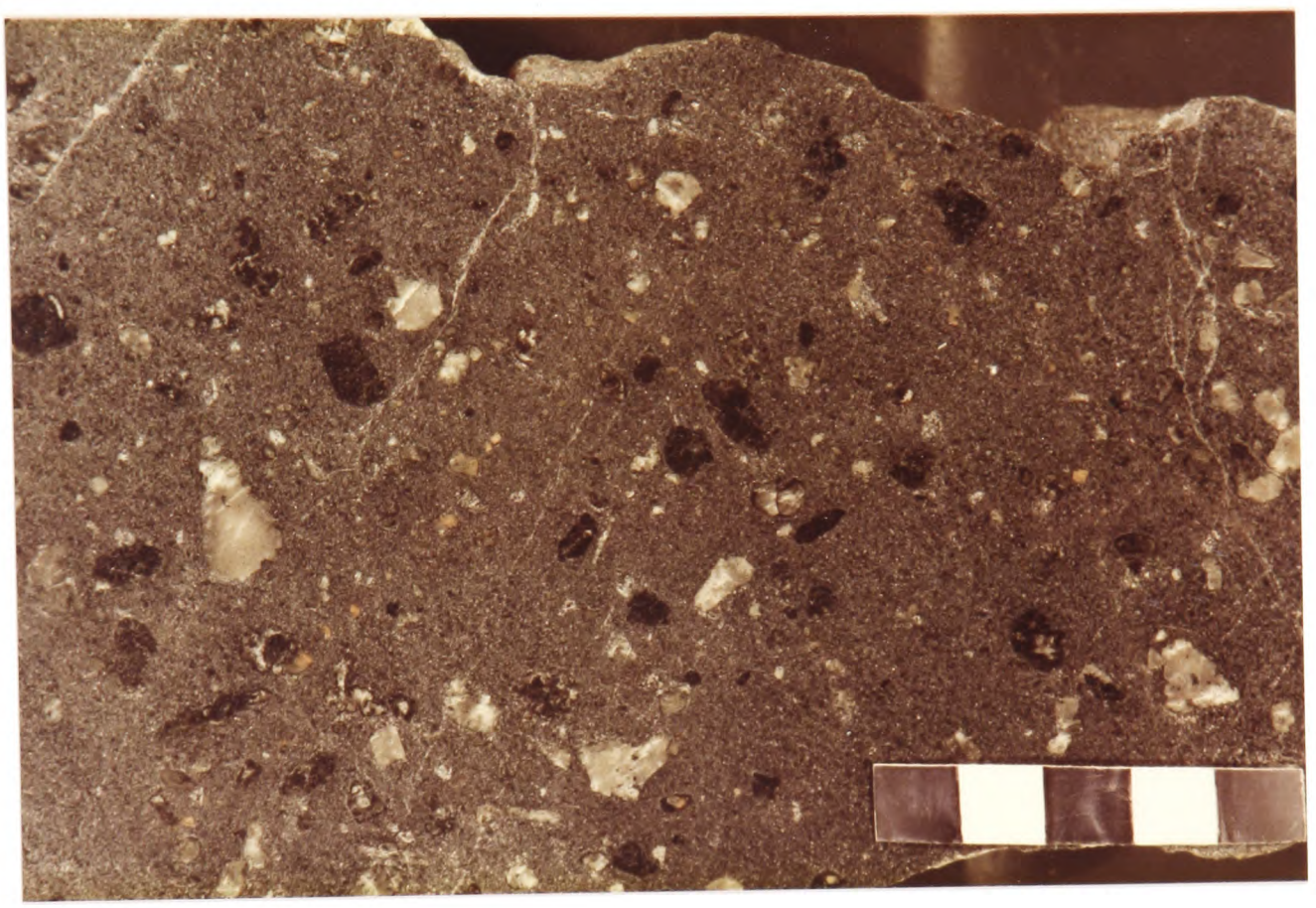


Plate 8.4. Polished slab of WL634 from the Lødingen Granite, 3km north of Rinøyvåg. This sample is typical of the Lødingen Granite: pink with dark aggregates of mafic phases; quartz, plagioclase and microcline comprise over 95% of the rock and microcline porphyroblasts occur. Green biotite is the main mafic phase, occurring in association with sphene and opaques. Epidote grains have allanite cores.

Plate 8.5. Polished slab of WL671 from the Lødingen Granite, 1km south of Kanstad road-junction. This sample contains the same phases as the samples with a smaller proportion of mafic phases (e.g. WL634, Plate 8.4).





Plate 8.6. Polished slab of WL421, from the Leknes Group metasediments at Leknes Airport. This sample is a kyanite-garnet-muscovite-biotite-quartz-plagioclase-staurolite schist.

Plate 8.7. A 5m wide pegmatite dyke of granitic composition, in the early Proterozoic supracrustal gneisses, north of Å, Moskenesøy. These pegmatites are restricted to the southern part of Moskenesøy. They cross-cut the earlier red monzonite sheets. They have been dated as Caledonian and as such represent the youngest recognized rock-forming event in the Lofoten-Vesterålen province.

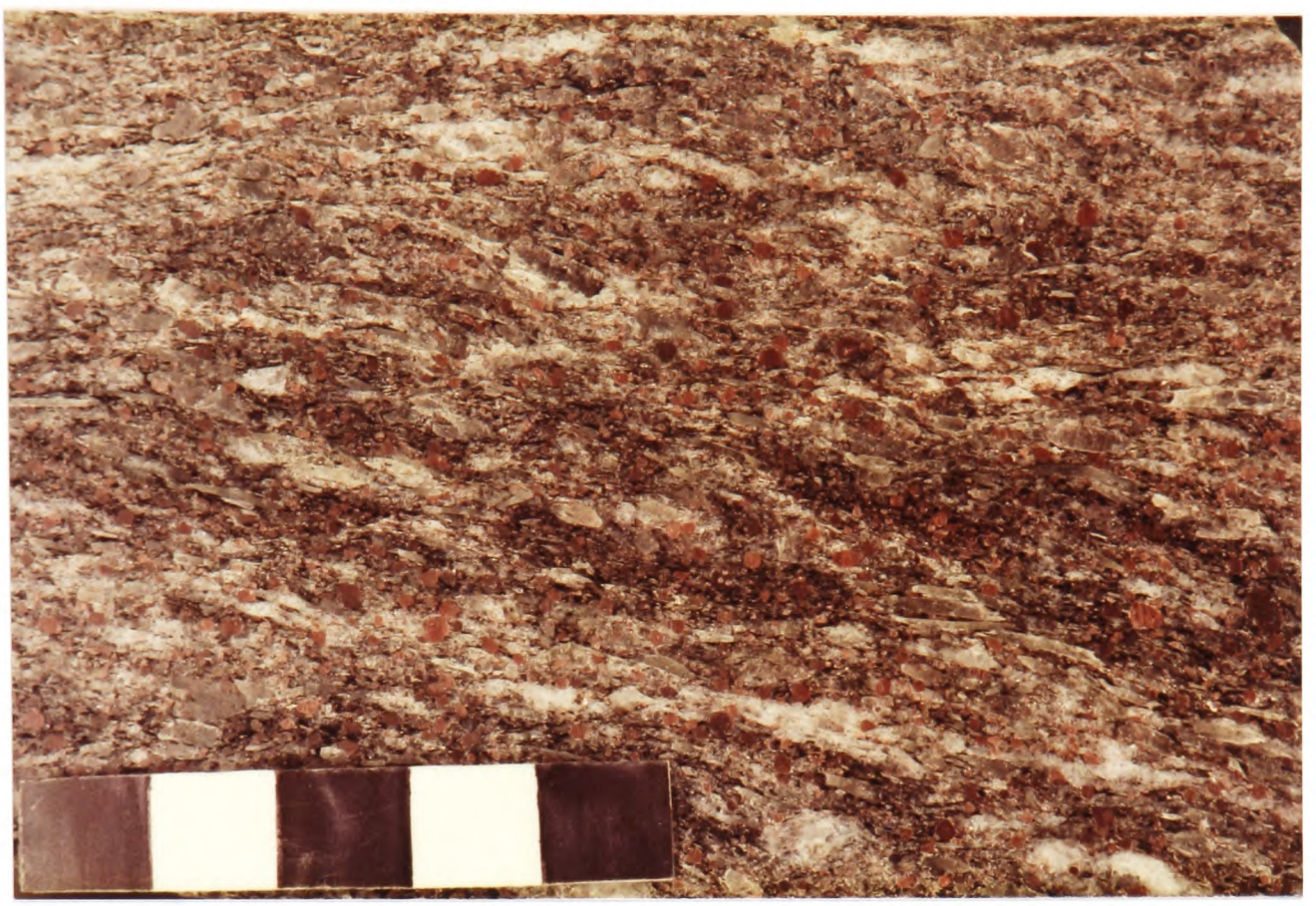




Table 8.1

Major Element Compositions and CIPW Norms for the Lødingen Granite

	WL629	WL634	WL666	WL677	WL690
SiO_2	77.39	63.65	60.90	61.21	77.66
Al_2O_3	11.83	17.36	11.10	16.14	11.46
TiO_2	0.11	0.68	1.53	0.69	0.14
Fe_2O_3	1.41	3.18	12.67	5.93	1.67
MgO	0.02	0.51	1.66	4.33	0.08
CaO	0.50	1.11	2.91	1.89	0.22
Na_2O	3.53	5.47	3.78	5.14	2.34
K_2O	4.56	6.92	3.35	3.52	6.46
MnO	0.03	0.10	0.23	0.10	0.02
P_2O_5	0.00	0.07	0.26	0.23	0.01
LOI	0.36	0.92	1.37	1.27	0.36
Total	99.75	99.97	99.75	100.45	100.43
Norms calculated with $Fe^{3+}/Fe^{3+} + Fe^{2+}$ =	0.25	0.25	0.15	0.15	0.25
Q	38.71	3.81	18.94	9.00	38.71
Or	26.95	40.90	19.80	20.80	38.18
Ab	29.87	46.29	31.99	43.50	19.80
An	1.09	1.50	3.44	2.97	0.64
C	0.69	0.32	-	2.78	0.38
Cc	0.64	1.64	2.44	2.26	0.18
Di	-	-	3.35	-	-
Hy	0.48	1.55	7.56	13.20	0.68
Ol	-	-	-	-	-
Mt	0.54	1.23	2.87	1.34	0.62
Il	0.21	1.29	2.90	1.31	0.27
Ap	-	0.15	0.57	0.50	0.02
Plag(An_x)	6	6	17	11	6
Mg/Mg+Fe*	0.13	0.85	0.52	0.85	0.35

*for ferromagnesian minerals

Table 8.2

Sm-Nd Data for the Lødingen Granite

Sample	Sm(ppm)	Nd(ppm)	$^{147}Sm/^{144}Nd$	$^{143}Nd/^{144}Nd$	T_{CHUR}(Ga)	T_{DM}(Ga)
WL629	7.097	47.671	0.09048	0.511088	2.20	2.39
WL634	14.043	110.002	0.07759	0.511067	2.99	2.19
WL666	46.023*	306.695*	0.09121	0.511177*	2.08	2.30
WL677	6.700	39.024	0.10436	0.511498	1.86	2.13
WL690	8.369	53.461	0.09514	0.511189	2.15	2.36
Errors (2σ)	±0.02%	±0.02%	±0.10%	±0.000025	±0.04	±0.06

unless asterisked (*) and listed below

WL666	±0.075%	±0.151%	±0.17%	±0.000028

Table 8.3

Major Element Compositions and CIPW Norms for the Leknes Metasediments

	WL421	WL424
SiO_2	54.37	52.89
Al_2O_3	22.06	14.97
TiO_2	1.64	1.80
Fe_2O_3	13.95	12.80
MgO	3.33	6.75
CaO	1.77	7.11
Na_2O	0.29	1.36
K_2O	1.54	1.21
MnO	0.29	0.22
P_2O_5	0.14	0.22
LOI	0.17	0.74
Total	99.55	100.06
Norms calculated with $Fe^{3+}/Fe^{3+} + Fe^{2+} = 0.20$		
Q	36.65	15.26
Or	9.10	7.15
Ab	2.45	11.51
An	7.21	30.98
C	17.27	0.07
Cc	0.30	1.32
Di	-	-
Hy	12.82	20.43
Ol	-	-
Mt	4.23	3.86
Il	3.11	3.41
Ap	0.31	0.48
Plag(An_x)	85	84
Mg/Mg+Fe*	0.71	0.86

*for ferromagnesian minerals

Table 8.4

Rb-Sr Data for the Leknes Metasediments

Sample	Rb(ppm)	Sr(ppm)	$^{87}Rb/^{86}Sr$	$^{87}Sr/^{86}Sr$
WL 421	58	175	n.d.	n.d.
WL422	43	195	0.6350	0.71510
WL424	45	327	n.d.	n.d.
Errors (2σ)	±5%	±5%	±1%	±0.00005

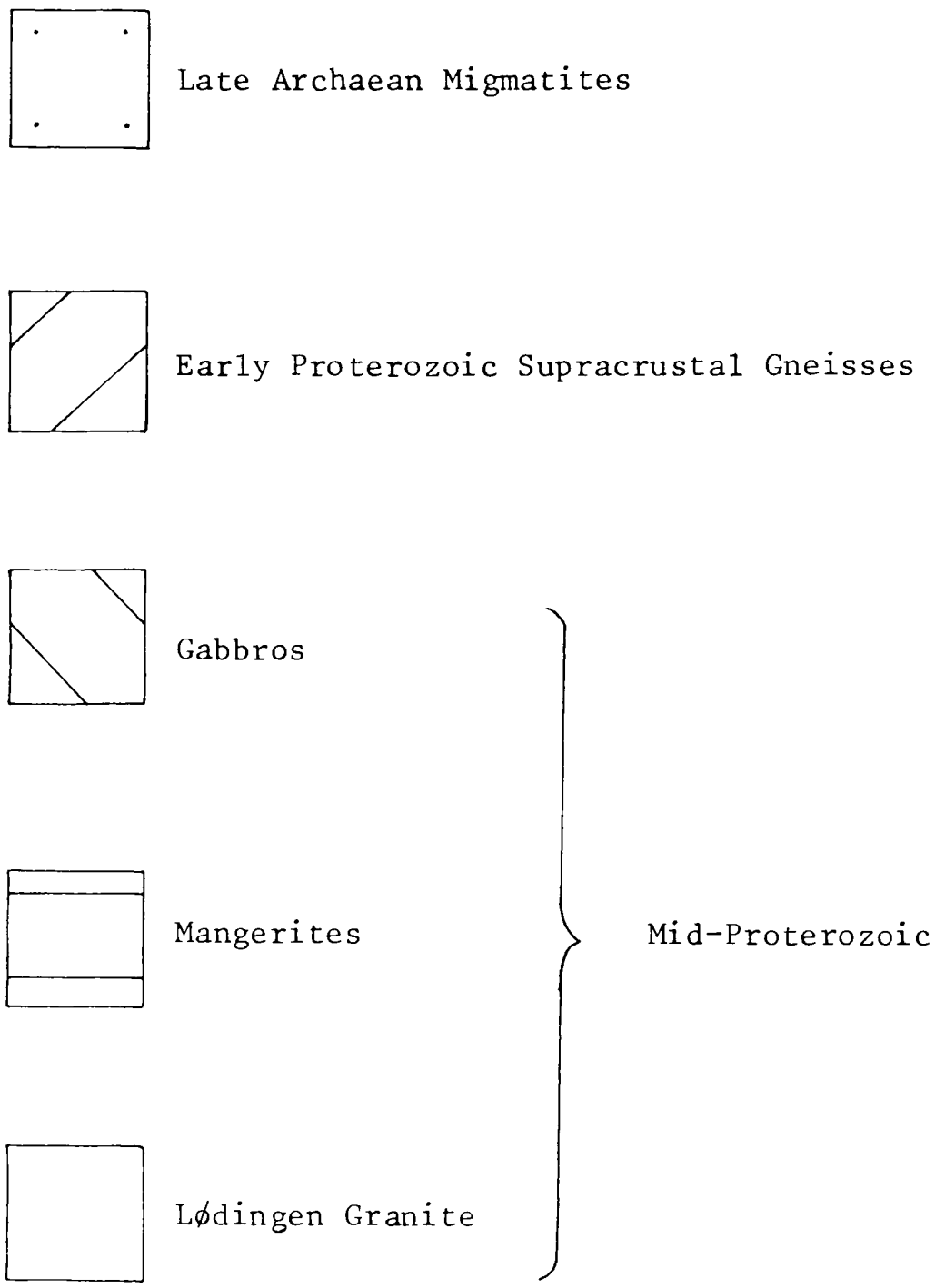
n.d. = not determined

Table 8.5

Sm-Nd Data for the Leknes Metasediments

Sample	Sm(ppm)	Nd(ppm)	$^{147}Sm/^{144}Nd$	$^{143}Nd/^{144}Nd$	T_{CHUR}(Ga)	T_{DM}(Ga)
WL421	19.701	110.377	0.10848	0.411933	1.20	1.58
WL424	5.875	24.407	0.14631	0.512307	0.98	1.63
Errors (2σ)	±0.02%	±0.02%	±0.10%	±0.000025	±0.04	±0.04

Fig. 8.1. Sample Locality Map for the Mid-Proterozoic Lødingen Granite



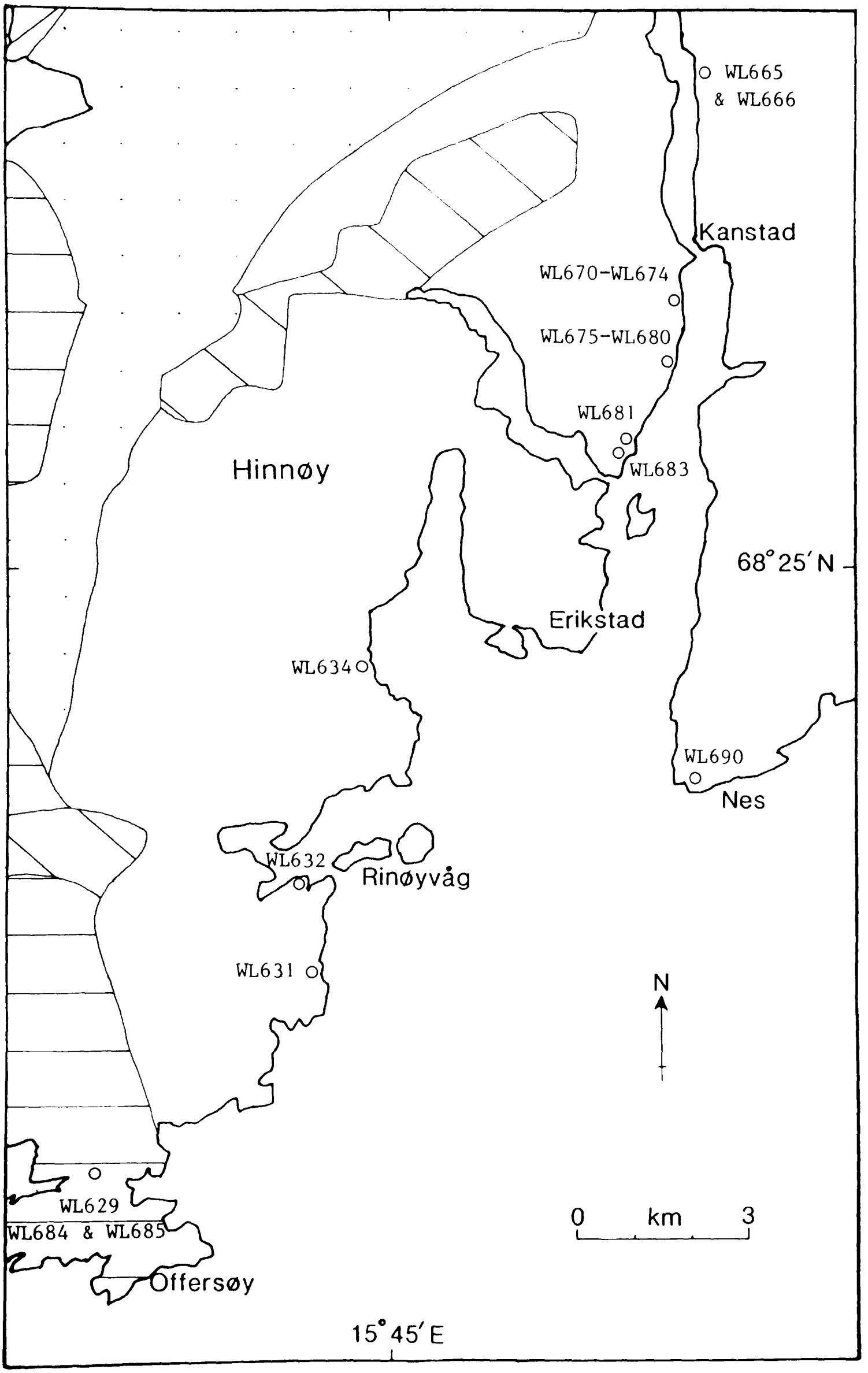

WL665
& WL666
Kanstad
WL670-WL674
WL675-WL680
WL681
WL683
Hinnøy
68°25'N
Erikstad
WL634
WL690
Nes
WL632
Rinøyvåg
WL631
N
WL629
WL684 & WL685
0 km 3
Offersøy
15°45'E

Fig. 8.2.

Rb-Sr isotope data and whole-rock isochron for twenty samples from the Lødingen Granite. The granite is a heterogeneous body with many litholigies present, all of which are represented in the samples included here:

WL629, WL631, WL632, WL634, WL665, WL670, WL675, WL683, WL684, WL685 and WL690 are pink, felsic granites (Plate 8.4);
WL666, WL671, WL676 and WL681 are more mafic granites (Plate 8.5); WL672 and WL673 are granitic pegmatites; WL679 is a fine-grained granite; and WL677 and WL678 are amphibolite xenoliths. The precision of the isochron is not altered by exclusion of particular samples. The ten-point isochron age for the Lødingen Granite published in Andresen and Tull (1983) is 1644 ± 36Ma (2σ) and $(^{87}Sr/^{86}Sr)_{1.8}$ is 0.70780 ± 74.

LØDINGEN GRANITE

SAMPLE NAME	Rb ppm	Sr ppm	87Rb/86Sr	87Sr/86Sr
WL629	123	27	28.9000	1.39686
WL631	111	194	1.7658	0.74811
WL632	102	229	1.3443	0.73747
WL634	83	94	2.9443	0.77488
WL665	127	84	4.6063	0.80556
WL666	94	80	3.8893	0.78705
WL670	124	205	1.8855	0.75029
WL671	156	278	1.6464	0.74448
WL672	233	42	18.1160	1.17419
WL673	207	55	11.9330	0.97633
WL675	106	68	4.9284	0.81201
WL676	100	424	0.6933	0.72180
WL677	152	282	1.6387	0.74361
WL678	120	192	1.9362	0.74485
WL679	70	71	3.5609	0.78694
WL681	84	593	0.4102	0.71376
WL683	107	83	4.5163	0.81467
WL684	107	241	1.3592	0.74228
WL685	129	179	2.2704	0.76437
WL690	180	83	7.6900	0.85604

Slope	0.023625	Error	0.000078 (1 Sigma)
Intercept	0.704849	Error	0.000114 (1 Sigma)
Centroid	1.042138	0.729469	
Squared residuals	1244.640		
M.S.W.D.	69.147		
No. of Cycles	3		

Slope	0.023625	Error	0.000645 (1 Sigma)
Intercept	0.704849	Error	0.000948 (1 Sigma)
Centroid	1.042138	0.729469	
Squared residuals	18.000		
M.S.W.D.	1.000		
No. of Cycles	3		

Age 1644.4 +/- 88.7 Ma. (2 sigma)

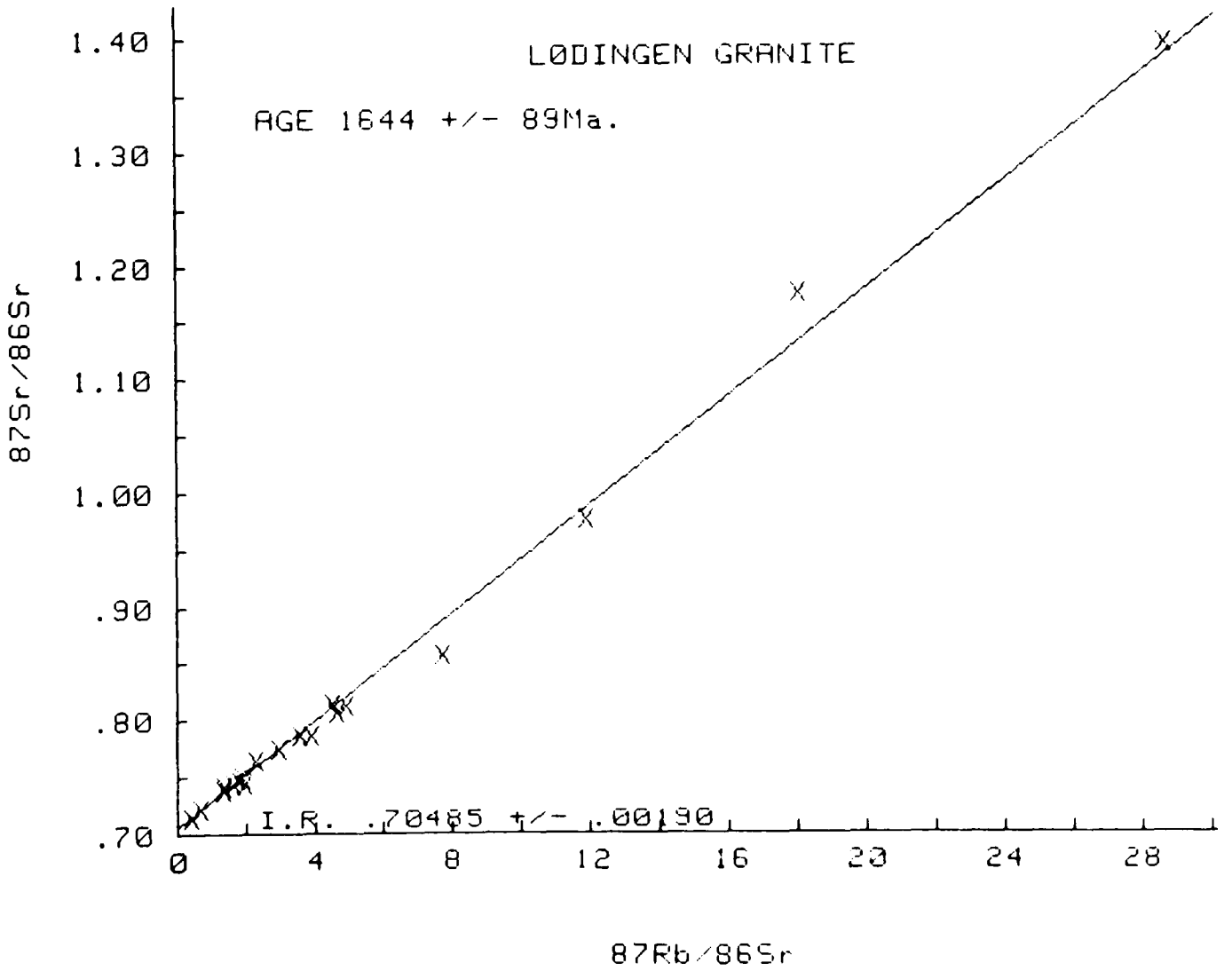


Fig. 8.3.

Sm-Nd evolution diagram for the Lødingen Granite, Southern Hinnøy (data in Table 8.2). This intrusion was emplaced at 1.65Ga (Fig. 8.2). (The vertical lines define the age range 1.55 - 1.7Ga). The range in initial $^{143}Nd/^{144}Nd$ ratios (at 1.65Ga) is sufficiently large to preclude Sm-Nd whole-rock isochron dating for the Lødingen Granite. The T_{DM} model ages for this intrusion imply that the granite contains a crustal component older than 1.65Ga. The isotope ratios and model ages are within the range of these values for the mangerites.

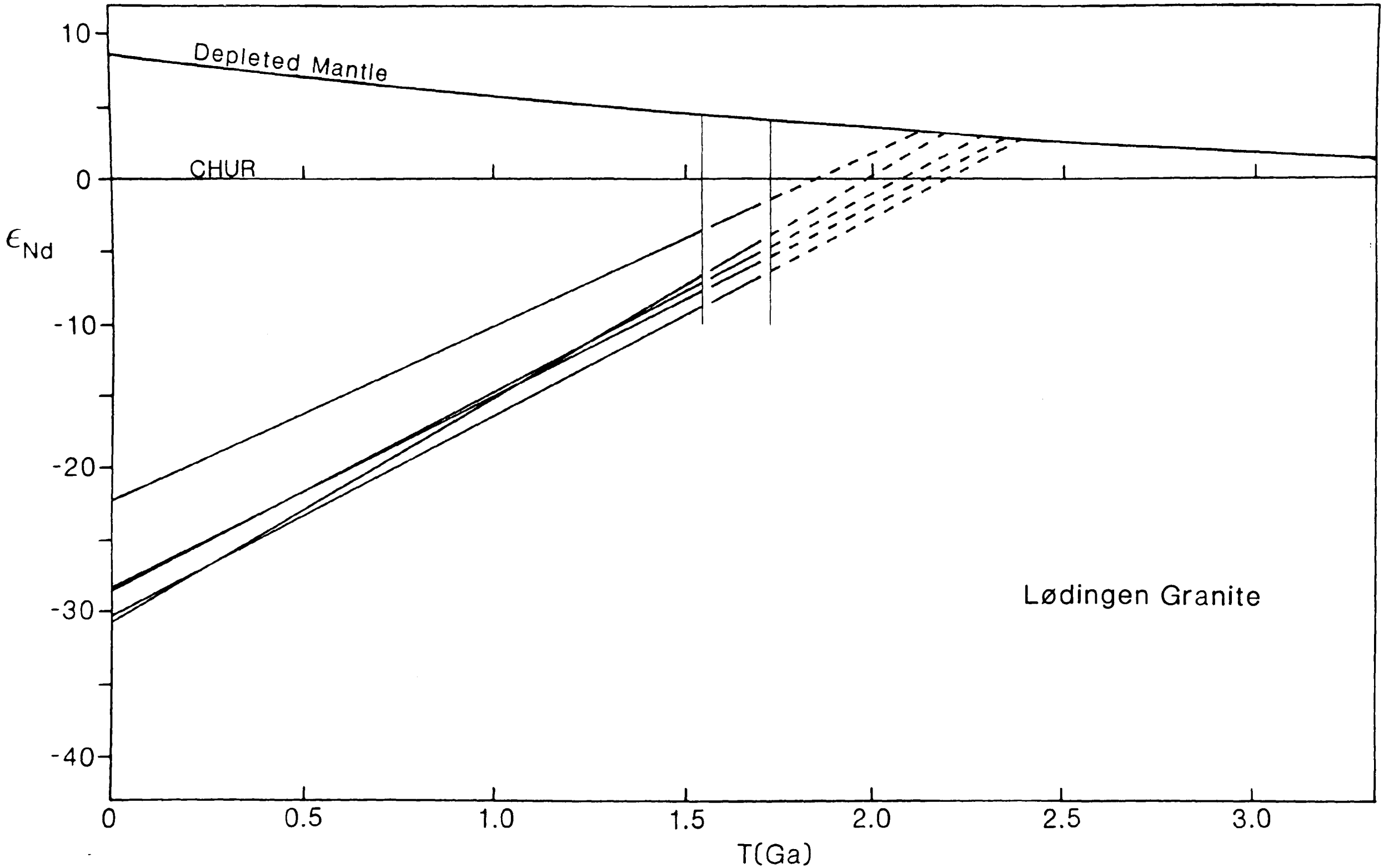
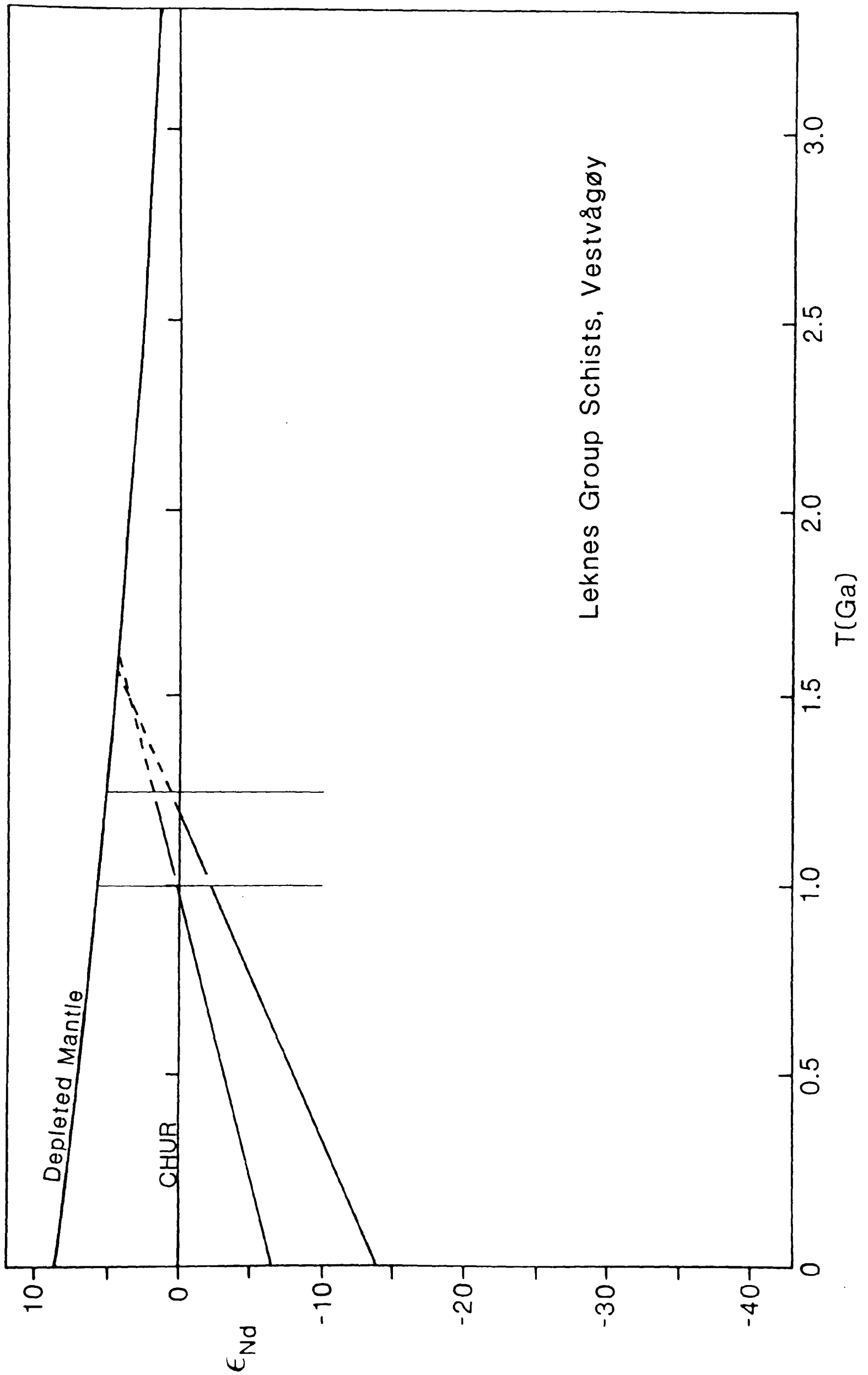

10
0
-10
-20
-30
-40
ϵ_{Nd}
Depleted Mantle
CHUR
Lødingen Granite
0
0.5
1.0
1.5
2.0
2.5
3.0
T(Ga)

Fig. 8.4.

Sm-Nd evolution diagram for the Leknes Group Metasediments, Vestvågøy (data in Table 8.5). The Rb-Sr whole-rock isochron age of these rocks is 1.15Ga (Griffin et al., 1978). (The vertical lines define the age range 1.0 - 1.25Ga). The T_{DM} model ages for the samples shown (WL421 and WL424) are both within error of 1.6Ga, proving that a mantle-derived crustal addition has been made to the Lofoten-Vesterålen province subsequent to the emplacement of the mangerites at 1.8Ga (so far unidentified). Nonetheless the model ages are older than the poorly-defined Rb-Sr whole-rock isochron age implying that the Leknes Group is older than 1.15Ga or that it has been derived from rocks with a previous crustal history.


Leknes Group Schists, Vestvågøy
Depleted Mantle
CHUR
ϵ_{Nd}
10
0
-10
-20
-30
-40
0
0.5
1.0
1.5
2.0
2.5
3.0
T(Ga)

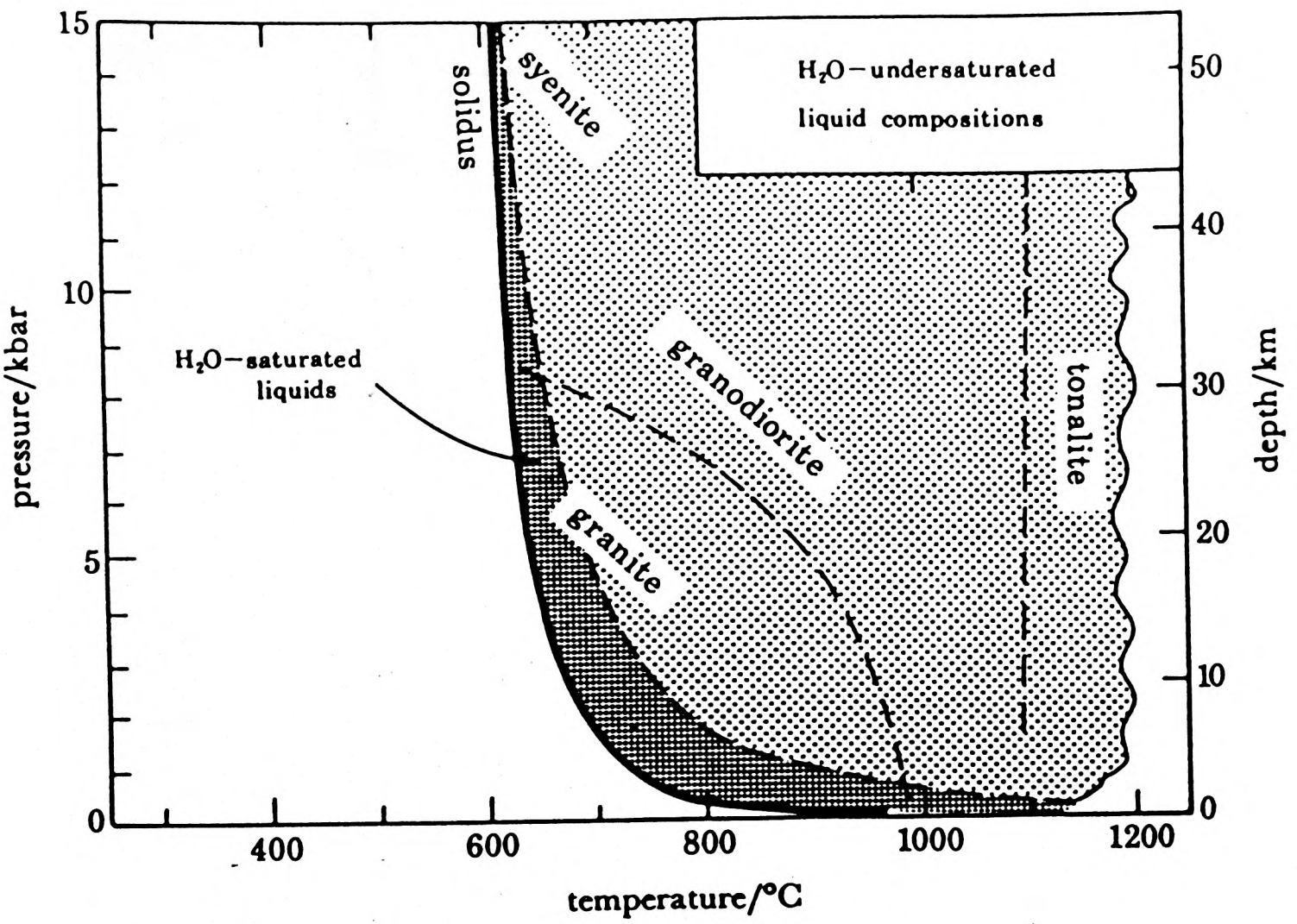


Fig. 9.1. Compositions of liquids generated within the melting interval of rocks of continental crust in presence of H_2O.

N.B. For thickened crust, the near-solidus liquid approaches syenite composition (Huang and Wyllie, 1981)

Diagram after Wyllie (1977, 1984).

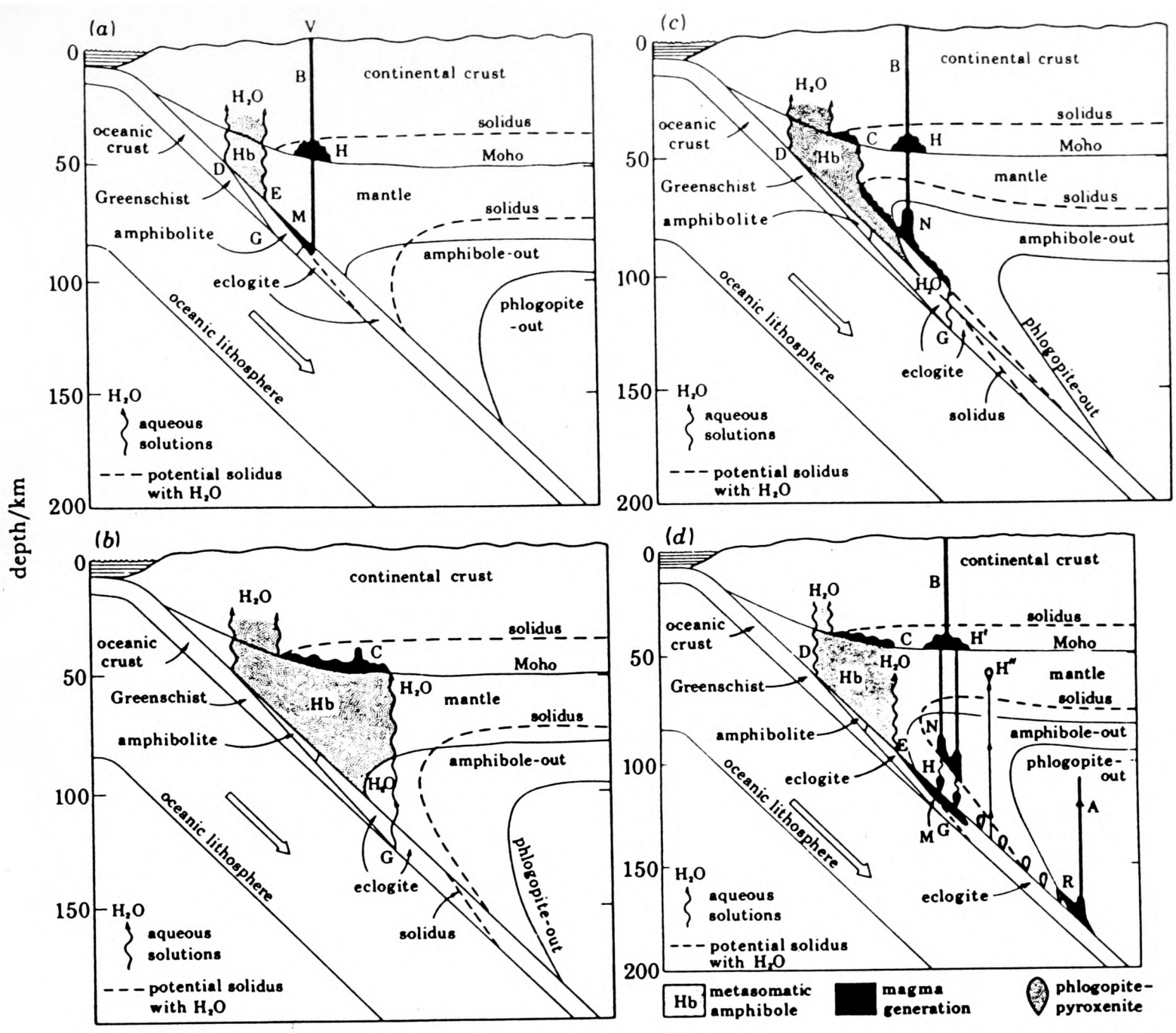


Fig. 9.2. Locations of dehydration, metasomatism, and melting in subduction zones from results of experimental petrology, according to four thermal structures obtained by combinations of warm or cool (by endothermic dehydration) subducted ocean crust, with cool or warm (by induced convection) mantle. (a) Cool mantle-warm crust. (b) Cool mantle-cool crust. (c) Warm mantle-cool crust. (d) Warm Mantle-warm crust.

High K, U and Th levels in the early Proterozoic mean that the mantle wedge beneath the Lofoten-Vesterålen province was probably warm, hence Figs. 9.2c and 9.2d are likely to be the most relevant for early Proterozoic magmatic processes in the province.

Diagrams after Wyllie (1984)